ARMY RESEARCH LABORATORY

ARL

Eaton Throat-Valve Element Modifications Preliminary Report

Marcela R. Stacey
James G. Arendts
Ray A. Berry
Gary E. Korth
Paul R. Schwieder
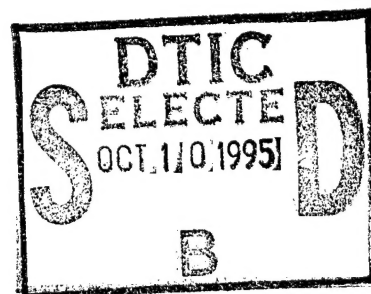Joseph P. Sekot
Spencer D. Snow

ARL-CR-239

July 1995

prepared by

DTIC
SELECTED
OCT 10 1995
B

19951005 007

DTIC QUALITY INSPECTED 8

NOTICES

Destroy this report when it is no longer needed. DO NOT return it to the originator.

The findings of this report are not to be construed as an official Department of the Army position, unless so designated by other authorized documents.

The use of trade names or manufacturers' names in this report does not constitute endorsement of any commercial product.

REPORT DOCUMENTATION PAGE

1. AGENCY USE ONLY (Leave blank)	2. REPORT DATE July 1995	3. REPORT TYPE AND DATES COVERED Final, July 1993 - December 1993

4. TITLE AND SUBTITLE

Eaton Throat-Valve Element Modifications Preliminary Report

5. FUNDING NUMBERS

DOE C: DE-AC07-761D01570

6. AUTHOR(S)

Marcela R. Stacey, James G. Arendts, Ray A. Berry, Gary E. Korth, Paul R. Schwieder, Joseph P. Sekot, and Spencer D. Snow

7. PERFORMING ORGANIZATION NAME(S) AND ADDRESS(ES)

Idaho National Engineering Laboratory
EG&G Idaho, Inc.
Idaho Falls, ID 83415

8. PERFORMING ORGANIZATION REPORT NUMBER

9. SPONSORING/MONITORING AGENCY NAMES(S) AND ADDRESS(ES)

Monitoring: U.S. Army Research Laboratory
ATTN: AMSRL-WT-NC
Aberdeen Proving Ground, MD 21005-5066

10. SPONSORING/MONITORING AGENCY REPORT NUMBER

ARL-CR-239

11. SUPPLEMENTARY NOTES

The agency sponsoring this study is: Defense Nuclear Agency, 6801 Telegraph Road, Alexandria, VA 22310.

12a. DISTRIBUTION/AVAILABILITY STATEMENT

Approved for public release; distribution is unlimited.

12b. DISTRIBUTION CODE

13. ABSTRACT (Maximum 200 words)

This report documents the development and findings of a computer model that simulates the behavior of the Eaton-Throat Valve Element (ETVE) prototype, and describes a proposed modification concept for the ETVE. This high-speed valve was designed for the U.S. Army Research Laboratory, Aberdeen Proving Ground, MD, to control the simulation of the dynamic effects of a nuclear blast.

The computer model reveals three main findings: (1) the ETVE chatters during the open cycle, (2) the chatter is caused by the high gas forces on the sliding sleeve as the driver gas passes through its portholes, and (3) the chatter is aggravated because there is insufficient damping in the system.

The INEL recommends opening the ETVE by sliding the sleeve toward the downstream end of the valve instead of toward the upstream end, as the ETVE is presently configured, and to provide additional damping to the system. However, neither of these configuration changes can be achieved easily, and a redesign and analysis of the ETVE must be completed prior to performing any work on the current ETVE prototype. The ETVE simulation model proved to be an extremely valuable tool in analyzing the qualitative nature of the valve's operation. Further development of the model is recommended for quantitative analysis and design of the ETVE. This report explains the model and stress analysis findings, and proposes a redesign concept.

14. SUBJECT TERMS

blast valves, shock tubes, valve elements, fast acting valves, sliding-sleeve valves, blast simulators

15. NUMBER OF PAGES 217

16. PRICE CODE

17. SECURITY CLASSIFICATION OF REPORT UNCLASSIFIED	18. SECURITY CLASSIFICATION OF THIS PAGE UNCLASSIFIED	19. SECURITY CLASSIFICATION OF ABSTRACT UNCLASSIFIED	20. LIMITATION OF ABSTRACT UL

INTENTIONALLY LEFT BLANK.

ACKNOWLEDGMENTS

INTENTIONALLY LEFT BLANK.

TABLE OF CONTENTS

LIST OF FIGURES

INTENTIONALLY LEFT BLANK.

SUMMARY

This report documents the development and findings of a computer model that simulates the behavior of the Eaton-Throat Valve Element (ETVE) prototype, and describes a proposed modification concept for the ETVE. This high-speed valve was designed for the U. S. Army Research Laboratory, Aberdeen Proving Ground, Maryland, to control the simulation of the dynamic effects of a nuclear blast.

The computer model reveals three main findings: (1) the ETVE chatters during the open cycle, (2) the chatter is caused by the high gas forces on the sliding sleeve as the driver gas passes through its portholes, and (3) the chatter is aggravated because there is insufficient damping in the system

The ETVE simulation model has proven to be an extremely valuable tool in assessing the qualitative nature of the current valve's operation and is indispensable in assessing the effects of valve modifications or redesigns. The ETVE's complex nonlinear behavior is impossible to predict in any way other than numerical simulation, even if the numerical simulations are accepted on a qualitative basis only.

In addition, the model can be used to input new Belleville washer characterization data for different washer configurations and then assess the qualitative effects of each configuration on the overall valve behavior.

The INEL recommends opening the ETVE by sliding the sleeve toward the downstream end of the valve instead of toward the upstream end, as the ETVE is presently configured, and to provide additional damping to the system. The main areas of redesign follow.

1. Increase the length of the sleeve by approximately 1.6 in. and add two sets of seals in the added length to seal the last row of body portholes. Reduce the length of the liner by 0.7 in.

2. Place the sleeve upstream (from its current as-built location) as indicated in Figure 5-1 so the pneumatics can slide the sleeve forward to its open position.

3. Increase the length of the ETVE body to house approximately 32 Belleville washers on the open chamber and 8 washers in the close chamber. This modification requires retapping the pneumatic actuation lines.

4. Lengthen the piston rod to accommodate the added number of washers.

5. Increase the stop plate size and increase the number and size of bolts used to fasten the stop plate to the valve body.

3. The close-cycle actuation needs to be evaluated and redesigned to overcome the driver gas forces that will make the valve difficult to close.

4. Any general design concepts should be evaluated by using the already developed valve sleeve dynamic simulation model to qualitatively predict and evaluate the design concept's effects on the ETVE performance.

INTENTIONALLY LEFT BLANK.

1. INTRODUCTION

1.1 Background

As part of an ongoing effort to improve techniques for simulating nuclear blasts, the U.S. Army Research Laboratory (ARL) has been studying the merits of computer-controlled valves. The valve studies have been aimed at providing the Department of Defense (DOD) with the capacity to conduct nuclear blast and thermal survivability testing on full-scale tactical vehicles. In support of this DOD objective, two new simulators are currently under development: (1) the Large Blast/Thermal Simulator (LB/TS), a Defense Nuclear Agency facility currently under construction at the White Sands Missile Range, and (2) the ARL 1/6-scale Test bed, a technology demonstrator currently undergoing characterization testing at the Aberdeen Proving Ground, Maryland. If use of computer controlled-valves proves feasible and cost effective, it is expected that the computer-controlled valves will replace the more labor-intensive rupture disks currently used to simulate nuclear blasts. The computer-controlled valves would be retrofitted first to the ARL Test Bed and then to the LB/TS at the White Sands Missile Range.

In support of the U.S. Army's work, the Idaho National Engineering Laboratory (INEL) studied a number of valve design concepts and determined that a multi-element valve would best control blast simulation. A multi-element valve is formed from an array of small valves whose openings and closings are coordinated to give the required total output through the valve as a whole. The INEL subcontracted Eaton Consolidated Controls to build the valve element prototype, called the Eaton Throat-Valve Element (ETVE), which uses a pneumatically-driven sliding-sleeve (see Figure 1-1). The term throat was given to the prototype since the valve acts like a throat in that the driver-gas released is funneled through an opening much narrower than the driver cross section. We tested this prototype ETVE at the INEL during 1991. The test results revealed segmented shock waves, which suggested the possibility that the ETVE chattered during the ETVE opening cycle. We also observed that the duration of the chatter increased with increased gas pressure in the upstream pressure chamber (hereafter called driver tube).

The primary objective of our work performed during 1993 has been to develop a computational fluid dynamics model of the valve and then use it to propose a preliminary modification design concept of the ETVE to meet the original design requirements. If the U.S. Army approves the design, and funds are available, the INEL may perform the final analysis, design, modification, and testing of the ETVE, and then ship the valve back to ARL to perform full conditions testing there (700°F and 1800 psi nitrogen driver gas).

1.2 Valve Testing History at the INEL

The INEL tested the ETVE's performance in two separate phases: the first phase during 1989, the second during 1991. The 1989 phase used the ETVE; however, the effort was focused on the equipment that had been purchased from Thermal Sciences Incorporated of St. Louis, Missouri. The equipment consisted of the high-pressure tube (called the driver tube), its interior insulation, and the gas heater.[1]

The 1991 phase focused on testing the performance of the ETVE, during which testing the chattering condition was diagnosed as a possible malfunction.[2] The main objection to the ETVE's chatter is its effect on the downstream shock signal; as the valve chatters, the effective flow area for the driver gas changes, causing a segmented wave downstream, which is unacceptable for blast simulation.

1
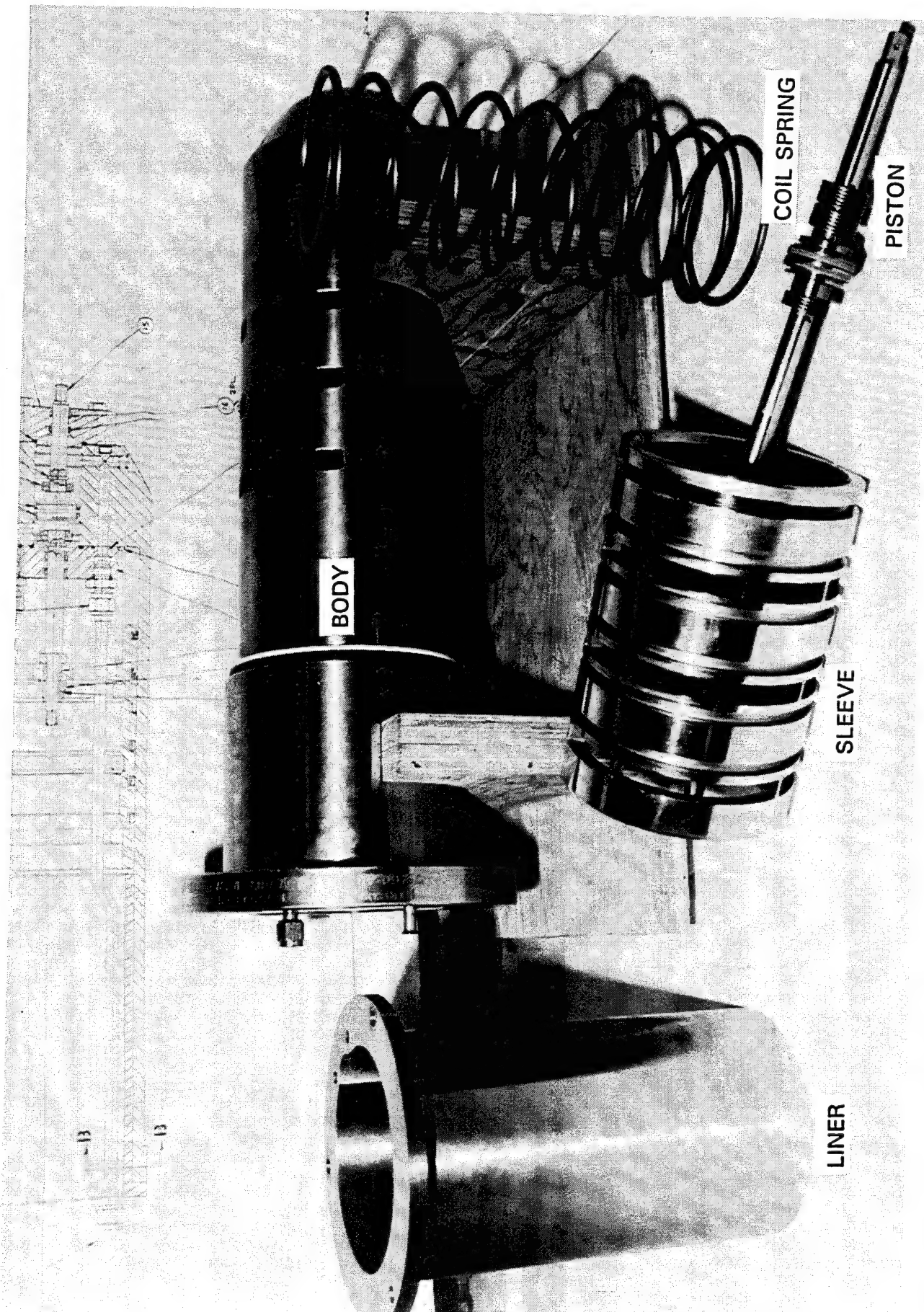
Figure 1-1. Photograph of ETVE main components.

1.3 Current ETVE Configuration

Figure 1-2 illustrates the current ETVE configuration . The main features of the current configuration are as follows:

- The ETVE is designed with three rows of portholes in both the ETVE body and sleeve. When the corresponding portholes are aligned, the gas in the upstream driver tube flows freely through these portholes.

- The ETVE is closed when the sliding sleeve is in its most downstream position, as indicated in Figure 1-2.

- The ETVE is actuated back to its open position by an electronic signal sent to the open-solenoid, which opens a 2000-psi gas supply line. The gas pressurizes the open-actuating line and the open-chamber. As the chamber is pressurized, the piston, which is rigidly connected to the sliding sleeve, will move to align the body and sleeve portholes. This is the ETVE open position, illustrated in Figure 1-3.

- The ETVE is actuated to its closed position by an electronic signal that actuates both the close-solenoid to supply 2000 psi to the close-chamber, and the open-solenoid to relieve the pressure in the open-chamber and its actuating line.

1.4 Purpose

The primary objective of the work performed during 1993 has been to develop a computational fluid dynamics model of the ETVE that can be used to propose a preliminary modification design concept to meet the ETVE's original design requirements. The gas dynamics model uses the ETVE moving parts equation of motion and associated parameters calculated in the mechanical dynamics subroutine. This subroutine calculates these parameters by using the results from tests we performed on the ETVE to characterize the sleeve's displacement history, and from tests we performed on Belleville washer stacks similar to those in the ETVE. Note that the characterization of the ETVE sleeve displacement was performed under ambient pressure and temperature conditions on the upstream end of the ETVE. This report presents the results from the characterization tests for the sleeve and the Belleville washers, and the results from the mechanical dynamics subroutine and the gas dynamics model.

3
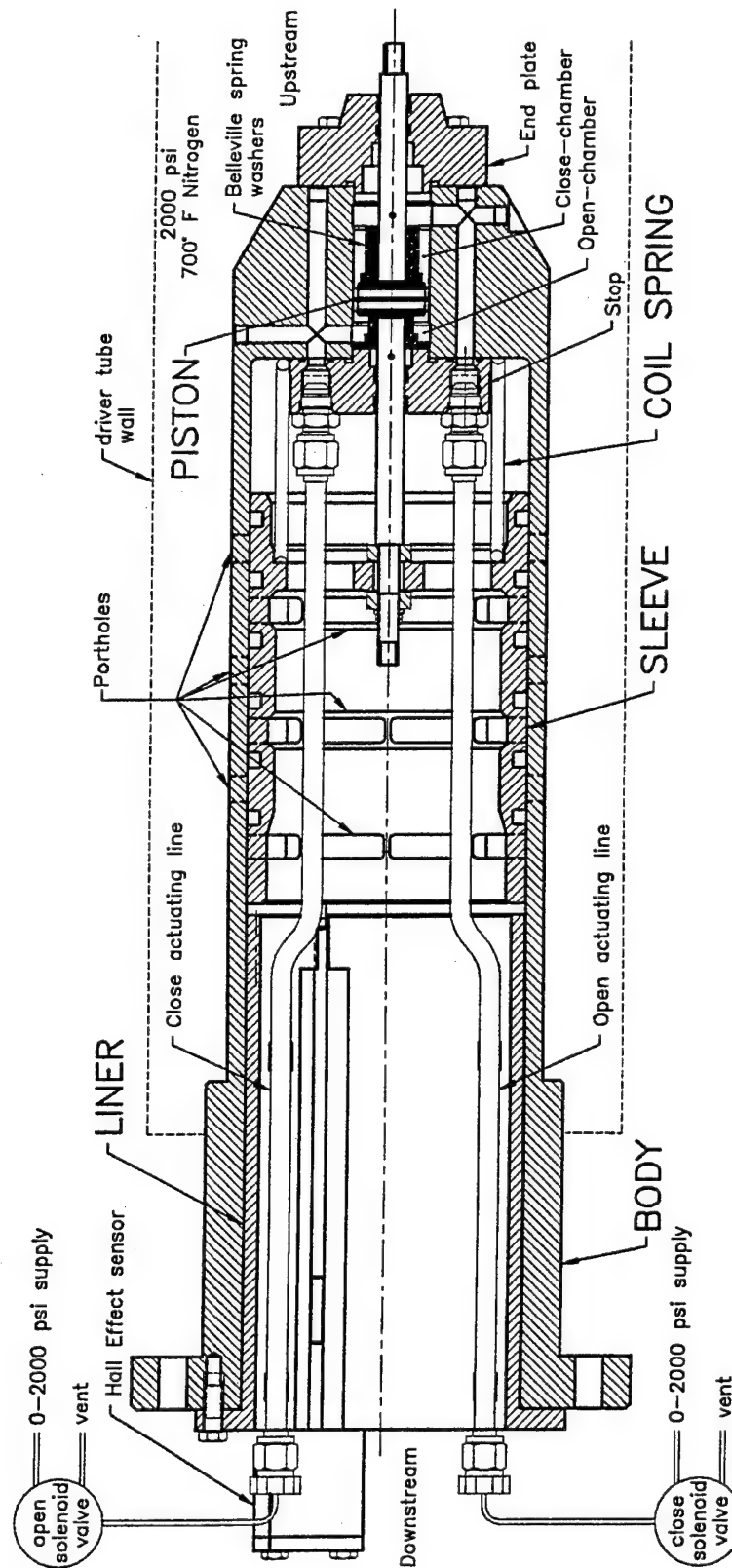
Figure 1-2. Current ETVE configuration—ETVE closed.

4
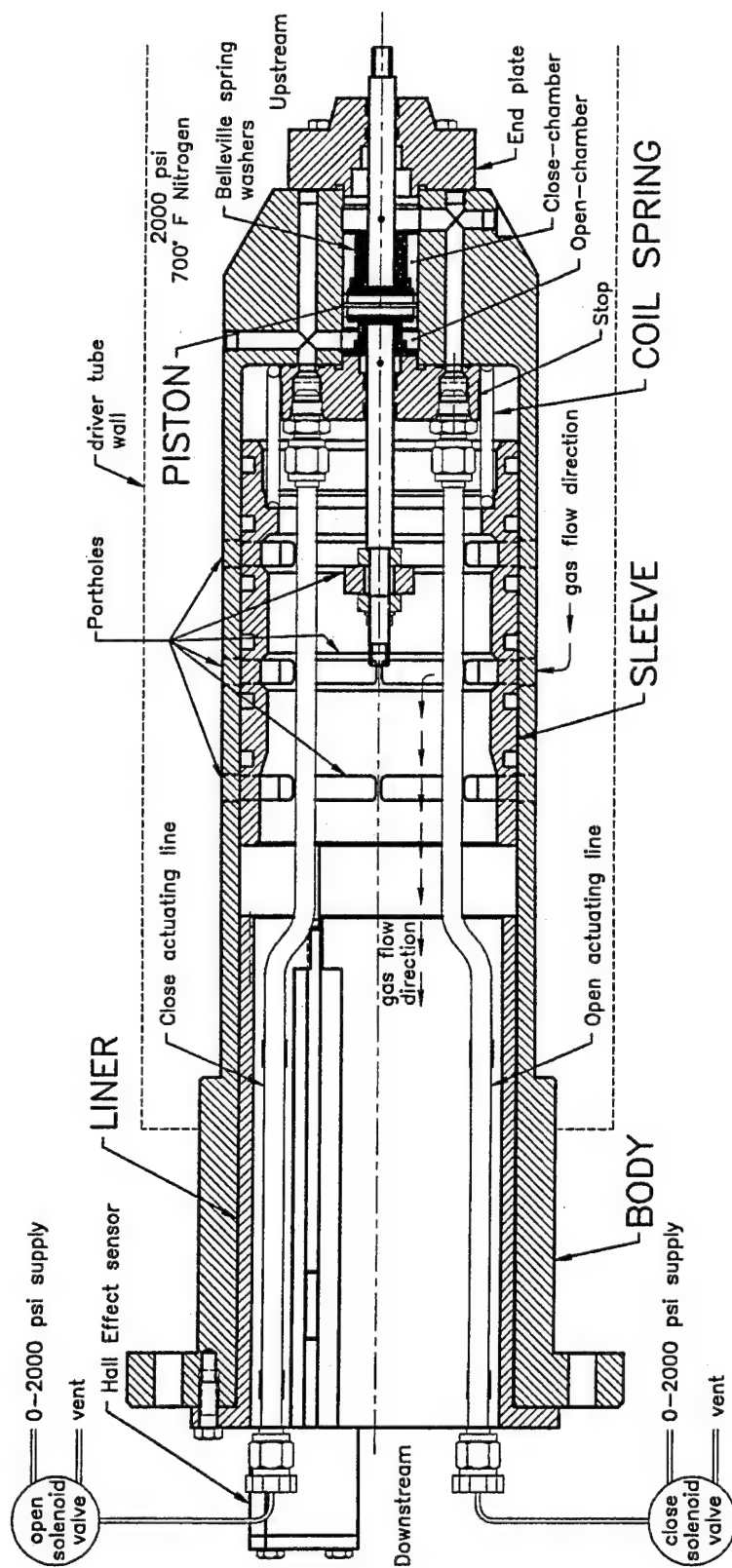
Figure 1-3. Current ETVE configuration—ETEV opened.

5

INTENTIONALLY LEFT BLANK.

2. VALVE COMPONENT CHARACTERIZATION AND VALVE MODELING

We developed the computer model in four phases: (1) characterization of the sleeve's displacement history, (2) characterization of the Belleville washer stack behavior under quasi-static loading, (3) development of the mechanical dynamics subroutine, and (4) development of the gas dynamics model. The sleeve displacement and Belleville washer characterization tests were necessary to complete the mechanical dynamics subroutine. In turn, the mechanical dynamics subroutine was necessary prior to finishing the gas dynamics model. Each of the four phases are described in this section.

2.1 ETVE Characterization Testing for the Existing Configuration

We performed two sets of tests to characterize the behavior of the ETVE under its existing configuration. The first test characterized the ETVE sleeve's displacement behavior using a linear variable displacement transducer (LVDT). The LVDT data were used in the development of the ETVE moving parts mechanical dynamics subroutine. The second test set explored the effects of varying the open- and close-actuating solenoids sequencing to reduce or eliminate the ETVE chatter. Appendix A describes this work in greater detail.

2.1.1 Characterization Test 1 — LVDT Testing. The tests performed at the INEL during 1991 indicated that the ETVE was possibly chattering during the opening cycle before achieving steady-state open position. At that time, when the ETVE arrived at the INEL for its initial testing in 1989,[1] it was not possible to exactly confirm the chatter, since the only means provided to detect the sleeve's movement was a Hall Effect Sensor. This instrument provided only qualitative displacement information. Prior

to characterizing the sleeve's displacement history, we purchased and installed an LVDT and used it to obtain a high-resolution sampling of the ETVE's sliding sleeve displacement during the open cycle. It is important to note that we tested the ETVE at ambient temperature and pressure because the driver tube was not available for use at the INEL facility during this 1993 work.

2.1.2 Characterization Test 2 — Damping with Solenoid Valves. We performed these tests to explore the possibility of reducing or eliminating the chatter by varying the sequencing of the actuating-solenoids. We tried two different actuating sequences:

1. We used 2000 psi to open the ETVE while the close-chamber was pressurized to 1000 psi; we then vented the close-chamber 70 msec after the LVDT detected any movement (see Appendix A for detailed test information).

2. Similar to Sequence 1, we pressurized the close-chamber to 1000 psi and used 2000 psi to actuate the ETVE to open. However, we kept the close-chamber pressurized at 1000 psi for 500 msec after the LVDT detected any movement before venting it. Figure 2-1 shows overlaid plots of the ETVE sleeve displacement for the tests results in the two sequences. The initial LVDT test results are described in Section 2.1.1.

These tests show that the actuating sequences described in sequences 1 and 2 did not change the chattering considerably. Furthermore, the overlaid plots clearly show that pressurizing the close-chamber before opening the valve increases the valve open time considerably, approximately 60 msec.

Characterization Test 1—LVDT Testing
2000 psi actuating open pressure with close-chamber
at ambient pressure

Characterization Test 2—Damping with Solenoid Valves
Sequence 1—2000 psi actuating open pressure with
1000 psi actuating close pressure on close-chamber for
70 msec.

These plots show that pressurizing the close-chamber
prior to opening the valve does not eliminate the
chatter; it only increases the valve open time by
approximately 60 msec compared to the valve open
time for the close-chamber at ambient pressure prior to
opening the valve.

Characterization Test 2—Damping with Solenoid Valves
Sequence 2—2000 psi actuating open pressure with
1000 psi actuating close pressure on close-chamber for
500 msec.

Displacement (inches)

Time (second)

Figure 2-1. Overlaid LVDT test plots.

2.2 Belleville Washer Characterization Testing

We characterized the Belleville washers under quasi-static load-deflection behavior for the current washer configuration and for other alternative configurations. We tested the washers in compression and monitored the deflection with respect to the load applied for each washer configuration.

The tests reveal that the Belleville washers experience a significantly different loading and unloading force-displacement behavior, and that damping decreases exponentially as the loading approaches the design load. To provide high-load damping, we believe it is necessary to stack several washers (eight to ten) in parallel and connect them in series with one or more similar stacks. Appendix B describes in detail the test results for the different washer stack configurations.

In addition to characterizing the washers, we developed a simple FORTRAN program using the mechanical dynamics subroutine to study the washer's damping behavior. We observe that overloading the washers reduces the effective damping significantly; however, *the Belleville washers are an effective method to provide damping for the system if designed correctly.* Appendix C describes the FORTRAN program in greater detail and discusses the conclusions drawn from its use.

2.3 Mechanical Dynamics Model

We analyzed the ETVE's moving parts (sleeve, piston, piston rod, and Belleville washers) and derived the equation of motion for their configuration. The resulting solution of the non-linear equation of motion is represented as explicit time-difference equations. Appendix D details the FORTRAN implementation of the motion solution and its supporting subroutines; namely "belspr," "fact," and "motion."

2.3.1 General Code. Since all of the moving parts of the ETVE are rigidly connected, the mechanical dynamics model developed uses a single degree-of-freedom rigid-body dynamic model, represented in Figure 2-2. The gas dynamic model described in Section 2.4 calls up the mechanical dynamics model as a subroutine. The LVDT test results provided the sleeve displacement information used in the subroutine. The Belleville damping characteristics were obtained from the quasi-static compression tests described in Section 2.2.

2.3.2 Description of Subroutines.
Subroutine *belspr* — This subroutine computes the Belleville springs' stiffness from the force-displacement characterization values specified in BLOCK DATA. The subroutine is only called from the main program once (prior to first call to *motion*).

Subroutine *fact* — This subroutine calculates the current actuator force acting on the moving ETVE parts. This subroutine must be called prior to each call of motion.

Subroutine *motion* — This subroutine calculates the incremental motion of the ETVE movable parts and outputs their displacement, velocity, and acceleration. Arguments passed to the subroutine are current calculation time, current time increment, net fluid dynamic force acting on the moving mass, and an integer flag. The flag indicates whether a Belleville spring is loading or unloading, which is very important owing to the very large changes in the motion parameters that occur in the transition between relatively free motion (neither Belleville spring is compressed) and very stiff resistance (either of the Belleville springs are compressed). The remaining section of the subroutine consists of logic blocks wherein the applicable motion parameters are specified, and, finally, the updated motion variables are computed. Appendix D presents this subroutine in Table D-3.

9
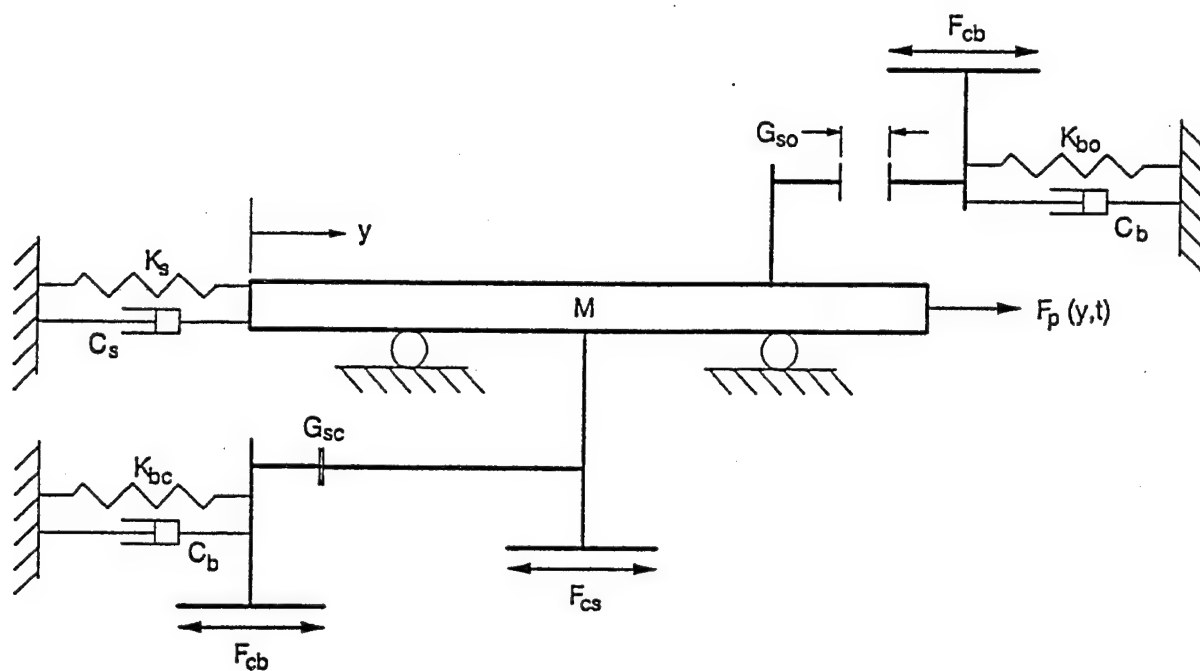
Gso = Sleeve opening gap
Gsc = Sleeve closing gap

M = Mass of the moving parts

Fcs = Coulomb damping on sleeve
Fcb = Coulomb damping on the Belleville washers

Cs = Stiffness and viscous damping on the sleeve
Ks = Stiffness and viscous damping on the coil spring

Kbc = Closing Belleville washers stiffness
Kbo = Opening Belleville washers stiffness
Cb = Belleville washer viscous damping

Externally applied force resulting from the time-dependent actuator pressure
and hydrodynamic gas pressure (time- and sleeve position-dependent)—
$F_p(y,t)$

Figure 2-2. Mechanical dynamic model.

2.3.3 Findings. Once the mechanical dynamic model was completed, the *actual* system's damping characteristics were obtained by running several algorithm predictions and varying different parameters until the axial displacement history matched the actual test data obtained from the tests described in Section 2.1 and 2.2. We found that the following damping parameters produce a reasonable fit to the test data:

Sleeve Coulomb damping force = 100 lbf

Sleeve viscous damping ratio = 0.0

Belleville washers Coulomb damping force = 0.0

Belleville washers viscous damping ratio = 0.08.

Figure 2-3 compares the subroutine-calculated ETVE displacement response damping data with the test data obtained from actuating the ETVE to open at ambient pressure and temperature, as described in Section 2.1.1.

2.4 Gas Dynamics Model

Figure 2-4 shows the gas dynamic simulation model representing the ETVE configuration. The stationary and moving valve parts are approximated as rectangular solid blocks; the mesh spacing used is $\partial x = \partial y = 1$ mm, in the axial and radial direction, respectively. Constant pressure boundary conditions were applied at the inlet and outlet boundaries of the flow model. On the high-pressure boundary (upstream in Figure 1-2) the pressure is set to 1800 psi and 700°F; the low-pressure boundary (downstream in Figure 1-2) is set to 14 psi and ambient temperature. Appendix E presents the gas dynamics model work in detail.

2.4.1 Description of the Model. We used the compressible Euler equations formulated for two-dimensional, axisymmetric coordinate systems to describe the gas dynamics of the ETVE during the actuating open cycle. The code uses a variable *thickness* or *depth* in the radial direction for each mesh cell, named A.

In two-dimensional computations, the volume of a cell of width ∂x and height ∂y is $A\partial x\partial y$, giving a quasi-three-dimensional effect. The physical assumption underlying the variable depth description is that the flow variables are depth-averaged in the depth direction to give mean values with variation only in the x and y dimensions, or equivalently, that the flow variables are independent of displacement in the depth direction.

The variable-depth equations are used because they greatly increase the geometrical flexibility of the description without increasing its complexity. The variable, A, may be used to represent flow through a two-dimensional duct of gradually varying thickness. The use of zero values of A in selected mesh cells provides a convenient means of including internal obstacles in the flow region. In particular, a cell with A = 0 will allow no flow across its boundaries. The stationary obstacles (valve internal parts) are represented with this technique. Axisymmetric coordinates are generated by having A increase linearly with the distance from the axis. Since the ETVE valve is approximately axisymmetrical, this feature is also used. As presently coded, the A-quantity must be a constant in time.

Equations and Constitutive Relations — The Euler equations describing the dynamics of an inviscid gas have been cast in many forms. The dependent variables are chosen here to be the mass density, ρ, the gas velocities, u and v, and the internal energy per unit volume, E. In terms of the chosen dependent variables, the basic two-dimensional Euler equations used in the code are the continuity, the momentum, and the internal energy equations.

In these equations, the independent variables are time, t, and coordinates, x and y. The gravitational acceleration terms, the heat conduction terms, and the viscous terms have been neglected, owing to their insignificance. To complete these equations, a constitutive relation, which relates pressure, p, and internal energy per unit volume, E, is defined. The following equation is based on the assumption that the gas obeys the perfect gas laws.

11
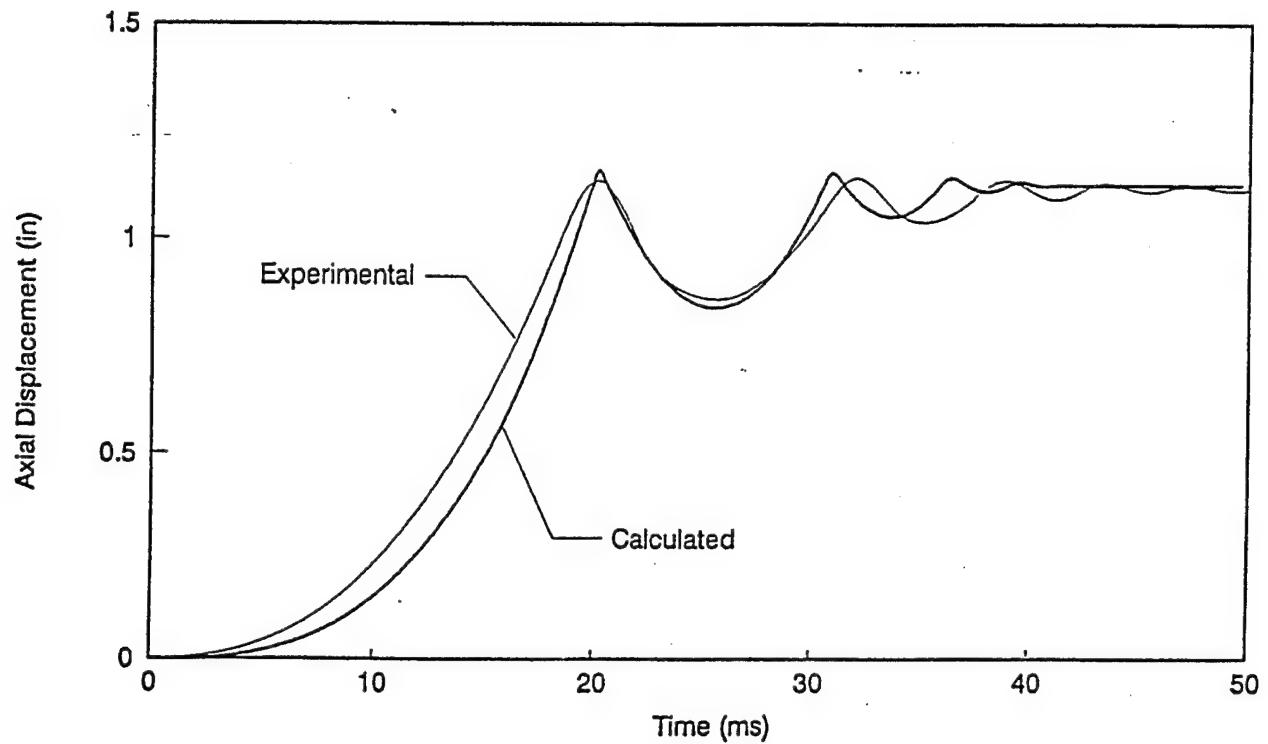
Comparison of actual LVDT test data with the Mechanical Dynamics Model output for ambient pressure and temperature driver gas. Valve actuated to open position with 2000 psi, ambient pressure in the close-chamber.

Figure 2-3. Calculated versus actual ETVE displacement history.
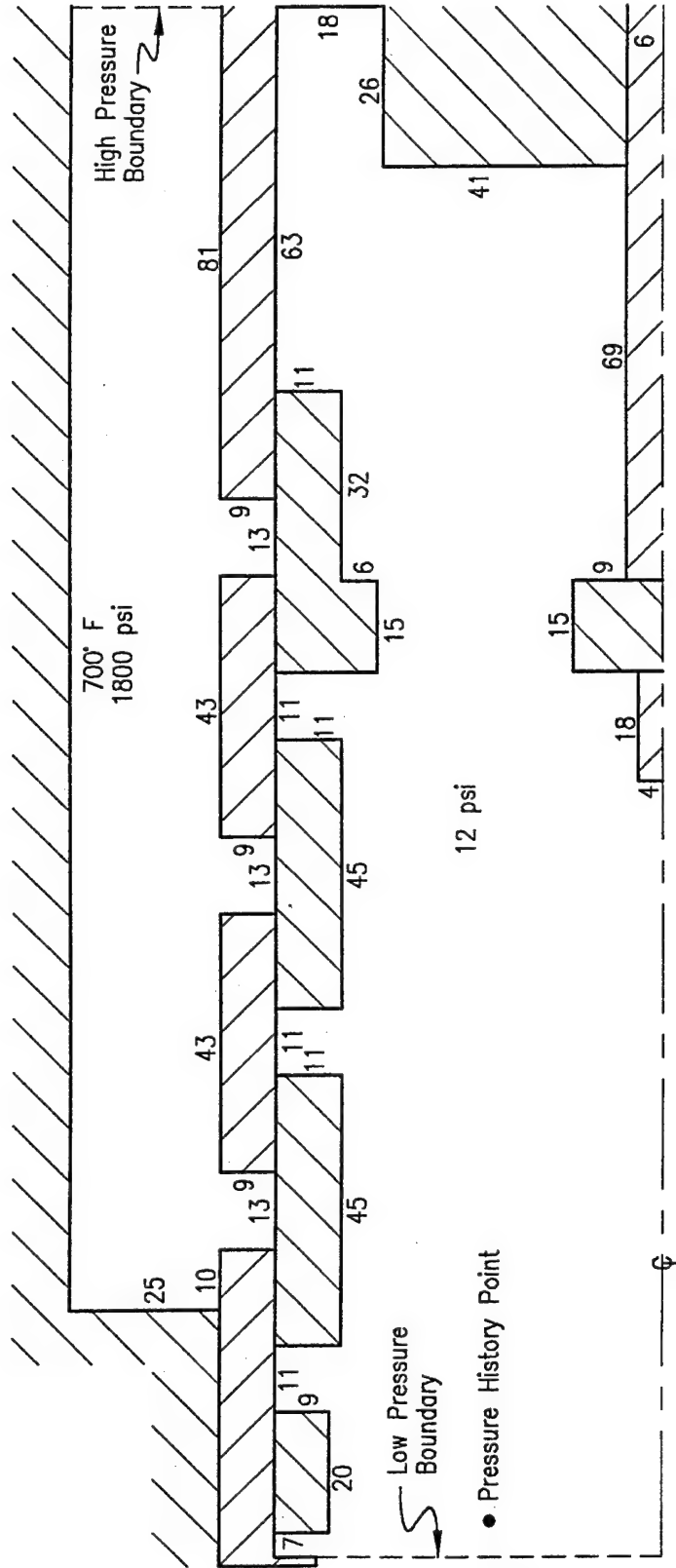
Figure 2-4. Gas dynamics model.

13

$p = (\gamma - 1) E$

The relation γ is the ratio of specific heats.

Dynamical Coupling — To represent the valve opening dynamics, the moving parts of the valve must be coupled to the subsequent fluid dynamics of the gas as it flows through the valve. The gas surrounding the valve moving parts exerts a force (the dominant force) on these moving parts to produce its motion. The ETVE sleeve motion, in turn, influences the gas directly with its motion and indirectly by opening or closing the portholes to alter the gas flow dynamics. The ETVE sleeve motion is also influenced by the dynamic response of other components and phenomena such as the coil spring, the ETVE sleeve friction, the Belleville spring loading and unloading, and the actuating pneumatics. The gas dynamic system and ETVE sleeve moving parts dynamics are solved together in a fully coupled manner.

2.4.2 Findings from the Current ETVE Configuration.

The overall ETVE model clearly shows that the driver gas dynamic force on the sleeve portholes dominates and is responsible, when coupled with the Belleville washer force, for the sleeve's oscillations during the open cycle. The other dynamical forces, such as the actuating pneumatics, the coil spring, and the coulomb damping forces during the open cycle have little effect on the ETVE sleeve motion, as is seen in the following discussion. Examination of the driver gas dynamic force on the sleeve shows that this force predominantly acts on the left side of the portholes or toward the direction of valve closure for the current configuration.

Figure 2-5 plots the predicted displacement of the sleeve with respect to time. The plot was generated by running the model using 8% Belleville washer viscous damping. Figures 2-6 plots the predicted displacement of the sleeve using 16% Belleville washer viscous damping.

The model predicts oscillation rates similar to those observed during the 1991 tests at the INEL. The 1991 tests suggest average oscillations of 153 cycles per second. The model predicts average oscillations of approximately 180 cycles per second for 8% viscous damping, and 125 cycles per second for 16% viscous damping. These results indicate that shifting the system's viscous damping can shift the system's frequency response.

It is important to keep in mind that (1) the model is an idealized situation with an infinite supply of gas at 1800 psi, contrasted to the actual test situation where the drive gas pressure decreases very quickly, and (2) the model uses driver gas at 700°F, contrasted to the actual test situations where the driver gas temperature was ambient for that time of the year at the INEL (approximately 30°F). Appendix E contains plots of other variables such as the sleeve velocity, sleeve acceleration, and gas pressure at the pressure plot point with respect to time.

Since the model shows that the driver gas forces dominate the open cycle, we began exploring different ETVE configurations to use the driver gas forces to our advantage, or to reduce their overall effect on the valve. Section 3. describes the different configurations explored.

8% Viscous + 100 lbf Bellville Damping

- Sleeve viscous damping set at 8%
- Belleville washers Coulomb damping set at 100 lbf
- Portholes are fully aligned at the 1.12 inch mark on the displacement axis
- Belleville washers are fully compressed at the 1.2 inch mark on the displacement axis: 1.12 inches to alignment of downstream edges of portholes, plus 0.05 inches portholes width mismatch (washers begin to be compressed at 1.17 inches), plus 0.03 inches maximum washer deflexion (form Appendix B data plots).

- Finer inlaid plot of force represents the net force on the moving parts (sleeve, piston, piston rod, and Belleville washers) acting in the axial direction. A positive value represents force in the upstream direction.

Figure 2-5. Eight percent Belleville washer viscous damping-model plot.

16% Viscous + 100 lbf Bellville Damping
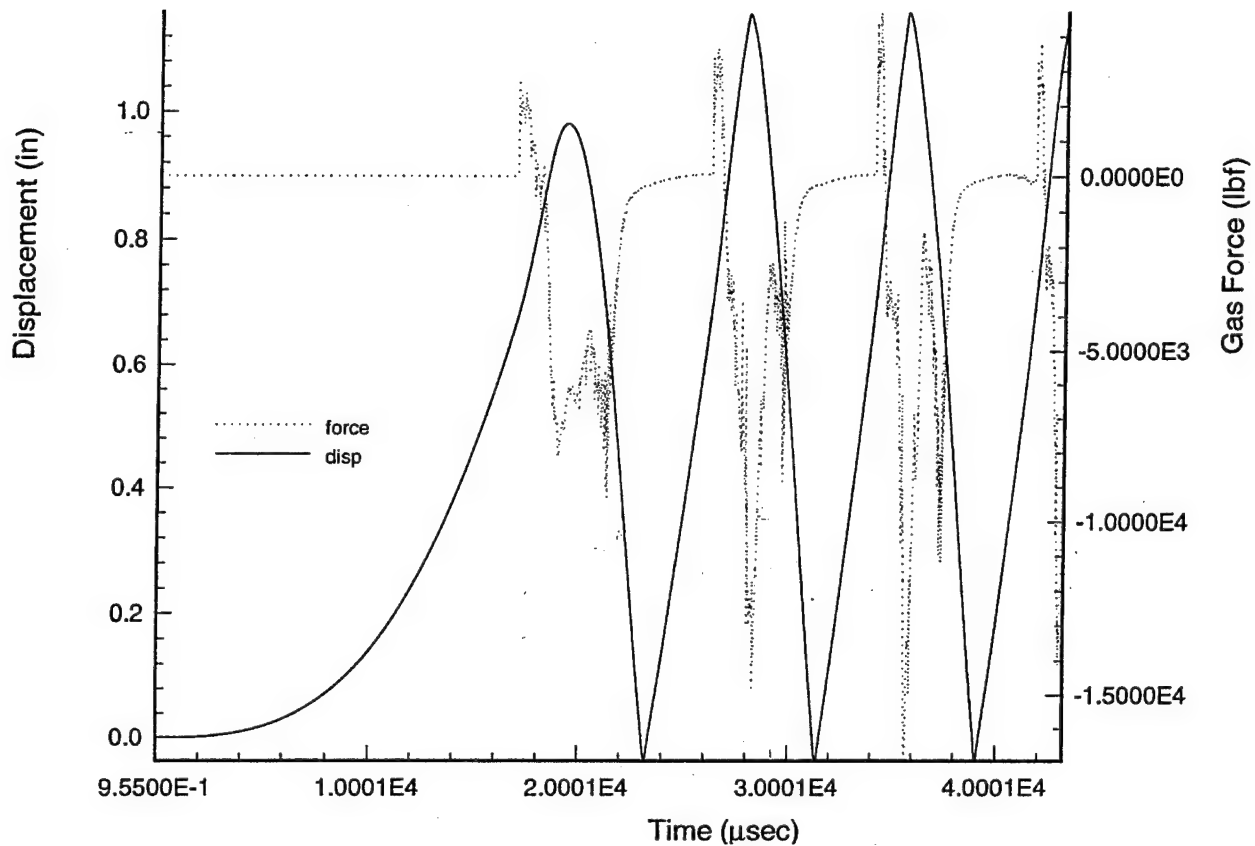
- Sleeve viscous damping set at 16%
- Belleville washers Coulomb damping set at 100 lbf
- Portholes are fully aligned at the 1.12 inch mark on the displacement axis
- Belleville washers are fully compressed at the 1.2 inch mark on the displacement axis: 1.12 inches to alignment of downstream edges of portholes, plus 0.05 inches portholes width mismatch (washers begin to be compressed at 1.17 inches), plus 0.03 inches maximum washer deflexion (form Appendix B data plots).

- Finer inlaid plot of force represents the net force on the moving parts (sleeve, piston, piston rod, and Belleville washers) acting in the axial direction. A positive value represents force in the upstream direction.

Figure 2-6. Sixteen percent Belleville washer viscous damping-model plot.

16

3. EVALUATION OF ALTERNATIVE CONFIGURATIONS

3.1 Model Runs

The main objective of reconfiguring the valve is to diminish or eliminate the valve chatter effects on the shock wave produced by the opening of the valve. We made many different configuration runs; however, only those configurations that show the most significant results are described here.

3.1.1 Beveled Portholes. The first configuration change attempted was to bevel the downstream edge of each porthole in the sleeve. This intuitive approach was to obtain the least obstruction possible to the gas thereby decreasing the net force by the gas on the sleeve. Figure 3-1 shows the configuration used in the attempt. The sleeve's response frequency changed somewhat, but the sleeve still oscillated violently during the open cycle (see Figure 3-2).

3.1.2 Backward Sleeve Configuration. Since beveling the portholes had no net effect on reducing the driver gas forces on the sleeve, we changed the ETVE configuration so that the initial sleeve position was shifted to the right (upstream), with the sleeve ports on the right side of the stationary ports. This configuration reverses the opening motion to the left (downstream), as illustrated in Figure 3-3. We term this configuration backward. The intuitive thinking in this case was that, perhaps, the gas dynamic forces on the sleeve would assist the open actuating force to thrust the valve into the open position.

Running the model with the sleeve backward forced us to lengthen the downstream end of the sleeve, for two reasons: (1) to maintain the required alignment of the seals and portholes, and (2) to block the gas flow through the body's most downstream portholes when the ETVE is to be in the close position.

The backward configuration model runs show that the gas dynamic forces thrust the valve into a strongly open position after 3 to 4 small bounces on the Belleville washers. Beyond this initial opening transient, we observe that the valve maintains the open position with a slightly growing, high-frequency oscillation imposed on a fairly significant steady Belleville washer compression (see Figure 3-4).

The growing, high-frequency oscillation is seen to correspond with the gas dynamic force on the sleeve. However, the net average gas dynamic force on the sleeve is shifting toward the open position. In the interest of time, we did not run the model any more time steps to determine if the sleeve's apparent growing oscillation could eventually grow to the point of blocking enough of the flow port to force the sleeve motion into another transient form. We recommend performing a longer run (at least the duration of the longest expected blast) to determine the oscillations trend and prove or disprove the possibility of another transient in the open cycle.
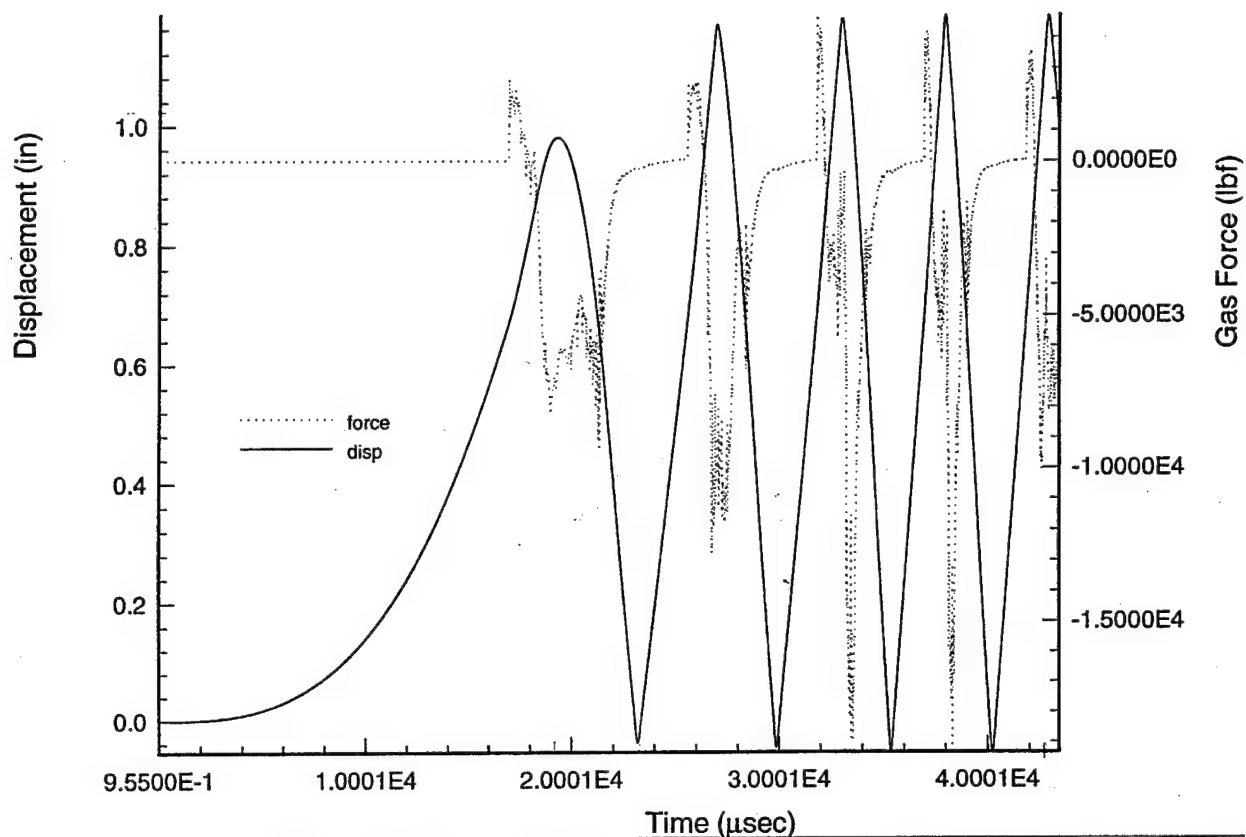
Figure 3-4 plots the predicted displacement of the sleeve with respect to time. The plot was generated by running the model with the sleeve in the backward configuration using 8% Belleville washer viscous damping. The finer inlaid plot of force in the plot represents the net force on the moving parts (sleeve, piston, and piston rod) acting in the axial direction. A positive value represents a force in the upstream direction.

3.2 Stress Analysis

Since the ETVE was not designed to run with the sleeve in the backward configuration, we performed a cursory stress analysis on the ETVE stop plate, and we calculated the maximum allowable width for the body portholes for the original design conditions (700°F and 1800 psi). Appendix F presents this portion of the work in greater detail.

17

Sleeve
end view

Sleeve

45°
REF 37°

4°
REF

Beveled edges

45°
24 PLCS
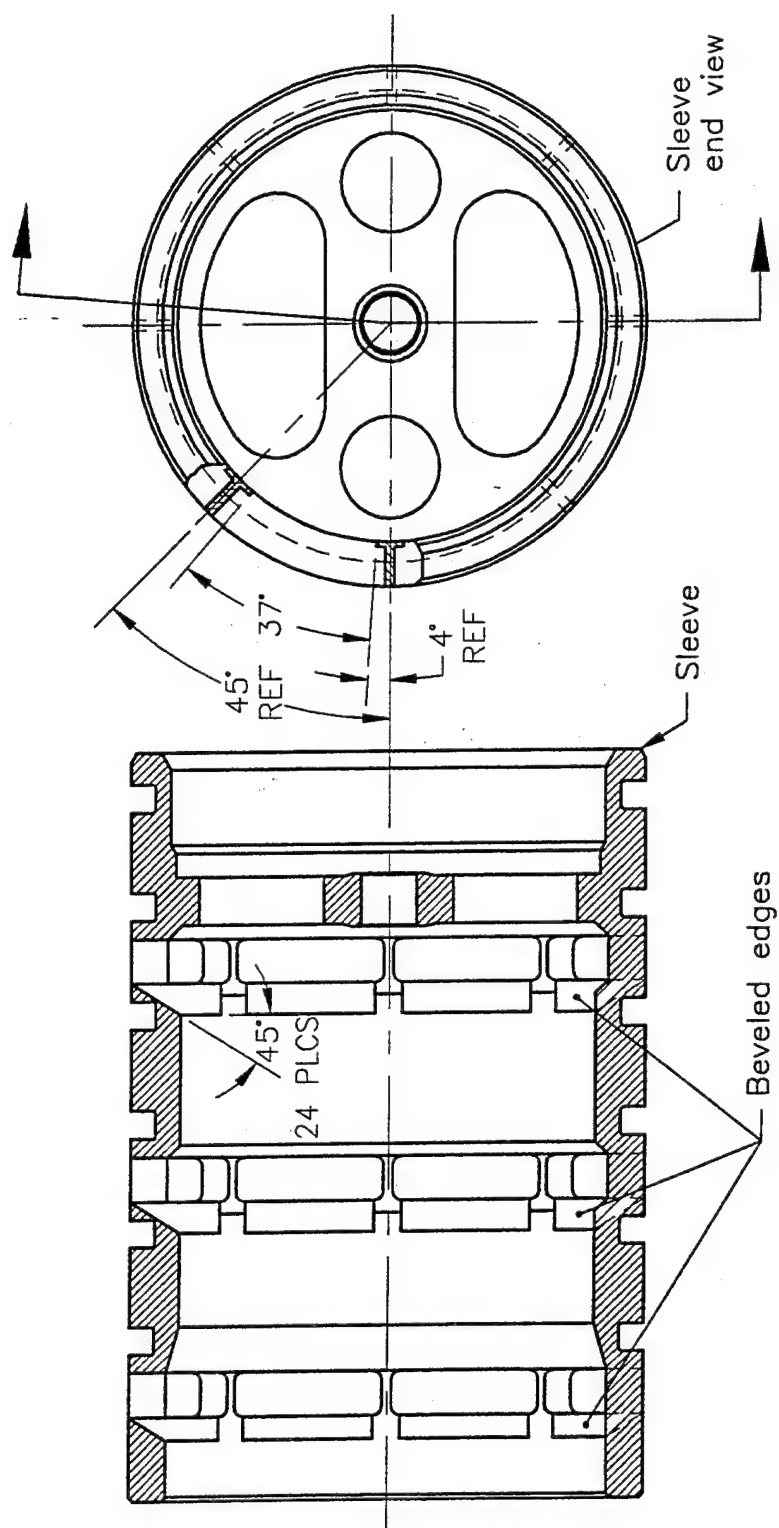
Side and end view schematics of the sleeve with beveled portholes. The portholes were beveled 45° only on the downstream side of the porthole.

Figure 3-1. Sleeve portholes beveled 45 degrees.

18

**8 % Viscous + 100 lbf Bellville Damping
Beveled (45°) Downstream Slider Ports**
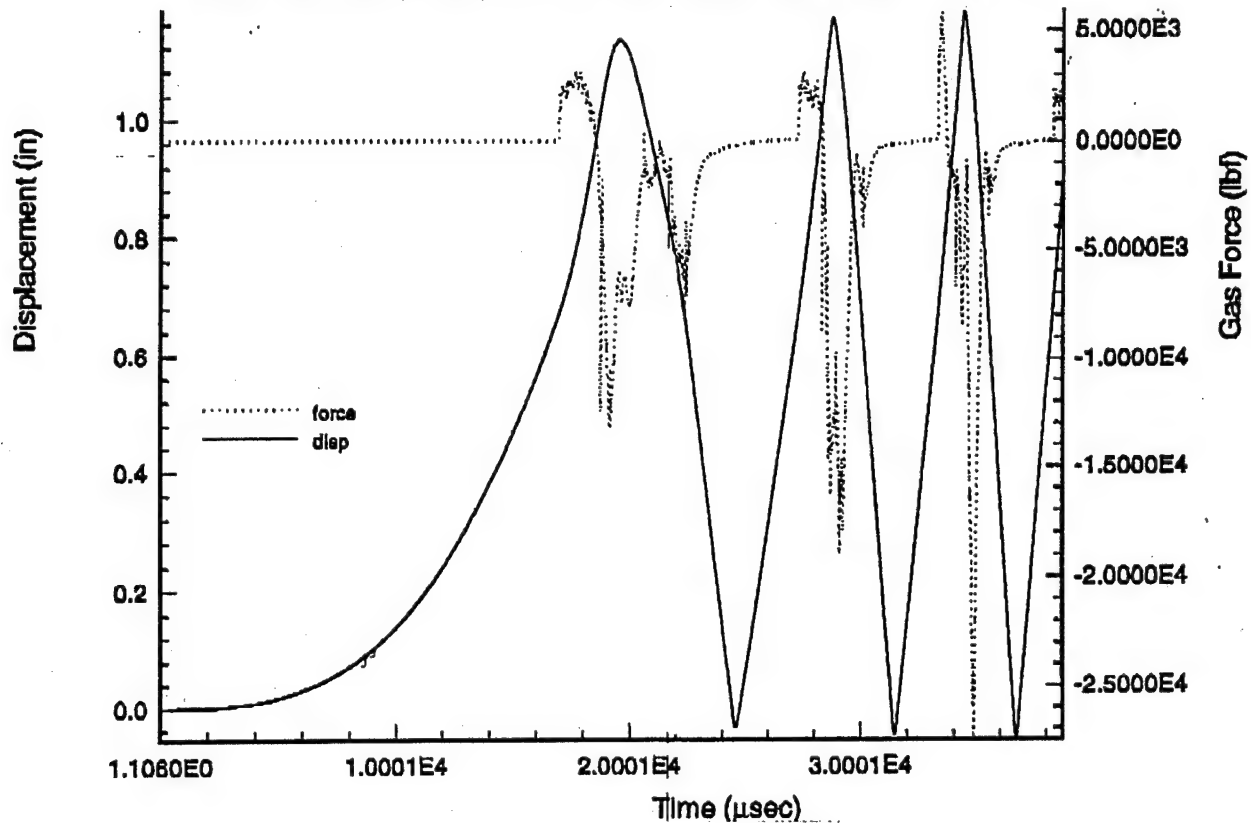
- Sleeve portholes are beveled at a 45-degree angle on the downstream edge of each porthole
- Sleeve viscous damping set at 8%
- Belleville washers Coulomb damping set at 100 lbf
- Portholes are fully aligned at the 1.12 inch mark on the displacement axis
- Belleville washers are fully compressed at the 1.2 inch mark on the displacement axis: 1.12 inches to alignment of downstream edges of portholes, plus 0.05 inches portholes width mismatch (washers begin to be compressed at 1.17 inches), plus 0.03 inches maximum washer deflexion (form Appendix B data plots).

- Finer inlaid plot of force represents the net force on the moving parts (sleeve, piston, piston rod, and Belleville washers) acting in the axial direction. A positive value represents force in the upstream direction.

Figure 3-2. Predicted displacement history for the sleeve with 45-degree beveled portholes.

19
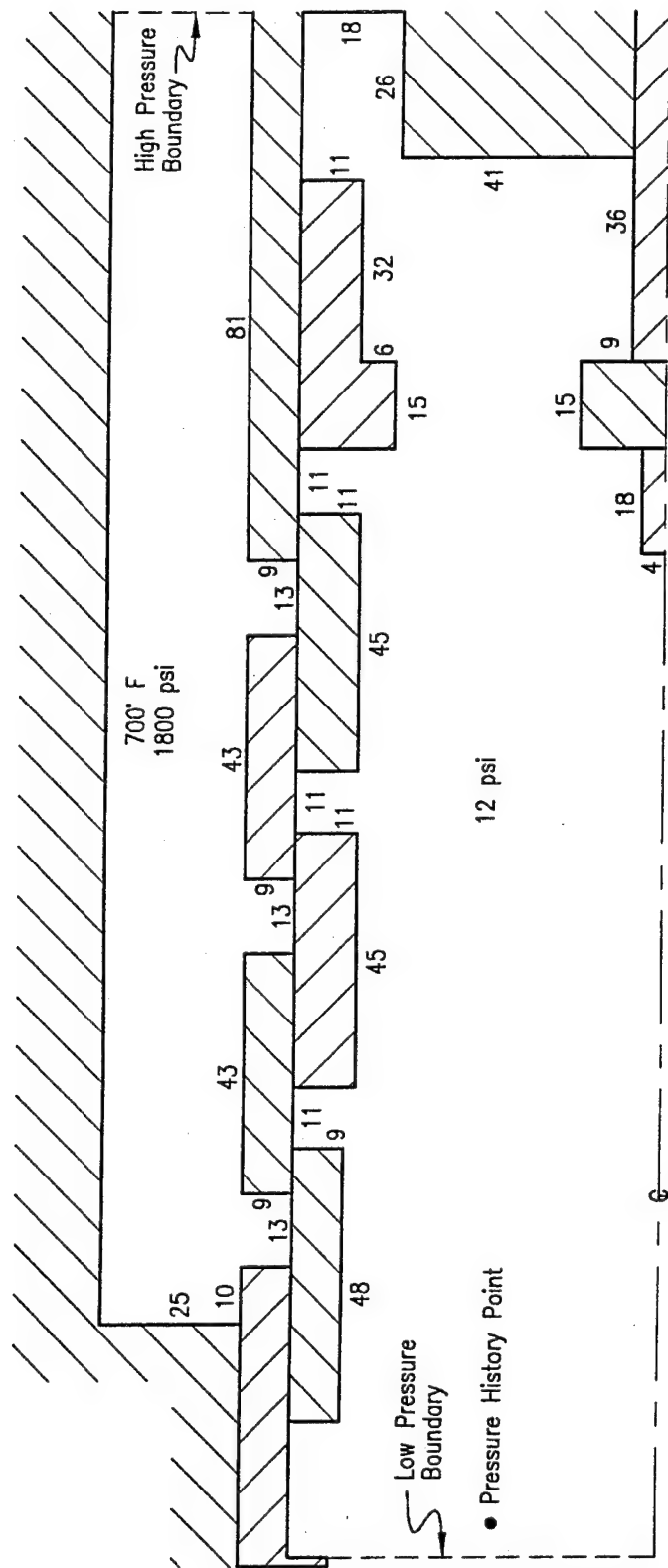
Figure 3-3. Gas dynamic model for sleeve in the backward configuration.

8% Viscous + 100 lbf Bellville Damping
Backward Opening / Lengthened Spool
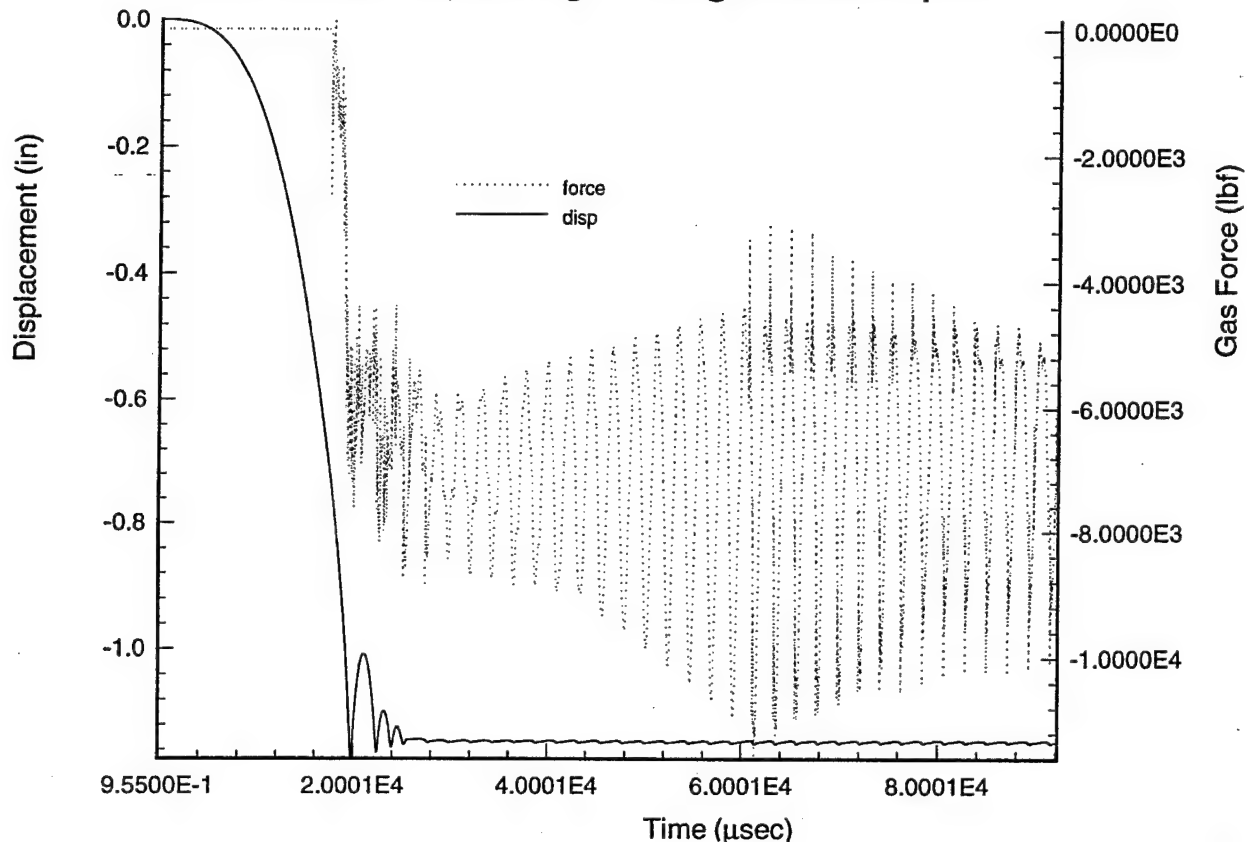
- Valve opens by sliding the sleeve in the upsteam direction—backward configuration
- Sleeve viscous damping set at 8%
- Belleville washers Coulomb damping set at 100 lbf
- Portholes are fully aligned at the 1.12 inch mark on the displacement axis
- Belleville washers are fully compressed at the 1.2 inch mark on the displacement axis: 1.12 inches to alignment of downstream edges of portholes, plus 0.05 inches portholes width mismatch (washers begin to be compressed at 1.17 inches), plus 0.03 inches maximum washer deflexion (form Appendix B data plots).

- Finer inlaid plot of force represents the net force on the moving parts (sleeve, piston, piston rod, and Belleville washers) acting in the axial direction. A positive value represents force in the upstream direction.

Figure 3-4. Model predictions for running sleeve in the backward configuration.

21

3.2.1 Wider Portholes in Body. As the sleeve portholes oscillate around the body portholes during the opening cycle, the effective flow area changes. This change in the flow area generates a segmented shock wave which is unacceptable for blast simulation.

Since the real requirement is to maintain a constant effective flow area, one possible configuration would be to increase the width of the body portholes to allow the sleeve to oscillate, yet maintain the effective flow area constant. We analyzed the valve to determine the largest width the portholes could be widened to and still maintain its integrity under operating conditions (700°F and 1800 psi).

The stress analysis determined that the portholes in the ETVE body could be widened to 0.76 in. centered on the existing portholes centerlines, as shown in Figure 3-5. This means that the sleeve's centerline can oscillate at an amplitude of 0.155 in. to either side of the body porthole centerline and still maintain a constant effective flow area.

3.2.2 Stress analysis on stop. When the ETVE is actuated open in the current configuration, the actuating piston slides to the back (upstream) end to impact on the end plate. However, in the proposed backward configuration, the actuating piston will move to the front (downstream) to impact on the stop, exposing it to much larger forces than it was originally designed for.

The analysis revealed that the stop would experience stresses over 400 ksi; the six bolts fastening the stop to the body would experience 224.9 ksi; and the ETVE body around the portholes would experience stresses in excess of 58 ksi. All these stresses exceed the maximum allowable stress of 32 ksi for these components (defined in the ASME Boiler and Pressure Vessel Code, Section VIII, Rules for Construction of Pressure Vessels).

The large dynamic (impulse) forces created by the deceleration of the piston and sleeve are aggravated by the stiffness of the Belleville washer stack; the stack is clearly very stiff and has a short distance to travel before bottoming out. However, the piston impulse forces can be greatly reduced if either of the following modifications are made:

- Arrange (or add to) the stack of Belleville washers so that the effective travel length (before bottoming out) is much longer. Note that this recommendation is based on the observations from the washer characterization tests; when the washers bottom-out, their stiffness increases tremendously, which in turn increases the piston/sleeve decelerations.

- Employ Belleville washers (or other springs) that have a lower stiffness value and a longer travel length. This will reduce the magnitude of the piston/sleeve deceleration.
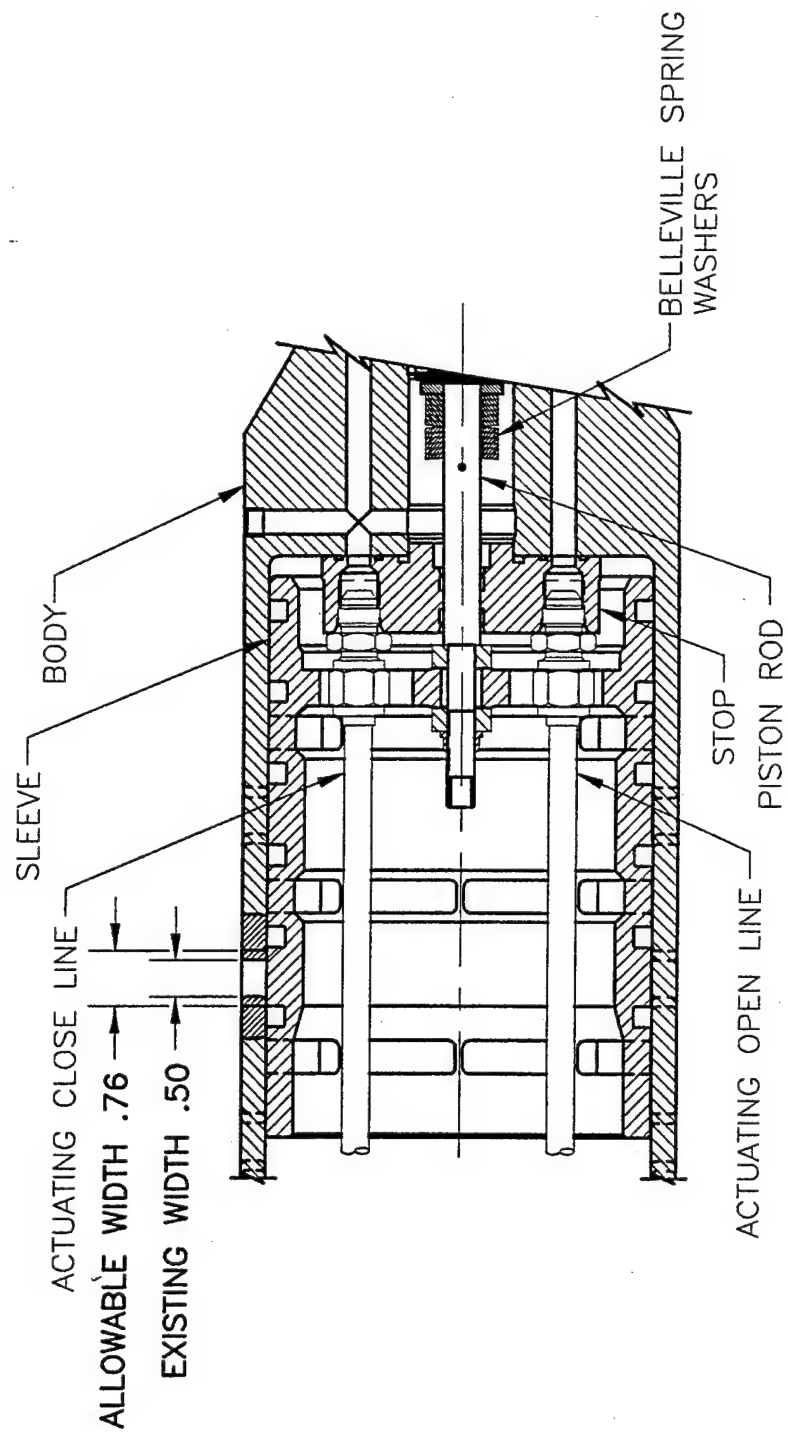
Figure 3-5. Widened portholes.

23

INTENTIONALLY LEFT BLANK.

4. SEALS STUDY

The 1991 ETVE tests at the INEL revealed another area of the ETVE's performance that needs further development: the main valve seals. Several kinds of seals were used during testing, but none were successful under the operating conditions (700°F and 2000 psi). We performed a cursory seal manufacturer and material study to determine the available seal materials and configurations capable of withstanding the operating conditions. Appendix G presents this work in detail.

The study concludes that no commercial seals are readily available that will withstand the operating conditions. We recommend testing different types of seals, including split-metal piston ring type seals and VESPEL seals. Appendix G presents a Draft Proposed Seal Test Program to evaluate existing seal technologies.

All vendor information gathered will be maintained in EG&G Idaho, Inc., Project File 93-713, and a copy will be transmitted to the U. S. Army Research Laboratory technical monitor, Mr. Richard J. Pearson.

INTENTIONALLY LEFT BLANK.

5. CONCLUSIONS AND RECOMMENDATIONS

The ETVE simulation model has proven to be an extremely valuable tool in assessing the qualitative nature of the current valve's operation and is indispensable in assessing the effects of valve modifications or redesigns. The ETVE's complex nonlinear behavior is impossible to predict in any way other than numerical simulation. Even if the numerical simulations are accepted on a qualitative basis only, they increase understanding of behavior, show trends and sensitivities, and suggest alternative designs. On the other hand, the alternative, iterative "cut and try" approach to design would be a long, tedious, and expensive route to valve design/redesign. In addition, the model can be used to input new Belleville washer characterization data for different washer configurations and then assess the qualitative effects of each configuration on the overall valve behavior.

For future design/analysis work and to predict accurate quantitative performance, we recommend that the numerical technique developed to simulate the gas dynamics be modified in four main areas:

1. Modify the model to give a partially implicit time integration instead of the explicit time integration (this would reduce the CPU time required to make runs and should increase the accuracy by reducing the large number of time steps required for the model runs)

2. Examine the importance of viscous effects, especially in the valve-open position where the high-speed flow through the ports could possibly place significant shear forces on the sleeve, and, therefore, influence its motion

3. Modify the model to study the ETVE close cycle under operating conditions

4. Design the valve's effective damping with either Belleville washers or another damping system for both the open and close cycles.

5.1 PROPOSED MODIFICATION

We propose the ETVE configuration change (Figure 5-1) as a preliminary concept only, and strongly caution that further design and analysis work must be performed prior to executing any actual modification to the existing ETVE. Furthermore, we recommend taking advantage of the already developed valve sleeve dynamic simulation model to characterize the performance of the ETVE under its proposed modified configuration or any other configuration that may be developed by further analysis and research.

The study described in Section 3.2.1 analyzing widened portholes in the body is left as a matter of consideration for the next redesign phase. Time precluded our running the model with widened portholes. Since we do not have model predictions for this configuration, we do not include widened portholes as part of the proposed modification concept.

The preliminary concept makes reference only to correcting the chatter in the open cycle; however, no analysis was performed on the close cycle. The proposed concept evolved from the results of the dynamic simulation model of the open cycle, the stress analysis performed on the stop plate and the valve body, and from the Belleville washers characterization studies.

The modification concept is best illustrated in Figure 5-1. Its main areas of redesign follow.

1. Increase the length of the sleeve by approximately 1.6 in. and add two sets of seals in the added length to seal the last row of body portholes. Reduce the length of the liner by 0.7 in.

2. Place the sleeve upstream (from its current as-built location) as indicated in Figure 5-1 so the pneumatics can slide the sleeve forward to its open position.

27
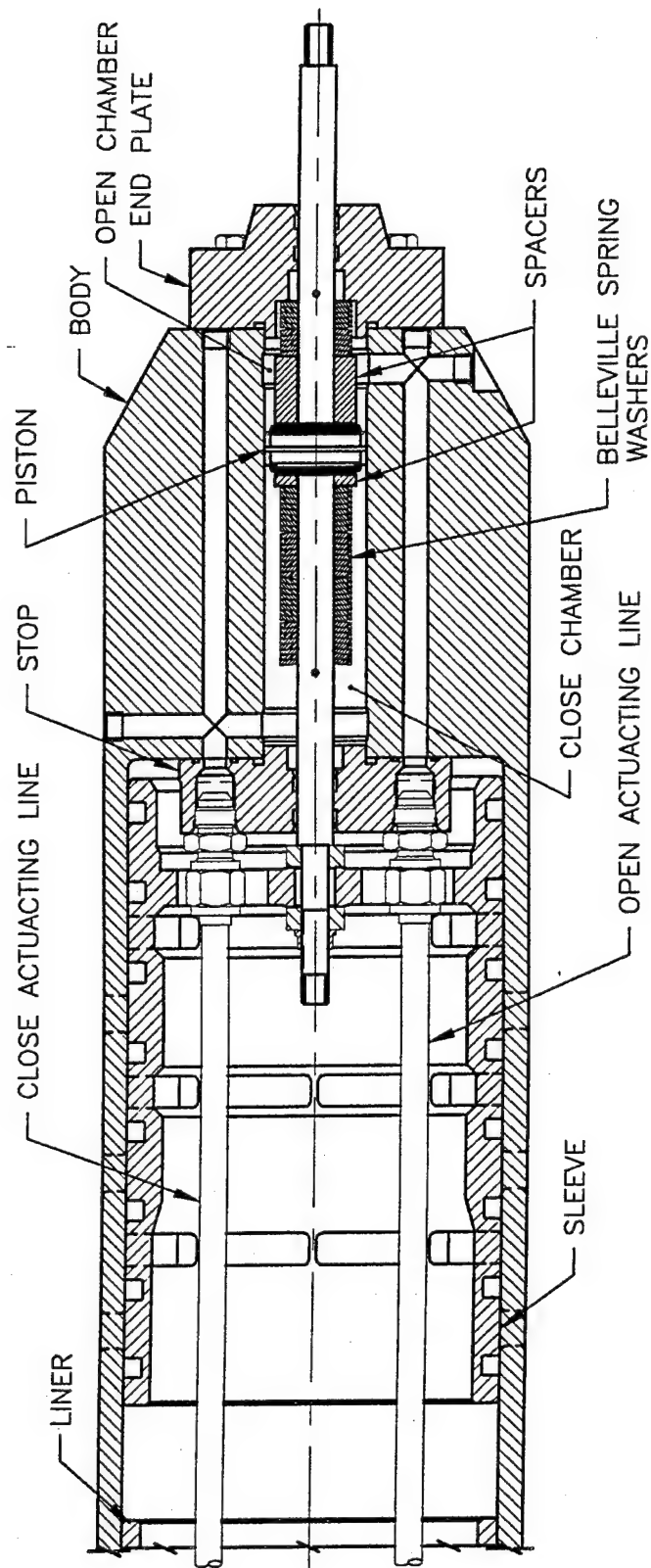
Figure 5-1. Proposed preliminary concept for ETVE configuration.

3. Increase the length of the ETVE body to house approximately 32 Belleville washers on the open chamber and 8 washers in the close chamber. This modification requires retapping the pneumatic actuation lines.

4. Lengthen the piston rod to accommodate the added number of washers.

5. Increase the stop plate size and increase the number and size of bolts used to fasten the stop plate to the valve body.

A full set of nonreleased drawings for this proposed configuration is included in the engineering design file at EG&G Idaho, and a copy is being sent to U. S. Army research Laboratory technical monitor, Mr. Richard J. Pearson.

5.2 CONCLUSIONS

1. The ETVE sleeve dynamic simulation model confirms that the ETVE does undergo chattering during the opening cycle. In fact, we observe, from Figure 2 no indication that the total amplitude of the sleeve oscillations decreases within the first 40 msec. We also observed, during the 1991[1] testing at the INEL, that the duration of the sleeve oscilla-tion increased as the driver gas pressure increased. From these two observations, we deduce that the sleeve will continue to oscil-late for as long as there is a relatively high pressure driver gas flow through its port-holes. The model reveals that the main dri-ving force causing the chatter is generated by the driver gas as it flows through the sleeve portholes. The model also reveals that the ETVE does not have sufficient damping to absorb energy from the moving sleeve.

2. The ETVE should not be used under its current configuration in high-pressure or high-temperature gas conditions. Furthermore, the current ETVE configuration requires significant redesign, analysis, and refabrication to meet its original design requirements .

3. The close-cycle actuation needs to be evaluated and redesigned to overcome the driver gas forces that will make the valve difficult to close.

4. Any general design concepts should be evaluated by using the already developed valve sleeve dynamic simulation model to qualitatively predict and evaluate the design concept's effects on the ETVE performance.

29

INTENTIONALLY LEFT BLANK.

6. REFERENCES

1. M. R. Stacey, *Large Blast/Thermal Simulator Insulation/Valve Testing*, EGG-ME-9358, November 1990.

2. M. R. Stacey, *Performance Tests of a Fast-acting Valve for the Driver Tubes of a Large Blast/Thermal Simulator*, Report BRL-CR-687, Ballistics Research Laboratory, Maryland, May 1992.

31

INTENTIONALLY LEFT BLANK.

APPENDIX A

EATON THROAT-VALVE ELEMENT PROTOTYPE
1993 TESTING

Paul Schwieder

INTENTIONALLY LEFT BLANK.

Appendix A

Eaton Throat-Valve Element Prototype 1993 Testing

I performed two sets of tests in November 1993 at the Idaho National Engineering Laboratory (INEL) to characterize the behavier of the Eaton Throat-Valve Element (ETVE) under existing configuration. The first test characterized the ETVE sleeve's displacement behavior with a linear variable displacement transducer (LVDT). The LVDT data then contributed to J. G. Arendts' analytical development of a computer model of the mechanical dynamics of the ETVE prototype moving parts (see Apendix D). The second test determined whether different sequencing of the open and close actuating sloenoid valves could reduce the valve chatter observed in the initial testing of the ETVE prototype at the INEL.

This report describes and documents the two sets of tests. The system setup was slightly different for each test, so a block diagram of each configuration is presented in the following discussiond for each.

C2. CHARACTERIZATION OF THE ETVE

The initial ETVE tests performed at the INEL indicate that the ETVE was possibly chattering during the opening cycle berfore achieving steady-state open position. However, the instrumentation available at the time could not give a detailed displacemnt history of the ETVE's sliding sleeve. Therefore, in order to subsequently characterize the suspected chatter, a linear variable displacement transducer (LVOT) was purchased and installed (STARRET Model 254, Serial Number 702168), and the ETVE characterization test was performed to obtain a high sampling of the ETVE's sliding sleeve during the open cycle. The testing was performed at the INEL's North Holmes Laboratory in Idaho Falls, Idaho. Since the pressure tube that normally is pressurized during the Large Blast/Thermal Simulation tests was not available for use at the INEL facility, the tests were performed only at ambient temperature and pressure.

Figure A-1 shows the hardware configuration. The data system consisted of a Kaye MDAS 7000 data system with a 20-Mbyte hard drive and a 1.2-Mbyte floppy disk. Data were collected to memory then stored in ascii format to hard disk and floppy. The LVDT and pressure transducers where both calibrated (see Attachment 1), and the data were converted to the corresponding values in engineering units before being saved to disk. Two separate tests were performed under this configuration.

2.1.2 CHARACTERIZATION TEST 1.

Under this test condition, 1200 psi were used to open the ETVE. The data acquisition system was then used to measure the sleeve displacement, open pressure used and fire signal from the Eaton control box. When the fire button was pressed on the Eaton control box, a signal was sent to the data acquisition system to start collecting data at 10,000 samples per second for 1.5 seconds. Attachment 2 contains the results of this test.

2.1.2 CHARACTERIZATION TEST 2.

Under this test condition 2000 PSI was used to open the ETVE. The data acquisition system was then used to measure the sleeve displacement, open pressure and fire signal from the Eaton control box. When the fire button was pressed on the Eaton control box, a signal was sent to the data acquisition to start collecting data at 10,000 samples per second for 1.5 seconds. Attachment 3 contains the results of this test.

2.2 Damping Testing

The characterization test confirmed that the ETVE chattered during the open cycle. This test set was performed to determine whether pressuring the close side of the valve would dampen the chatter. During the testing, both the close and openactuating pressures and the sleeve displacemtn were measured. The data system was triggered from the

LVDT movement (see Figure A-2). The system was modified so that the Eaton control box controlled only the ETVE opening. The close solenoid was controlled by the Kaye data system through a solenoid state relay. A 28 volt dc power supply was connectted across this relay to actuate the close solenoid. With this control system, it was possible to apply a pressure to the close side of the valve and then release that pressure an arbitrary time from when the valve moved. Two tests were run with this configuration.

2.2.1 Damping Test 1. Test 1 was set so that the close pressure would be relieved in the middle of the valve opening stroke. See appendix D for these test results.

2.2.2. Damping Test 2. Test 2 was set so that the close pressure was left on for 0.5 seconds after the valve was actuated open. This configuration allowed the valve fully open and stabilize before the close pressure was released. See Attachment 5 for the plotted test results. Both test used a open pressure of 2000 psi and a close pressure of 1000 psi. The data was collected at 10,000 samples per second for 1 sec for both of these tests. Figure A-3 shows the ETVE's sleeve displacement overlayed for both damping tests.
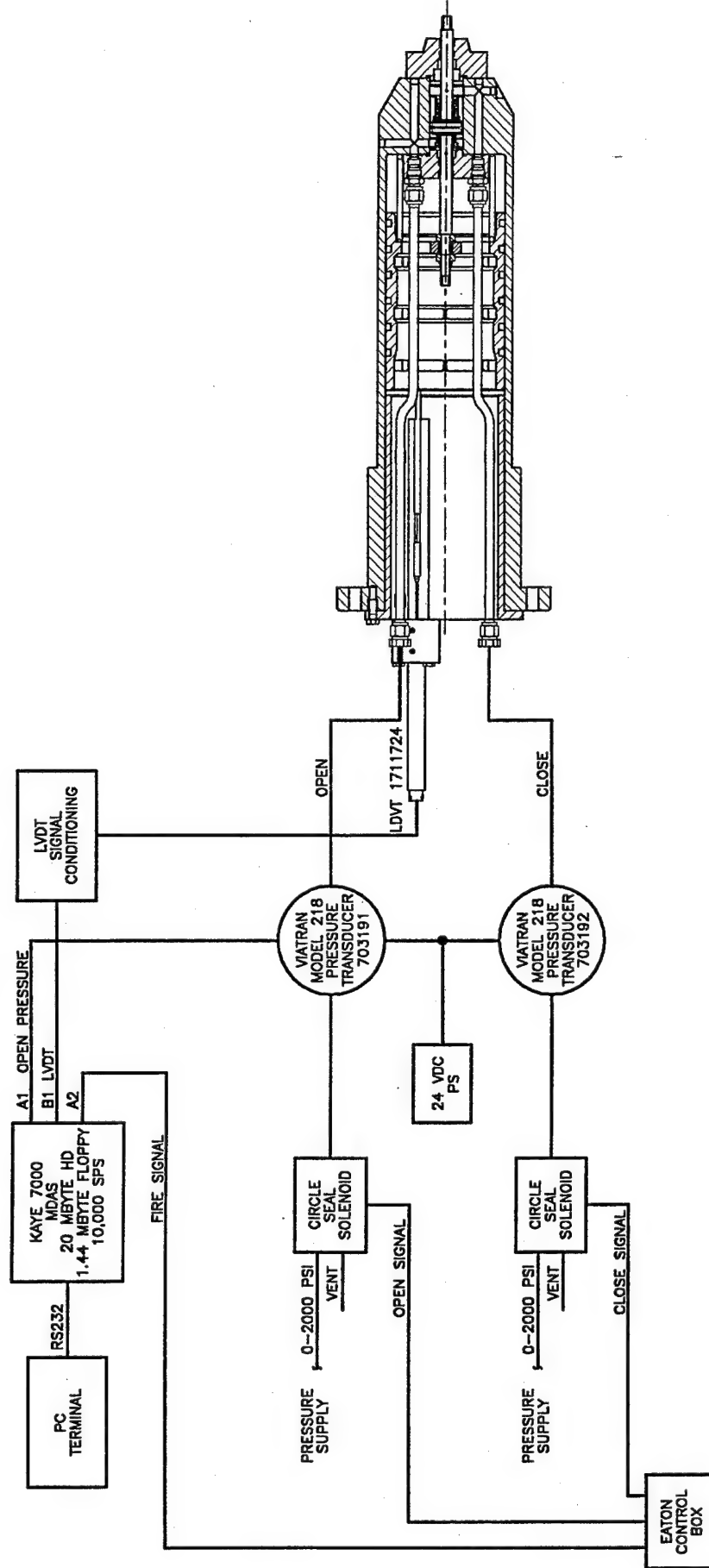
Figure A-1. Characterization test setup.
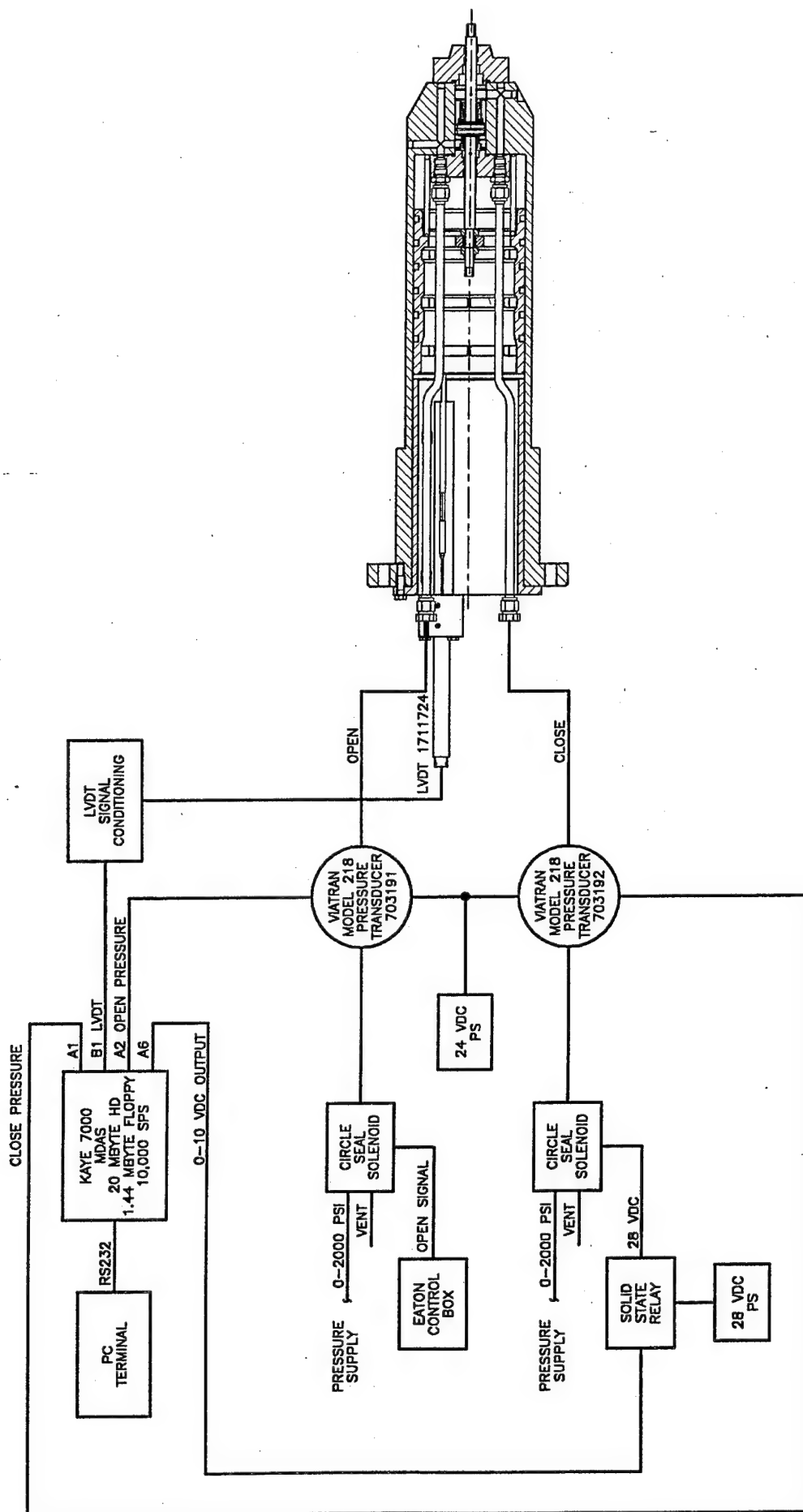
Figure A-2. Damping test setup.

Dataset Name:	Unspecified	Sample Rate:	1e+004
Version Number:	0	Maximum:	1.69507
Series Name:	Unspecified	Minimum:	1.6715
Date Acquired:	12-09-1993	Comments: Close pressure left	
Time Acquired:	14:53:52.32	on for .5 seconds open pressure	
Vert Units:	INCHES	set 2000 psi close pressure at	
Horiz Units:	Sec	1000 psi	
Num Samples:	250		

W9: CLS_PRES_TRIG_LVDT vs CLS_PRES_ON_LVDT

Figure A-3. ETVE's sleeve displacement overlayed for both damping tests.

CALIBRATION DATA
FOR THE
LINEAR VARIABLE DISPLACEMENT TRANSDUCER AND
PRESSURE TRANSDUCERS

EG&G Idaho, Inc.
STANDARDS & CALIBRATION LABORATORY
CALIBRATION DATA SHEET

DATE: 08/24/1993

MANUFACTURER:	NOMENCLATURE:	MODEL #:	PROPERTY #:
VIATRAN	PRESSURE TRANSDUCER	218	703192

SERIAL #:	PROCEDURE #:	NOMINAL INTERVAL:	NEXT DUE DATE:
295578	3043	15 MONTHS	11/24/1994

PRESSURE HIGH SIDE	NOMINAL mV	ACTUAL mV INCREASING	ACTUAL mV DECREASING	mV HYSTERISIS	LINEARITY LOWER LIMIT	UPPER LIMIT
0.00000	-3.9000	-3.9000	-3.2000	-0.7000	-15.9064	8.1064
300.00000	296.2600	295.8000	296.8000	-1.0000	284.2536	308.2664
600.00000	596.4200	595.8000	596.9000	-1.1000	584.4136	608.4264
900.00000	896.5800	896.0000	896.9000	-0.9000	884.5736	908.5864
1200.00000	1196.7400	1196.2000	1197.5000	-1.3000	1184.7336	1208.7464
1500.00000	1496.9000	1496.3000	1497.1000	-0.8000	1484.8936	1508.9064
1800.00000	1797.0600	1796.6000	1797.3000	-0.7000	1785.0536	1809.0664
2100.00000	2097.2200	2096.8000	2097.4000	-0.6000	2085.2136	2109.2264
2400.00000	2397.3800	2397.2000	2397.6000	-0.4000	2385.3736	2409.3864
2700.00000	2697.5400	2697.5000	2697.7000	-0.2000	2685.5336	2709.5464
3000.00000	2997.7000	2997.7000	2997.7000	0.0000	2985.6936	3009.7064

THE HYSTERESIS, IN mV, MUST BE LESS THAN   12.0064

PRESSURE IN UNITS OF PSI
FULL SCALE PRESSURE: 3000.0000 PSI
LINEARITY ACCURACY: 0.4000 %
HYSTERESIS ACCURACY: 0.4000 %
EXCITATION VOLTS: 14.0000 VOLTS
TECHNICIAN: K.ANDERSON 10
CALIBRATED FOR: B.COLSON

REMARKS: A-9
INPUT 1+ 2-/OUTPUT 3+ 4-

EG&G Idaho, Inc.
STANDARDS & CALIBRATION LABORATORY
CALIBRATION DATA SHEET

DATE: 08/24/1993

MANUFACTURER:	NOMENCLATURE:	MODEL #:	PROPERTY #:
VIATRAN	PRESSURE TRANSDUCER	218	703191

SERIAL #:	PROCEDURE #:	NOMINAL INTERVAL:	NEXT DUE DATE:
295478	3043	15 MONTHS	11/24/1994

PRESSURE HIGH SIDE	NOMINAL mV	ACTUAL mV INCREASING	ACTUAL mV DECREASING	mV HYSTERISIS	LINEARITY LOWER LIMIT	UPPER LIMIT
0.00000	2.3000	2.3000	3.4000	-1.1000	-9.6880	14.2880
300.00000	302.0000	302.1000	303.4000	-1.3000	290.0120	313.9880
600.00000	601.7000	602.0000	603.3000	-1.3000	589.7120	613.6880
900.00000	901.4000	901.9000	903.2000	-1.3000	889.4120	913.3880
1200.00000	1201.1000	1201.8000	1203.0000	-1.2000	1189.1120	1213.0880
1500.00000	1500.8000	1501.5000	1502.8000	-1.3000	1488.8120	1512.7880
1800.00000	1800.5000	1801.1000	1802.3000	-1.2000	1788.5120	1812.4880
2100.00000	2100.2000	2100.6000	2101.6000	-1.0000	2088.2120	2112.1880
2400.00000	2399.9000	2400.2000	2401.0000	-0.8000	2387.9120	2411.8880
2700.00000	2699.6000	2699.7000	2700.0000	-0.3000	2687.6120	2711.5880
3000.00000	2999.3000	2999.3000	2999.3000	0.0000	2987.3120	3011.2880

THE HYSTERESIS, IN mV, MUST BE LESS THAN   11.9880

PRESSURE IN UNITS OF PSI
FULL SCALE PRESSURE: 3000.0000 PSI
LINEARITY ACCURACY: 0.4000 %
HYSTERESIS ACCURACY: 0.4000 %
EXCITATION VOLTS: 24.0000 VOLTS
TECHNICIAN: K.ANDERSON
CALIBRATED FOR: B.COLSON

REMARKS:
INPUT 1+ 2-/OUTPUT 3+ 4-

vitran 703191

0	0.0023
300	0.3021
600	0.602
900	0.9019
1200	1.2018
1500	1.5015
1800	1.8011
2100	2.1006
2400	2.4002
2700	2.6997
3000	2.9993
3000	2.9993
2700	2.7
2400	2.401
2100	2.1016
1800	1.8023
1500	1.5028
1200	1.203
900	0.9032
600	0.6033
300	0.3034
0	0.0034

```
          Regression Output:
Constant                      -3.40787
Std Err of Y Est              0.685176
R Squared                            1
No. of Observations                 22
Degrees of Freedom                  20

X Coefficient(s)   1001.186
Std Err of Coef.   0.154164
```

vitran 703192

0	-0.0039
300	0.2958
600	0.5958
900	0.896
1200	1.1962
1500	1.4963
1800	1.7966
2100	2.0968
2400	2.3972
2700	2.6975
3000	2.9977
3000	2.9977
2700	2.6977
2400	2.3976
2100	2.0974
1800	1.7973
1500	1.4971
1200	1.1975
900	0.8969
600	0.5969
300	0.2698
0	-0.0032

```
          Regression Output:
Constant                      7.544301
Std Err of Y Est              5.557849
R Squared                     0.999969
No. of Observations                 22
Degrees of Freedom                  20

X Coefficient(s)   997.8521
Std Err of Coef.    1.24637
```

EG&G Idaho

STANDARDS & CALIBRATION LABORATORY
CALIBRATION DATA SHEET

Page 1 of 2

FORM EG&G-1510B
(Rev. 04-80)

DATE **8-24-93**

MANUFACTURER LUCAS/ SCHAEVITZ	NOMENCLATURE LVDT		MODEL NO. 1000 HCA-2181	SERIAL NO. 4072
PROPERTY NO. 711724	PROCEDURE NO. 3550	INTERVAL 12 MO.	CALIBRATED FOR:	

CALIBRATION EQUIPMENT USED
STANDARDS CERTIFIED TRACEABLE TO THE NATIONAL BUREAU OF STANDARDS
(Records on file in the EG&G Standards & Calibration Laboratory. CF-698)

MANUFACTURER	MODEL NO.	SERIAL NO.	RECALL DATE	MANUFACTURER	MODEL NO.	SERIAL NO.	RECALL DATE
STARRETT	254	702168	9-25-93				
FLUKE	8050A	701652	10-11-93				

CALIBRATION DATA

PROCEDURE STEP NO.	FUNCTION TESTED	NOMINAL	IN TOLERANCE (CK)	OUT OF TOLERANCE (READING)	ADJUSTMENT (CK)	TOLERANCES	
						LOWER LIMIT	UPPER LIMIT

The LVDT was lightly clamped in a V-Block resting on two angle plates.

The core was attached to a holding rod secured to a Height Gage support arm. It was moved up or down in the LVDT with the height adjustment of the Height Gage.

Three separate runs were made over the full range of the LVDT. The output voltage was measured at 0.1" intervals over ± 1.0" of core travel. Output data is listed on page 2.

The output was from an ATA-101 Analog Transducer Amplifier, S/N-2824 and Property No. 711725, to which the LVDT was connected.

(Diagram labels: Support Arm, Holding Rod, Core, LVDT, Vee Block, Angle Plate, Angle Plate)

TYPE OF DATA:

☐ TEST REFERRAL

P.O. # _____

☐ CALIBRATION

☐ CERTIFICATION

☐ EVALUATION

☐ CROSS CHECK

☐ SPECIAL MEASUREMENT

REMARKS: The ATA-101 Amplifier was calibrated for ± 10 Volt DC output as outlined in the Manufacturer's instruction manual. Unit meets the linearity specification of 0.24 %.

TECHNICIAN W. R. Rodeback	HRS. 9.0	DATE NEXT CALIBRATION DUE 8-24-94

CALIBRATION DATA

PROCEDURE STEP NO.	FUNCTION TESTED	NOMINAL	IN TOLERANCE (CK)	OUT OF TOLERANCE (READING)	ADJUSTMENT (CK)	TOLERANCES	
						LOWER LIMIT	UPPER LIMIT
	MEASUREMENT POSITION in Inches		LVDT ✱ OUTPUT Volts DC				
	−1.000		−9.975				
	−0.900		−8.961	✱ These are an average			
	−0.800		−7.956	of the values from			
	−0.700		−6.947	three separate runs.			
	−0.600		−5.941				
	−0.500		−4.940				
	−0.400		−3.945				
	−0.300		−2.952	NOTE: All measurements were			
	−0.200		−1.972	made with reference			
	−0.100		−0.986	to the null point −			
	0 (null)		0	where output voltage			
	+0.100		+0.993	reads zero.			
	+0.200		+1.973				
	+0.300		+2.953				
	+0.400		+3.944				
	+0.500		+4.943				
	+0.600		+5.947				
	+0.700		+6.955				
	+0.800		+7.970				
	+0.900		+8.984				
	+1.000		+10.000				

0   10

0.1	8.984
0.2	7.97
0.3	6.955
0.4	5.947
0.5	4.943
0.6	3.944
0.7	2.953
0.8	1.973
0.9	0.993
1	0
1.1	-0.986
1.2	-1.972
1.3	-2.952
1.4	-3.945
1.5	-4.94
1.6	-5.941
1.7	-6.947
1.8	-7.956
1.9	-8.961
2	-9.9752

```
              Regression Output:
Constant                         1.000416
Std Err of Y Est                 0.002634
R Squared                        0.999983
No. of Observations                    21
Degrees of Freedom                     19

X Coefficient(s)   -0.10054
Std Err of Coef.   0.000095
```
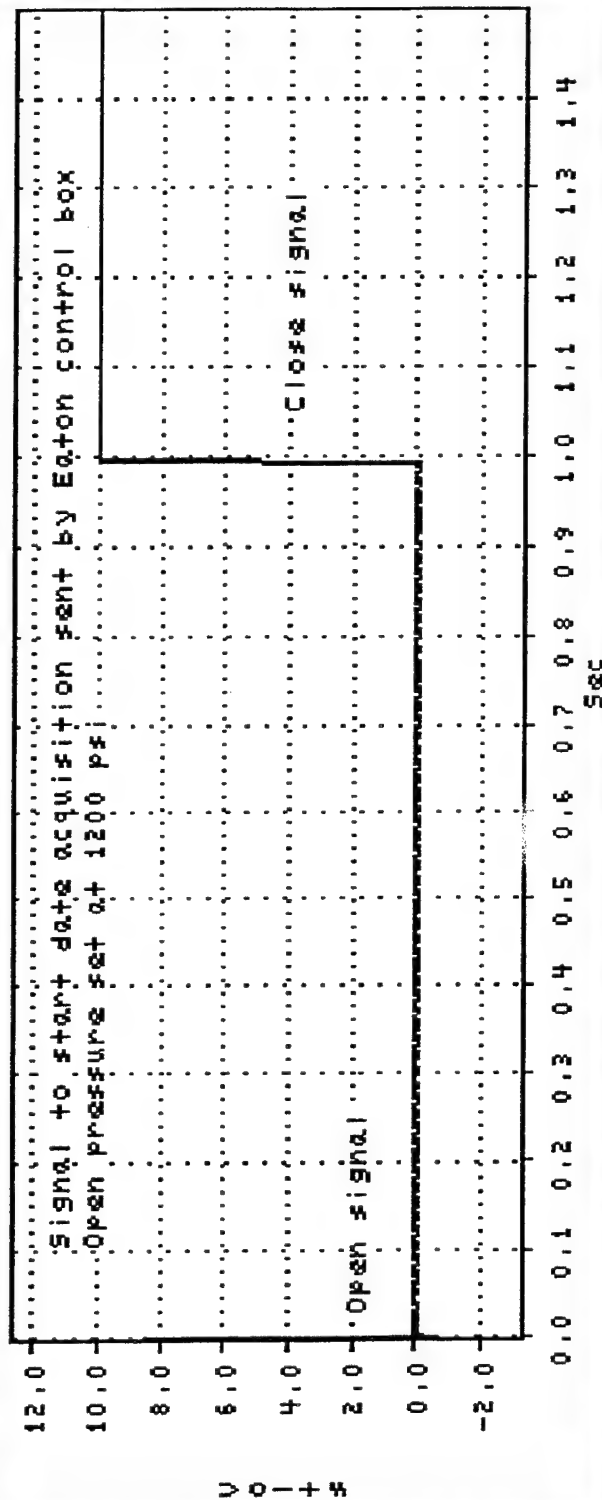
ETVE CHARACTERIZATION TEST DATA PLOTS

TEST 1

Open actuating pressure: 1200 psi
Data sampling rate: 10,000 samples per second
Data sampling time: 1.5 seconds

Dataset Name:	FIRE1200
Version Number:	1
Series Name:	1200PSI
Date Acquired:	9-24-1993
Time Acquired:	9:36:28.67
Vert Units:	Volts
Horiz Units:	Sec
Num Samples:	15000

Sample Rate:	1e+004
Maximum:	9.99512
Minimum:	-0.551758
Comments:	Signal to start data system sent from Eaton control box

W1: FIRE1200,1,1200PSI

Signal to start data acquisition sent by Eaton control box
Open pressure set at 1200 psi

Open signal

Close signal

Sec

Dataset Name:	LVDT2000
Version Number:	1
Series Name:	1200PSI
Date Acquired:	9-24-1993
Time Acquired:	9:36:28.67
Vert Units:	INCHES
Horiz Units:	Sec
Num Samples:	15000

Sample Rate:	1e+004
Maximum:	1.72108
Minimum:	0.572827
Comments:	Valve position signal from LVDT

Valve position measured by LVDT
Open pressure set at 1200 psi

W2: LVDT1200,1,1200PSI

Dataset Name:	OPEN1200
Version Number:	1
Series Name:	1200PSI
Date Acquired:	9-24-1993
Time Acquired:	9:36:28.67
Vert Units:	PSI
Horiz Units:	Sec
Num Samples:	15000

Sample Rate:	1e+004
Maximum:	1252.12
Minimum:	-1956.02
Comments:	Pressure measurement on the open side of valve

W3: OPEN1200,1,1200PSI
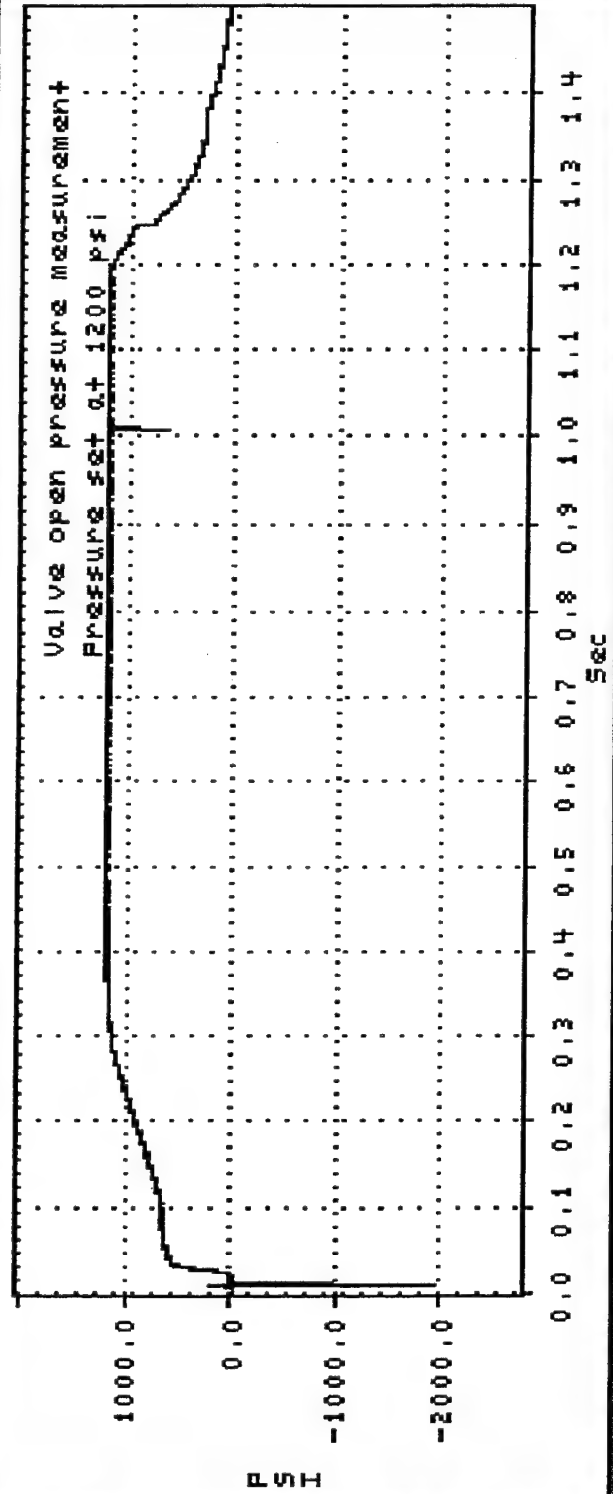
Valve open pressure measurement+

Pressure set at 1200 psi

Dataset Name:	Unspecified
Version Number:	0
Series Name:	Unspecified
Date Acquired:	12-09-1993
Time Acquired:	14:11:21.86
Vert Units:	INCHES
Horiz Units:	Sec
Num Samples:	1000

Sample Rate:	1e+004
Maximum:	1.72108
Minimum:	0.576754
Comments:	

W4: Extrac+CW2,500,1000>
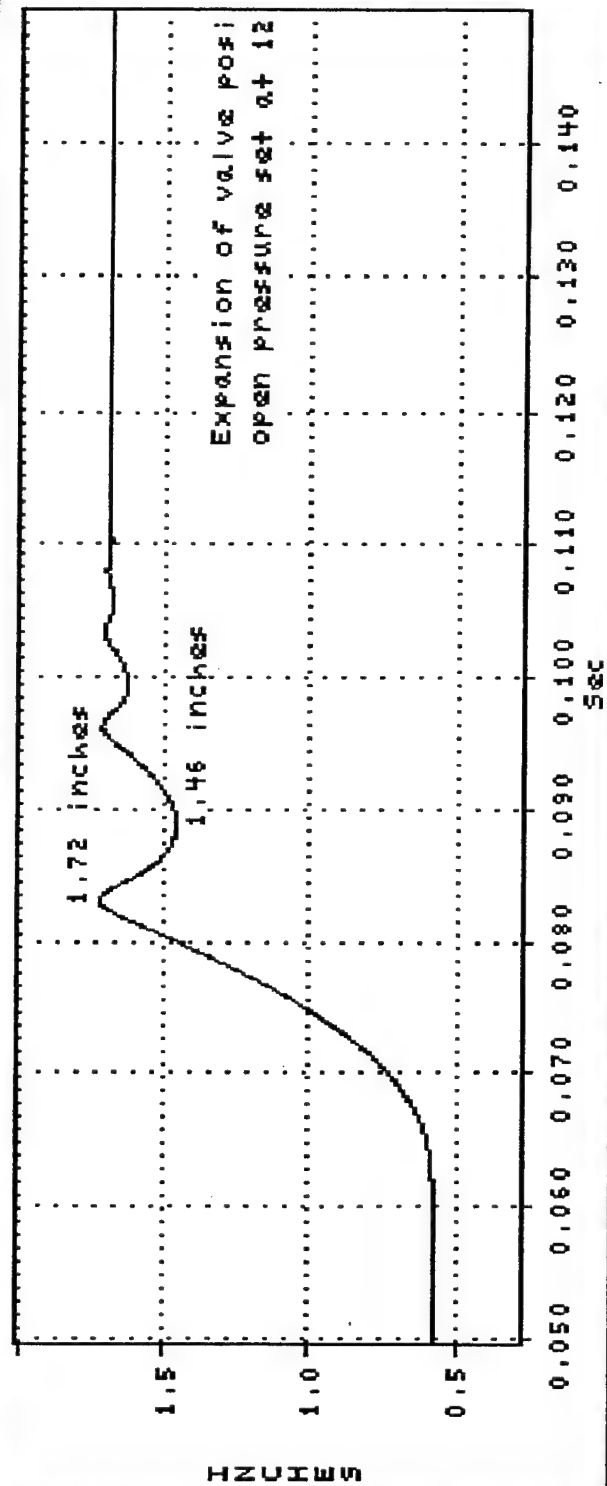
Expansion of valve posi
open pressure set at 12

1.72 inches

1.46 inches

INCHES

Sec

Dataset Name:	Unspecified
Version Number:	0
Series Name:	Unspecified
Date Acquired:	12-09-1993
Time Acquired:	14:40:40.63
Vert Units:	INCHES
Horiz Units:	Sec
Num Samples:	1000

Sample Rate:	1e+004
Maximum:	1.69114
Minimum:	0.572827
Comments:	Valve position signal
	from LVDT

WS: Extract+CW2.13000,1000)

LVDT measurement at valve closure
Open pressure set at 1200 psi

INCHES

Sec

1.300 1.310 1.320 1.330 1.340 1.350 1.360 1.370 1.380 1.390
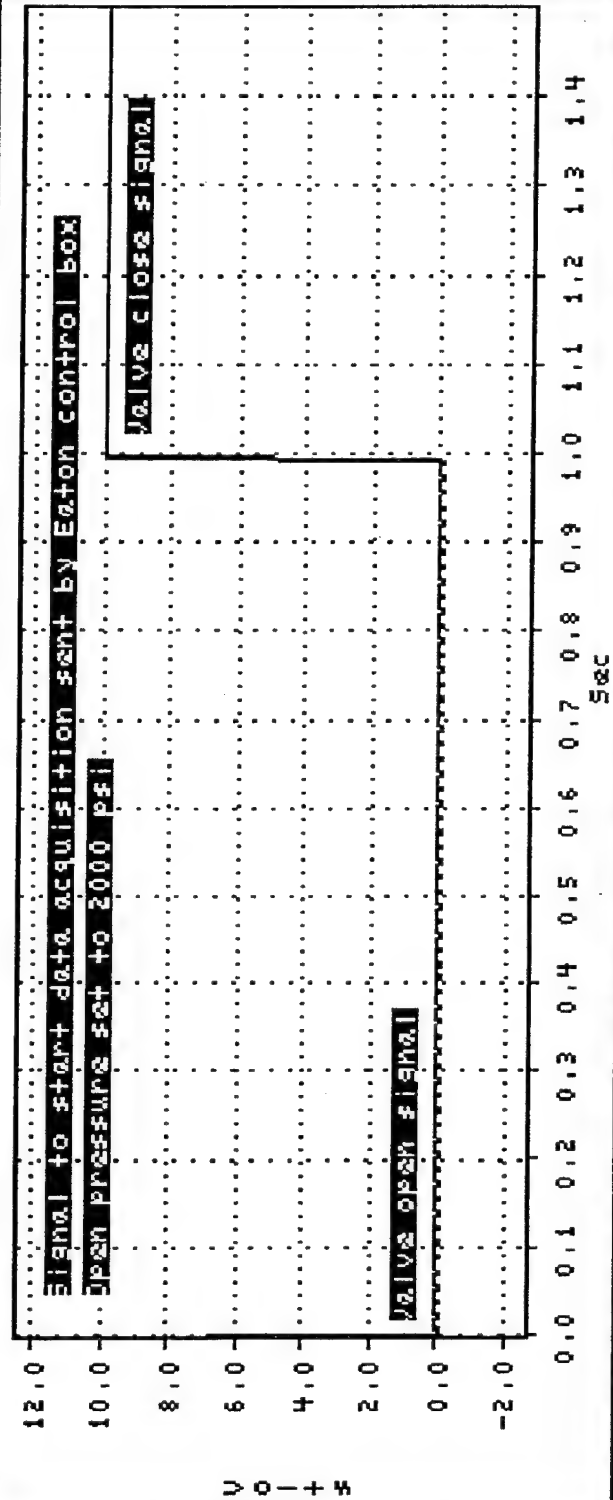
1.5

1.0

0.5

ETVE CHARACTERIZATION TEST DATA PLOTS

TEST 2

Open actuating pressure: 2000 psi
Data sampling rate: 10,000 samples per second
Data sampling time: 1.5 seconds

Dataset Name:	FIRE2000	Sample Rate:	1e+004
Version Number:	1	Maximum:	9.99512
Series Name:	2000PSI	Minimum:	-0.078125
Date Acquired:	9-24-1993	Comments:	Signal to start data
Time Acquired:	9:36:28.67		system sent from Eaton control
Vert Units:	Volts		box
Horiz Units:	Sec		
Num Samples:	15000		

W1: FIRE2000,1,2000PSI

Signal to start data acquisition sent by Eaton control box

Open pressure set to 2000 psi

Valve close signal

Valve open signal

Sec

Dataset Name:	LVDT2000
Version Number:	1
Series Name:	2000PSI
Date Acquired:	9-24-1993
Time Acquired:	9:36:28.67
Vert Units:	INCHES
Horiz Units:	Sec
Num Samples:	15000

Sample Rate:	1e+004
Maximum:	1.71961
Minimum:	0.567917
Comments:	Valve position signal from LVDT

Valve position measured by LVDT
open pressure set at 2000 psi

W2: LVDT2000,1,2000PSI
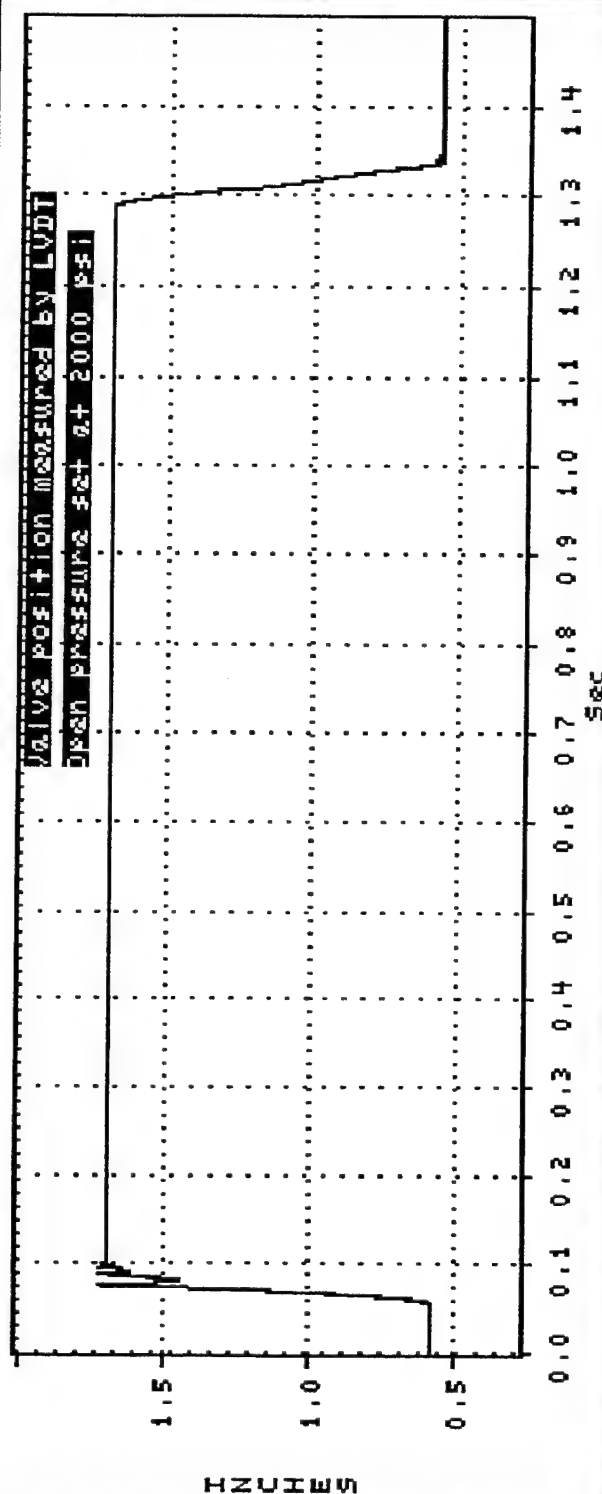
Dataset Name:	OPEN2000
Version Number:	1
Series Name:	2000PSI
Date Acquired:	9-24-1993
Time Acquired:	9:36:28.67
Vert Units:	PSI
Horiz Units:	Sec
Num Samples:	15000

Sample Rate:	1e+004
Maximum:	2499.48
Minimum:	-1333.18
Comments:	Pressure measurment
	on the open side of valve

W3: OPEN2000,1,2000PSI
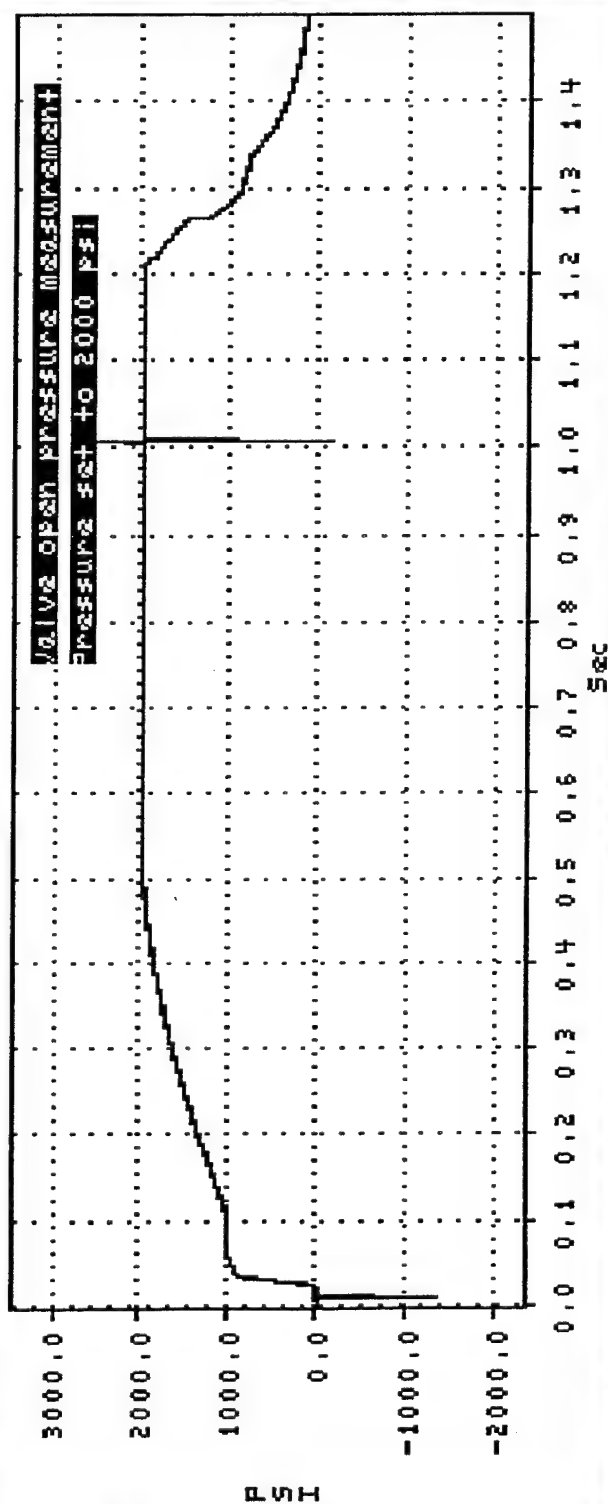
Valve open pressure measurement.
Pressure set to 2000 psi

Sample Rate:	1e+004
Maximum:	1.71961
Minimum:	0.576754
Comments:	Expansion of LVDT
	measurement when valve comes
	fully open
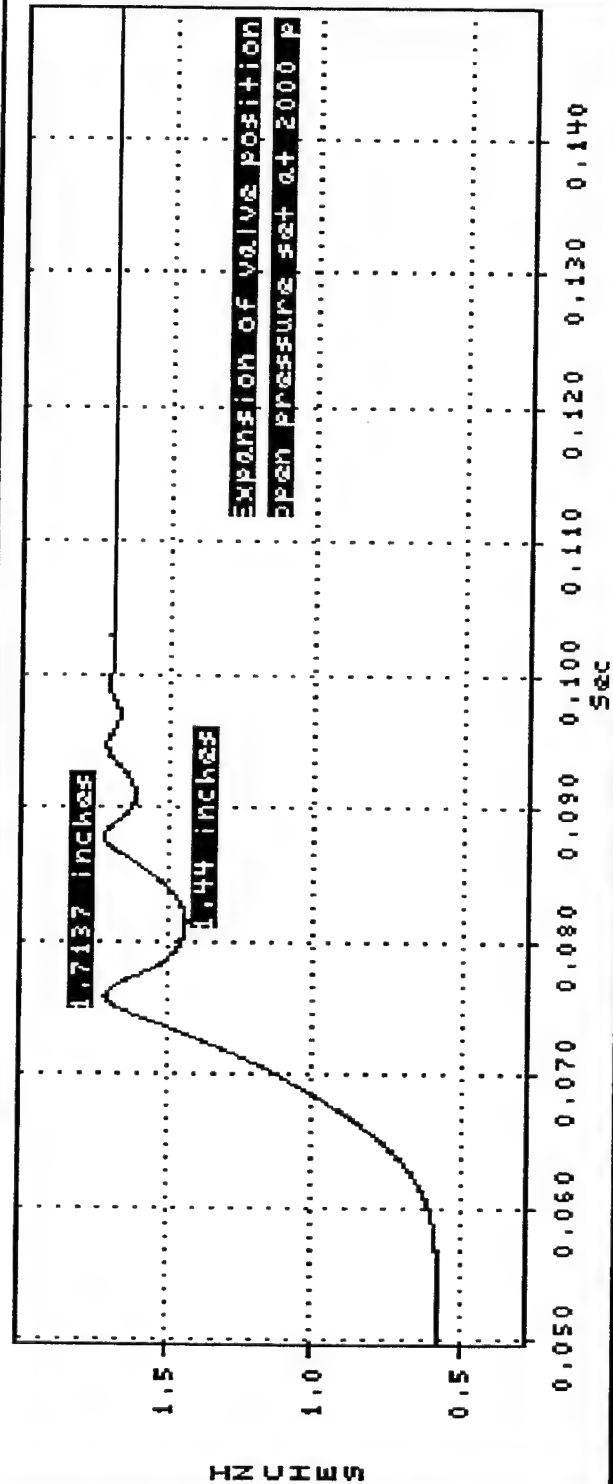
Dataset Name:	Unspecified
Version Number:	0
Series Name:	Unspecified
Date Acquired:	9-24-1993
Time Acquired:	9:46:45.20
Vert Units:	INCHES
Horiz Units:	Sec
Num Samples:	1000

W4: Extrac+CW2,500,1000?

Expansion of valve position
open pressure set at 2000 p

1.7137 inches

1.44 inches

INCHES

Sec

0.050 0.060 0.070 0.080 0.090 0.100 0.110 0.120 0.130 0.140

0.5 1.0 1.5

A-25

Dataset Name:	Unspecified
Version Number:	0
Series Name:	Unspecified
Date Acquired:	9-24-1993
Time Acquired:	9:45:38.69
Vert Units:	INCHES
Horiz Units:	Sec
Num Samples:	1000

Sample Rate:	1e+004
Maximum:	1.6931
Minimum:	0.567917
Comments:	Expansion of LVDT at
valve closure	
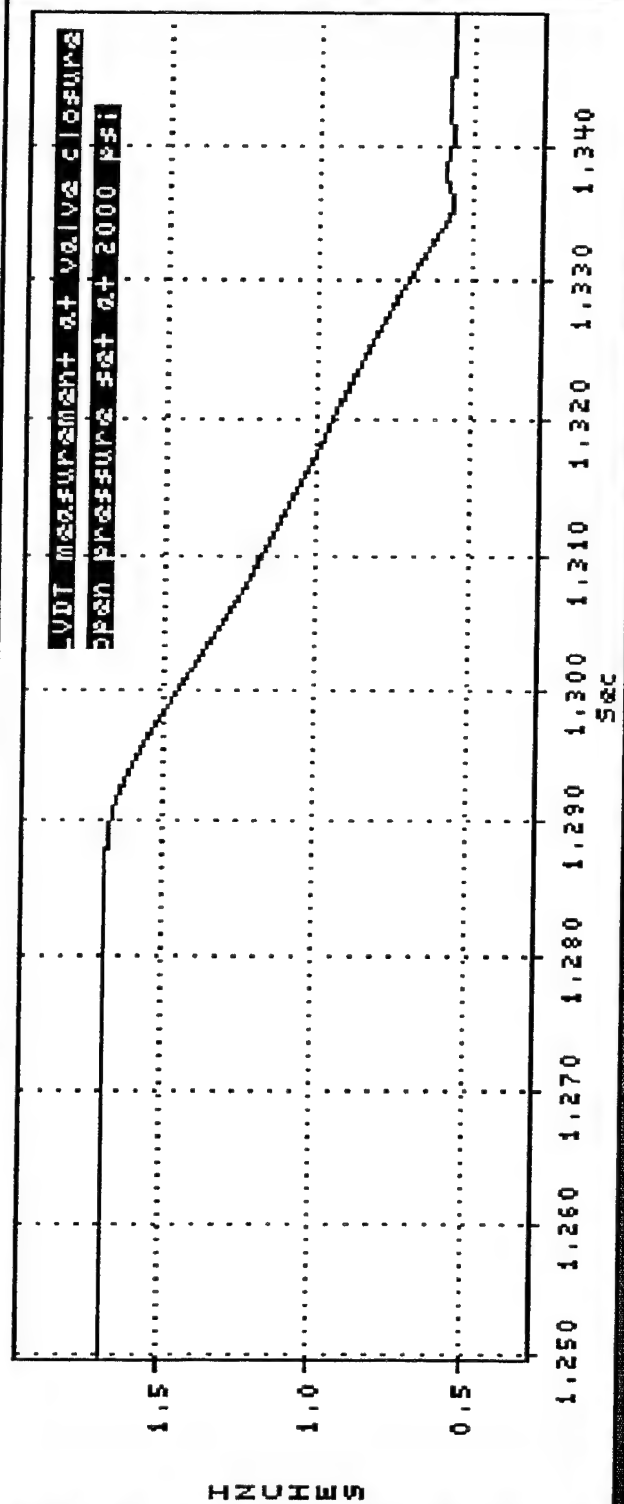
WS: Extrac+CW2,12500,1000)

LVDT measurement at valve closure
open pressure set at 2000 psi

ETVE DAMPING TEST DATA PLOTS

## TEST 1

Open actuating pressure: 2000 psi
Close actuating pressure: 1000 psi
Close actuating pressure—release time: 70 msec
    from start of sleeve displacement
Data sampling rate: 10,000 samples per second
Data sampling time: 1 second

Dataset Name:	CLOSE
Version Number:	1
Series Name:	CLS_PRES_ON
Date Acquired:	12-09-1993
Time Acquired:	14:47:02.52
Vert Units:	PSI
Horiz Units:	Sec
Num Samples:	10000

Sample Rate:	1e+004
Maximum:	1167.44
Minimum:	-14.3174
Comments:	Close pressure left
	on for .5 seconds open pressure
	set 2000 psi close pressure at
	1000 psi

W1: CLOSE,1,CLS_PRES_ON
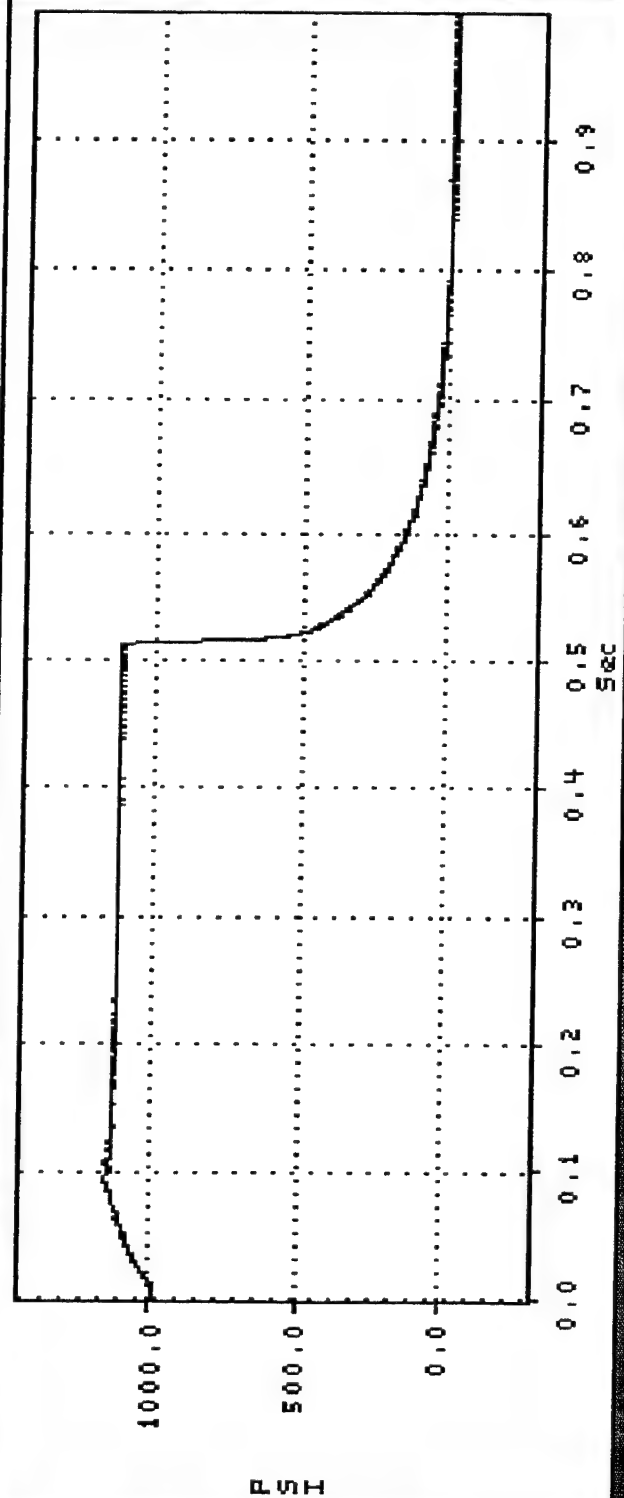
Dataset Name:	OPEN
Version Number:	1
Series Name:	CLS_PRES_ON
Date Acquired:	12-09-1993
Time Acquired:	14:47:02.52
Vert Units:	PSI
Horiz Units:	Sec
Num Samples:	10000

Sample Rate:	1e+004
Maximum:	1998.7
Minimum:	1201.33
Comments:	Close pressure left
	on for .5 seconds open pressure
	set 2000 psi close pressure at
	1000 psi

W2: OPEN.1.CLS_PRES_ON
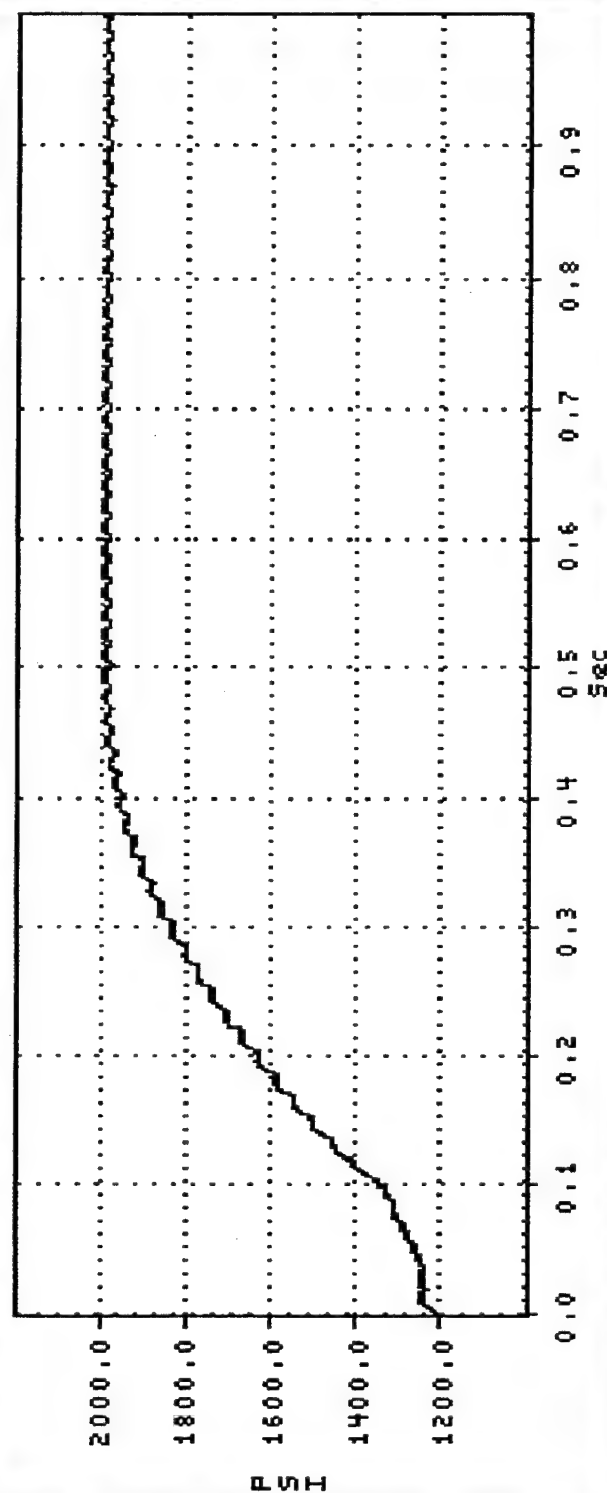
Dataset Name:	LVDT
Version Number:	1
Series Name:	CLS_PRES_ON
Date Acquired:	12-09-1993
Time Acquired:	14:47:02.52
Vert Units:	INCHES
Horiz Units:	Sec
Num Samples:	10000

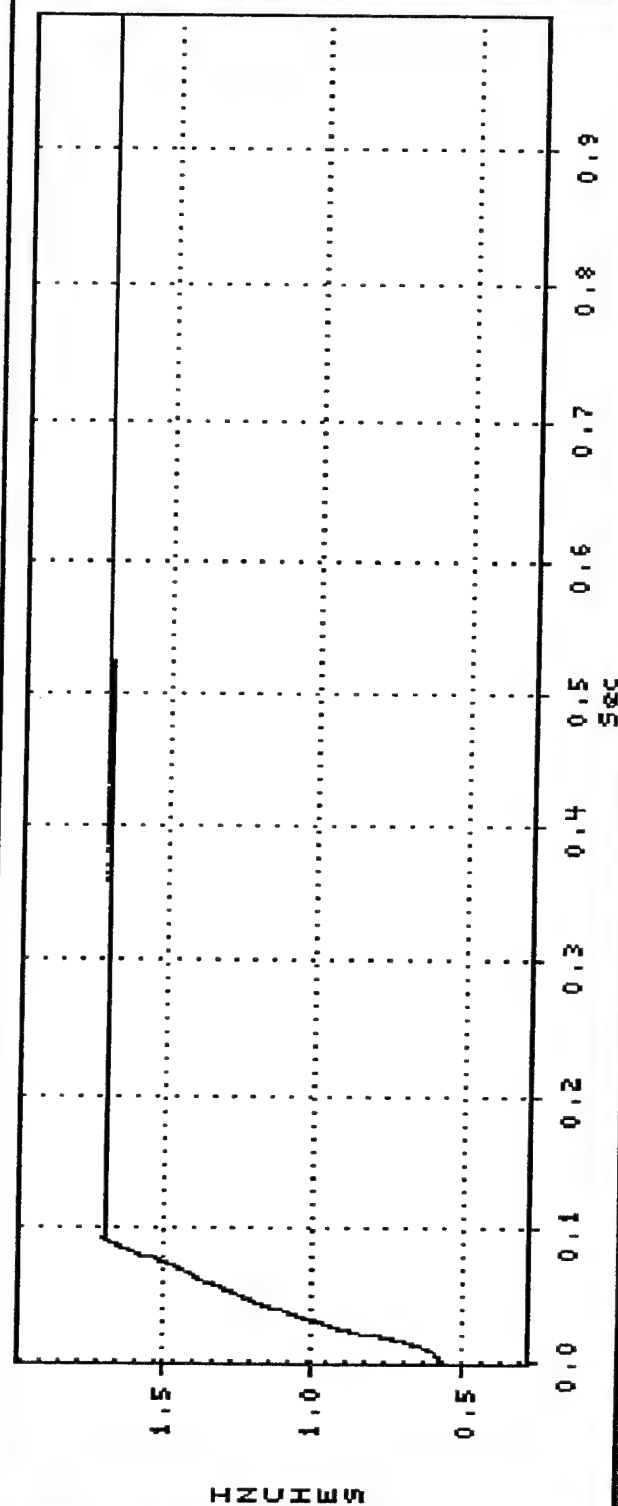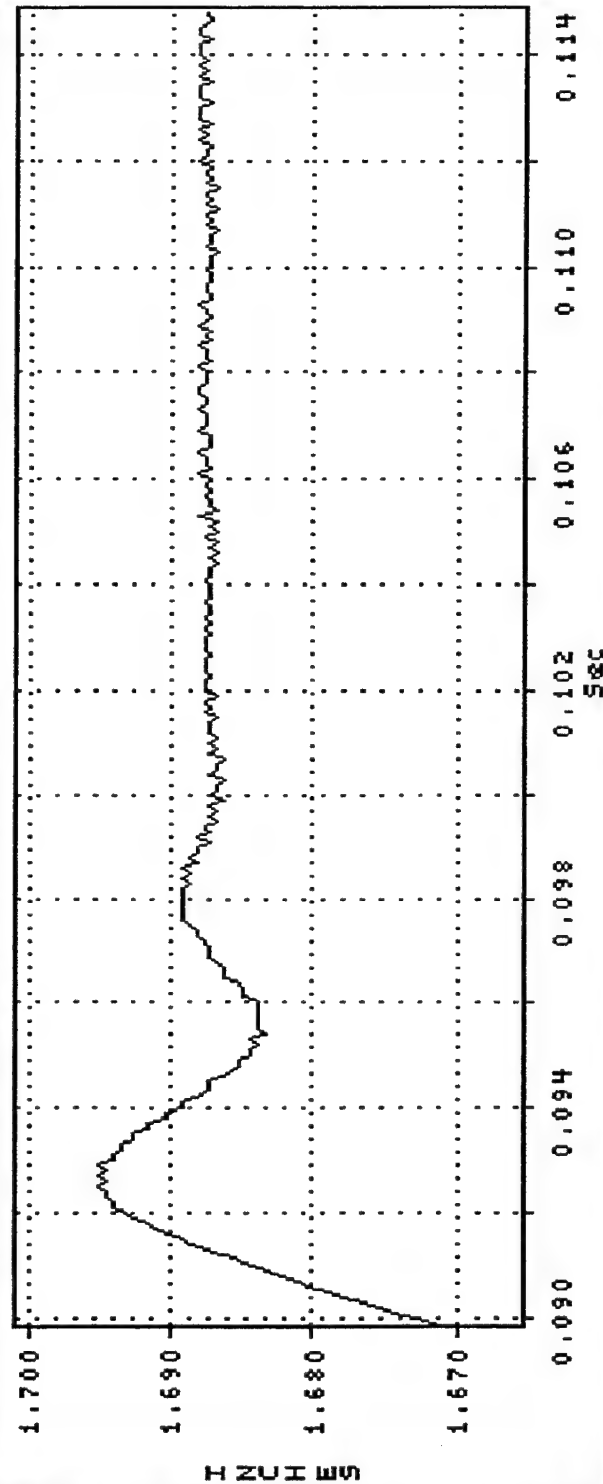| Sample Rate: | 1e+004 |
Maximum:	1.6985
Minimum:	0.577736
Comments:	Close pressure left on for .5 seconds open pressure set 2000 psi close pressure at 1000 psi

W3: LVDT.1.CLS_PRES_ON

Dataset Name:	Unspecified
Version Number:	0
Series Name:	Unspecified
Date Acquired:	12-09-1993
Time Acquired:	14:53:52.38
Vert Units:	INCHES
Horiz Units:	Sec
Num Samples:	250

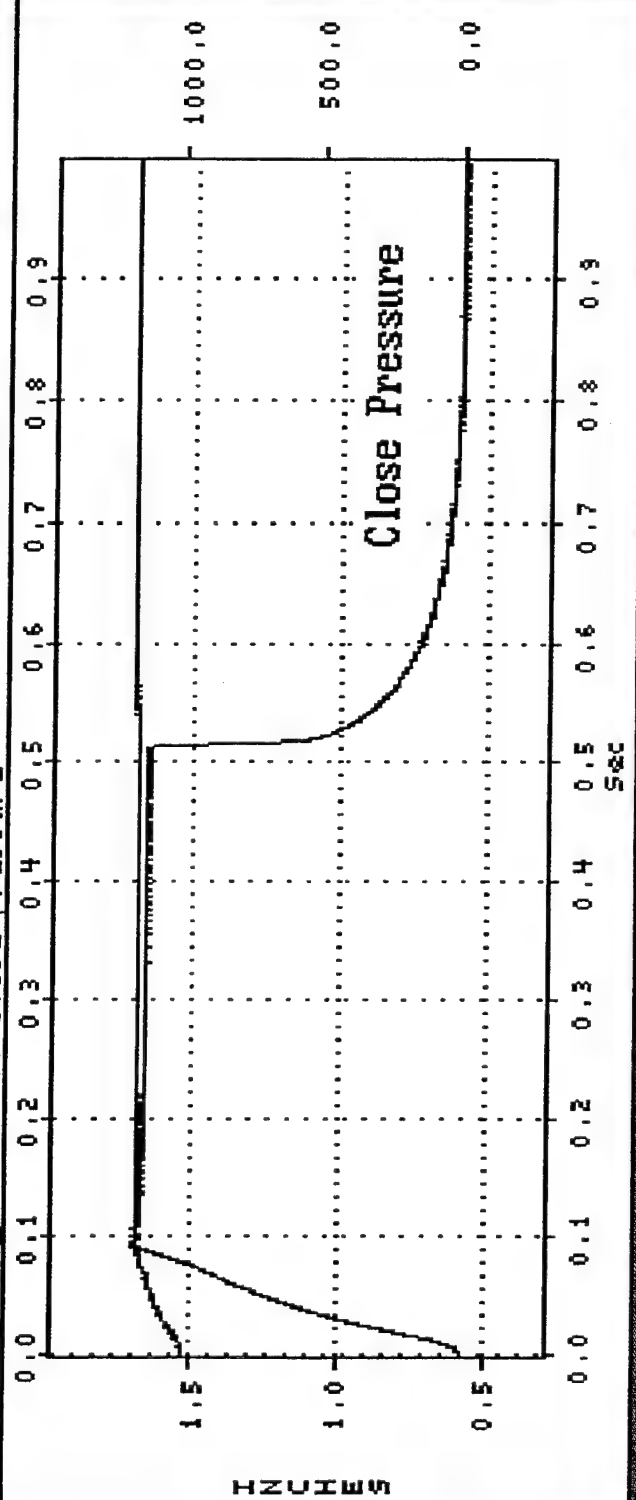| Sample Rate:	1e+004
Maximum:	1.69507
Minimum:	1.6715
Comments:	Close pressure left on for .5 seconds open pressure set 2000 psi close pressure at 1000 psi

W8: CLS_PRES_ON LVDT expanded at valve open

Dataset Name:	LVDT	Sample Rate:	1e+004
Version Number:	1	Maximum:	1.6985
Series Name:	CLOSE_ON	Minimum:	0.577736
Date Acquired:	12-06-1993	Comments:	
Time Acquired:	15:19:18.37		
Vert Units:	INCHES		
Horiz Units:	Sec		
Num Samples:	10000		

W10: CLS_PRES_ON LVDT vs close pressure
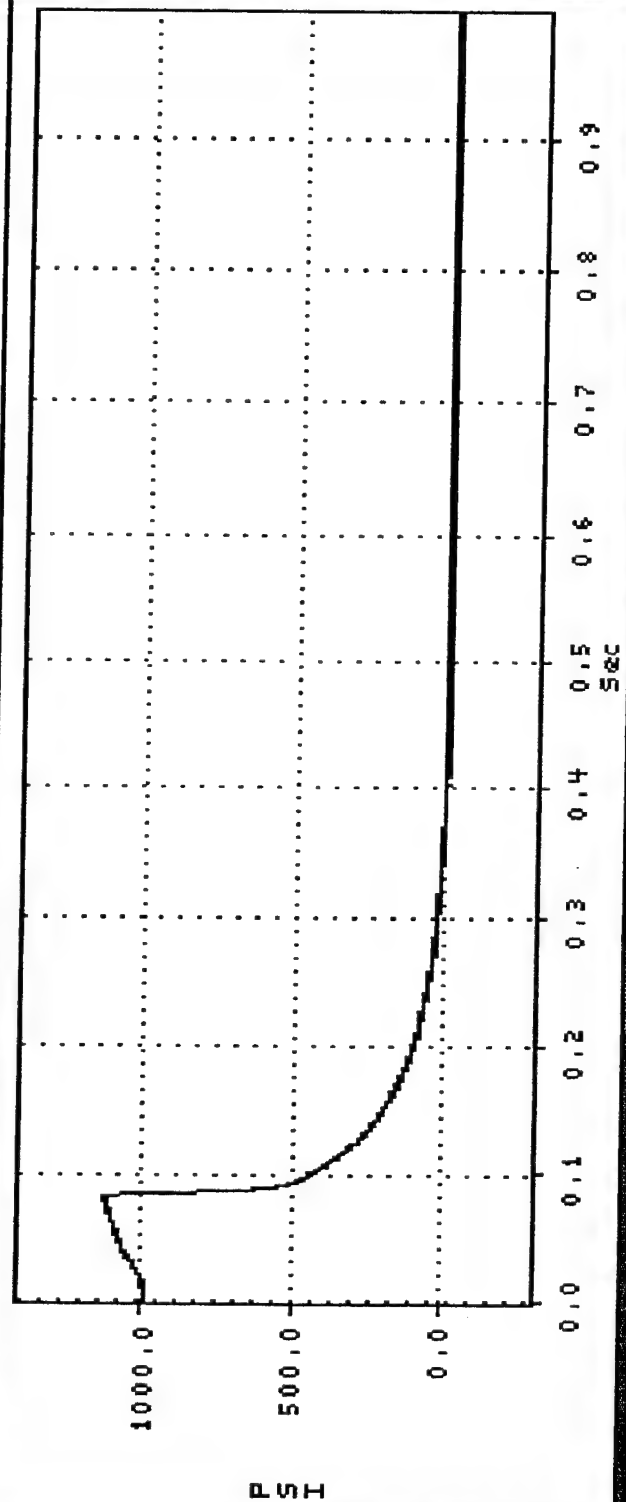
Close Pressure

ETVE DAMPING TEST DATA PLOTS

TEST 2

Open actuating pressure: 2000 psi
Close actuating pressure: 1000 psi
Close actuating pressure—release time: 0.5 sec
Data sampling rate: 10,000 samples per second
Data sampling time: 1 second

Dataset Name:	CLOSE
Version Number:	2
Series Name:	CLS_PRES_TRIG
Date Acquired:	12-09-1993
Time Acquired:	14:52:42.40
Vert Units:	PSI
Horiz Units:	Sec
Num Samples:	10000

Sample Rate:	1e+004
Maximum:	1135.33
Minimum:	-15.6139
Comments:	Close pressure on for 3/4 open cycle then released. open pressure set at 2000 psi close pressure set at 1000 psi

W4: CLOSE.2.CLS_PRES_TRIG

Dataset Name:	OPEN
Version Number:	2
Series Name:	CLS_PRES_TRIG
Date Acquired:	12-09-1993
Time Acquired:	14:52:42.40
Vert Units:	PSI
Horiz Units:	Sec
Num Samples:	10000

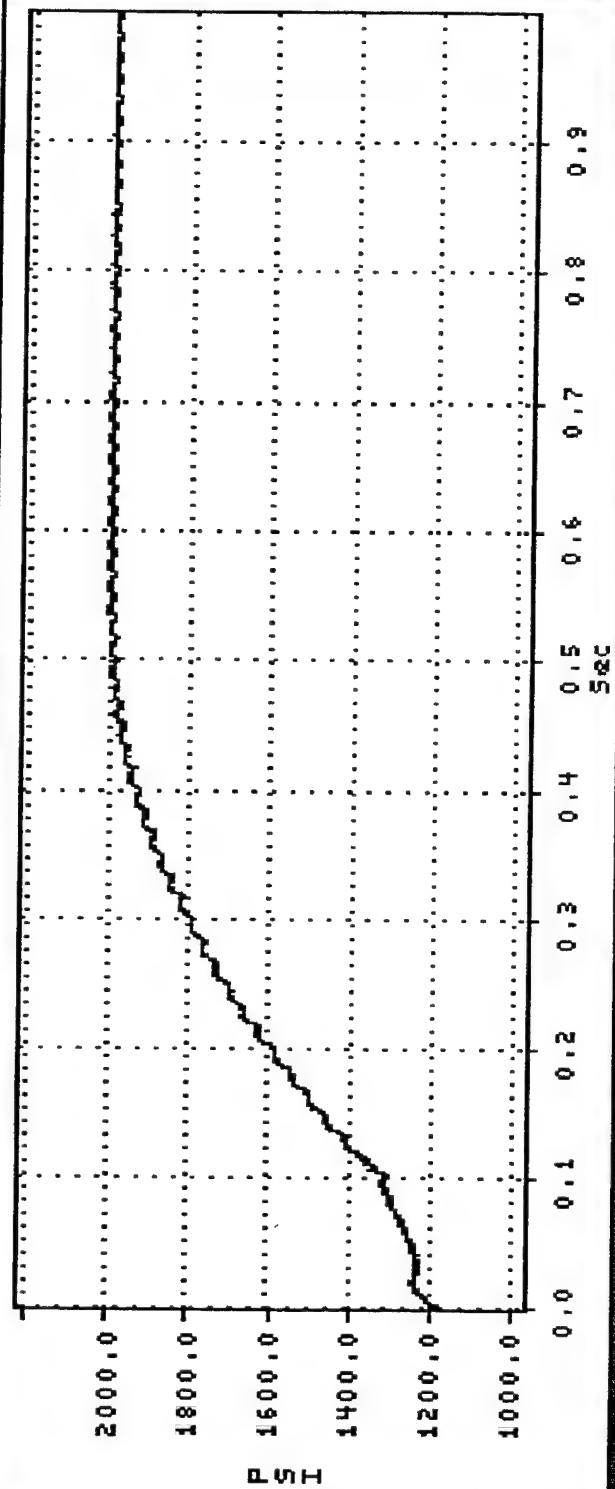|	
Sample Rate:	1e+004
Maximum:	2013.6
Minimum:	1176.58
Comments:	Close pressure on for 3/4 open cycle then released. open pressure set at 2000 psi close pressure set at 1000 psi

W5: OPEN.2.CLS_PRES_TRIG

Dataset Name:	LVDT
Version Number:	2
Series Name:	CLS_PRES_TRIG
Date Acquired:	12-09-1993
Time Acquired:	14:52:42.40
Vert Units:	INCHES
Horiz Units:	Sec
Num Samples:	10000

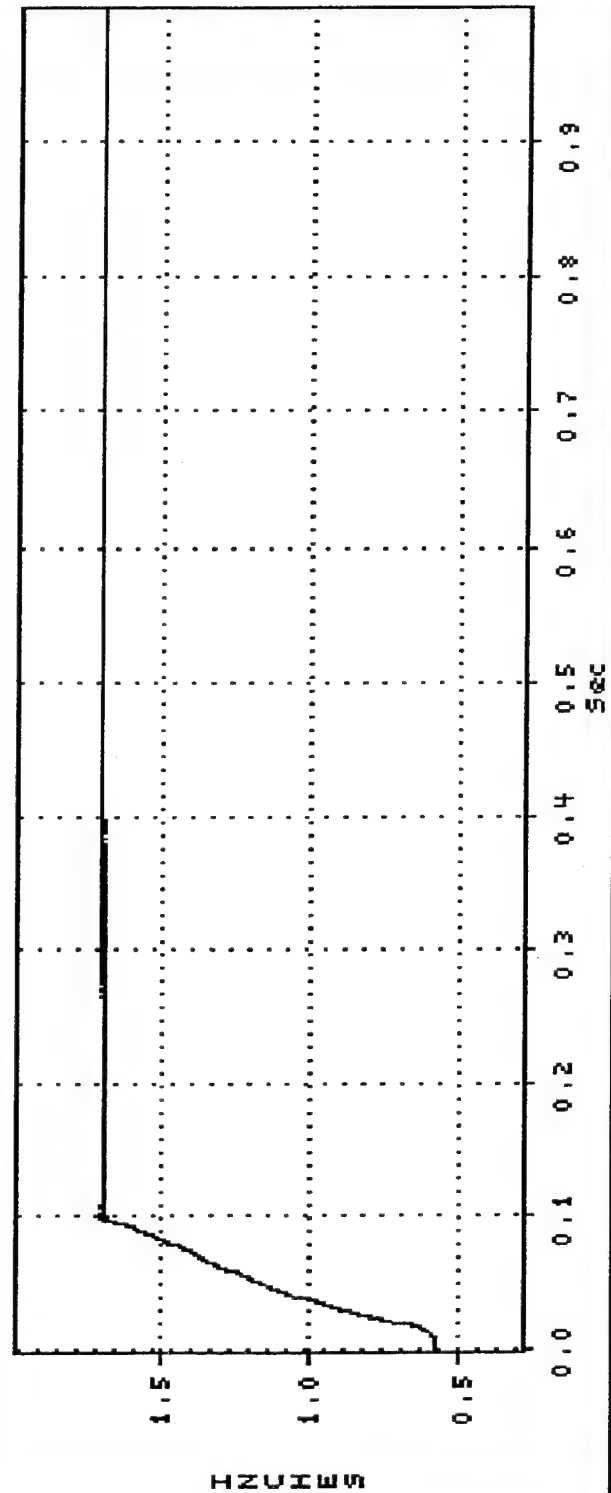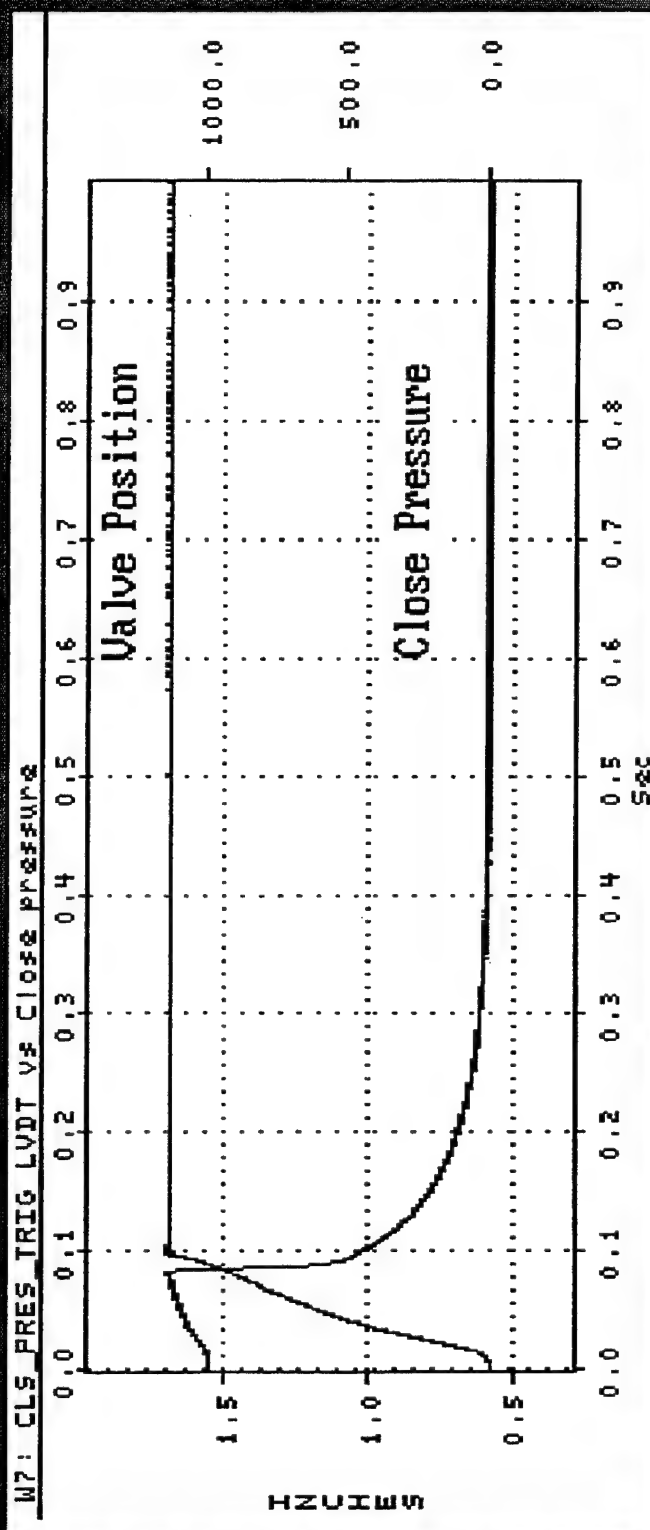|	
Sample Rate:	1e+004
Maximum:	1.70341
Minimum:	0.577245
Comments:	Close pressure on for 3/4 open cycle then released. open pressure set at 2000 psi close pressure set at 1000 psi

W6: LVDT,2,CLS_PRES_TRIG

Dataset Name:	LVDT	Sample Rate:	1e+004
Version Number:	1	Maximum:	1.70341
Series Name:	CLOSE_OFF	Minimum:	0.577245
Date Acquired:	12-06-1993	Comments:	Close pressure on for
Time Acquired:	15:19:18.37		3/4 open cycle then released.
Vert Units:	INCHES		open pressure set at 2000 psi
Horiz Units:	Sec		close pressure set at 1000 psi
Num Samples:	10000		

W7: CLS_PRES_TRIG LVDT vs Close pressure

Valve Position

Close Pressure

| Dataset Name:	Unspecified
Version Number:	0
Series Name:	Unspecified
Date Acquired:	12-09-1993
Time Acquired:	14:58:17.01
Vert Units:	INCHES
Horiz Units:	Sec
Num Samples:	250

Sample Rate:	1e+004
Maximum:	1.70341
Minimum:	1.56841
Comments:	Close pressure on for 3/4 open cycle then released. open pressure set at 2000 psi close pressure set at 1000 psi

W11: CLS_PRES_ON LVDT expanded at valve open
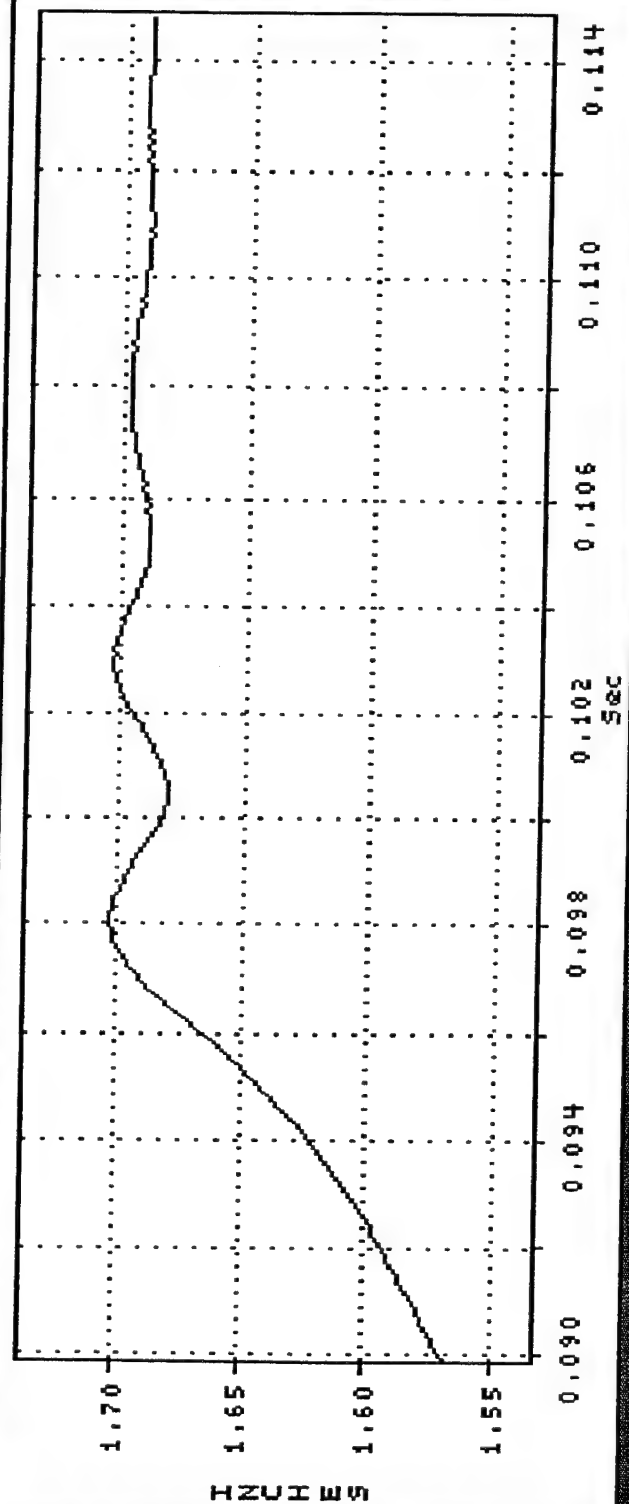
APPENDIX B

BELLEVILLE WASHER CHARACTERIZATION TESTING

G. E. Korth

INTENTIONALLY LEFT BLANK.

<u>Objective of Tests:</u> These tests were conducted to determine the quasi-static load-deflection behavior of different configurations of Belleville washers used or proposed to be used in the Eaton Throat Valve prototype. This loading behavior provides input for the numerical modeling task of the dynamic valve evaluation.

<u>Description of Material:</u> The test specimens were made from 17-7PH CH900 CRES (AMS 5529). They were nominally 1.00 inch in diameter with a 0.50 inch hole and 0.073 inches thick. The part number of these washers is B1000-073-S. A free standing height of one washer without load is 0.088 to 0.090 inches.

<u>Description of Test Equipment:</u> The washers were tested in a compression mode using an Instron Model 1128 Universal load frame. This load frame is a four post screw-driven machine with maximum capacity of 100,000 pounds. The washers were loaded between two compression platens. The accuracy of the load cell is within ± 0.5% of the indicated load or ± 0.25% of the load range in use. Deflection was monitored between the compression platens with a linear variable capacitance transducer with an accuracy of within 0.02% of full range (0.50 inches).

Test Procedure: The washers were tested either dry (as received) or lubed with DN-600 Polar Start grease manufactured by Conoco. They were placed directly on the compression platen in various configurations as shown in Figure 1. The load frame cross-head was manually moved down until the first indication of load was noted and then the electronic cross-head positioner was zeroed so upon unloading the cross-head would come back to that same position. Using this technique, permanent deformation would be evident on unloading or in subsequent cycles of the same stack. The cross-head was programmed to move with a speed of 0.05 to 0.50 inches/minute. After the desired load was reached the reverse was activated and the stack was unloaded with the same cross-head velocity (0.05 to 0.50 in./min.). Compliance was measured on the system by loading the compression platens without any washers present (See Chart 16). The compliance of the machine can probably be neglected since it was measured to be 1.25×10^{-8} inches/pound.

The same set of washers were used for the dry and lubed tests of configuration (a) and (b), but for all other configurations, a new set of as-received washers were used with one exception: configuration (1) used four washers which had also been tested in the configuration (k) stack. The load and deflection were recorded on an X-Y plotter with the load range, load calibration, and deflection calibration noted on each chart. The test temperature was ambient laboratory temperature (approximately 22-24°C).
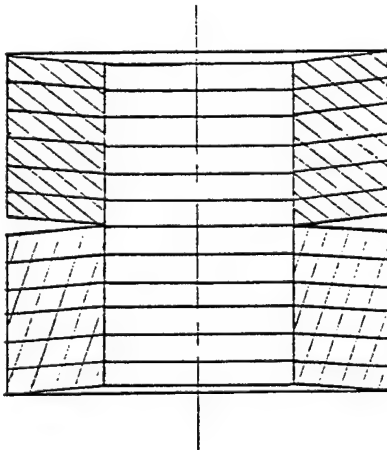
Results: The loading and unloading behavior of the various stack configurations shown in Fig.1 is described by the X-Y plots. The matrix of tests conducted is listed in Table 1 which also lists the maximum load and deflection for each configuration stack.
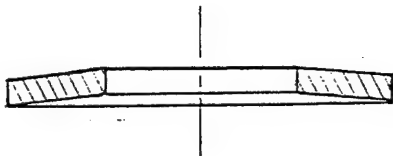
Configuration (a)
Stack of 1
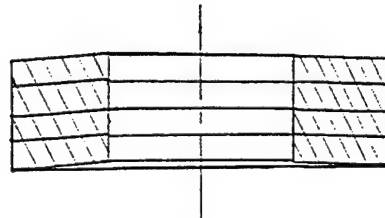
Configuration (b)
Stack of 4

Configuration (c)
Stack of 12

Configuration (d)
Stack of 16

Figure 1. Stack configurations used in testing Belleville washers
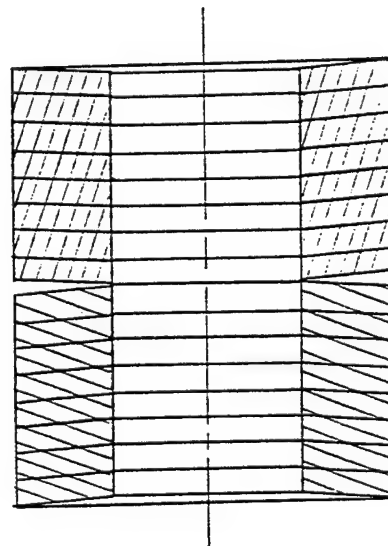
Configuration (e), Stack of 20

Configuration (f), Stack of 12
Configuration (g), Stack of 16
Configuration (h), Stack of 20

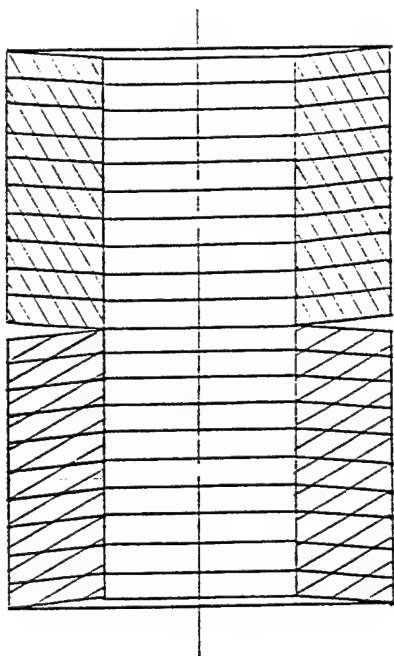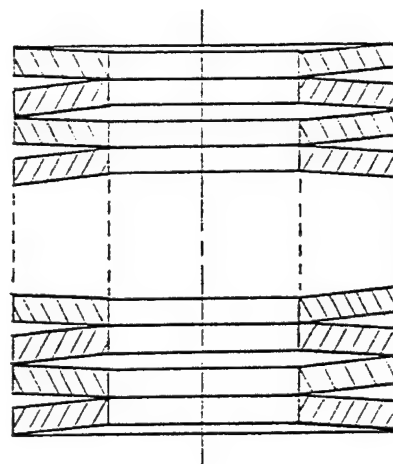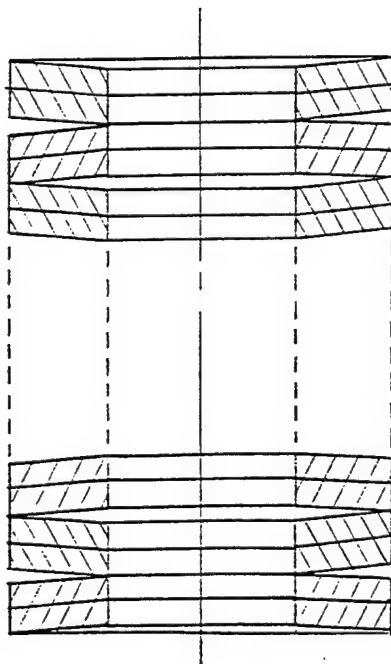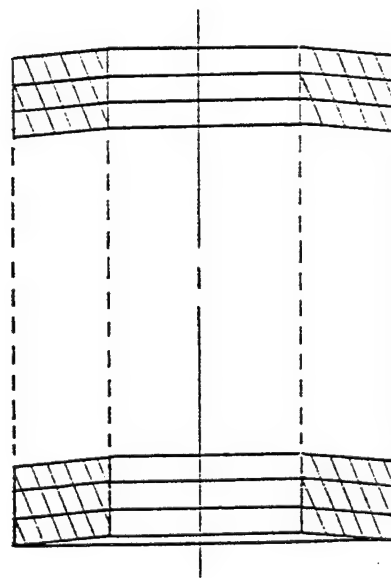Configuration (i), Stack of 20

Configuration (j), Stack of 12
Configuration (k), Stack of 16
Configuration (l), Stack of 20

Figure 1. (cont'd) Stack configurations used in testing Belleville washers

Table 1. Belleville washer load-deflection stack tests.

Stack Configuration (Fig.1)	Configuration Description	Lube	Max. Load (lbs)	Max. Defl. 10^{-3} in.	No. Cycles	Chart No.
a	Single	N	3,500	14.5	3	1
a	Single	Y	3,500	14.5	3	1
b	4 Parallel	N	14,000	16.1	3	2
b	4 Parallel	Y	14,000	17.3	10	2,3
c	12(Two 6's)	N	21,000	34.2	3	4
c	12(Two 6's)	Y	21,000	38.8	10	5,6
d	16(Two 8's)	Y	45,000	39.4	6	7,8
e	20(Two 10's)	Y	70,000	65.0	5	9
f	12(Alternating)	Y	4,500	176.5	5	10
g	16(Alternating)	Y	4,500	228.5	5	11
h	20(Alternating)	Y	4,500	264.0	5	12
i	20(Ten sets of alternat. 2's)	Y	14,000	146.5	5	13
j	12 Parallel	Y	70,000	29.3	5	14
k	16 Parallel	Y	80,000	42.2	5	15
l	20 Parallel	Y	100,000	74.0	5	16

8/30/93

Single Washer (Dry)

Cycle 1

Cycle 2

End of Dry Cycle

Cycle 3

New Single Washer
(Lubed w/Polarstart)

Cycle 1

Cycle 2

Cycle 3

5000 lbs. = 10V

$Y - \dfrac{5000 \text{ lbs.}}{10V} \quad \dfrac{1V}{10 \text{ div.}}$

$\dfrac{1}{1 \text{ div.}}$

$X - \dfrac{500 \text{ in.}}{10V} \quad \dfrac{1V}{10 \text{ div.}}$

$\dfrac{.0005 \text{ in.}}{\text{div.}}$

$\dfrac{1}{1 \text{ div.}}$

Tested with Instron 1/28

Configuration (a)

Actual Test (above)

.0885" As Rec'd

.0875 After 3500 lbs.

h (hydraulic press)

.0885 in. Original
.0885 After 5000 lbs.
.0880 After 10,000 lbs.
.0870 After 20,000 lbs.

Chart 1

B-8

Chart 2

8/30/93

Stack of 4 (Dry)

Loading

Unloading

Cycle 2 (Dry)

Cycle 3 (Dry)

Lubed (Polarstart)
Same Stack of 4

Cycle 1 (Lube)

Cycle 2 (Lube)

Configuration (b)

.0005 in.
div.

200 lbs.
div.

B-9

Stack of 4
(Cont'd)

- Cycle 3
(Lubed)

- Cycle 4

- Cycle 5

- Cycle 6

- Cycle 7

- Cycle 8

- Cycle 9

- Cycle 10

200 lbs.
div.

.0005 in.
div.

Configuration (b) cont'd.

Chart 3

8/30/93

Stack of 12 (Dry)

500 lbs. div.

.0005 in. div.

- Cycle 2 (Dry)

- Cycle 3 (Dry)

Configuration (c)

Chart 4

B-11

47 0700

- Cycle 1

- Cycle 2

- Cycle 5

- Cycle 6

- Cycle 3

- Cycle 4

Tested wth Instron 1/28

Y - 50,000 lbs.   1V
     10V   10 div.

500 lbs.   1
div.   1 div.

X - 500 in.   1V
    10V   10 div.

.0005 in.
div.   1 div.

Configuration (c) cont'd.

Chart 5

B-12

Y - 50,000 lbs. / 10V   1V / 10 div.

500 lbs. / div.   1V / 1 div.

X - 500 in. / 10V   1V / 10 div.

.0005 in. / div.   1V / 1 div.

Configuration (c) cont'd.

- Cycle 7
- Cycle 8
- Cycle 9
- Cycle 10
- Cycle 11
- Cycle 12
- Cycle 13

Chart 6

B-13

12-13-93 — Cycle 1

— Cycle 2

— Cycle 3

.0025 in.
div.

.0025 in.
div.

or .0005 in.
div.

.0005 in.
div.

Y (Load)
50,000 lbs/10V
Plotter 1V/10 div.
500 lbs/div.

X (Deflection)
0.5 in./10V
Plotter (.5V/10 div.)
(.1V/10 div.)

Configuration (d)
16 washers total

Configuration (d)
16 washers total
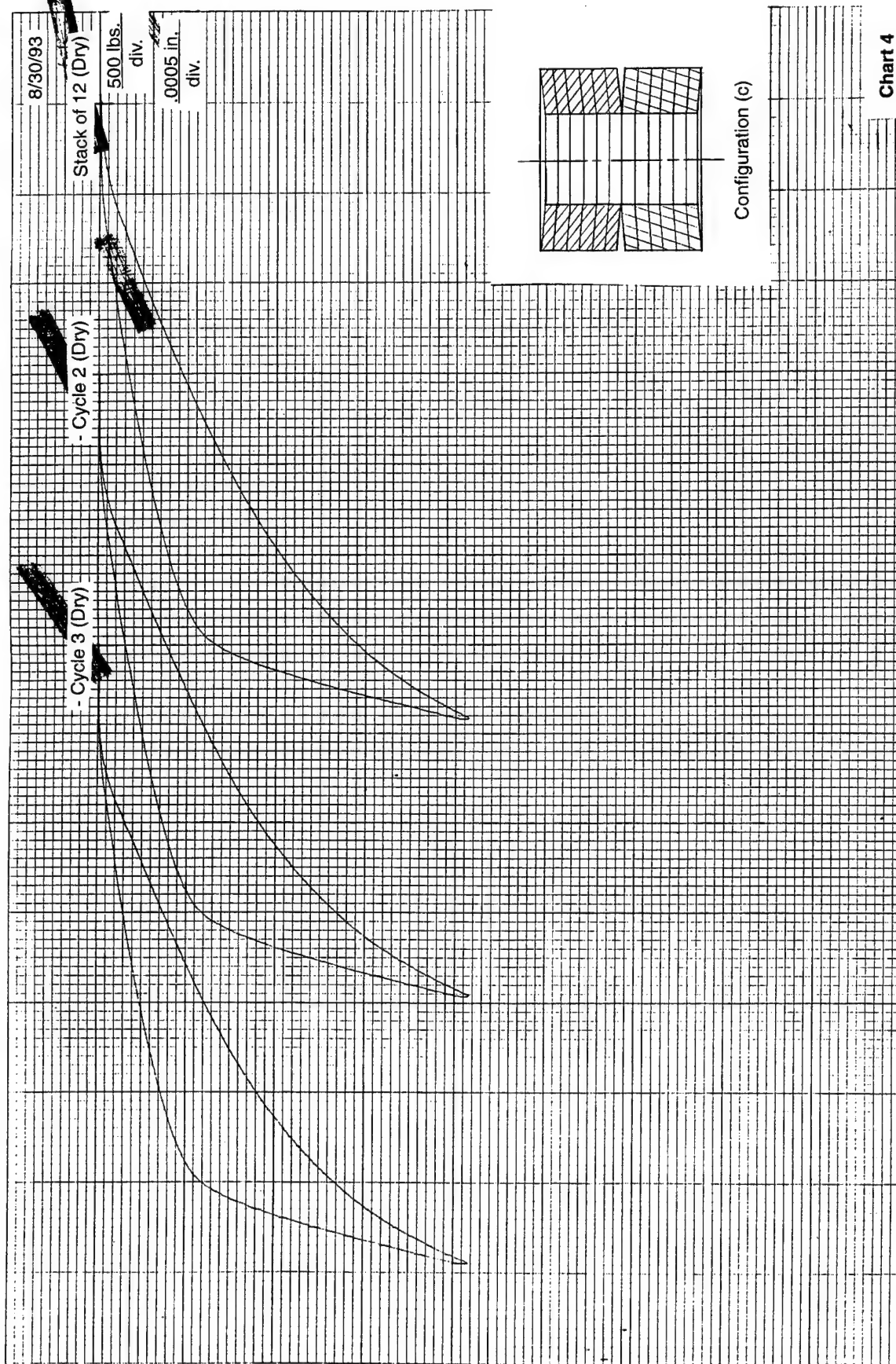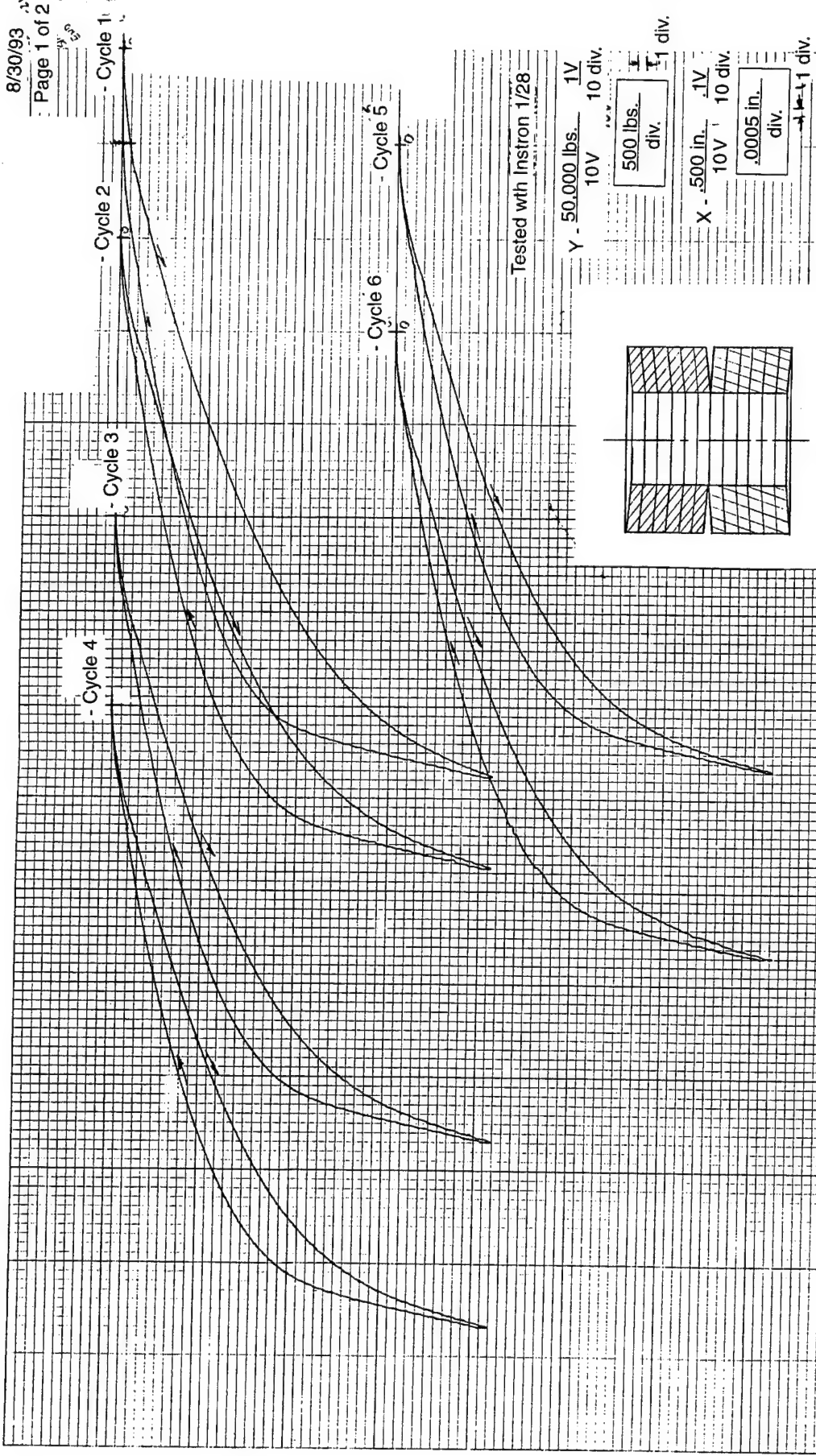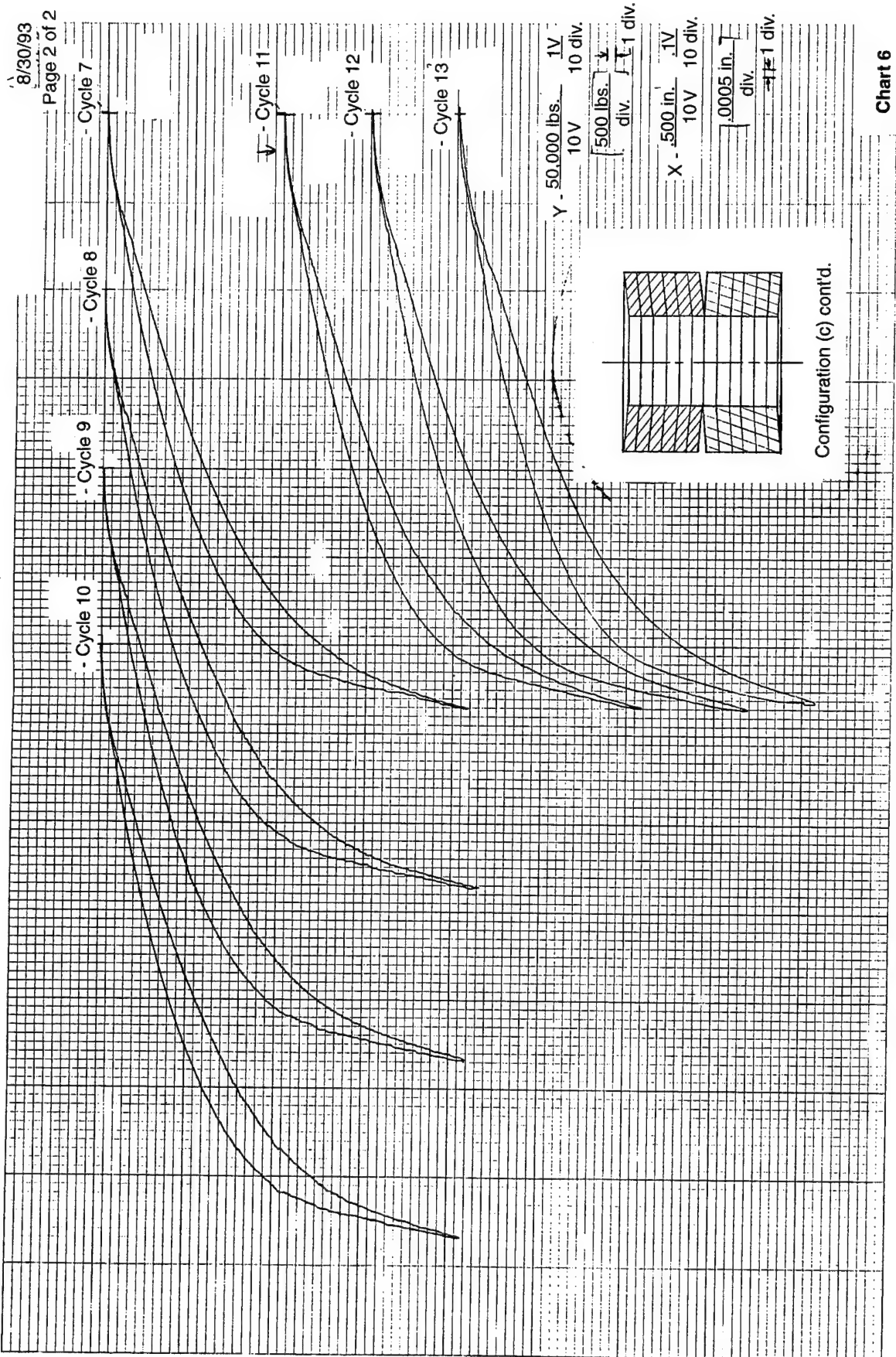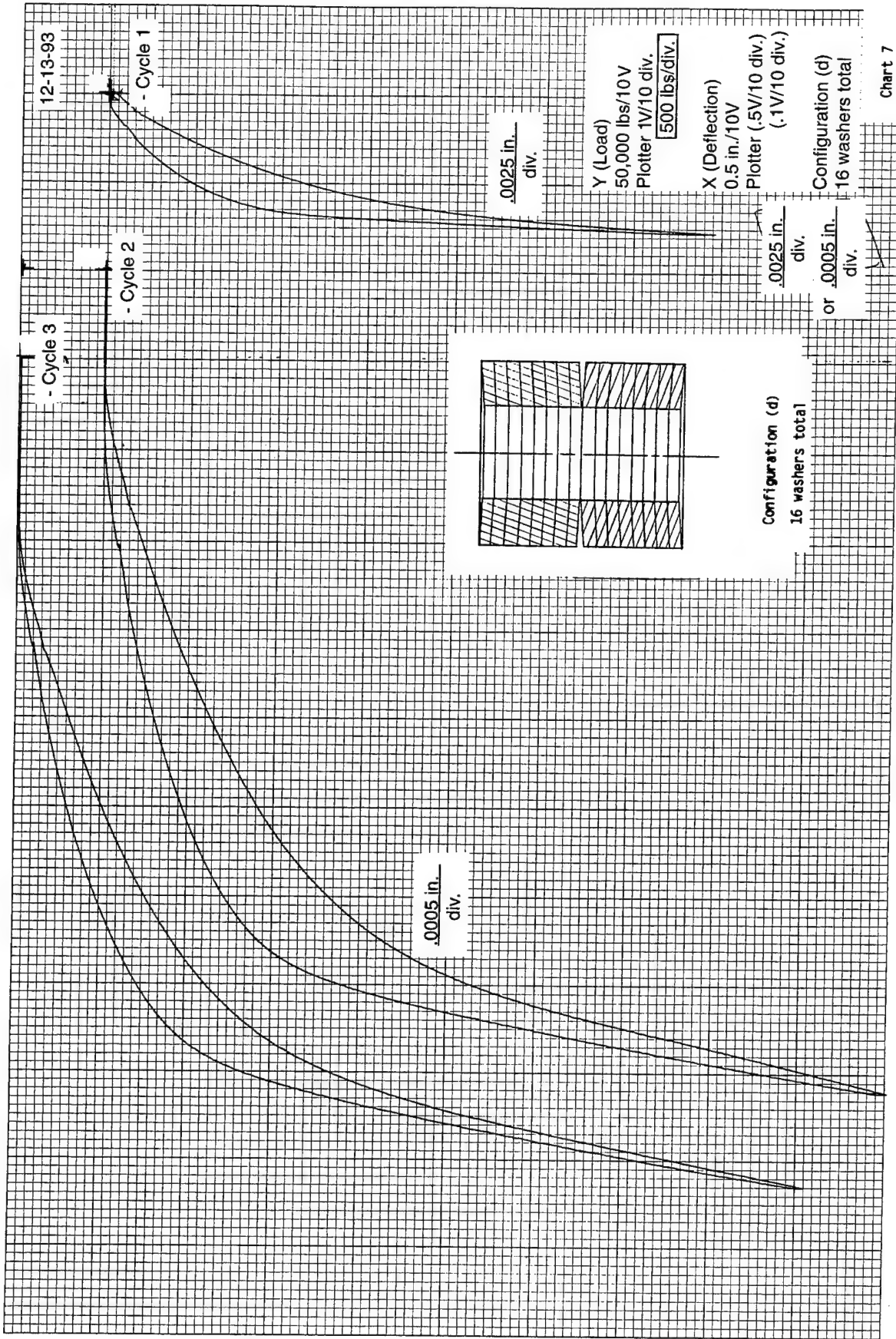
Chart 7

47 0700

K+E 10 X 10 TO THE INCH • 10 X 15 INCHES
KEUFFEL & ESSER CO. MADE IN U.S.A.

Chart 8
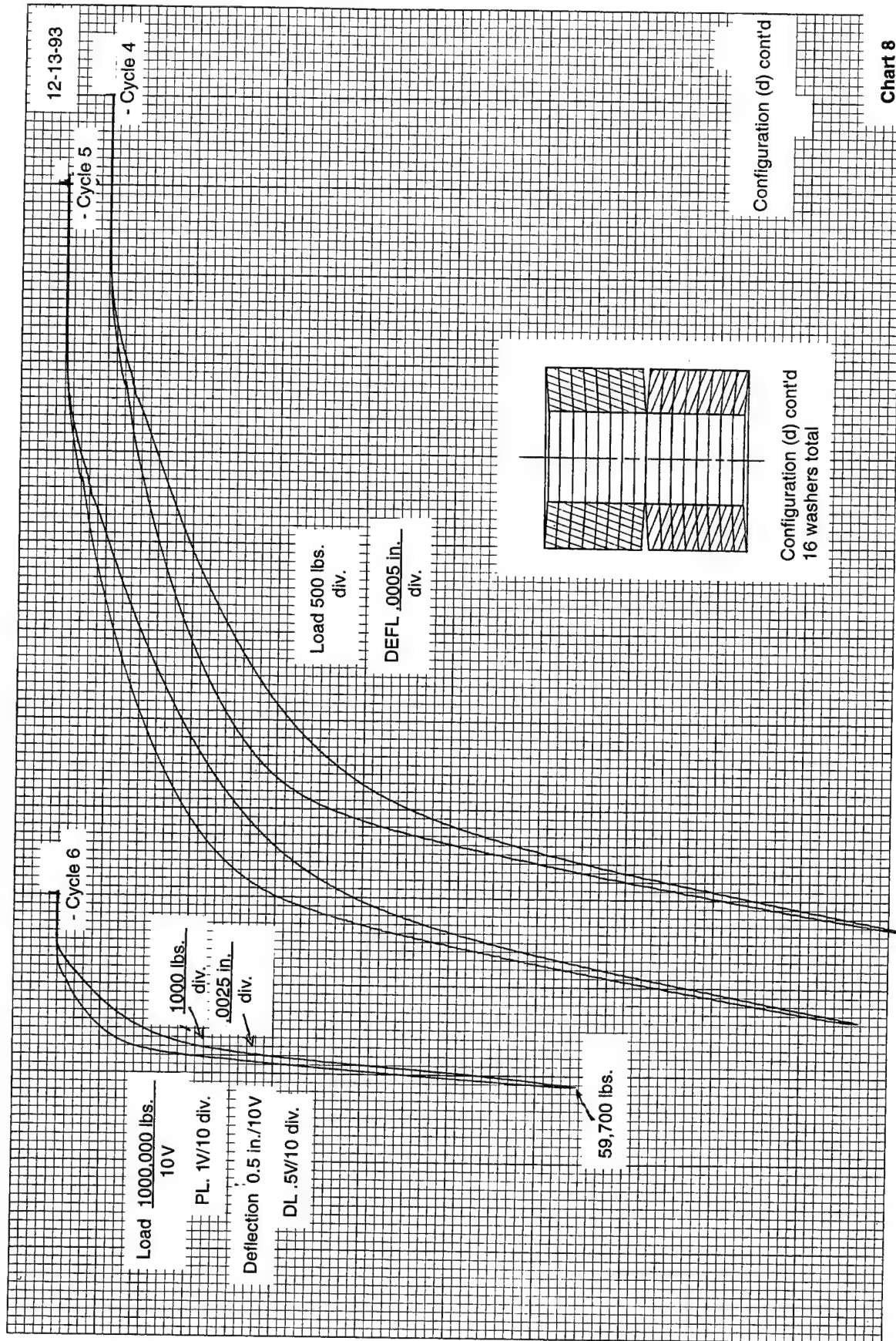
12-13-93

- Cycle 4
- Cycle 5
- Cycle 6

Configuration (d) cont'd

Configuration (d) cont'd
16 washers total

Load 500 lbs.
div.

DEFL .0005 in.
div.

1000 lbs.
div.
.0025 in.
div.

Load 1000,000 lbs.
10V

PL. 1V/10 div.

Deflection 0.5 in./10V

DL .5V/10 div.

59,700 lbs.

12-13-93

- Cycle 1
- Cycle 2
- Cycle 3
- 4
- 5

Configuration (e)
20 washers total

Y (Load)
100,000 lbs./10V
Plotter 1V/10 div.

X (Deflection)
0.5 in./10V
Plotter .5V/10 div.

1000 lbs.
div.

.0025 in.
div.

Configuration (e)

Chart 9

47 0700

K+E 10 X 10 TO THE INCH • 10 X 15 INCHES
KEUFFEL & ESSER CO. MADE IN U.S.A.

Cycle 1

2

3

4

5

Configuration (f)
12 Washers total

Y (Load)
5000 lbs./10V
Plotter 1V/10 div.

50 lbs.
div.

X (Deflection)
0.5 in./10V
Plotter 1V/10 div.

.005 in.
div.

Chart 10

Configuration (f)

47 0700

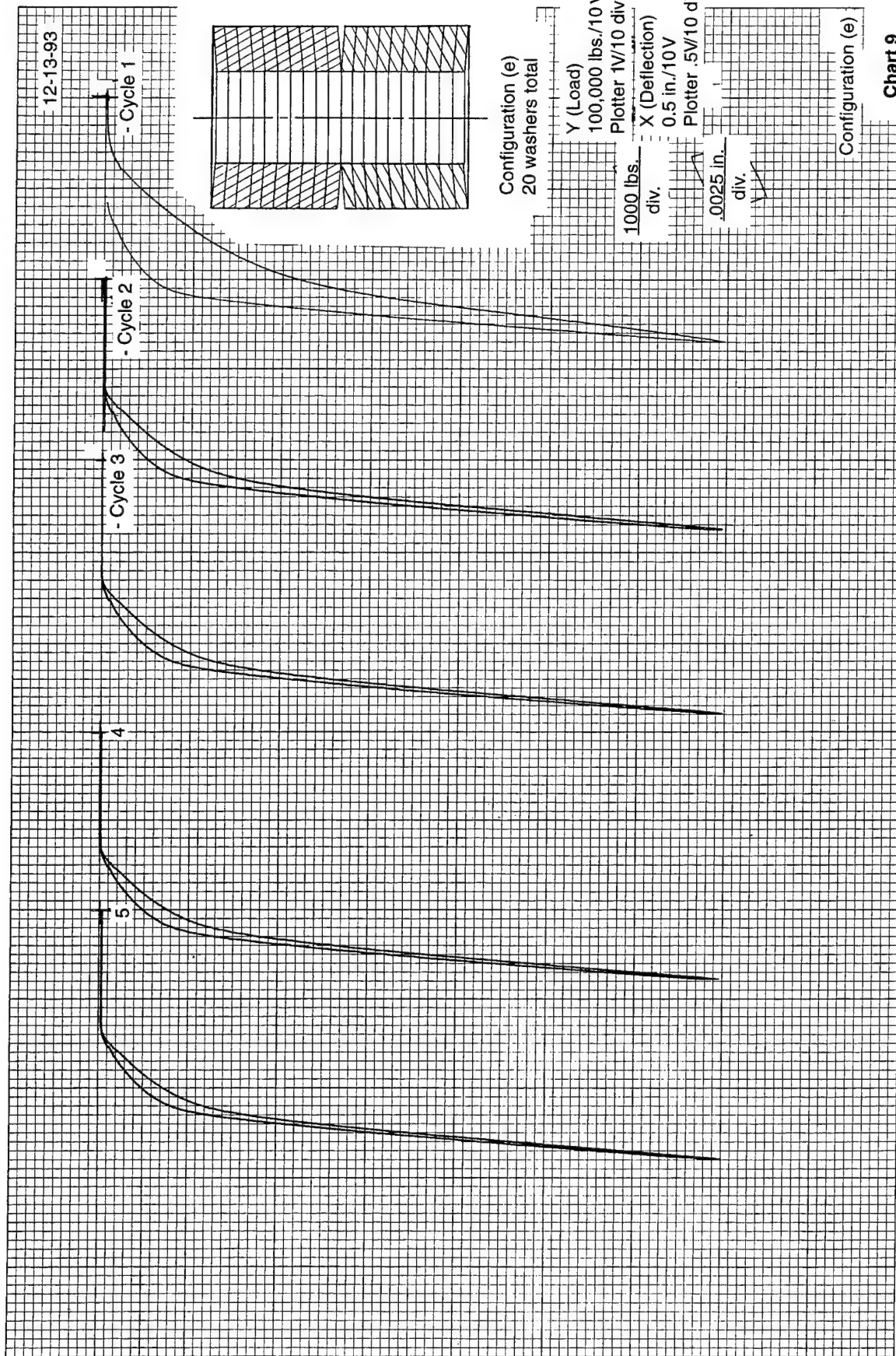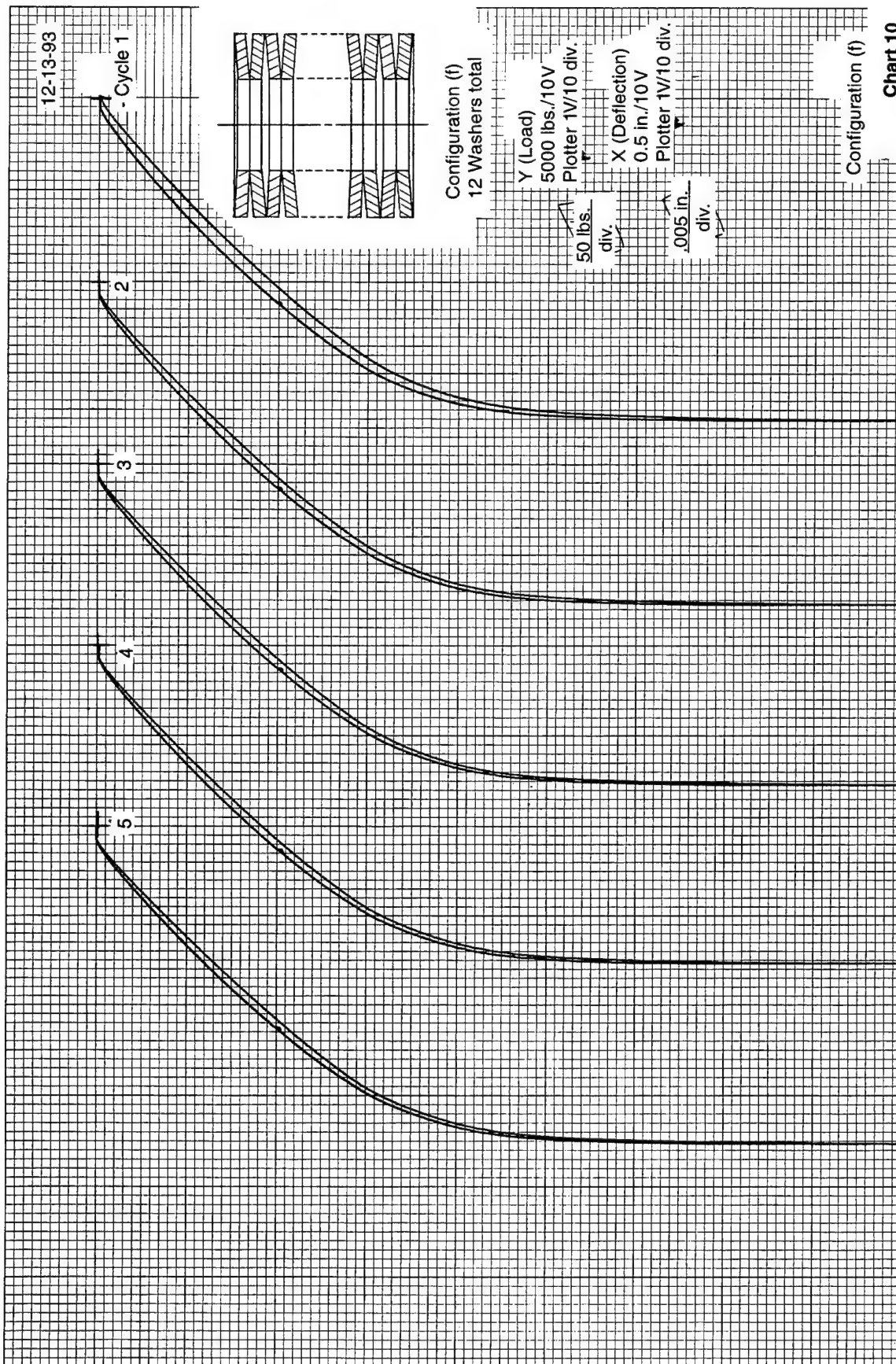K•E 10 X 10 TO THE INCH • 10 X 15 INCHES
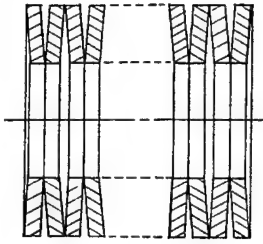KEUFFEL & ESSER CO. MADE IN U.S.A.

12-13-93

Cycle 1

2

3

4

5

Configuration (g)
16 washers total

Y (Load)
5000 lbs./10V
Plotter: 1V/10 div.
X (Deflection)
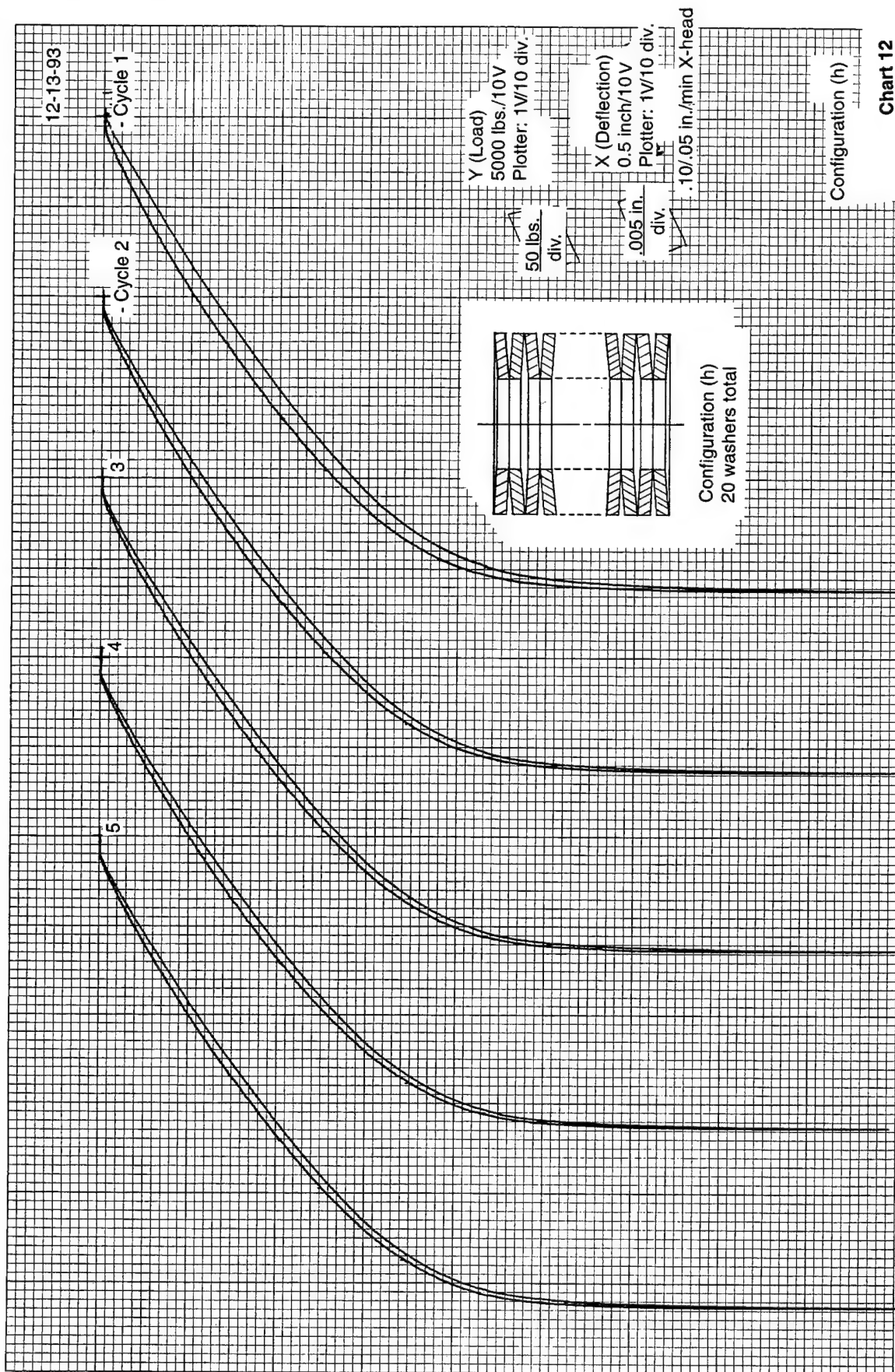0.5 in./10V
Plotter: 1V/10 div.

0.05 in./min.
&
0.5 in./min.

50 lbs.
div.

.005 in.
div.
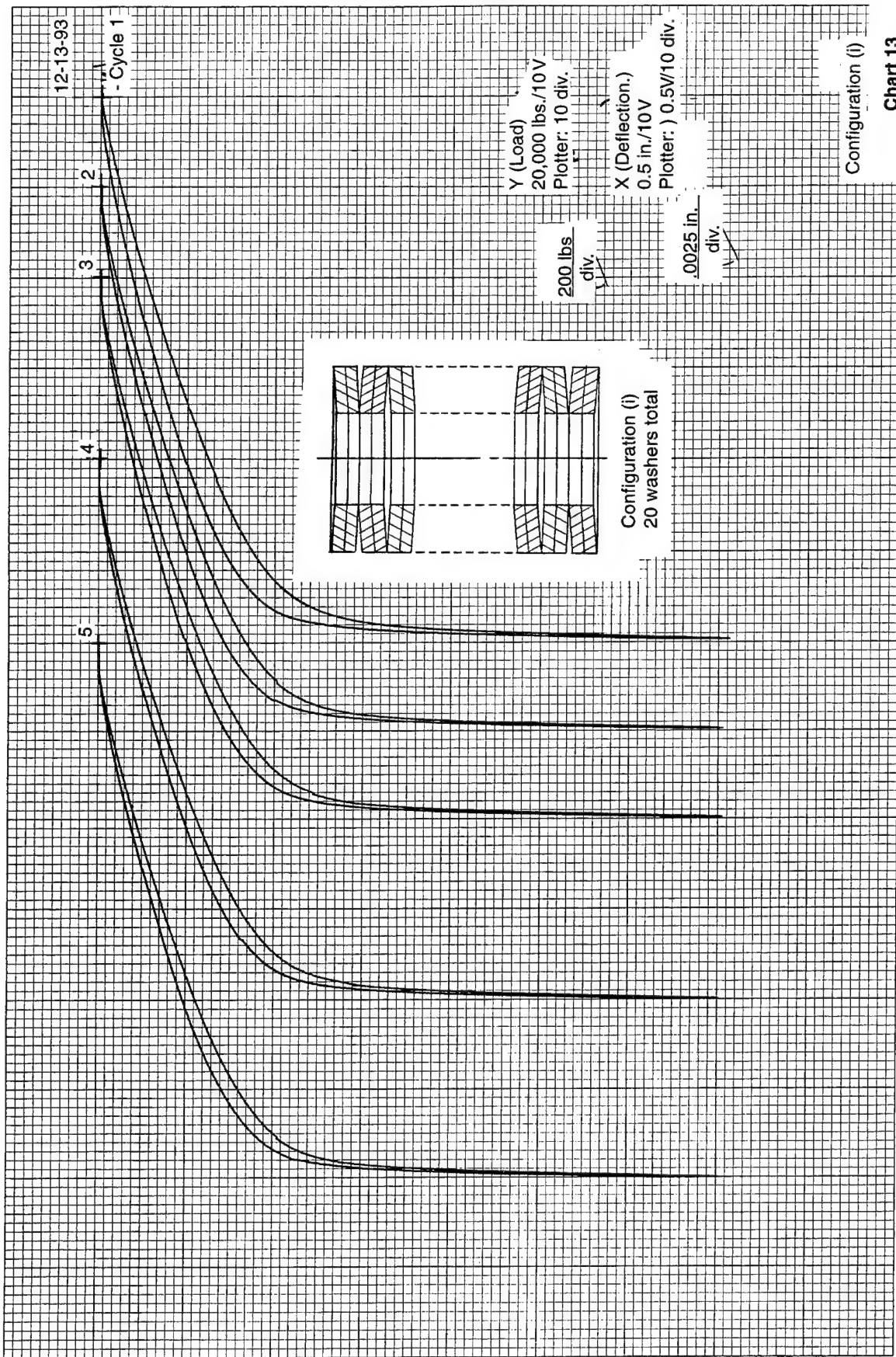
Configuration (g)

Chart 11

12-13-93

Cycle 1

Cycle 2

3

4

5

Y (Load)
5000 lbs./10V
Plotter: 1V/10 div.

50 lbs.
div.

X (Deflection)
0.5 inch/10 V
Plotter: 1V/10 div.

.005 in.
div.

.10/.05 in./min X-head

Configuration (h)
20 washers total

Configuration (h)

Chart 12

12-13-93

- Cycle 1

Y (Load)
20,000 lbs./10V
Plotter: 10 div.

X (Deflection.)
0.5 in./10V
Plotter:) 0.5V/10 div.

200 lbs
div.

.0025 in.
div.

Configuration (i)
20 washers total

Configuration (i)

Chart 13

12-13-93

- Cycle 1

5

2.

3

4.

Y (Load)
100,000 lbs./10 V
Plotter: 1v/10 div.

1000 lbs.
div.

X (Deflection)
0.5 inch/10 V
Plotter: 0.1V/10 div.

.0005 in.
div.

Configuration (J)
12 washers total

Configuration (J)

Chart 14

47 0700

K+E KEUFFEL & ESSER CO. MADE IN U.S.A.
10 X 10 TO THE INCH • 10 X 15 INCHES

Chart 15

Y(Load)
100,000 lbs./10v
Plotter: 1V/10 div.

$\dfrac{1000\ lbs.}{div.}$

X(Deflection)
0.5in./10V
Plotter: 0.1V/10 div.

$\dfrac{.0005\ in.}{div.}$

Configuration (k)
16 Washers Total

- Cycle 1
- Cycle 2
- Cycle 3
- Cycle 4
- Cycle 5

12/13/93

12/13/93

- Cycle 1

- Cycle 2

- Cycle 3

- Cycle 4

- Cycle 5

Y(Load)
100,000 lbs./10V
Plotter: 2V/10 div.

X(Deflection)
0.5in./10V
0.5V/10 div.

2000 lbs.
div.

.0005 in.
div.

Configuration (I)
20 Washers Total

Chart 16

12-16-93

5

- Cycle 1

Y (Load)
100,000 lbs./10V
Plotter: 1V/10 div.

X (Deflection)
0.5 in./10 V
Plotter: .5V/10 div.

$\dfrac{1000 \text{ lbs.}}{\text{div.}}$

$\dfrac{.0025 \text{ in.}}{\text{div.}}$

Configuration (m)
(32 washers total)

Used washers from
configurations f & h

2

3

4

Configuration m
(4) Parallel stacks of 8
32 total

APPENDIX C

BELLEVILLE WASHER DAMPING CHARACTERIZATION

J. G. Arendts

INTENTIONALLY LEFT BLANK.

APPENDIX C

BELLEVILLE WASHER DAMPING CHARACTERIZATION

Unloaded initial displacement ringdown of the Belleville washers is examined herein to ascertain the damping behavior of the Eaton Throat-Valve Element Prototype (ETVE). The ideal spring behavior assumed is that described in Appendix A of this report. I wrote a simple FORTRAN program to use the ETVE mechanical motion subroutines described in Appendix D. Ringdown behavior of both ETVE opening and closing Belleville washer stacks is observed; we see that overload of either washer significantly reduces its effective damping.

Ringdown Model

Figure C-1 illustrates the mechanical motion ringdown model used. A single degree-of-freedom mass is allowed to oscillate between two identical ideal Belleville washers. Mass and washer stiffness properties are those defined in Appendix A of this report. An initial displacement, $y(0)$, is imposed, followed by free oscillation of the mass. Figure C-2 illustrates a typical ringdown displacement history for an idealized Belleville washer subjected to moderate initial displacement. Observe that the absolute values of succeeding displacement relative minima and maxima decrease with respect to the absolute values of time.

Damping Models

Again, referring to Figure C-2, the envelope curve tangent to the displacement history relative maxima is defined to be $Y(t)$. If, for a simple washer-mass system, $Y(t)$ is linear with respect to time, the damping behavior is termed Coulomb or friction damping, having the following description, $Y_c(t)$:

$$Y_c(t) = y(0) - F_c\left(\frac{T}{\pi^2 M}\right) t$$

where

$y(0)$ = The initial displacement

F_c = The Coulomb damping force

M = The mass of the system

T = The natural vibration period.

Thus, if the mass is known and the period is measured from the actual decay curve, the equivalent Coulomb damping force may be found through substituting $y(t)$ and a relative maxima and corresponding time into the above relationship.

An exponentially decaying definition, $Y_v(t)$, of the envelope defines classical viscous damping of

$$Y_v(t) = y(0)\sqrt{\frac{1}{1-\zeta^2}}\; e^{\frac{-2\pi\zeta t}{T}}$$

a simple washer-mass-dashpot system:
where

ζ = the viscous critical damping ratio

T = the natural vibration period.

In this case, z is easily found by means of a technique termed logarithmic decrement; if the natural logarithm of the ratio of adjacent relative maxima or minima of $y(t)$ is found,

$$\zeta = \frac{1}{2\pi}\; \ln\left[\frac{y(\bar{t})}{y(\bar{t}+T)}\right]$$

History Calculations

A simple FORTRAN program, listed in Table C-1, numerically determines the ringdown behavior of an ideal Belleville washer. Force-displacement behavior of the ideal washer, as described in Appendix D of this report, is defined in BLOCK

---

a. Figures and tables are found in a section beginning on page 5.

DATA (respectively listed in Tables C-2 and C-3 for the opening and closing washers). Variables input during program execution are initial displacement, calculation duration, and file output interval. ASCII file output records consist of the following: time, displacement, velocity, and acceleration.

Opening Belleville Washer

Figures C-3 and C-4 illustrate results of two ringdown calculations for the opening Belleville washer (12 washers). The first figure represents behavior where the initial displacement is set to be d3 (idealized characterization data, Appendix D) which represents normal loading of the washer. The second figure represents behavior where initial displacement is greater than d3 (overloaded condition). It is seen that effective damping is significantly reduced for the overload case. Also, it is seen that the damping envelope is essentially linear, which indicates that the equivalent simple washer-mass damping is predominantly frictional (Coulomb). If the mass of the moving parts of the ETVE is taken to be 0.0324 lbf-s2/in., then, from Figure C-3 (T = 0.0023 s, y(0) = 0.0327 in., Yc(0.0043 s) = 0.0159 in.), the equivalent Coulomb damping force for normal Belleville washer ringdown is

$$F_{cn} = 540 \text{ lbf.}$$

However, from Figure C-4, if the initial displacement of the Belleville washer is increased to 0.050 in., damping is significantly reduced. In this case, the equivalent damping force is approximately

$$F_{co} = 310 \text{ lbf} .$$

Logarithmic decrement of the latter relative maxima and minima from Figure F-3 results in an average equivalent critical viscous damping ratio:

$$\zeta_n = 0.066 \quad .$$

Closing Belleville Washer

Figures C-5 and C-6 present the results of ringdown calculations for the ETVE closing Belleville washer (4 washers). Again, the first figure illustrates results for initial displacement, representing normal loading on the washer. The second figure depicts results of an overload condition is. In this case, the ratio of the overload initial displacement to the normal initial displacement is not as great as this ratio was for the opening washer comparison. We see that the reduction of equivalent damping is not as great as in the opening washer comparison. Coulomb damping force calculations, similar to those previously performed, indicate
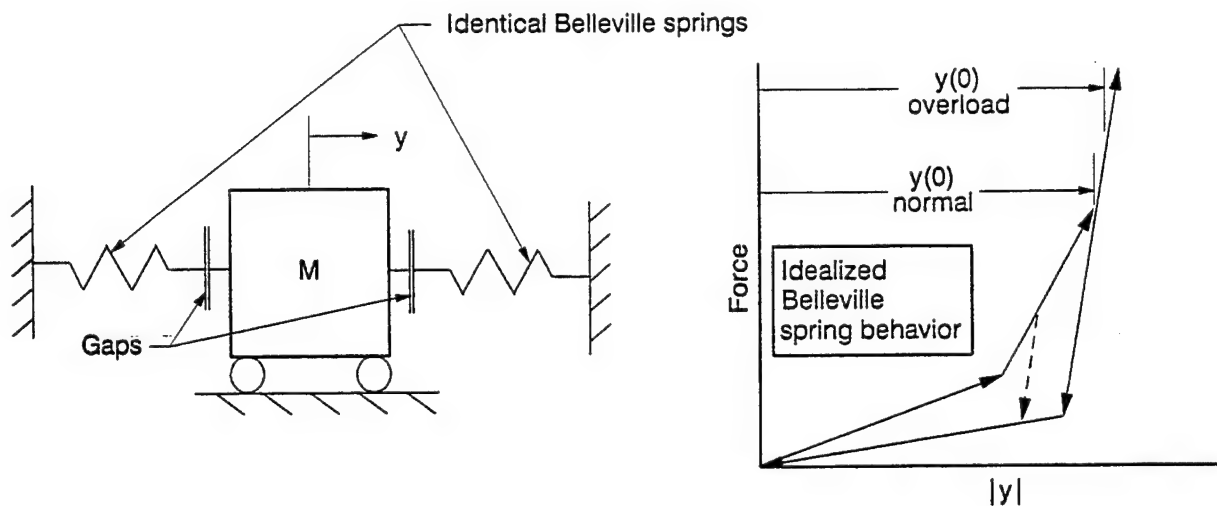
$$F_{cn} = 360 \text{ lbf}$$
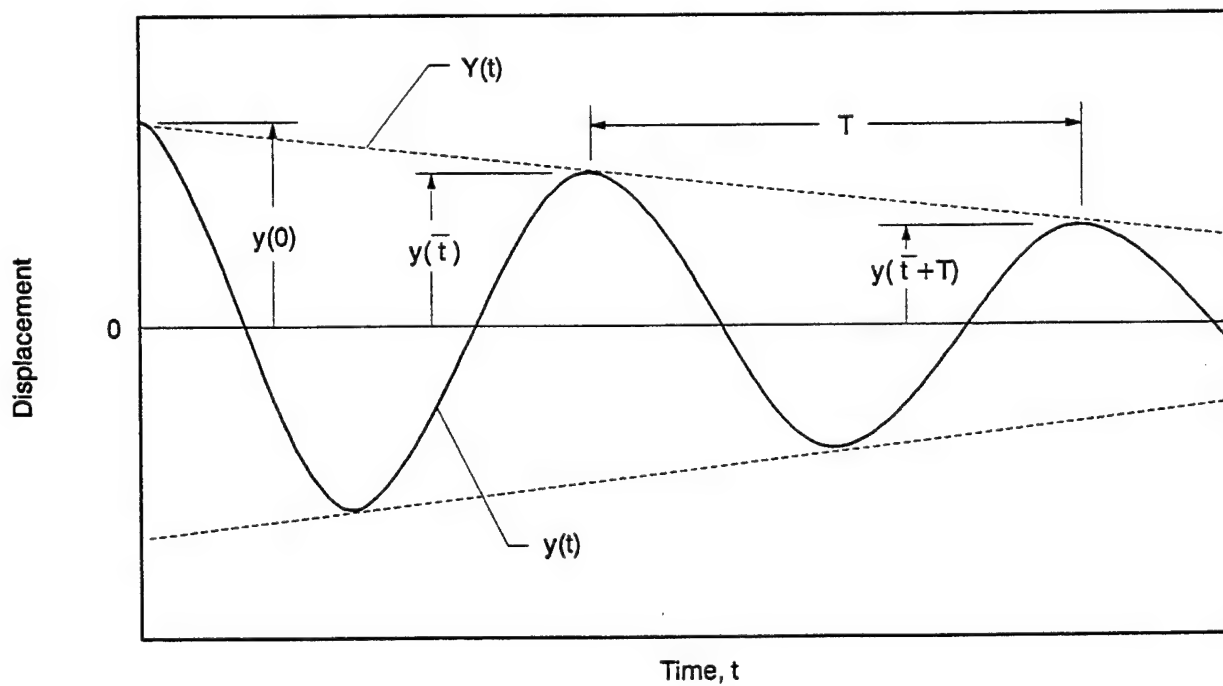
$$F_{co} = 240 \text{ lbf} .$$

Logarithmic decrement calculations for the normally loaded ringdown case result in an average equivalent viscous critical damping ratio:
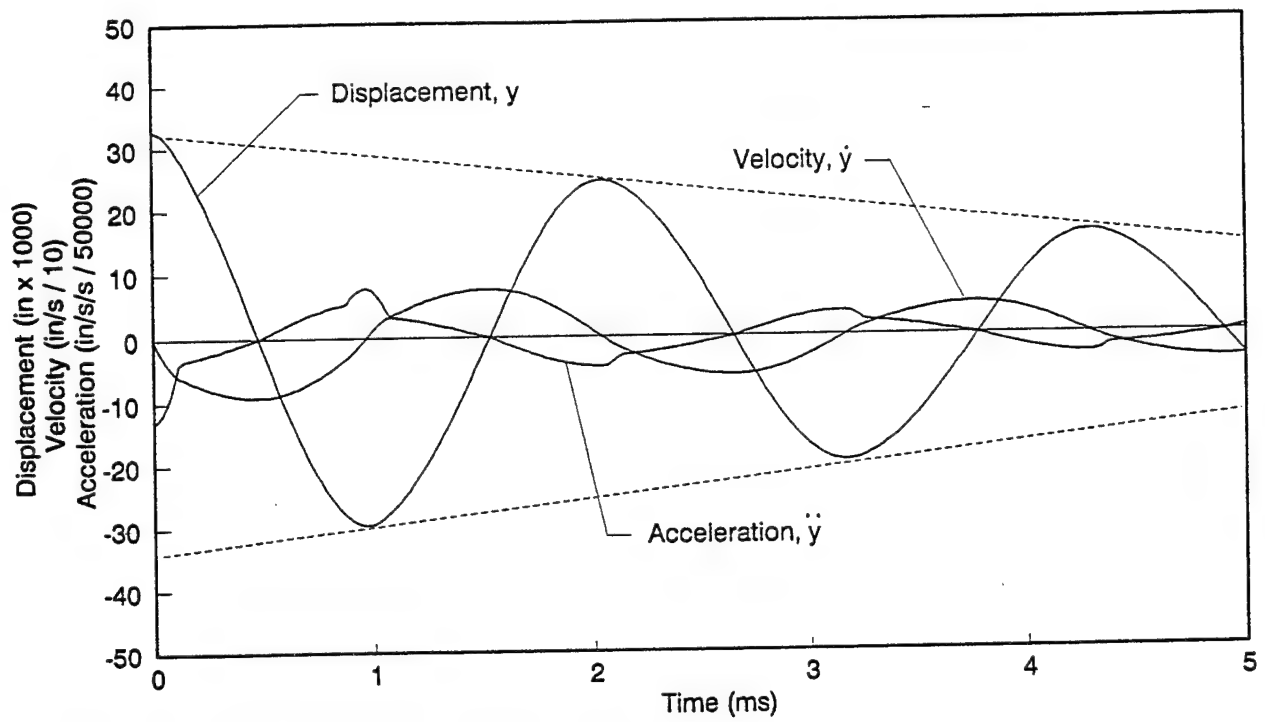
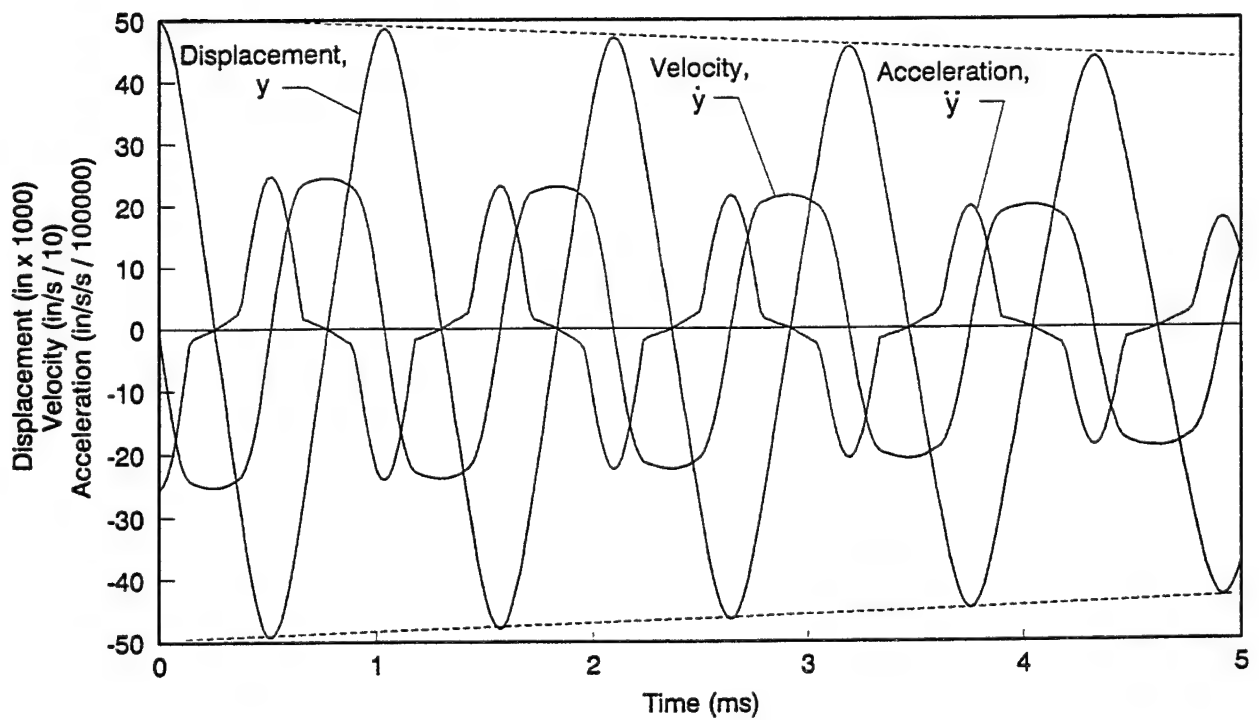$$\zeta_n = 0.055 .$$

Figures and Tables

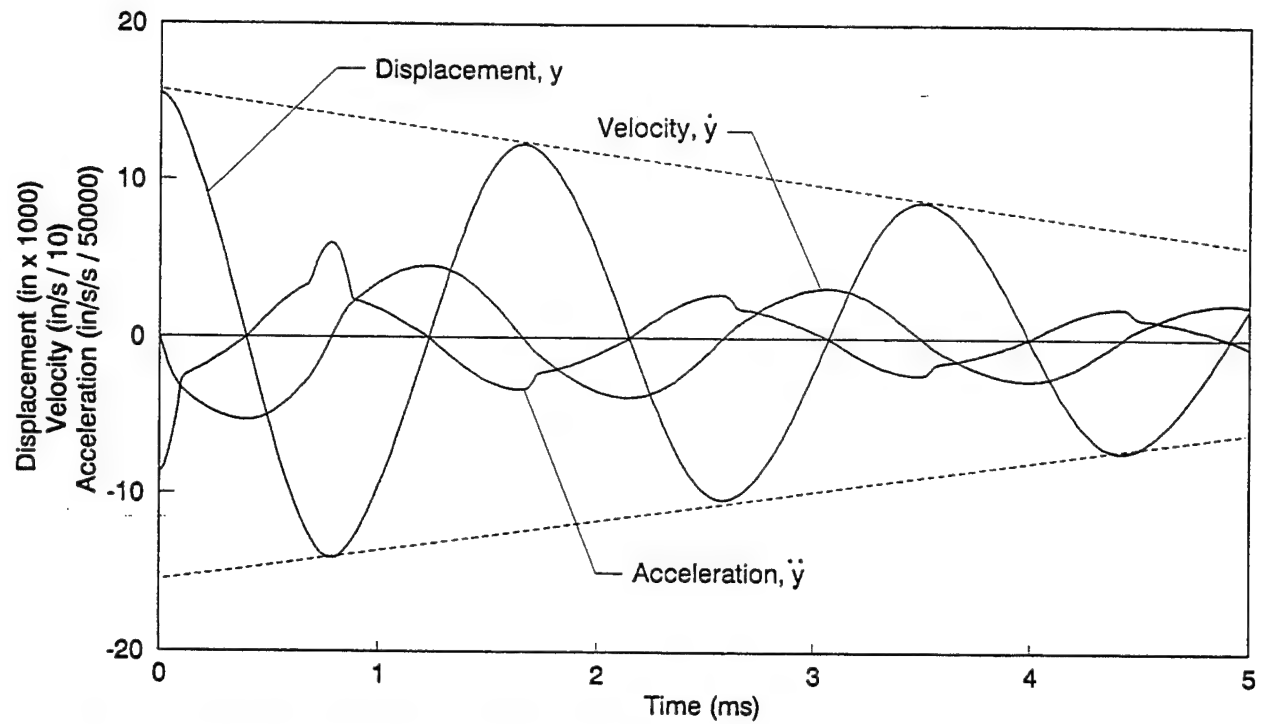**Figure C-1.** Belleville washer ringdown model.

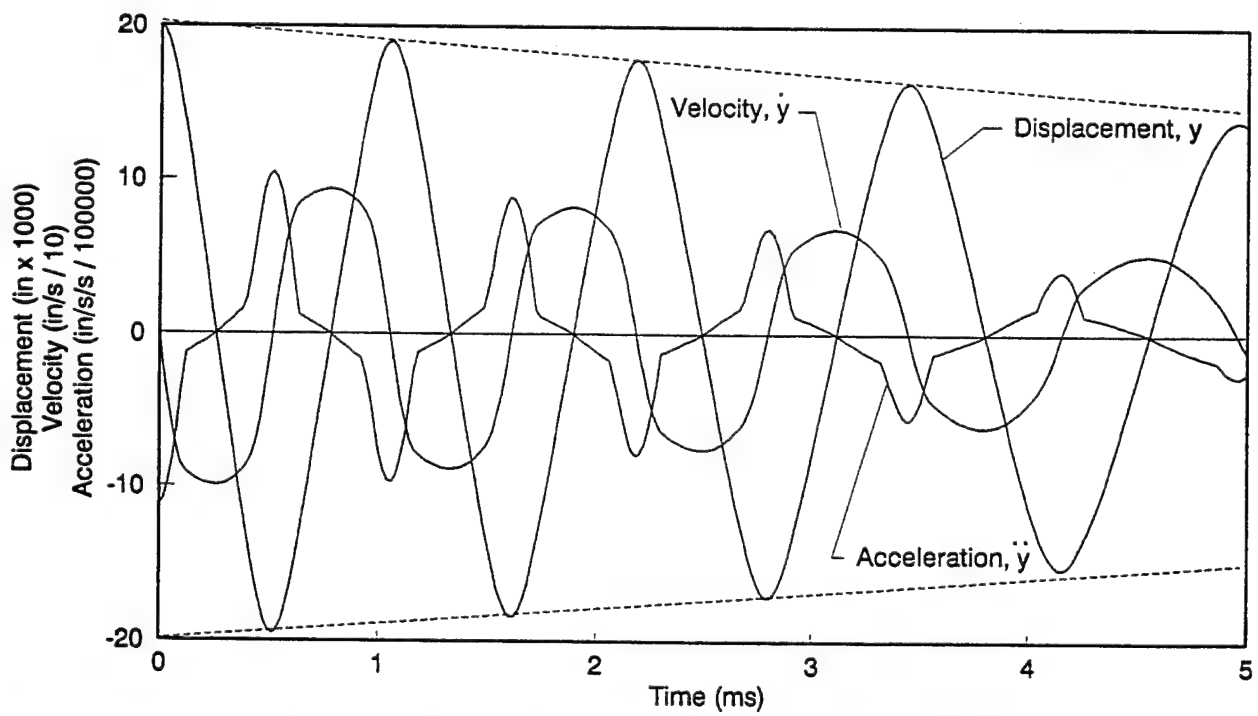**Figure C-2.** Typical Belleville washer damping behavior.

Figure C-3. Normal ringdown—opening Belleville washer.

Figure C-4. Overload ringdown—opening Belleville washer.

Figure C-5. Normal ringdown—closing Belleville washer.

Figure C-5. Overload ringdown—closing Belleville washer.

Table C-1. Belleville Spring Ringdown Program Listing -

```
C       Program damp --- Calculates Belleville spring ringdown history.
C           An initial displacement is specified for a mass located
C           between two identical Belleville springs and allowed to
C           oscillate with no external applied force.
C           Displacement, velocity, and acceleration are calculated and
C           output to file for subsequent analysis.

C       Developed in support of ETVE behavior coupled hydrodynamic -
C           mechanical motion prediction code for U.S. Army.

C       J. G. Arendts, INEL/EG&G Idaho, Dec. 1993.

        PROGRAM damp
        IMPLICIT REAL*8 (a-h, o-z)
        CHARACTER*12 z_fout
        COMMON /mtn/       tmass, gap_sc, gap_so,  f_act,
       &                   f_cdc,  f_cdb,  s_csp,  c_csp,  c_bsp,
       &                   d_cur,  d_upd,  v_cur,  v_upd,  a_cur,  a_upd
        COMMON /bspr/   f1_bsc, f2_bsc, f3_bsc, f1_bso,  f2_bso, f3_bso,
       &                d1_bsc, d2_bsc, d3_bsc, d1_bso,  d2_bso, d3_bso,
       &                s1_bsc, s2_bsc, s3_bsc, s4_bsc,
       &                s1_bso, s2_bso, s3_bso, s4_bso

C *** Calculate Belleville spring characteristics ***

        CALL belspr

C *** Open output file ***

        PRINT *, 'Output File Name: '
        READ *, z_fout
        OPEN (UNIT=2, FILE=z_fout)

C *** Input data ***

        PRINT *, 'Initial Displacement: '
        READ *, d_upd
        PRINT *, 'Calculation Duration: '
        READ *, t_end
        PRINT *, 'Output Interval: '
        READ *, t_del
```

Table C-1. (continued)

```
C *** Initialize ***

      iu_flg = 0

C *** Time loop ***

      time = - t_del
   10 time = time + t_del
      d_cur = d_upd
      v_cur = v_upd
      a_cur = a_upd
      WRITE (2,FMT=' (4E20.6)') time, d_cur, v_cur, a_cur
      CALL motion (time, t_del, 0.0, iu_flg)

C *** End time loop **

      IF (time.LT.t_end) GO TO 10
      CLOSE (2)
      STOP
      END
```

Table C-2. Opening Spring Ringdown Block Data Listing

```
      BLOCK DATA
      IMPLICIT REAL*8 (a-h, o-z)
      COMMON /mtn/    tmass, gap_sc, gap_so,  f_act,
     &                f_cdc,  f_cdb,  s_csp,  c_csp,  c_bsp,
     &                d_cur, d_upd, v_cur, v_upd, a_cur, a_upd
      COMMON /bspr/  f1_bsc, f2_bsc, f3_bsc, f1_bso, f2_bso, f3_bso,
     &               d1_bsc, d2_bsc, d3_bsc, d1_bso, d2_bso, d3_bso,
     &               s1_bsc, s2_bsc, s3_bsc, s4_bsc,
     &               s1_bso, s2_bso, s3_bso, s4_bso
      DATA            tmass, gap_sc, gap_so, f_act
     &             / 0.0324,    0.0, 1.0E-6,  0.0                    /
      DATA            f_cdc,  f_cdb,  s_csp,  c_csp,  c_bsp
     &             /   0.0,    0.0,    8.0,    0.0,    0.0       /
      DATA            d_cur,  d_upd,  v_cur,  v_upd,  a_cur,  a_upd
     &             /   0.0,    0.0,    0.0,    0.0,    0.0,    0.0/

C *** Initialize Belleville spring force-displacement data here ***

      DATA            f1_bsc, f2_bsc, f3_bsc, f1_bso, f2_bso, f3_bso
```

```
      &                / 8.5E+3, 5.5E+3, 2.1E+4, 8.5E+3, 5.5E+3, 2.1E+4/
      DATA              dl_bsc, d2_bsc, d3_bsc, dl_bso, d2_bso, d3_bso
      &                / 0.0280, 0.0285, 0.0328, 0.0280, 0.0285, 0.0328/

C ******************************************************************

      DATA             s1_bsc, s2_bsc, s3_bsc, s4_bsc
      &                /   0.0,    0.0,    0.0,    0.0              /
      DATA             s1_bso, s2_bso, s3_bso, s4_bso
      &                /   0.0,    0.0,    0.0,    0.0              /
      END
```

Table C-3.   Closing spring ringdown block data list.

```
      BLOCK DATA
      IMPLICIT REAL*8 (a-h, o-z)
      COMMON /mtn/     tmass, gap_sc, gap_so,  f_act,
      &                 f_cdc,  f_cdb,  s_csp,  c_csp,  c_bsp,
      &                 d_cur,  d_upd,  v_cur,  v_upd,  a_cur,  a_upd
      COMMON /bspr/   f1_bsc, f2_bsc, f3_bsc, f1_bso, f2_bso, f3_bso,
      &                 dl_bsc, d2_bsc, d3_bsc, dl_bso, d2_bso, d3_bso,
      &                 s1_bsc, s2_bsc, s3_bsc, s4_bsc,
      &                 s1_bso, s2_bso, s3_bso, s4_bso
      DATA              tmass, gap_sc, gap_so,  f_act
      &                / 0.0324,    0.0, 1.0E-6,    0.0                 /
      DATA              f_cdc,  f_cdb,  s_csp,  c_csp,  c_bsp
      &                /   0.0,    0.0,    8.0,    0.0,    0.0         /
      DATA              d_cur,  d_upd,  v_cur,  v_upd,  a_cur,  a_upd
      &                /   0.0,    0.0,    0.0,    0.0,    0.0,    0.0/

C *** Initialize Belleville spring force-displacement data here ***

      DATA             f1_bsc, f2_bsc, f3_bsc, f1_bso, f2_bso, f3_bso
      &                / 5.6E+3, 4.1E+3, 1.4E+4, 5.6E+3, 4.1E+3, 1.4E+4/
      DATA             dl_bsc, d2_bsc, d3_bsc, dl_bso, d2_bso, d3_bso
      &                / 0.0127, 0.0135, 0.0155, 0.0127, 0.0135, 0.0155/

C ******************************************************************

      DATA             s1_bsc, s2_bsc, s3_bsc, s4_bsc
      &                /   0.0,    0.0,    0.0,    0.0              /
      DATA             s1_bso, s2_bso, s3_bso, s4_bso
      &                /   0.0,    0.0,    0.0,    0.0              /
      END
```

C-10

APPENDIX D

MECHANICAL DYNAMICS SUBROUTINE
FOR THE EATON THROAT-VALVE ELEMENT PROTOTYPE

J. G. Arendts

INTENTIONALLY LEFT BLANK.

Appendix D

Mechanical Dynamics Subroutine
for the Eaton Throat-Valve Element Prototype

This appendix presents the analytical development of the mechanical dynamic model representing the Eaton Throat-Valve Element (ETVE) prototype moving parts. The ETVE's moving parts (sleeve, piston, piston rod, and Belleville washers) are analyzed, from which the equation of motion for the ETVE's configuration is derived. The resulting solution of the nonlinear equation of motion is presented as explicit time-difference equations. The paper also presents FORTRAN implementation of the motion solution, with supporting subroutines.

Analytical Model

Since all of the moving parts of the ETVE are rigidly connected and, thus, move together, we assume a single degree-of-freedom rigid body dynamic model. Figure D-1 represents the assumed model. We see that nonlinearities are introduced owing to the slide opening and closing gaps (G_{so} and G_{sc}, respectively) and Coulomb damping friction forces acting on the sliding mechanism and Belleville washers (F_{cs} and F_{cb}, respectively). Stiffness and viscous damping of the coil spring and slide mechanism are represented, respectively, as K_s and C_s. Since the closing and opening rebound Belleville washers have differing stiffness properties, their
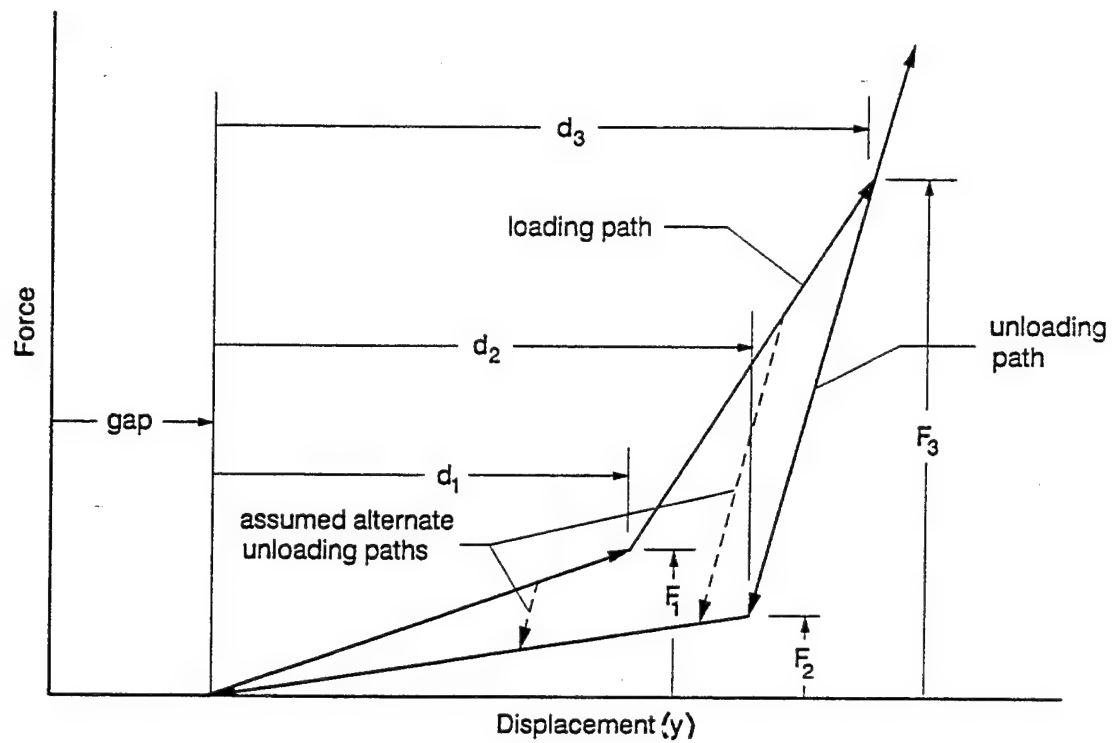
respective stiffness properties are represented as K_{bc} and K_{bo}. Viscous damping of the Belleville washers is represented as C_b. Finally, externally applied force, resulting from time-dependent actuator pressure and hydrodynamic gas pressure (both time- and slide position-dependent), is represented as $F_p(y,t)$.

Belleville Spring Characterization

Quasi-static compression tests of representative ETVE Belleville spring stacks indicate significantly different loading and unloading force-displacement behavior. Figure D-2 represents idealized quadrilinear Belleville spring behavior. We see that the entire ideal behavior may be represented through specification of three force-displacement coordinate pairs, (F_i, d_i), where i = 1, 2, 3. The four stiffnesses that represent the overall Belleville spring behavior are then found as the slopes of the linear curve segments. For maximum compressive forces exceeding F_3, unloading behavior follows the bounding unloading curves. However, for maximum spring compressive forces less than F_3, initial unloading behavior is assumed to follow a curve parallel to the bounding initial unloading curve until intersection with the final bounding unloading curve, at which time unloading behavior follows the latter curve.

Figure D-1. ETVE mechanical motion model.

Figure D-2. Idealized Belleville spring behavior.

$$F_r = F_i + K(y - d_i - g)$$
$$= Ky - F_{es}$$
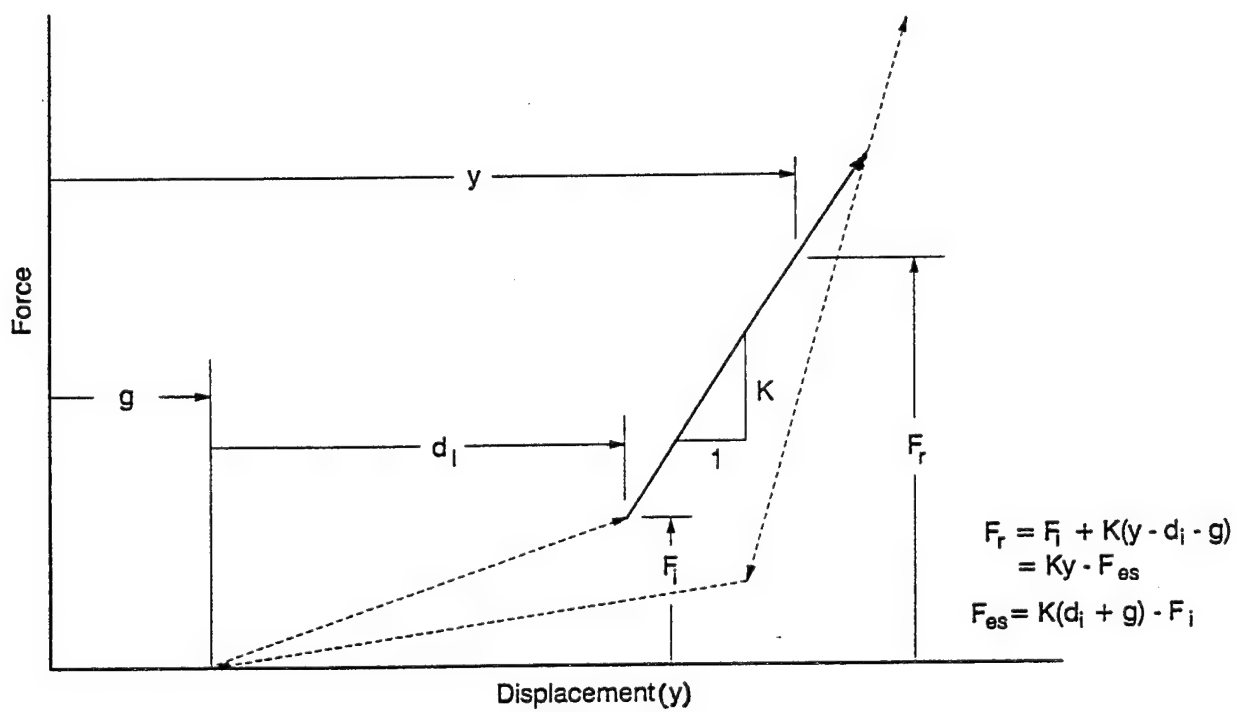$$F_{es} = K(d_i + g) - F_i$$

Figure D-3. Typical Belleville spring load segment restoring force.

D-4

Equivalent Spring Force

Since the Belleville spring force-displacement characterization curves do not necessarily pass through the origin of the force-global displacement coordinate system, the restoring force acting on the moving mass caused by the Belleville spring compression is not equal to the current global displacement multiplied by the corresponding stiffness. Figure D-3 illustrates the Belleville spring restoring force F_r, as related to global displacement, y, for a typical spring characterization curve. We see that F_r is equal to Ky less F_{es}, the equivalent spring force. Note that when neither of the gaps is closed, the equivalent spring force is zero, and the coil spring restoring force is equal to $K_s y$.

Equation of Motion

Equating restoring forces acting on the single degree-of-freedom mass (inertial, viscous damping, spring, and Coulomb friction) with the total disturbing force from actuator and hydrodynamic pressures yields the following equation of motion:

$$M\ddot{y} + C(y)\,\dot{y} + K(y)\,y - F_{es}(y) + F_c(y,\dot{y}) = F_p(y,t)$$

where

$\quad$ M = the total mass of all moving valve parts

$\quad$ C(y) = the viscous damping function

$$C(y) = C_s\,,\ -G_{sc} \le y \le G_{so}$$
$$C(y) = C_b\,,\ y < -G_{sc}\ \text{or}\ y > G_{so}$$

$\quad$ K(y) = the stiffness function

$$K(y) = K_s,\ -G_{sc} \le y \le G_{so}$$
$$K(y) = K_{bc},\ y < -G_{sc}$$
$$K(y) = K_{bo},\ y > G_{so}$$

$\quad$ $F_{es}(y)$ = the equivalent spring force function

$$F_{es}(y) = 0,\ -G_{sc} \le y \le G_{so}$$
$$F_{es}(y) = ,\ F_{es},\ y < -G_{sc}$$
$$F_{es}(y) = F_{eso},\ y > G_{so}$$

$F_c(y,\dot{y})$ = the Coulomb damping force function

$$F_c(y,\dot{y}) = 0,\ \dot{y} = 0$$
$$F_c(y,\dot{y}) = F_{cs},\ -G_{sc} \le y \le G_{so},\ \text{and}\ \dot{y} > 0$$
$$F_c(y,\dot{y}) = -F_{cs},\ -G_{sc} \le y \le G_{so},\ \text{and}\ \dot{y} < 0$$
$$F_c(y,\dot{y}) = F_{cs},\ + F_{cb},\ y > G_{sc},\ \text{or}\ y < -G_{sc},$$
$$\text{and}\ \dot{y} > 0$$
$$F_c(y,\dot{y}) = -(F_{cs} + F_{cb}),\ y > G_{so},\ \text{or}\ y < -G_{sc},$$
$$\text{and}\ \dot{y} > 0$$

$F_p(y,t) = F_h(y,t) + F_a F(t)$ is the pressure

$\quad$ induced load history

$F_h(y,t)$ is the net hydrodynamic pressure

$\quad$ load history

$F_a(t)$ is the actuation pressure load history.

Linearized Equation of Motion

If $C(y)$, $K(y)$, $F_{es}(y)$, and $F_c(y,\dot{y})$ are constant over some small time, $\bar{t}$, $0 \le \bar{t} \le \Delta t$, and are equal to C, K, F_{es}, respectively; and if

$$F(\bar{t}) = F_p(y,t) + F_{es} - F_c$$

then

$$M\frac{d^2 y}{d\bar{t}^2} + C\frac{dy}{d\bar{t}} + ky = F(\bar{t}).$$

Frequency Description

If the following frequency terms are defined,

$\quad$ Undamped natural frequency, $\omega = (k/M)^{1/2}$

$\quad$ Damping factor frequency, $\beta = C/2M$

$\quad$ Damped natural frequency, $\omega_d = (\omega^2 - \beta^2)^{1/2}$

then,

$$\frac{d^2 y}{dt^2} + 2\beta \frac{dy}{dt} + \omega^2 y = \frac{1}{M} F(t).$$

Closed Solution

The above equation has the following general solution:

$$y(\bar{t}) = e^{-\beta \bar{t}} \left[\frac{1}{\omega_d} (\dot{y}_o + \beta y_o) \sin\omega_d \bar{t} + y_o \cos\omega_d \bar{t} \right]$$

$$+ \frac{1}{M\omega_d} \int_0^{\bar{t}} F(\tau) e^{-\beta(\bar{t}-\tau)} \sin\omega_d (\bar{t}-\tau) \, d\tau$$

$$= Y_h (\bar{t})$$

$$+ y_p (\bar{t})$$

where y_o and $\dot{y}_o$ are, respectively, displacement and velocity at $\bar{t} - 0$.

Particular Integral

Since the present linearized solution is to be used for explicit time integration, the disturbing force is set to be constant over the interval, $0 \le t \le \tau$,

$$F(\tau) = F_0 .$$

or,

$$y_p (\bar{t}) = \frac{1}{M\omega_d} \int_0^{\bar{t}} F(\tau) e^{-\beta(\bar{t}-\tau)} \sin\omega_d (\bar{t}-\tau) \, d\tau$$

$$= \frac{F_o}{M\omega_d} \int_0^{\bar{t}} e^{-\beta(\bar{t}-\tau)} \sin\omega_d (\bar{t}-\tau) \, d\tau .$$

Upon integration,

$$y_p (\bar{t}) = \frac{F_o}{K} \left[1 - e^{-\beta \bar{t}} \left(\frac{\beta}{\omega_d} \sin\omega_d \bar{t} + \cos\omega_d \bar{t} \right) \right] .$$

Upon combination of the above homogeneous and particular solutions and differentiation of the result, displacement, velocity, and acceleration are, respectively,

$$y (\bar{t}) = e^{-\beta \bar{t}} \left[\left(\frac{\beta}{\omega_d} y_o + \frac{1}{\omega_d} \dot{y}_o \right) \sin\omega_d \bar{t} + y_o \cos\omega_d \bar{t} \right]$$

$$+ \frac{F_o}{K} \left[1 - e^{-\beta \bar{t}} \left(\frac{\beta}{\omega_d} \sin\omega_d \bar{t} + \cos\omega_d \bar{t} \right) \right] .$$

$$\dot{y}(\bar{t}) = \frac{dy(\bar{t})}{d\bar{t}}$$

$$= e^{-\beta \bar{t}} \left[-\left(\frac{\omega^2}{\omega_d} y_o + \frac{\beta}{\omega_d} \dot{y}_o \right) \sin\omega_d \bar{t} + \dot{y}_o \cos\omega_d \bar{t} \right]$$

$$+ \frac{F_o \omega^2 e^{-\beta \bar{t}}}{K\omega_d} \sin\omega_d \bar{t} .$$

$$\ddot{y}(\bar{t}) = \frac{d^2 y(\bar{t})}{d\bar{t}^2}$$

$$= e^{-\beta \bar{t}} \left[\left(\frac{\beta\omega^2}{\omega_d} y_o - \frac{\omega_d^2 - \beta^2}{\omega_d} \dot{y}_o \right) \sin\omega_d \bar{t} \right.$$

$$\left. - (\omega^2 y_o + 2\beta\dot{y}_o) \cos\omega_d \bar{t} \right]$$

$$+ \frac{F_o \omega^2 e^{-\beta \bar{t}}}{K} \left(-\frac{\beta}{\omega_d} \sin\omega_d \bar{t} + \cos\omega_d \bar{t} \right) .$$

Explicit Time Integration

Let

$$y_o = y(t)$$

$$\dot{y}_o = \dot{y}(t)$$

be the previously calculated displacement and velocity at time, t. Then, from the closed solution, where $\bar{t} = \delta t$,

$$y(t + \delta t) = e^{-\beta\delta t} \left[\left(\frac{\beta}{\omega_d} y(t) + \frac{1}{\omega_d} \dot{y}(t) \right) \sin (\omega_d \delta t) \right.$$

$$\left. + y(t) \cos (\omega_d \delta t) \right]$$

$$+ \frac{F(t)}{K} \left[1 - e^{-\beta\delta t} \left(\frac{\beta}{\omega_d} \sin (\omega_d \delta t) + \cos (\omega_d \delta t) \right) \right] .$$

$$\dot{y}(t + \delta t) = e^{-\beta \delta t} \left[-\left(\frac{\omega^2}{\omega_d} y(t) + \frac{\beta}{\omega_d} \dot{y}(t) \right) \sin (\omega_d \delta t) \right.$$

$$\left. + \dot{y}(t) \cos (\omega_d \delta t) \right]$$

$$+ \frac{F(t) \omega^2 e^{-\beta \delta t}}{K \omega_d} \sin (\omega_d \delta t) \ .$$

$$\ddot{y}(t + \delta t) = e^{-\beta \delta t} \left(\frac{\beta \omega^2}{\omega_d} y(t) - \frac{\omega_d^2 - \beta^2}{\omega_d} \dot{y}(t) \right) \sin (\omega_d \delta t)$$

$$- e^{-\beta \delta t} (\omega^2 y(t) + 2\beta \dot{y}(t)) \cos (\omega_d \delta t)$$

$$+ \frac{F(t) \omega^2 e^{-\beta \delta t}}{K} \left(-\frac{\beta}{\omega_d} \sin (\omega_d \delta t) + \cos (\omega_d \delta t) \right) \ .$$

Experimental Characterization

To determine the Belleville washers' ideal stiffness behavior and dynamic model overall damping characteristics, results from quasi-static Belleville spring compression tests and ETVE opening tests are used.

Belleville Spring Characterization

Figures D-4 and D-5 illustrate the force-displacement idealized Belleville spring stiffness characteristic curves used herein. The closing spring is a stack of four parallel Belleville washers, whereas the opening spring is two stacks of six washers oriented in series. Also represented are actual average test data (see Appendix B of this report). The idealized curves are determined by visual best fit to the overall test data.

Actuator Force History Characterization

I used the results from a recent ETVE opening test that used 2000-psi actuator pressure (quickly applied and having a long duration) but no driver gas volume or pressure. Figure D-6 represents a typical actuator force history derived from mea-sured actuator pressures (see Appendix A of this report). Also shown is the ideal actuator history specified for the mechanical motion model. The time and force values referred to in Figure D-6 and used in the model are

$$t_{a1} = 0.05 \text{ sec}$$
$$t_{a2} = 0.50 \text{ sec}$$
$$F_{a1} = 1425 \text{ lbf}$$
$$F_{a2} = 2850 \text{ lbf}.$$

Overall Model Damping Characterization

We obtained the system's damping characteristics by running several algorithm predictions, varying different parameters until the axial displacement history matched the actual test data obtained from the tests described above (see Appendix A of this report). We found that the following damping parameters produced a reasonable fit to the test data:

Slide Coulomb damping force = 100 lbf
Slide viscous damping ratio = 0.0
Belleville spring Coulomb damping force = 0.0
Belleville spring viscous damping ratio = 0.08.

Figure D-7 compares the calculated ETVE displacement response damping data with the test data.

Subroutine Descriptions

Three FORTRAN subroutines that support and perform the ETVE motion calculations depicted above are described here. The only significant deviation from ANSI FORTRAN-77 is in the use of underscored variable names (which will be included in ANSI FORTRAN-90). Generic names are used for intrinsic library functions, 32 bit real words are implicitly defined, and constants are defined in either floating point or "E" formats. Three named common blocks are used for global variable storage and a BLOCK DATA segment is defined for global variable value initialization. The three subroutines, namely "belspr," "fact," and "motion," are described below. BLOCK DATA is also listed.
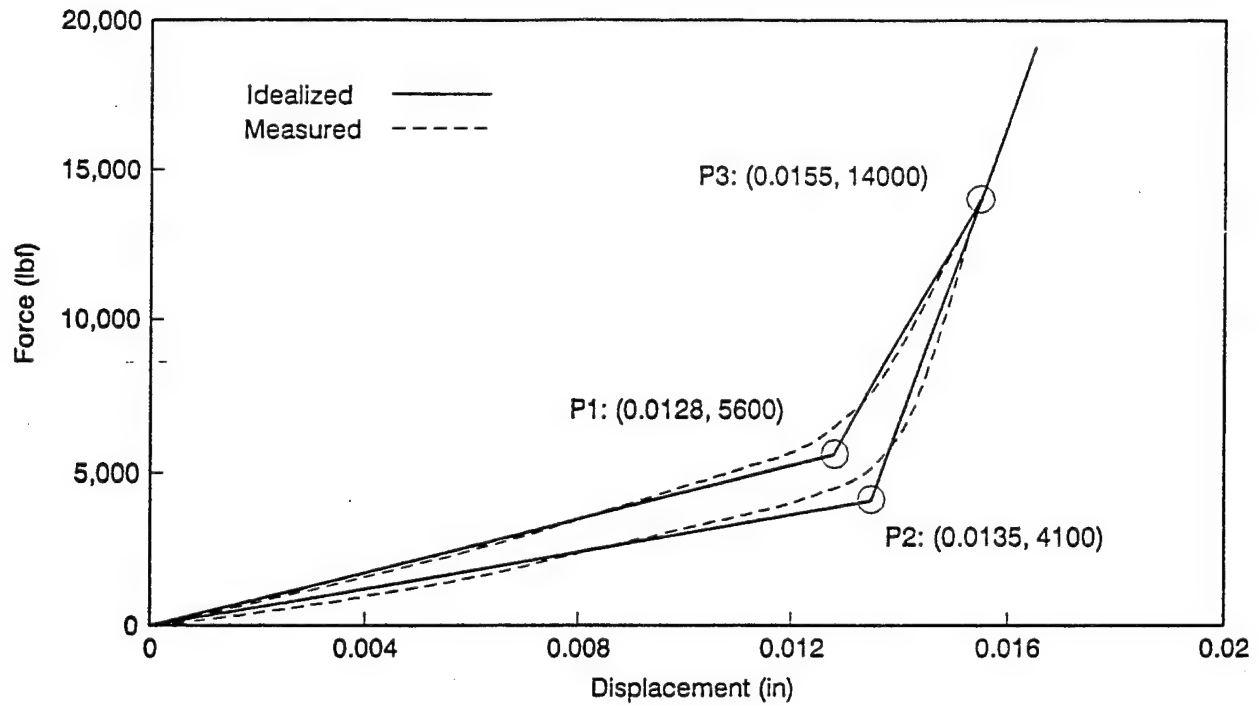
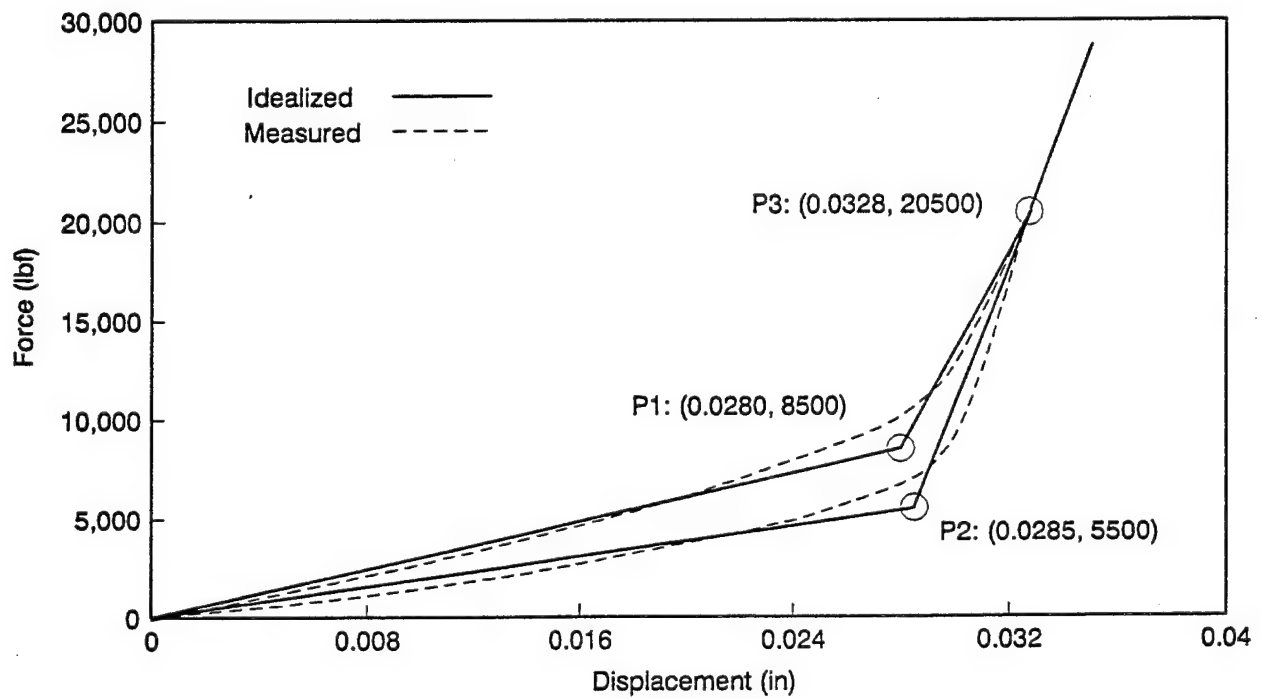Figure D-4. Belleville closing spring stiffness characteristics.

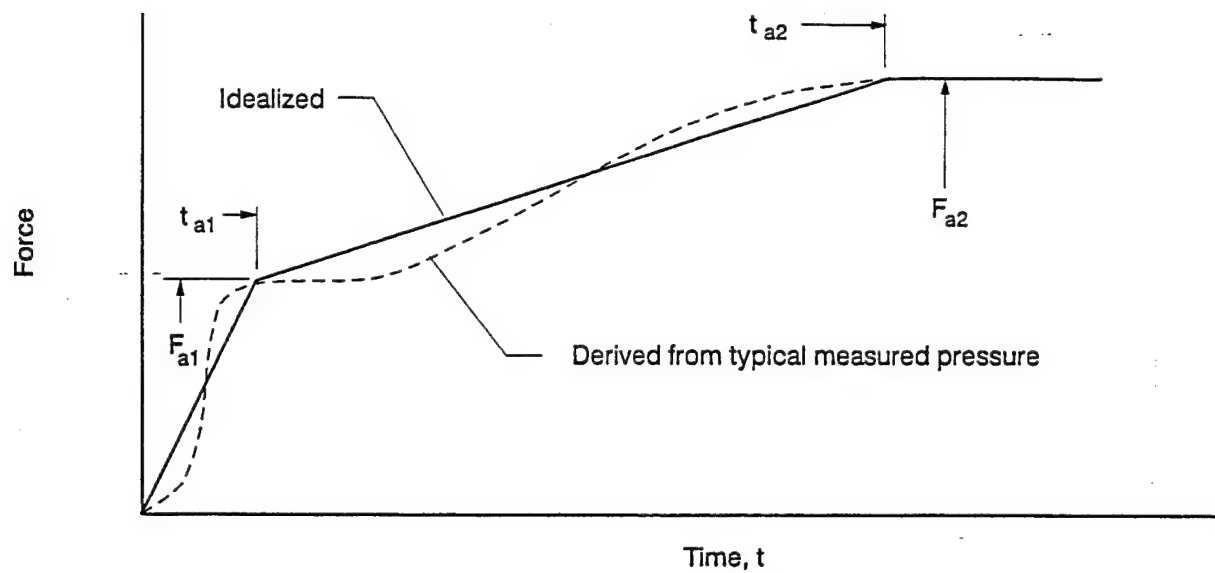Figure D-5. Belleville opening spring stiffness characteristics.
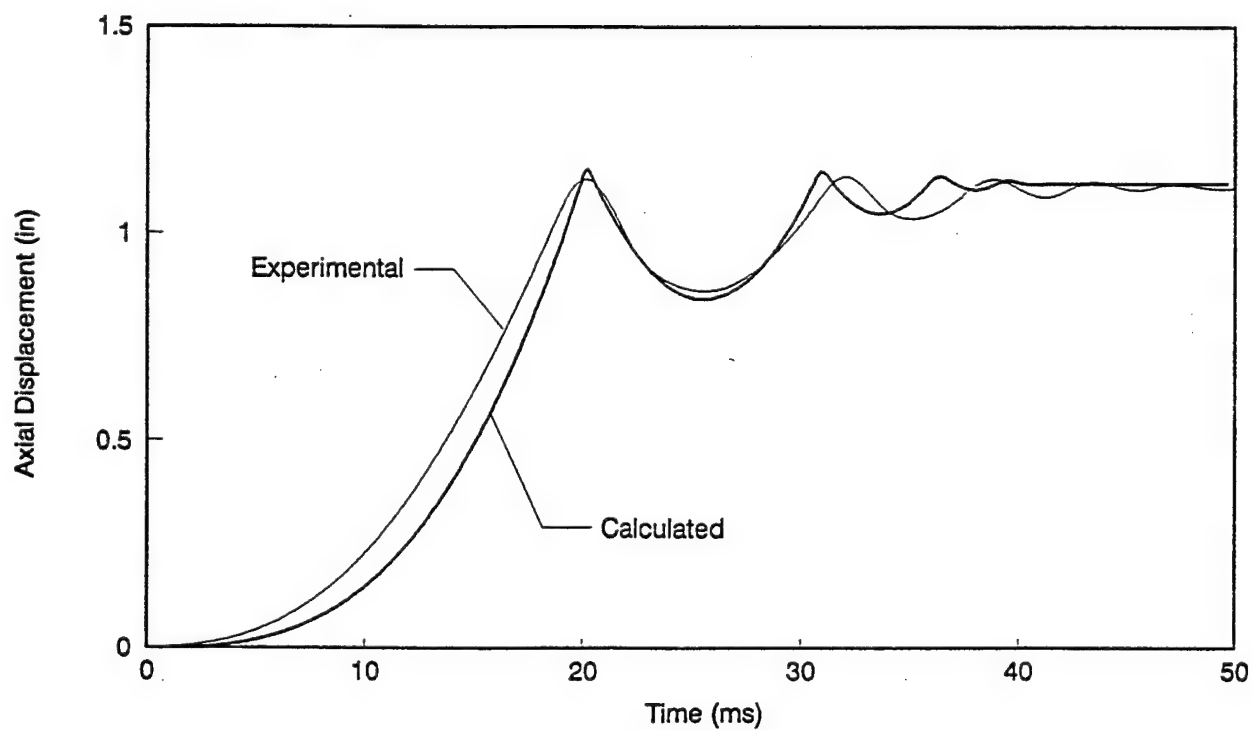
D-8

Figure D-6. Actuator force histories.

Figure D-7. ETVE opening transient displacement histories.

Subroutine "belspr"

The purpose of this subroutine is to compute the Belleville washers' stiffness from the force-displacement characterization values specified in BLOCK DATA. This subroutine is only called from the main program once (prior to first call to "motion"). The source list of this subroutine is given in Table D-1, and use of the variables is described as follows (see Figure D-2):

f1_bsc = F_1 (closing Belleville spring)
f2_bsc = F_2 (closing Belleville spring)
f3_bsc = F_3 (closing Belleville spring)
f1_bso = F_1 (opening Belleville spring)
f2_bso = F_2 (opening Belleville spring)
f3_bso = F_3 (opening Belleville spring)

d1_bsc = d_1 (closing Belleville spring)
d2_bsc = d_2 (closing Belleville spring)
d3_bsc = d_3 (closing Belleville spring)
d1_bso = d_1 (opening Belleville spring)
d2_bso = d_2 (opening Belleville spring)
d3_bso = d_3 (opening Belleville spring)
s1_bsc -
s4_bsc = calculated stiffnesses (closing Belleville spring)
s1_bso -
s4_bso = calculated stiffnesses (opening Belleville spring).

Subroutine "fact"

This subroutine calculates the current actuator force acting on the moving ETVE parts. One argu-

Table D-1. Subroutine "belspr" List.

```
C    Subroutine belspr -- Calculates Belleville spring stiffness
C            characteristics from force displacement values.

C    Developed for inclusion in ETVE behavior coupled hydrodynamic -
C    mechanical motion prediction code for U.S. Army.

C    J. G. Arendts, INEL/EG&G Idaho, Nov. 1993.

     SUBROUTINE belspr
     IMPLICIT REAL*8 (a-h, o-z)
     COMMON /bspr/ f1_bsc, f2_bsc, f3_bsc, f1_bso, f2_bso, f3_bso,
    &              d1_bsc, d2_bsc, d3_bsc, d1_bso, d2_bso, d3_bso,
    &              s1_bsc, s2_bsc, s3_bsc, s4_bsc,
    &              s1_bso, s2_bso, s3_bso, s4_bso

C *** Belleville closing spring characteristics ***

     s1_bsc = f1_bsc/d1_bsc
     s2_bsc = f2_bsc/d2_bsc
     s3_bsc = (f3_bsc-f1_bsc)/(d3_bsc-d1_bsc)
     s4_bsc = (f3_bsc-f2_bsc)/(d3_bsc-d2_bsc)

C *** Belleville opening spring characteristics ***

     s1_bso = f1_bso/d1_bso
     s2_bso = f2_bso/d2_bso
     s3_bso = (f3_bso-f1_bso)/(d3_bso-d1_bso)
     s4_bso = (f3_bso-f2_bso)/(d3_bso-d2_bso)

     RETURN
     END
```

ment is passed, the current solution time. This subroutine must be called prior to each call of "motion." The source list of this subroutine is given in Table D-2, and use of the variables is described as follows (see Figure D-6):

$$f1\_act = F_{a1}$$
$$f2\_act = F_{a2}$$
$$t1\_act = t_{a1}$$
$$t2\_act = t_{a2}$$
$$f\_act = \text{calculated current actuator force.}$$

Subroutine "motion"

This subroutine, listed in Table D-3, calculates the incremental motion of the ETVE movable parts in terms of the variables: displacement, velocity, and acceleration. Arguments passed to the subroutine are current calculation time, current time increment, net fluid dynamic force acting on the moving mass, and an integer flag, iu_flg, which indicates whether a Belleville spring is loading (iu_flg = 0) or unloading (iu_flg = 1). Note that iu_flg is not initialized in BLOCK DATA; it must be initialized to zero early in the main program.

The subroutine first determines if either of the the Belleville washers are compressed upon subroutine call or, if not, will a Belleville spring become compressed at the end of the time step. If either of the above cases are true, the motion calculational time step is reduced to $1.0 \times (10)^{-7}$ sec

and the incremental motion calculations are summarily performed until the argument passed time increment is attained. The reason for this small incremental motion calculation is due to the very large changes of the motion parameters that occur in the transition between relatively free motion (neither Belleville spring compressed) and very stiff resistance when either of the Belleville washers are compressed.

The following section of the subroutine consists of logic blocks wherein the applicable motion parameters are specified. Finally, the updated motion variables are computed. It is important to know that the subroutine does not update the current motion variables; rather, the updated (end of time increment) variables are re-computed in the subroutine. It is the responsibility of the calling program to update the current variables, either before "motion" is called, or after.

Parametric variables (mass, stiffnesses, and damping values), as well as motion variables and forces, are described in the subroutine listing and will not be repeated here.

Block Data

The purpose of BLOCK DATA, listed in Table D-4, is to initialize all global variables. General motion and spring parameters are specified here. Changes to these parameter values are easily made in the source module (with recompilation).

Table D-2. Subroutine "fact" List.

```
C      Subroutine fact --- Calculates actuator force as a function
C            of current time.

C      Developed for inclusion in ETVE behavior coupled hydrodynamic -
C            mechanical motion prediction code for U.S. Army.

C      J. G. Arendts, INEL/EG&G Idaho, Nov. 1993.
```

```
                     SUBROUTINE fact (time)
                     IMPLICIT REAL*8 (a-h, o-z)
                     COMMON /fac/    f_act, f1_act, f2_act, t1_act, t2_act


         C *** Current actuator force ***

                     IF ( time.LT.t1_act ) THEN
                         f_act = f1_act*time/t1_act
                     ELSE IF ( time.GT.t2_act ) THEN
                         f_act = f2_act
                     ELSE
                         f_act = f1_act+(f2_act-f1_act)*(time-t1_act)/(t2_act-t1_act)
                     ENDIF

                     RETURN
                     END
```

Table D-3. Subroutine "motion" list.

```
         C      Subroutine motion --- Calculates and updates displacement,
         C          velocity, and acceleration of single degree-of-freedom,
         C          damped, and forced (constant over time step)
         C          dynamic mechanical system.  A closed-form solution of
         C          equation-of-motion is utilized for explicit time integration.


         C      Developed for inclusion in ETVE behavior coupled hydrodynamic -
         C          mechanical motion prediction code for U.S. Army.


         C      J. G. Arendts, INEL/EG&G Idaho, Nov. 1993.


         C      Argument passed variables:
         C          time     = current absolute time (sec)
         C          t_del    = time increment (sec)
         C          f_hyd    = current net hydrodynamic force (lbf)
         C          iu_flg   = Belleville spring unlaoding flag (= 1 if unloading)


         C      Named common (motion) variables:
         C          tmass    = total mass of moving parts (lbf-sec**2/in)
         C          gap_sc   = slide closing gap (ref. to undisplaced position - in.)
         C          gap_so   = slide opening gap (ref. to undisplaced position - in.)
         C          f_act    = current actuator force (lbf)
         C          f_cdc    = coil spring Coulomb damping force (lbf)
         C          f_cdb    = Belleville spring (both) Coulomb damping force (lbf)
         C          s_csp    = coil spring stiffness (lbf/in)
         C          c_csp    = coil spring viscous critical damping ratio (dim.-less)
         C          c_bsp    = Belleville spring viscous critical damping ratio (")
         C          d_cur    = current displacement (in.)
         C          d_upd    = updated displacement (in.)
         C          v_cur    = current velocity (in/sec)
         C          v_upd    = updated velocity (in/sec)
```

```
C        a_cur    = current acceleration (in/sec**2)
C        a_upd    = updated acceleration (in/sec**2)

C     Calculated volatile variables:
C        fre_u    = undamped natural frequency (rad/sec)
C        fre_d    = damped natural frequency (rad/sec)
C        beta     = damping factor frequency (rad/sec)
C        f_cd     = velocity dependent Coulomb damping force (lbf)
C        f_es     = effective gap-closure spring force (lbf)

      SUBROUTINE motion (time, t_del, f_hyd, iu_flg)
      IMPLICIT REAL*8 (a-h, o-z)

      COMMON /mtn/    tmass,  gap_sc,  gap_so,
     &                f_cdc,  f_cdb,   s_csp,   c_csp,   c_bsp,
     &                d_cur,  d_upd,   v_cur,   v_upd,   a_cur,   a_upd
      COMMON /fac/    f_act, f1_act, f2_act, t1_act, t2_act
      COMMON /bspr/   f1_bsc, f2_bsc, f3_bsc, f1_bso, f2_bso, f3_bso,
     &                d1_bsc, d2_bsc, d3_bsc, d1_bso, d2_bso, d3_bso,
     &                s1_bsc, s2_bsc, s3_bsc, s4_bsc,
     &                s1_bso, s2_bso, s3_bso, s4_bso
      SAVE f2_bst, d2_bst

C *** Net external force ***

      f_ex = f_hyd + f_act

C *** Initialize ***

      tt = t_del
      tt_sum = 0.0
      d1 = d_cur
      v1 = v_cur
      g_sc = -gap_sc
      g_so = gap_so

C *** Set gap boundary and Belleville spring compression flags ***

      i_flg = 0
      IF ( d_cur.GT.g_so .OR. d_cur.LT.g_sc ) i_flg = 1
  10  j_flg = 0
      IF ( i_flg.EQ.1 .AND. t_del.GT.1.0E-07 ) tt = 1.0E-07

C *** Current stiffness, damping, and effective forces ***

  20  IF ( d1.GT.g_so ) THEN

C *** Belleville opening spring is active ***

          beta = c_bsp
          f_cd = f_cdc + f_cdb
          d_rel = d1 - g_so
          f_so = s_csp*g_so
          IF ( v1.GE.0.0 ) THEN
```

```
C *** The spring is loading ***

            iu_flg = 0
            IF ( d_rel.GT.d3_bso ) THEN
                stif = s4_bso
                f_es = s4_bso*(g_so+d3_bso) - f_so - f3_bso
            ELSE IF ( d_rel.LT.d1_bso ) THEN
                stif = s1_bso
                f_es = s1_bso*g_so - f_so
            ELSE
                stif = s3_bso
                f_es = s3_bso*(g_so+d1_bso) - f_so - f1_bso
            ENDIF

            ELSE

C *** The spring is unloading ***

                IF ( iu_flg.EQ.0 ) THEN

C *** Do this only for the initial unload step

                iu_flg = 1
                IF ( d_rel.LT.d1_bso ) THEN
                    d2_bst = d_rel*(s4_bso-s1_bso)/(s4_bso-s2_bso)
                    f2_bst = s2_bso*d2_bst
                ELSE IF ( d_rel.LT.d3_bso ) THEN
                    d2_bst = d_rel*(s4_bso-s3_bso) + d1_bso*s3_bso
                    d2_bst = (d2_bst-f1_bso)/(s4_bso-s2_bso)
                    f2_bst = s2_bso*d2_bst
                ELSE
                    d2_bst = d2_bso
                    f2_bst = f2_bso
                ENDIF
            ENDIF
            IF ( d_rel.GT.d2_bst ) THEN
                stif = s4_bso
                f_es = s4_bso*(g_so+d2_bst) - f_so - f2_bst
            ELSE
                stif = s2_bso
                f_es = s2_bso*g_so - f_so
            ENDIF
        ENDIF
    ELSE IF ( d1.LT.g_sc ) THEN

C *** Belleville closing spring is active ***

        beta = c_bsp
        f_cd = f_cdc + f_cdb
        d_rel = -d1 - gap_sc
        f_sc = s_csp*gap_sc
        IF ( v1.LE.0.0 ) THEN
```

```
C *** The spring is loading ***

            iu_flg = 0
            IF ( d_rel.GT.d3_bsc ) THEN
                stif = s4_bsc
                f_es = -s4_bsc*(gap_sc+d3_bsc) + f_sc + f3_bsc
            ELSE IF ( d_rel.LT.d1_bsc ) THEN
                stif = s1_bsc
                f_es = -s1_bsc*gap_sc + f_sc
            ELSE
                stif = s3_bsc
                f_es = -s3_bsc*(gap_sc+d1_bsc) + f_sc + f1_bsc
            ENDIF
        ELSE

C *** The spring is unloading ***

            IF ( iu_flg.EQ.0 ) THEN
                iu_flg = 1
                IF ( d_rel.LT.d1_bsc ) THEN
                    d2_bst = d_rel*(s4_bsc-s1_bsc)/(s4_bsc-s2_bsc)
                    f2_bst = s2_bsc*d2_bst
                ELSE IF ( d_rel.LT.d3_bsc ) THEN
                    d2_bst = d_rel*(s4_bsc-s3_bsc) + d1_bsc*s3_bsc
                    d2_bst = (d2_bst-f1_bsc)/(s4_bsc-s2_bsc)
                    f2_bst = s2_bsc*d2_bst
                ELSE
                    d2_bst = d2_bsc
                    f2_bst = f2_bsc
                ENDIF
            ENDIF
            IF ( d_rel.GT.d2_bst ) THEN
                stif = s4_bsc
                f_es = -s4_bsc*(gap_sc+d2_bst) + f_sc + f2_bst
            ELSE
                stif = s2_bsc
                f_es = -s2_bsc*gap_sc + f_sc
            ENDIF
        ENDIF
    ELSE

C *** Only the coil spring is active ***

        stif = s_csp
        beta = c_csp
        f_es = 0.0
        f_cd = f_cdc
    ENDIF

C *** Displacement and velocity dependent properties and forces ***

    fre_u = SQRT(stif/tmass)
    beta = beta*fre_u
    fre_d = SQRT(fre_u**2-beta**2)
    IF ( v1.GE.0.0 ) f_cd = -f_cd
```

D-15

```
            IF ( time.LT.tl_act ) f_cd = f_cd*f_act/fl_act
            f_tot = f_ex + f_cd + f_es

C *** Exponential and trig factors ***

            fac_e = EXP(-beta*tt)
            fac_s = SIN(fre_d*tt)
            fac_c = COS(fre_d*tt)

C *** Updated or incremental displacement ***

            d2 = fac_e *(fac_s *(d1*beta/fre_d + v1/fre_d) + fac_c*d1)
            d2 = d2 + f_tot*(1.0 - fac_e *(fac_s*beta/fre_d + fac_c))/stif

C *** Check gap boundary crossings ***

            IF ( i_flg.EQ.0 ) THEN
                IF ( d2.GT.g_so .OR. d2.LT.g_sc ) THEN
                    i_flg = 1
                    j_flg = 1
                ENDIF
            ENDIF
            IF ( j_flg.EQ.1 ) GO TO 10

C *** Updated or incremental velocity ***

            v2 = -fac_s *(d1*fre_u**2/fre_d + v1*beta/fre_d)
            v2 = fac_e *(v2 + fac_c*v1)
            v2 = v2 + f_tot*fac_e*fac_s*fre_u**2/stif/fre_d

C *** Updated or incremental acceleration ***

            a2 = d1*beta*fre_u**2/fre_d - v1 *(fre_d**2 - beta**2)/fre_d
            a2 = fac_e *(a2*fac_s - fac_c *(d1*fre_u**2 + 2.0*v1*beta))
            a2 = a2 + f_tot*fre_u**2*fac_e *(-fac_s*beta/fre_d + fac_c)/stif

C *** Check for end of step ***

            d1 = d2
            v1 = v2
            tt_sum = tt_sum + tt
            IF ( tt_sum.LT.t_del ) GO TO 20

C *** Finish-up ***

            d_upd = d2
            v_upd = v2
            a_upd = a2

            RETURN
            END
```

```
      BLOCK DATA
      IMPLICIT REAL*8  (a-h, o-z)
      COMMON /mtn/      tmass, gap_sc, gap_so,
     &                  f_cdc,  f_cdb,  s_csp,  c_csp,  c_bsp,
     &                  d_cur,  d_upd,  v_cur,  v_upd,  a_cur,  a_upd
      COMMON /fac/      f_act, f1_act, f2_act, t1_act, t2_act
      COMMON /bspr/     f1_bsc, f2_bsc, f3_bsc, f1_bso, f2_bso, f3_bso,
     &                  d1_bsc, d2_bsc, d3_bsc, d1_bso, d2_bso, d3_bso,
     &                  s1_bsc, s2_bsc, s3_bsc, s4_bsc,
     &                  s1_bso, s2_bso, s3_bso, s4_bso

C **** Initialize general motion parameters here ******************

      DATA              tmass, gap_sc, gap_so
     &          / 0.0324,    0.0,   1.12                          /
      DATA              f_cdc,  f_cdb,  s_csp,  c_csp,  c_bsp
     &          /  100.0,    0.0,    8.0,    0.0,   0.08          /
      DATA              d_cur,  d_upd,  v_cur,  v_upd,  a_cur,  a_upd
     &          /    0.0,    0.0,    0.0,    0.0,    0.0,    0.0/

C **** Initialize actuator force data here ************************

      DATA              f_act, f1_act, f2_act, t1_act, t2_act
     &          /    0.0, 1425.0, 2850.0,   0.05,    0.5          /

C **** Initialize Belleville spring force-displacement data here ***

      DATA              f1_bsc, f2_bsc, f3_bsc, f1_bso, f2_bso, f3_bso
     &          / 5.6E+3, 4.1E+3, 1.4E+4, 8.5E+3, 5.5E+3, 2.1E+4/
      DATA              d1_bsc, d2_bsc, d3_bsc, d1_bso, d2_bso, d3_bso
     &          / 0.0127, 0.0135, 0.0155, 0.0280, 0.0285, 0.0327/

C  *****************************************************************

      DATA              s1_bsc, s2_bsc, s3_bsc, s4_bsc
     &          /    0.0,    0.0,    0.0,    0.0                   /
      DATA              s1_bso, s2_bso, s3_bso, s4_bso
     &          /    0.0,    0.0,    0.0,    0.0                   /

      END
```

INTENTIONALLY LEFT BLANK.

APPENDIX E

GAS DYNAMIC SIMULATIONS

R. A. Berry

INTENTIONALLY LEFT BLANK.

APPENDIX B

GAS DYNAMIC SIMULATIONS

This appendix describes the gas dynamics of the Eaton Throat-Valve Element Prototype (ETVE) with compressible, inviscid, nonheat conducting, time-dependent Euler equations formulated for axisymmetric coordinate systems. The code is formulated with a variable *thickness* or *depth*, denoted by A for each mesh cell. In two-dimensional computations, the volume of a cell of width δx and height δx is $A\delta x^2$, giving a quasi-three-dimensional effect. The physical assumption underlying the variable depth description is that the flow variables are depth-averaged in the depth direction to give mean values with variation only in the x and y dimensions, or, equivalently, that the flow variables are independent of displacement in the depth direction. The variable-depth equations were used here because they greatly increase the geometrical flexibility of the description without correspondingly increasing its complexity. The variable A may be used to represent flow through a two-dimensional duct of gradually varying thickness. Axisymmetric coordinates are generated by having A increase linearly with distance from the axis. The use of zero values of A in selected mesh cells provided a convenient means of including stationary internal obstacles (valve internal parts) in the flow region. In particular, a cell with $A = 0$ will allow no flow across its boundaries. As presently coded, the A-quantity must be a constant in time.

The valve model uses an Eulerian description for the gas dynamics (with the stationary valve internals represented with zero depth, $A = 0$), while the moving valve parts are treated as a moving material interface. Various problems can arise in the treatment of material interfaces: (a) their discrete representation, (b) their evolution in time, and (c) the manner in which boundary conditions are imposed on them.

In an Eulerian representation, the computational grid remains fixed, and the identity of individual fluid elements is not maintained. It is then necessary to compute the flow of fluid through the mesh. This flow, or convective flux calculation, necessarily requires an averaging of the flow properties of all fluid elements that end up in a given mesh cell after some period of time. This convective averaging results in a smoothing of all variations in flow quantities, and, in particular, a smearing of surfaces of discontinuity such as material interfaces. In order to overcome this loss of boundary resolution, an adaptation of the VOF (fractional volume of fluid) technique[1] was incorporated that recognizes a discontinuity and avoids averaging across it.

With the modified VOF technique used here, a function $F(x,y,t)$ is defined whose value is zero at any point occupied by gas and unity elsewhere. When averaged over the cells of a computational mesh, the average value of F in a cell is equal to the fractional volume of the cell occupied by a solid. In particular, a zero value of F corresponds to a cell full of fluid, whereas a unit value indicates that the cell contains no fluid and is occupied totally by solid, moveable valve components. Cells with F values between zero and one contain a material interface.

The F function is also used to define where fluid is located in an interface cell. The nor-

mal direction to the boundary lies in the direction in which the value of F changes most rapidly. Because F is a step function, its derivative is computed in a special way, using a donor-acceptor method.[2]

This technique was used because it provides a means of following the gas-solid interfaces of the valve through an Eulerian mesh of stationary cells, and because it follows regions rather than boundaries; it avoids the logic problems associated with explicitly tracking interface surfaces.

Equations and Constitutive Relations

The Euler equations describing the dynamics of an inviscid gas have been cast in many forms. In the present case, is chosen the dependent variables are chosen to be the mass density ρ, the gas velocities u and v, and the internal energy per unit volume E. In terms of the chosen dependent variables, the basic two-dimensional Euler equations used in the code are the continuity equation,

$$\frac{\partial \rho}{\partial t} + \frac{1}{A}\left[\frac{\partial(\rho u A)}{\partial x} + \frac{\partial(\rho v A)}{\partial y}\right] = 0 \tag{1}$$

the momentum equations,

$$\frac{\partial u}{\partial t} + u\frac{\partial u}{\partial x} + v\frac{\partial u}{\partial y} = -\frac{1}{\rho}\frac{\partial p}{\partial x} \tag{2}$$

$$\frac{\partial v}{\partial t} + u\frac{\partial v}{\partial x} + v\frac{\partial v}{\partial y} = -\frac{1}{\rho}\frac{\partial p}{\partial y} \tag{3}$$

and the internal energy equation

$$\frac{\partial E}{\partial t} + \frac{1}{A}\left[\frac{\partial(E u A)}{\partial x} + \frac{\partial(E v A)}{\partial y}\right] = -\frac{(\gamma - 1)E}{A}\left[\frac{\partial(u A)}{\partial x} + \frac{\partial(v A)}{\partial y}\right] \tag{4}$$

In these equations, the independent variables are time t and coordinates x and y. The gravitational force terms have been neglected, as have the heat conduction term, assuming they are insignificant. The viscous terms have been dropped to simplify the model, with the assumption that reasonable approximations could be attained without their inclusion. The quantity A is the time-independent *thickness* or *depth* of the flow channel. Thus, the volume associated with an area δx wide and δy high is $A\delta x\delta y$. Suitably defined A values were used to represent cylindrical coordinates (A = y, the circumferential area per unit azimuthal angle) and stationary obstacle regions (A = 0).

To complete these equations, a constitutive relations relating pressure, p, and internal energy, E, must be defined. For this case, assume the gas to obey the perfect gas relationship

$$p = (\gamma - 1)E \tag{5}$$

where γ is the ratio of specific heats at constant pressure and at constant volume.

The time dependence of the solid volume fraction function F is governed by the equation,

$$\frac{\partial F}{\partial t} + u_s \frac{\partial F}{\partial x} = 0 \tag{6}$$

where $u_s(x,t)$ is the velocity of the moveable solid valve components in the x-coordinate direction since, or the valve considered, a single degree of freedom in the axial direction exists. The solid volume fraction function $F(x,y,t)$ takes on point values of 0 or 1– 0 if the point (x,y) is occupied by gas at time t, and 1 if the point is occupied by a solid at time t. In the numerical scheme, the mesh value of F is an average of the point values of F within a computational cell, which represents the volume fraction of that cell occupied by the solid. Obviously, the volume fraction of that cell occupied by gas is 1-F.

Dynamical Coupling

To represent the valve opening dynamics, the moving parts of the valve must be coupled to the subsequent fluid dynamics of the gas as it flows through the valve. The gas surrounding the moving valve parts exerts a force (in fact, the dominant force) on the valve parts to produce their motion. The valve sleeve motion, in turn, influences the gas directly with its motion and indirectly by opening or closing the port holes to alter the gas flow dynamics. The valve sleeve motion is also influenced by other components and phenomena such as the centering spring, sleeve friction, Belleville spring loading and unloading, and the actuating hydraulics. The gas dynamic system and valve slide train dynamics are solved together, in a fully coupled manner. Information is exchanged explicitly between the gas dynamic and sleeve dynamic models every gas dynamic time step. The sleeve dynamic model, however, may subcycle its time step to values smaller than a gas dynamic time step when appropriate (such as near the reversal times, etc.).

Numerical Methods

This section briefly describes the numerical technique used to integrate the gas dynamics and advecting solid fraction function. The numerical technique used to integrate the valve slide train dynamics is included in Appendix D.

For simplicity, the solution domain is divided into a two-dimensional array of rectangular cells or control volumes each of dimension δx by δy. To each of these cells, a cell-averaged density $\rho_{i,j}$, pressure $p_{i,j}$, internal energy $E_{i,j}$, depth $A_{i,j}$, and solid volume fraction $F_{i,j}$ are assigned. A staggered mesh is used wherein average velocities, $u_{i,j}$ and $v_{i,j}$ (respectively for the x- and y-coordinate directions), are assigned at the cell edges. For cell-centered quantities, the $_{i,j}$ subscripts indicate position ($i\delta x$, $j\delta y$); for edge-defined u-velocities, the $_{i,j}$ subscripts indicate position (($i+ \frac{1}{2}$)δx, $j\delta y$); for the edge-defined v-velocities, these subscripts indicate position ($i\delta x$, ($j+ \frac{1}{2}$)δy).

Since we expected rapid valve motions to produce significant gas dynamical waves, we used an explicit Euler method to integrate the conservation and F-advection equations in time. The convective terms are differenced spatially with a fixed variable weighted upwind differencing formula. By setting the parameter α equal to unity, full upwind differencing results; whereas, setting α to zero produces centered differencing. Setting α to a value between zero and one gives a linearly weighted combination of upwind and centered spatial differencing.

The first calculation in the solution sequence involves computing the forces on the moveable valve parts owing to the pressures in the gas. This is accomplished by assigning to each cell an index, the value of which depends on whether the cell is an interface cell. If it is an interface cell, its index value depends on the orientation of the interface. To compute the gas dynamic force on the sleeve, an individual cell's contributions are summed with appropriated coefficients determined by the cell's interface index. For example, if a cell's index does not indicate the cell to be an interface cell, the coefficient for this cell is zero, i.e., it contributes no force to the sleeve. On the other hand, if a cell's index indicates it has an interface with positive outward normal in the positive x-direction, the cell's coefficient is $-\delta y$, and its contribution to the total force on the sleeve is $-p_{i,j}\delta y$. Interface cells with orientation in the negative x-direction contribute $+p_{i,j}\delta y$ to the total force. Other cell interface orientations contribute nothing to the total sleeve force since a single degree of freedom (in the x-direction) was assumed for the valve sleeve spool.

Next, the valve dynamics are integrated for a time step, or, if warranted, several sub-time steps to get the new displacement, velocity, and acceleration of the moveable valve parts. With the new valve velocity, the F-function is advected for a time step to get the new gas dynamic flow configuration. With the flow configuration, the gas dynamic solution is ready to be updated (advanced one time step). First, the u- and v-velocity equations, Equations (2) and (3), are updated as

$$u_{i,j}^{n+1} = u_{i,j} + \delta t \left[\frac{2(p_{i,j} - p_{i+1,j})}{\delta x \, (\rho_{i,j} + \rho_{i+1,j})} - FUX - FUY \right] \tag{7}$$

$$v_{i,j}^{n+1} = v_{i,j} + \delta t \left[\frac{2(p_{i,j} - p_{i,j+1})}{\delta y \, (\rho_{i,j} + \rho_{i,j+1})} - FVX - FVY \right] \tag{8}$$

where

$$FUX = \frac{1}{2\delta x} [u_{i,j} (u_{i+1,j} - u_{i-1,j}) - \alpha \, |u_{i,j}| \, (u_{i+1,j} - 2u_{i,j} + u_{i-1,j})]$$

$$FUY = \frac{1}{8\delta y} [(v_{i,j} + v_{i+1,j} + v_{i,j-1} + v_{i+1,j-1}) (u_{i,j+1} - u_{i,j-1})$$

$$- \alpha \, |v_{i,j} + v_{i+1,j} + v_{i,j-1} + v_{i+1,j-1}| \, (u_{i,j+1} - 2u_{i,j} + u_{i,j-1})]$$

$$FVX = \frac{1}{8\delta x}[(u_{i-1,j+1} + u_{i,j+1} + u_{i-1,j} + u_{i,j})(v_{i+1,j} - v_{i-1,j})$$

$$- \alpha \mid u_{i-1,j+1} + u_{i,j+1} + u_{i-1,j} + u_{i,j} \mid (v_{i+1,j} - 2v_{i,j} + v_{i-1,j})]$$

$$FVY = \frac{1}{2\delta y}[v_{i,j}(v_{i,j+1} - v_{i,j-1}) - \alpha \mid v_{i,j} \mid (v_{i,j+1} - 2v_{i,j} + v_{i,j-1})]$$

In these discretized equations (and in all subsequent discretized equations), the superscripts indicate time level, e.g., $u_{i,j}^{n+1}$ indicates the u-velocity at

$$\text{time} = \sum_{i=1}^{n+1} \delta t_i$$

where δt_i is the time step size, and the absence of a superscript implies that the variable is evaluated at the current time level,

$$\text{time} = \sum_{i=1}^{n} \delta t_i \ .$$

Using the updated velocity field, the mass density is next updated to the new time level as

$$\rho_{i,j}^{n+1} = \rho_{i,j} - \frac{\delta t}{A_{i,j}}\left[\frac{FR - FL}{\delta x} + \frac{FT - FB}{\delta y}\right]$$

where

$$FR = \frac{ABR}{2}[u_{i,j}^{n+1}(\rho_{i,j} + \rho_{i+1,j}) + \alpha \mid u_{i,j}^{n+1} \mid (\rho_{i,j} - \rho_{i+1,j})]$$

$$FL = \frac{ABL}{2}[u_{i-1,j}^{n+1}(\rho_{i-1,j} + \rho_{i,j}) + \alpha \mid u_{i-1,j}^{n+1} \mid (\rho_{i-1,j} - \rho_{i,j})]$$

$$FT = \frac{ABT}{2}[v_{i,j}^{n+1}(\rho_{i,j} + \rho_{i,j+1}) + \alpha \mid v_{i,j}^{n+1} \mid (\rho_{i,j} - \rho_{i,j+1})]$$

$$FB = \frac{ABB}{2}[v_{i,j-1}^{n+1}(\rho_{i,j-1} + \rho_{i,j}) + \alpha \mid v_{i,j-1}^{n+1} \mid (\rho_{i,j-1} - \rho_{i,j})]$$

$$ABR = \frac{2A_{i,j}A_{i+1,j}}{A_{i,j} + A_{i+1,j}}$$

$$ABL = \frac{2A_{i,j}A_{i-1,j}}{A_{i,j} + A_{i-1,j}}$$

$$ABT = \frac{2A_{i,j}A_{i,j+1}}{A_{i,j} + A_{i,j+1}}$$

$$ABB = \frac{2A_{i,j}A_{i,j-1}}{A_{i,j} + A_{i,j-1}}$$

In a similar manner, using the new time velocities the energy equation is updated to the new time level, as follows:

$$E_{i,j}^{n+1} = E_{i,j} - \frac{\delta t}{A_{i,j}}\left[\frac{FER - FEL}{\delta x} + \frac{FET - FEB}{\delta y} + FWK\right] \tag{10}$$

where

$$FER = \frac{ABR}{2}[u_{i,j}^{n+1}(E_{i,j} + E_{i+1,j}) + \alpha\,|u_{i,j}^{n+1}|\,(E_{i,j} - E_{i+1,j})]$$

$$FEL = \frac{ABL}{2}[u_{i-1,j}^{n+1}(E_{i-1,j} + E_{i,j}) + \alpha\,|u_{i-1,j}^{n+1}|\,(E_{i-1,j} - E_{i,j})]$$

$$FET = \frac{ABT}{2}[v_{i,j}^{n+1}(E_{i,j} + E_{i,j+1}) + \alpha\,|v_{i,j}^{n+1}|\,(E_{i,j} - E_{i,j+1})]$$

$$FEB = \frac{ABB}{2}[v_{i,j+1}^{n+1}(E_{i,j-1} + E_{i,j}) + \alpha\,|v_{i,j-1}^{n+1}|\,(E_{i,j-1} - E_{i,j})]$$

$$FWK = (\gamma-1)E_{i,j}\left[\frac{u_{i,j}^{n+1}ABR - u_{i-1,j}^{n+1}ABL}{\delta x} + \frac{v_{i,j}^{n+1}ABT - v_{i,j-1}^{n+1}ABB}{\delta y}\right]$$

For the cell boundary depths, a linearly interpolated value is not used, but, instead, a combined geometric and arithmetic average is used. For example,

$$ABR = \frac{2A_{i,j}A_{i+1,j}}{A_{i,j} + A_{i+1,j}}$$

This choice has the convenient feature that a cell boundary depth vanishes when either of the cell depths on each side of boundary is zero, i.e., for this case, ABR vanishes whenever A_{ij} or A_{i+1j} is zero.

Finally, with the new time energy field, the pressure is updated as

$$p_{i,j}^{n+1} = (\gamma - 1)E_{i,j}^{n+1} \tag{11}$$

and the new time specific internal energy, e , can be obtained as

$$e_{i,j}^{n+1} = \frac{E_{i,j}^{n+1}}{\rho_{i,j}^{n+1}} \tag{12}$$

RESULTS

Figure E-1[a] shows the gas dynamic simulation model used for the ETVE. The stationary and moving valve elements are approximated as rectangular solid blocks. The mesh spacing used is $\delta x = \delta y = 1$ mm. Constant pressure boundary conditions were applied at the inlet and outlet boundaries of the flow model. For the first set of runs, the high-pressure boundary (upstream, right boundary in Figure E-1), is set to 1400 psi while the low-pressure boundary (downstream, left boundary) is set to 14 psi. Figures E-2 and E-3 show the results for runs with combined 8% viscous and 100 lbf coulomb damping on the Belleville washers; Figures E-4 and E-5 show the results for runs with a combined 16% viscous and 100 lbf coulomb damping on the Belleville washers. In Figures E-2 and E-4, the "a" figure is a plot of valve sleeves displacement with time, the "b" figure is a plot of its velocity with time, and the "c" and "d" figures are plots of its acceleration with time. The "e" figures show pressure in the gas as a function of time for a location 6 mm in from the low-pressure boundary and 29-mm radially outward from the axis of symmetry (labeled as pressure plot point in Figure E-1). In Figures E-2 and E-4, each of the plots also have the total gas static pressure loading acting on the valve sleeve as a function of time shown as a "ghost" dotted line. Figures E-3 and E-5 show the pressure distribution (spatial) at the instant in time corresponding to the last time step in each run; isobars are at 10-psi intervals.

Clearly, the gas dynamic force on the sleeve dominates and is responsible, when coupled with the Belleville spring force, for the severe oscillations. The other dynamical forces have little effect on the sleeve motion. Examination of the gas dynamic force on the sleeve shows that this force predominantly acts left or toward the direction of valve closure. In an attempt to reduce this large gas dynamic force on the sleeve, a run was made in which the downstream face of each of the sleeve ports was beveled along its entire face at a 45 degree angle. This had some effect, but not enough; the sleeve still oscillated violently.

Based on the above observation, the question was asked, what might happen if the initial sleeve position was shifted to the right with the sleeve ports on the other side of the stationary ports, with the opening motion now being to the left (reversed). Then, perhaps, the gas dynami-

---

a. The figures are found as a section of the report beginning on page E-12.

cal force on the sleeve would act to force the valve into the open position. When this change in geometry was made in the simulation model, that is exactly what was observed.

In order to reposition the valve sleeve as described above with the same sleeve travel length with the same dimensions between ports, it was necessary to lengthen the downstream end of the sleeve in order that the downstream stationary port hole be totally blocked (closed) in the initial configuration. Figure E-6 shows the gas dynamical simulation model for this new configuration. With this modification, and with 8% viscous and 100-lbf coulomb damping in the Belleville springs, the simulation produced the results shown in Figures E-7, E-8, and E-9. Figures E-7a and E-7b show the time history of the sleeve displacement and velocity, respectively. Figures E-7c and E-7d show the valve sleeve acceleration history. Figure E-7e shows the gas pressure history, again at the position 6 mm in from the left (low) pressure boundary and 29 mm radially out from the axis (pressure plot point in Figure E-6). Figure E-8a and E-8b show the phase portrait (displacement versus velocity) for the sleeve motion with Figure E-8b being an enlargement of the region around the region of attraction to the open position. Figure E-9 shows the spatial pressure distribution at the time corresponding to the last time step of the problem, with isobars at 10-psi intervals. These results shown that the gas dynamic forces do force the valve into a strongly open position after 3 to 4 small bounces from the Belleville spring. Beyond this initial opening transient, we observed that the valve maintains the open position with a growing, high-frequency oscillation imposed on a fairly significant steady Belleville spring compression. A growing, high-frequency oscillation is seen in the gas dynamic force on the sleeve. However, the average gas dynamic force on the sleeve is seen to be strongly toward the open position. It is not known whether this growing oscillation of the sleeve could eventually grow to the point of blocking enough of the flow through the portholes to force the sleeve motion into another transient form. We do not know whether this growing oscillation is physical or just numerical artifice.

For the second set of runs, the high-pressure boundary was increased to 1800 psi with conditions corresponding to 700°F, and the low-pressure boundary was lowered to 12 psi. Figure E-10 shows, in a manner similar to the earlier set of runs, the displacement, velocity, acceleration, and single point pressure histories with total static pressure gas load on the sleeve (dotted line) included, all for the case of 8% viscous damping plus 100 lbf coulomb damping. Figure E-11 shows the corresponding pressure distribution for this case at the last time step, with 12 psi isobar intervals. Similar data are shown in Figures E-12 and E-13 for the case of 16% viscous plus 100 lbf coulomb damping. Figures E-14 and E-15 show the same data arrangement displays for the modified, backward opening valve. Again, a high-frequency, low-amplitude wave form is seen imposed on the approximate steady state for later times, after the valve is open. The same caveat applies. We are unsure at this time of the physical reality of this phenomena.

In the pressure distribution figures, we noted the large pressure gradients occurring in the vicinity of the low-pressure boundary. This may be due to the fixed pressure boundary condition. If the flow local to the exit boundary is supersonic, it is no longer appropriate to impose a pressure at this boundary. To rule out the possibility of such a boundary condition causing the high-

frequency oscillations about the open position, the code's boundary condition subroutine was rewritten to impose an exit boundary condition as a local extrapolation from the interior of the flow field where the velocities are locally supersonic. The backward opening valve with lengthened spool was executed (8% viscous plus 100 lbf Belleville damping) with the new boundary conditions. Figure E-16 shows the displacement, velocity, acceleration, and pressure point histories, all plotted with the total gas dynamic force history on the valve spool (dotted line). Figure E-17 shows the pressure distribution (~13 psi between isobars) at the last time step. The large pressure gradients that were piling up at the exit boundary are now gone. However, the high-frequency oscillation is still present, and the valve opening dynamics are the same. While the new boundary condition is certainly appropriate, the oscillating phenomena cannot be attributed to the previously used, fixed pressure boundary condition.

CONCLUSIONS AND RECOMMENDATIONS

The coupled gas dynamic and valve slide dynamic simulation model has been found to be an extremely valuable tool in assessing the nature of the current valve's operation and is indispensible in assessing the effects of valve modifications or redesigns. Such complex nonlinear behavior is impossible to predict in any way other than numerical simulation. Even if the numerical simulations are accepted only on a qualitative basis, they increase understanding of behavior, show trends and sensitivities, and suggest alternate designs. On the other hand, the alternative, cut and try approach to design would be a long, tedious, and expensive route to valve design/redesign.

For future design/analysis work, we recommend that the numerical technique used to simulate the gas dynamics be modified to give a partially implicit time integration instead of the explicit time integration. This will reduce the CPU time required to make runs and should increase the accuracy by reducing the large number of time steps required for these runs. The importance of viscous effects should also be examined, especially in the valve open position where the high-speed flow though the ports could possibly place significant shear forces on the sleeve, and therefore influencing its motion.

REFERENCES

1. C. W. Hirt and B. D. Nichols, *Journal of Computational Physics, 39*, 201, 1981.

2. J. D. Ramshaw and J. A. Trapp, *Journal of Computational Physics, 21*, 438, 1976.
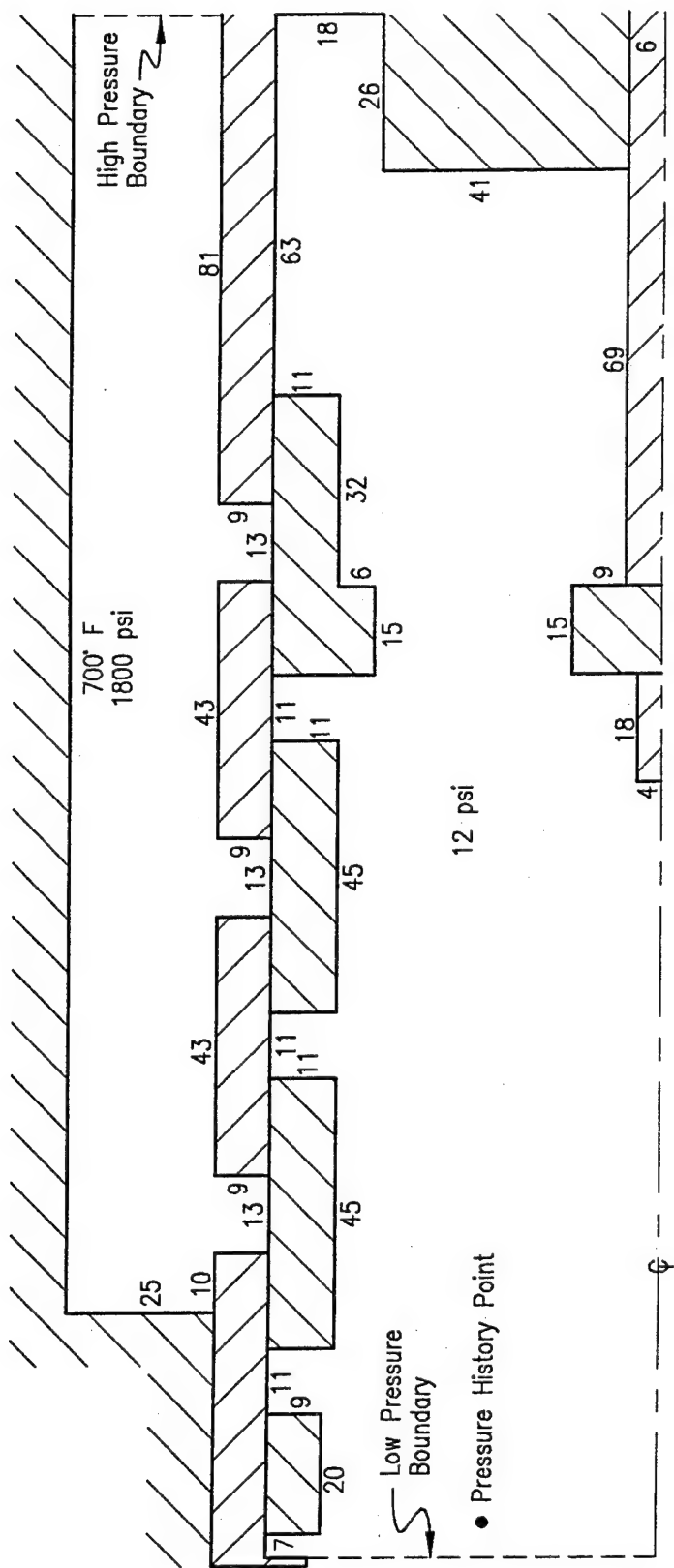
Figure E-1. ETVE gas dynamic simulation model.
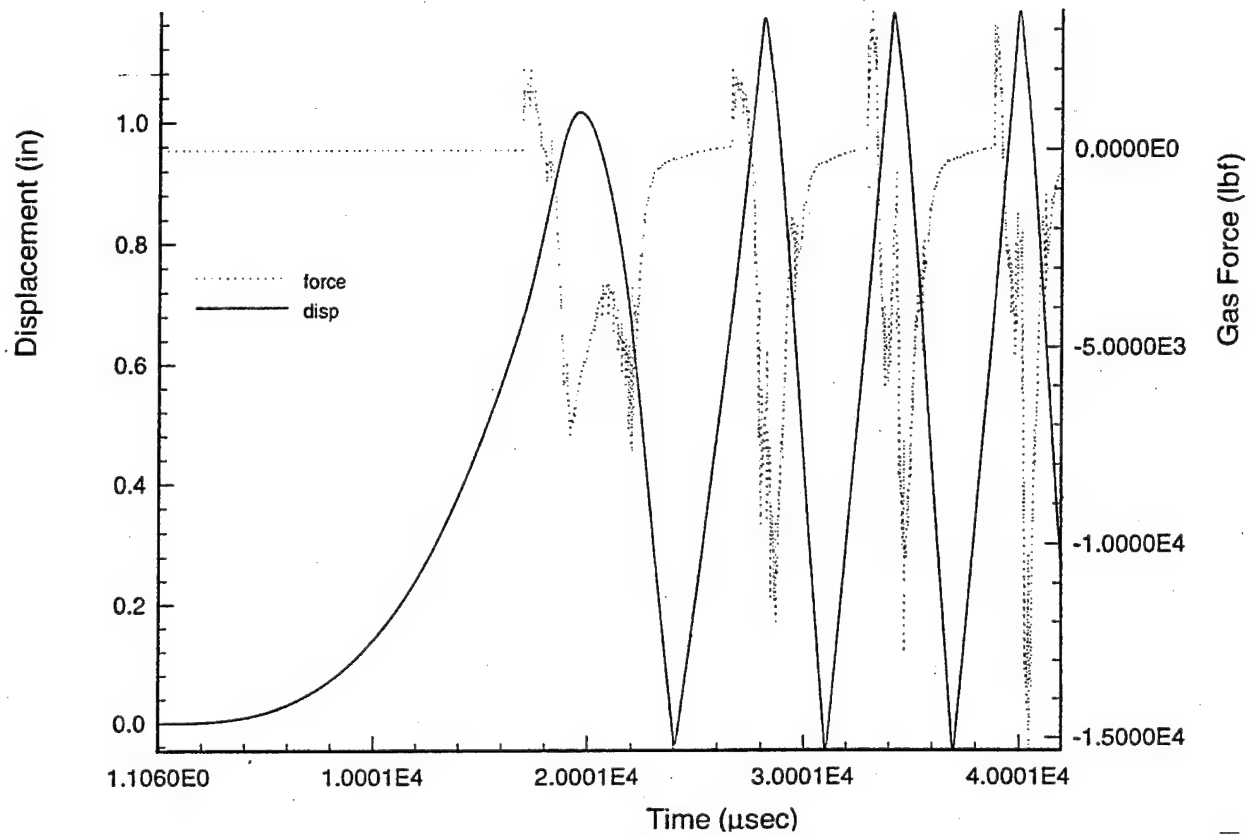
Figure E-2a. Histories of valve spool *displacement* and total gas dynamic force on valve spool. Damping forces are set at 8% viscous (on spool) plus 100lbf (on Belleville) Coulomb damping. The high-pressure boundary is 1400 psia; the low-pressure boundary is 14 psia.
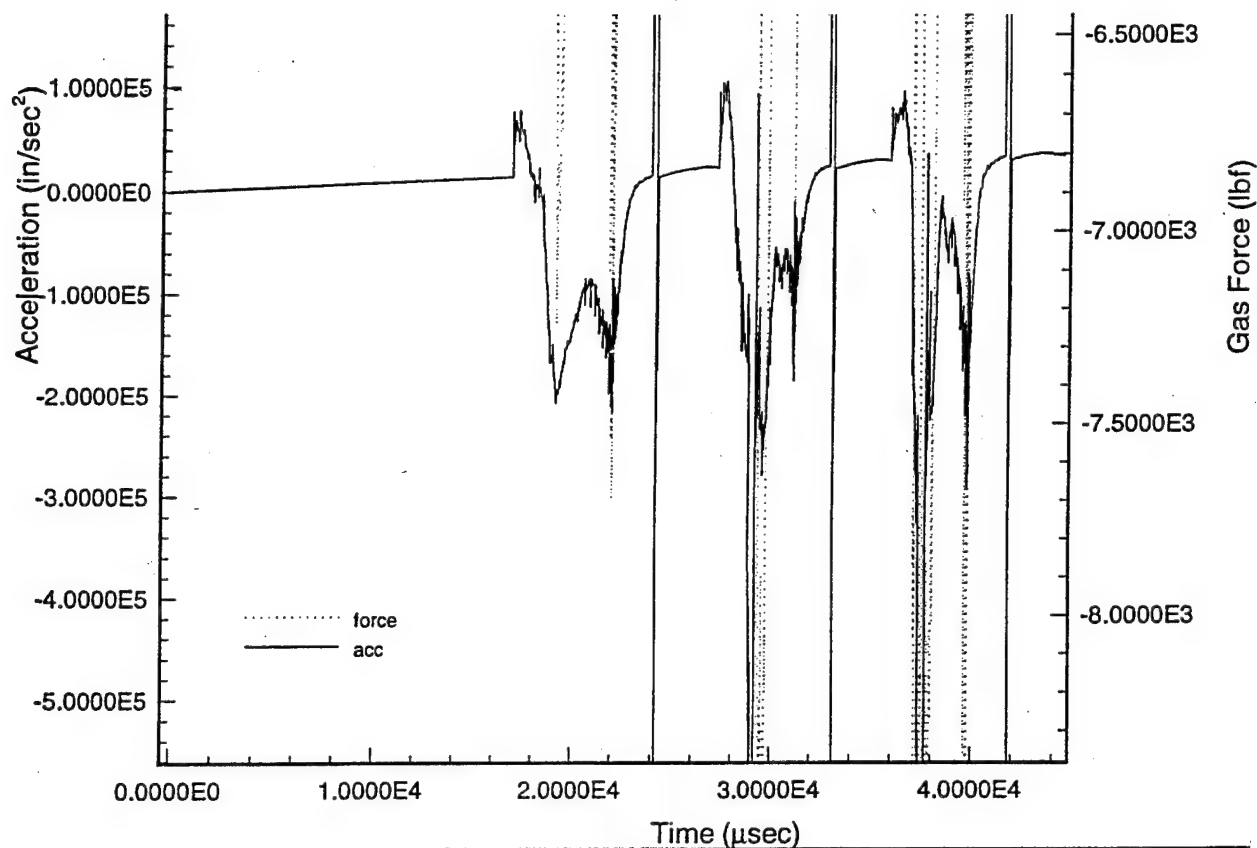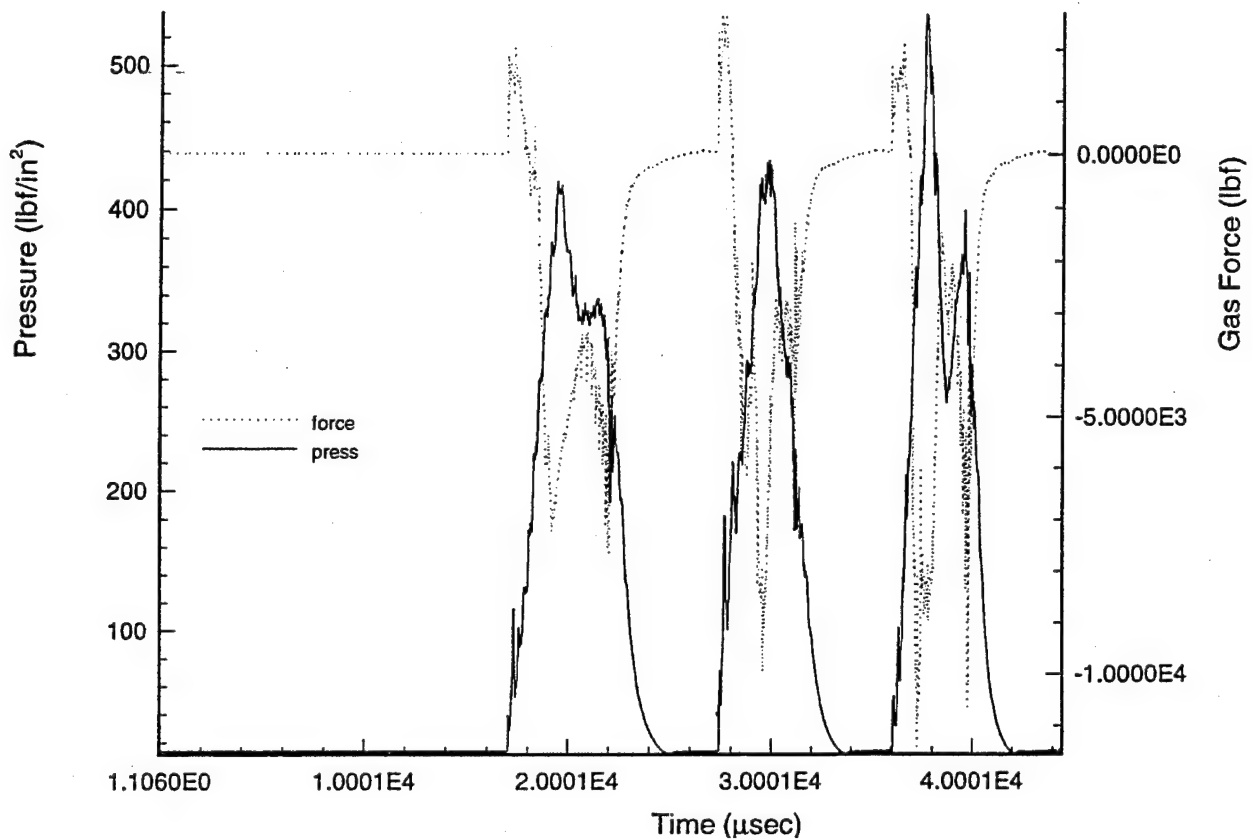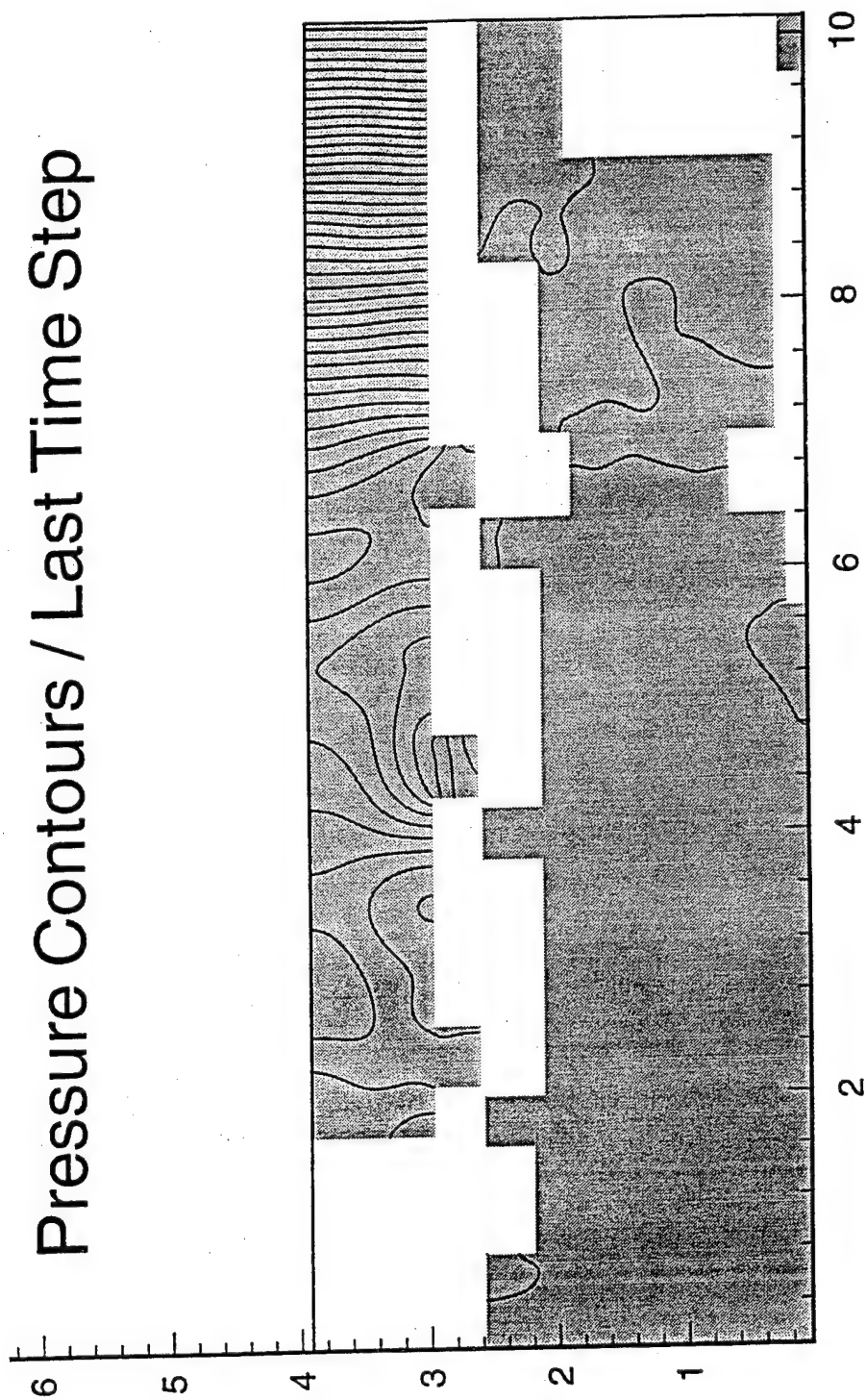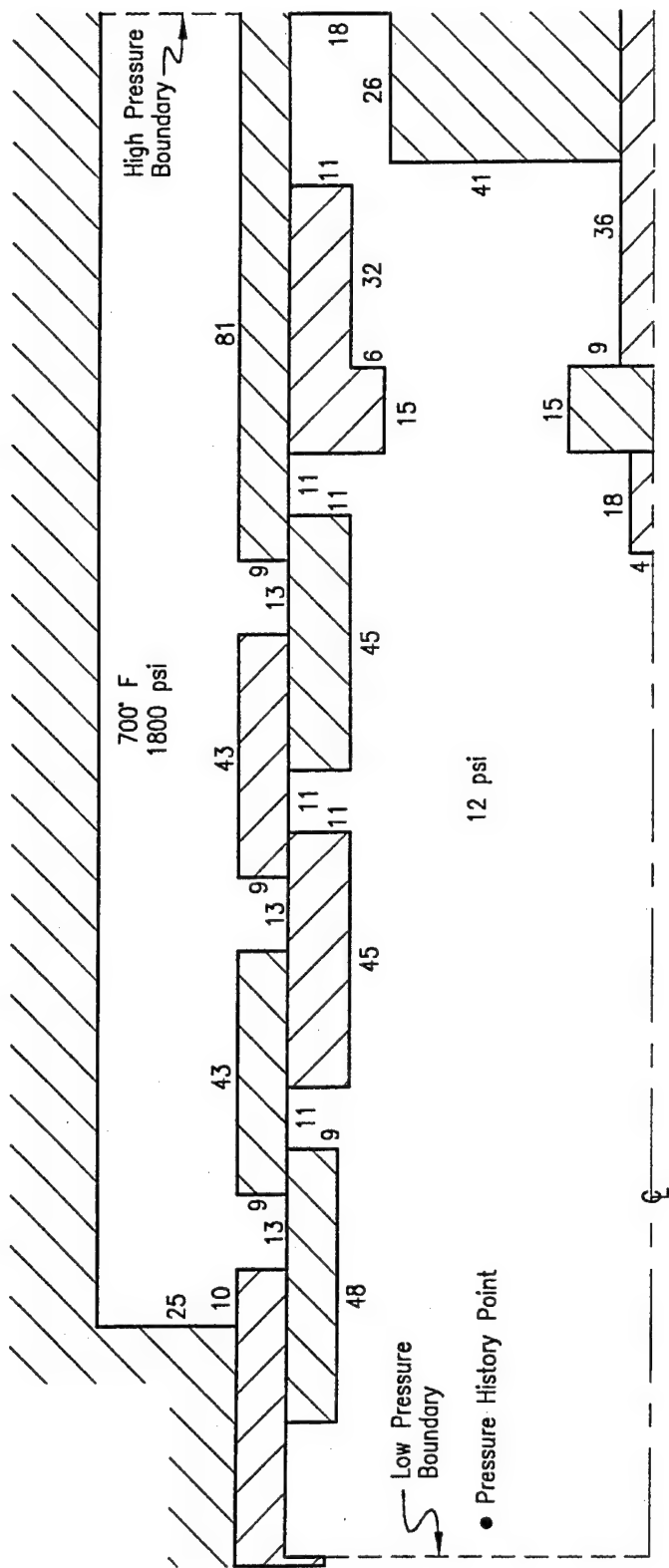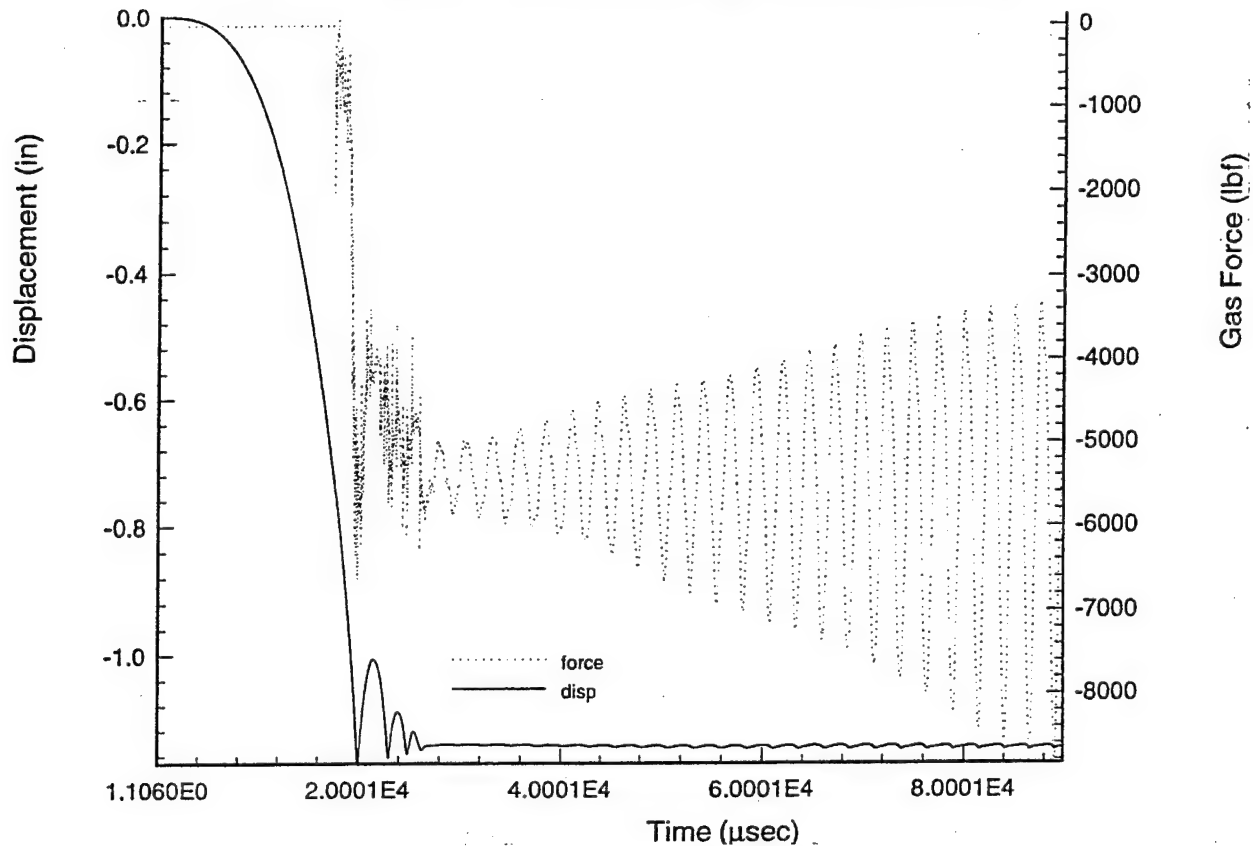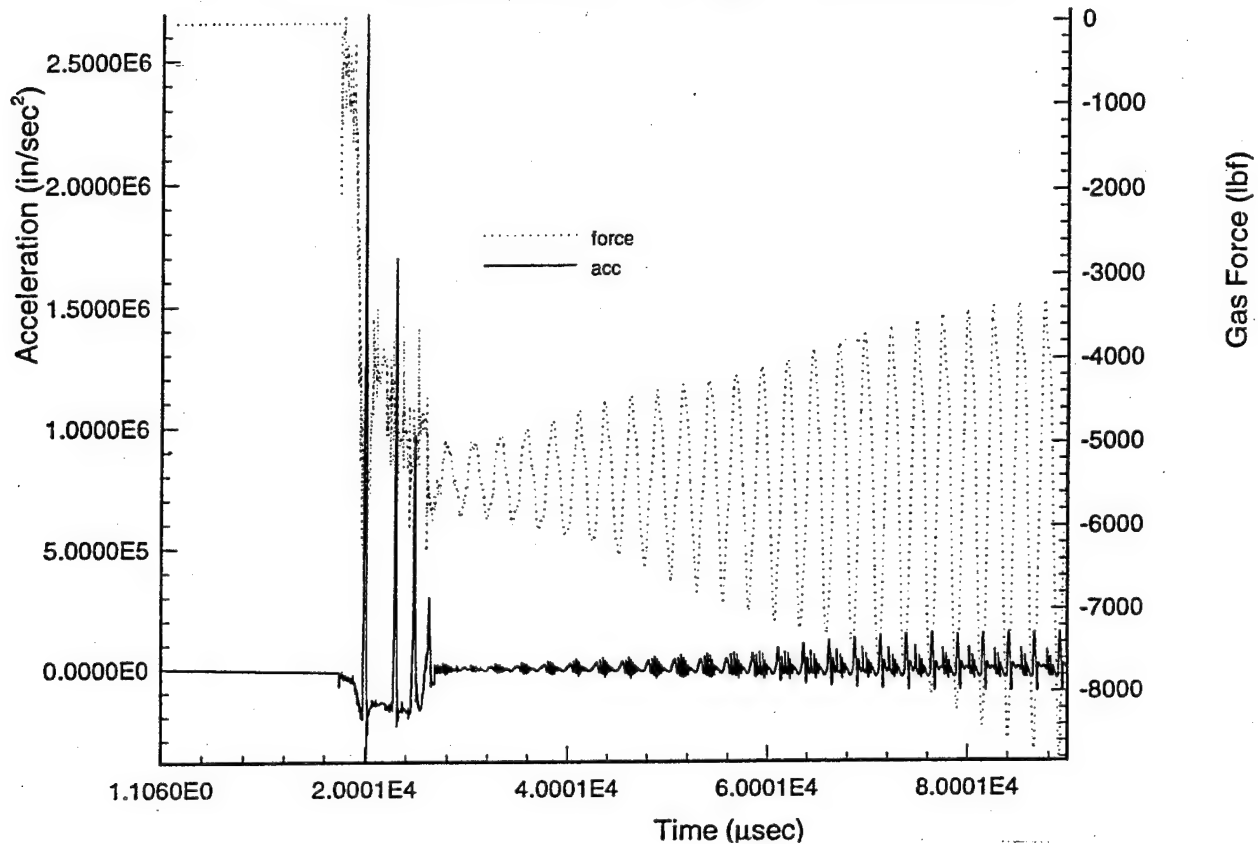
8 % Viscous + 100 lbf Bellville Damping
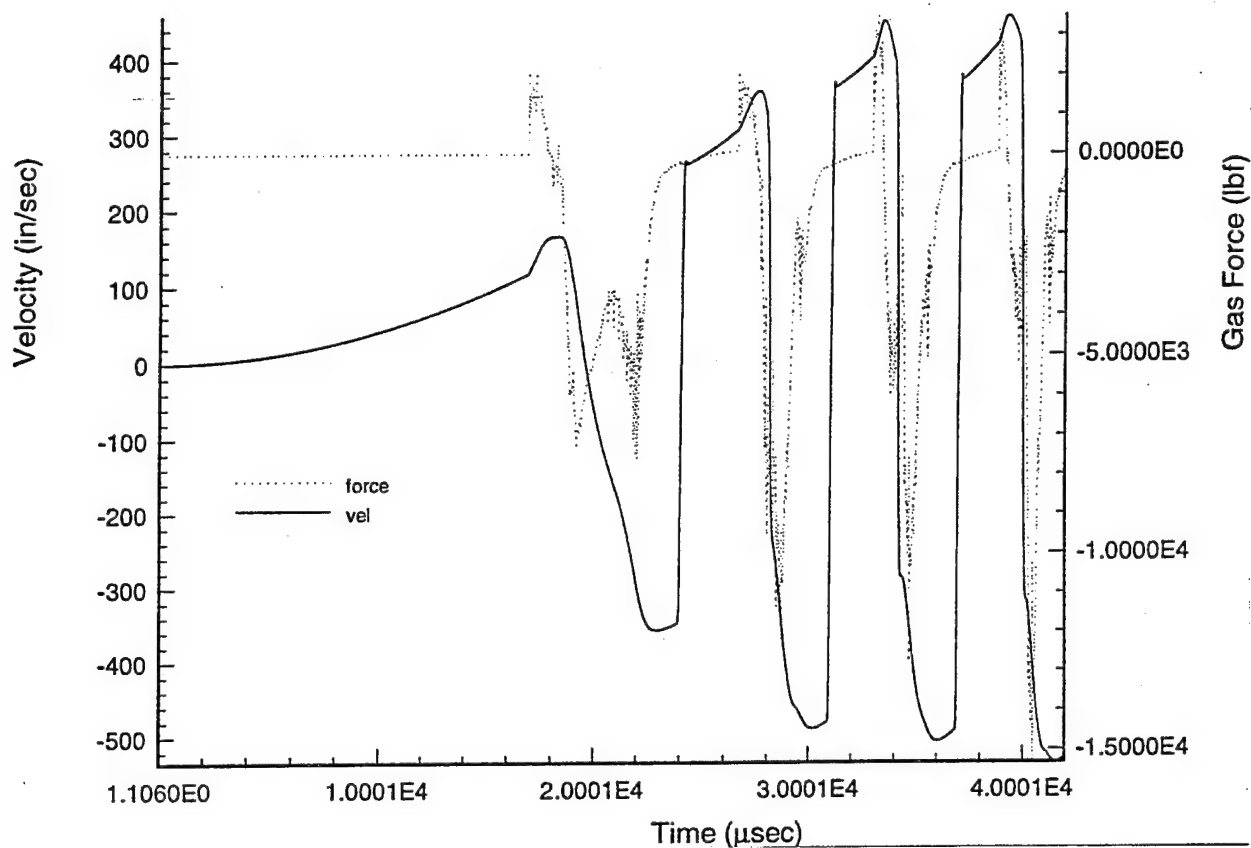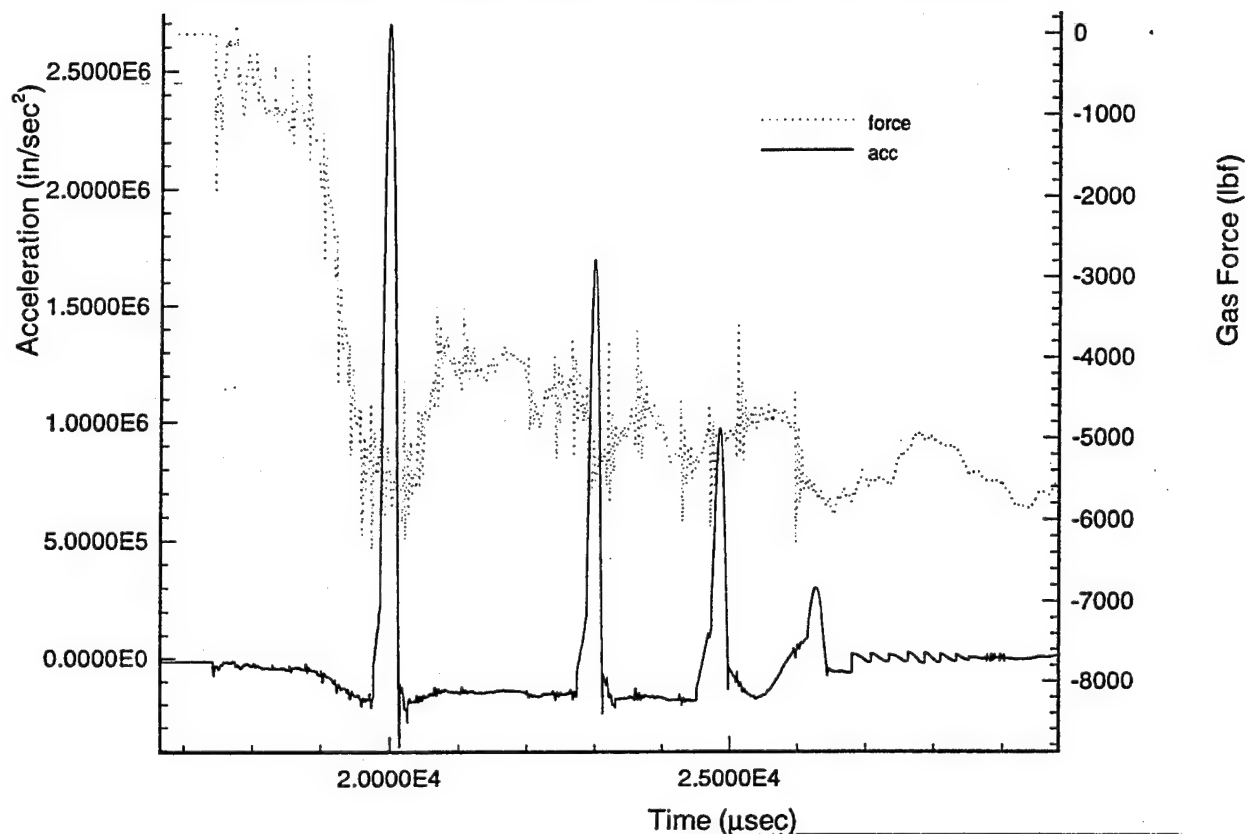

Figure E-2b. Histories of valve spool *velocity* and total gas dynamic force on valve spool. Damping forces are set at 8% viscous (on spool) plus 100lbf (on Belleville) Coulomb damping. The high-pressure boundary is 1400 psia; the low-pressure boundary is 14 psia.

8 % Viscous + 100 lbf Bellville Damping
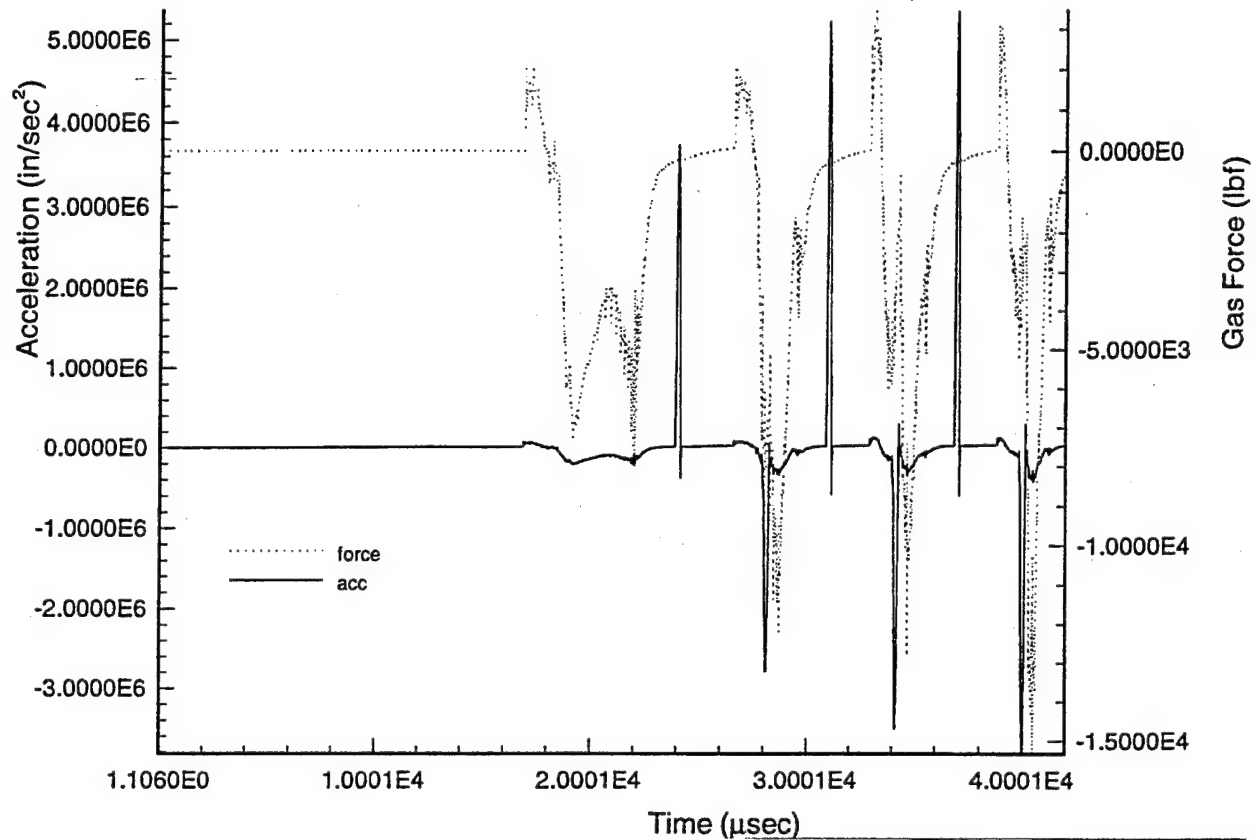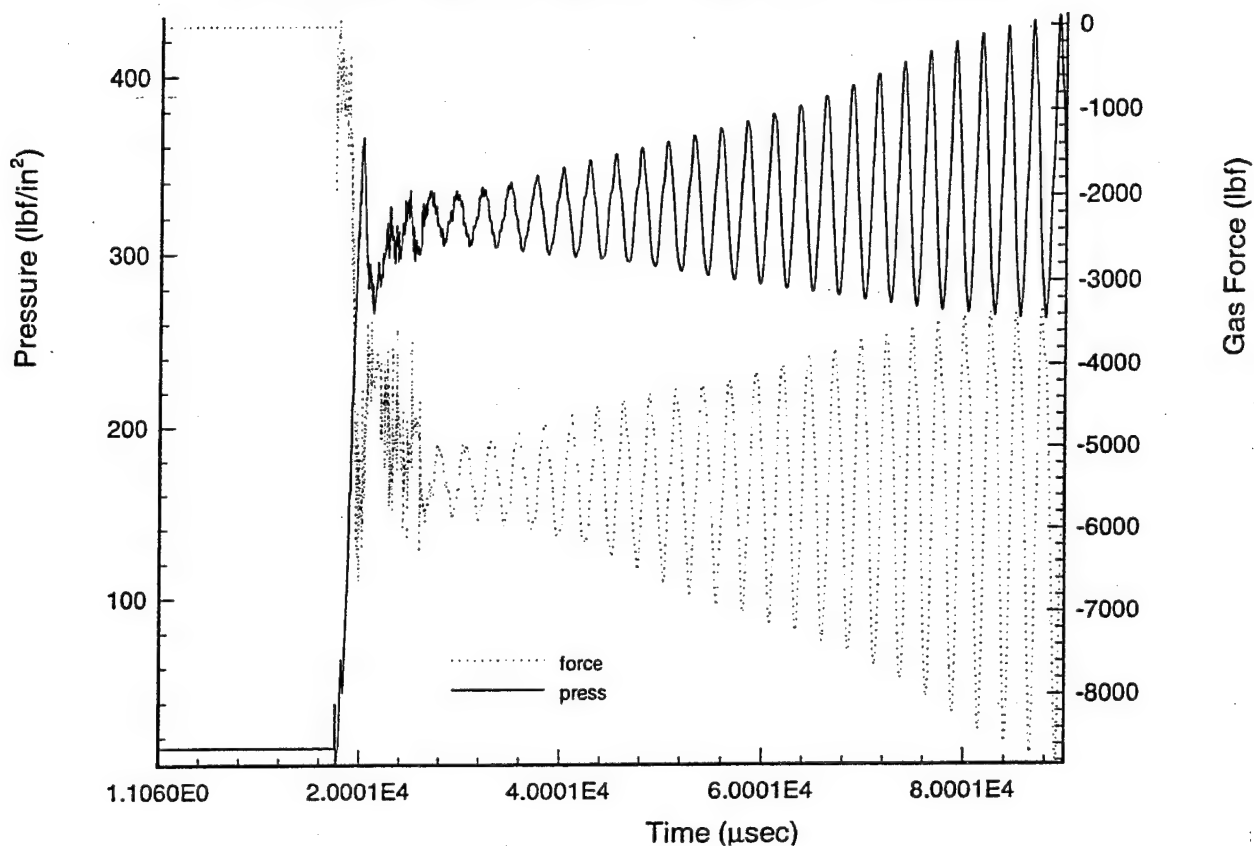

Figure E-2c. Histories of valve spool *acceleration* and total gas dynamic force on valve spool. Damping forces are set at 8% viscous (on spool) plus 100lbf (on Belleville) Coulomb damping. The high-pressure boundary is 1400 psia; the low-pressure boundary is 14 psia.
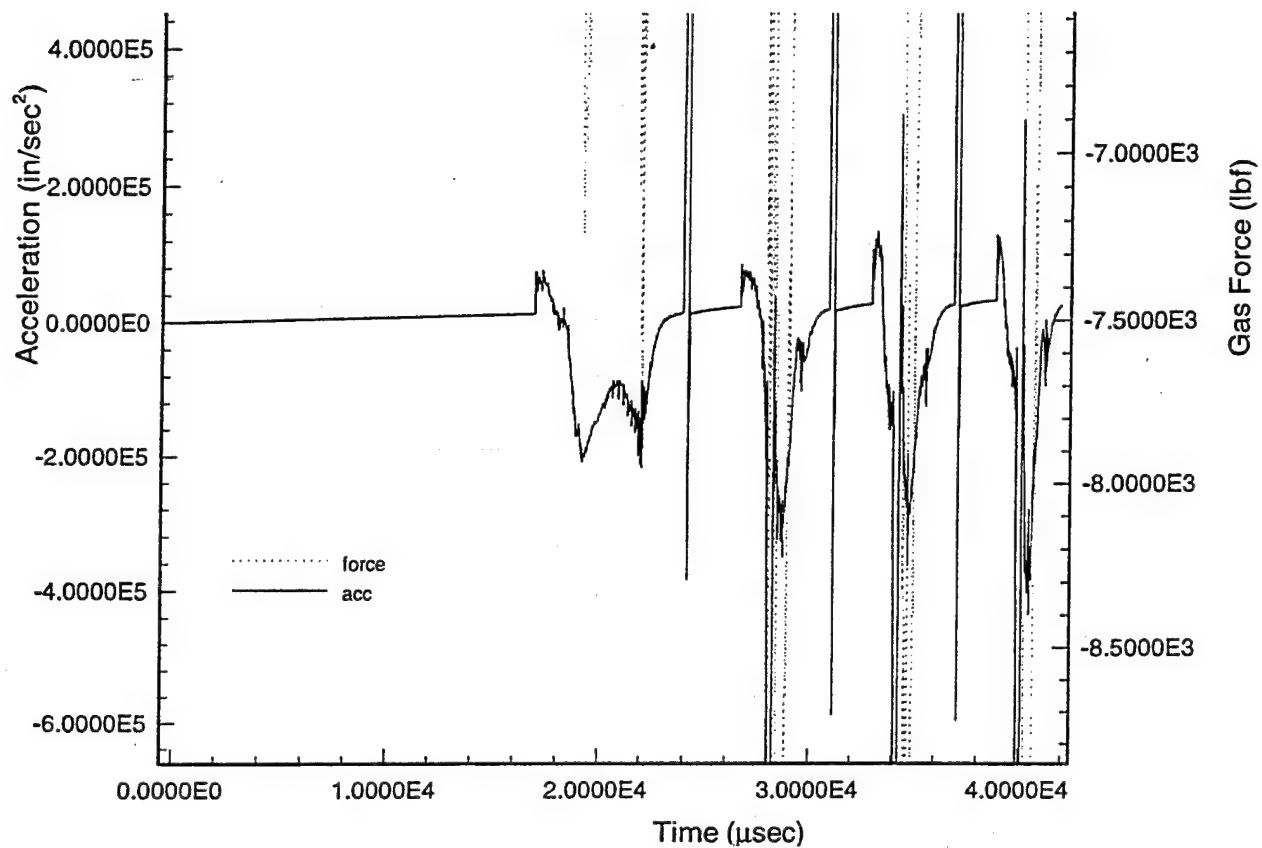
Figure E-2d. Histories of valve spool *acceleration (enlargement)* and total gas dynamic force on valve spool. Damping forces are set at 8% viscous (on spool) plus 100lbf (on Belleville) Coulomb damping. The high-pressure boundary is 1400 psia; the low-pressure boundary is 14 psia.
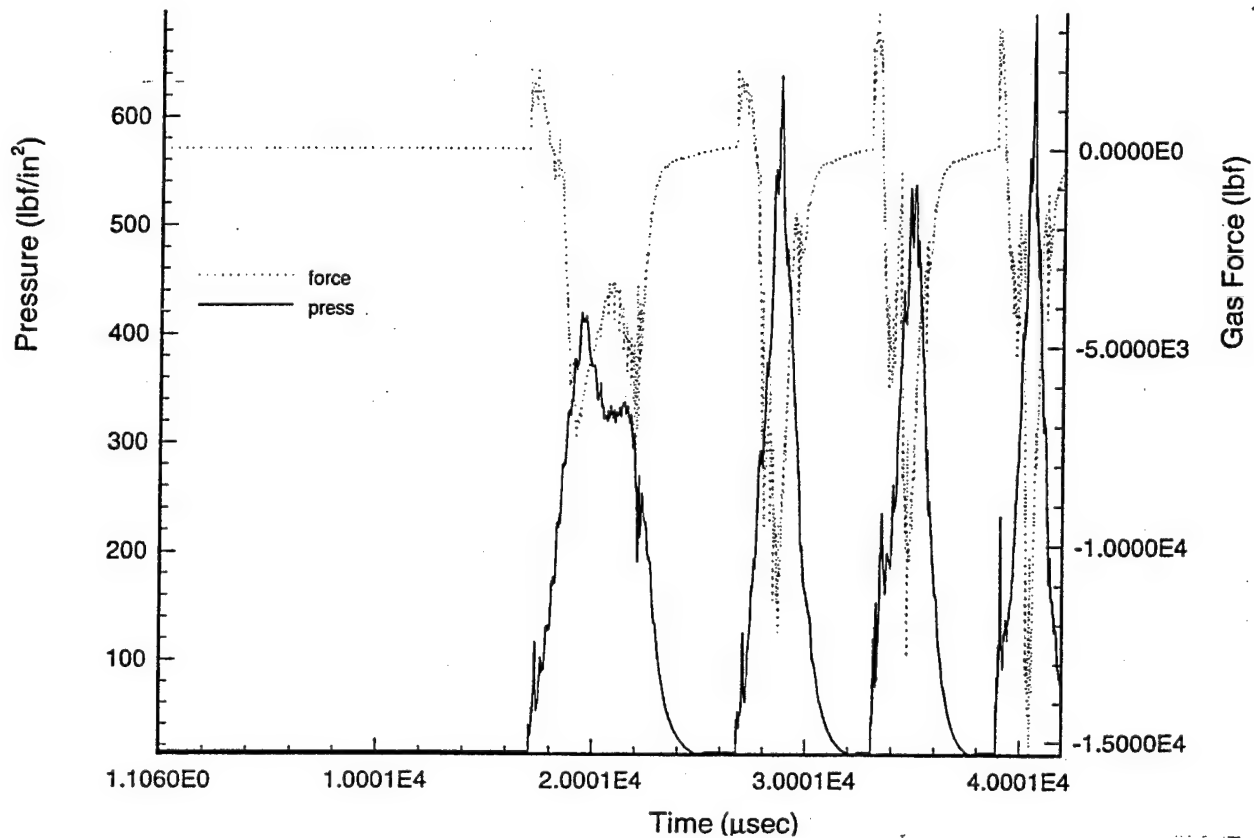
Figure E-2e. Pressure history at the pressure history point and total gas dynamic force on valve spool. Damping forces are set at 8% viscous (on spool) plus 100lbf (on Belleville) Coulomb damping. The high-pressure boundary is 1400 psia; the low-pressure boundary is 14 psia.

Pressure Contours / Last Time Step
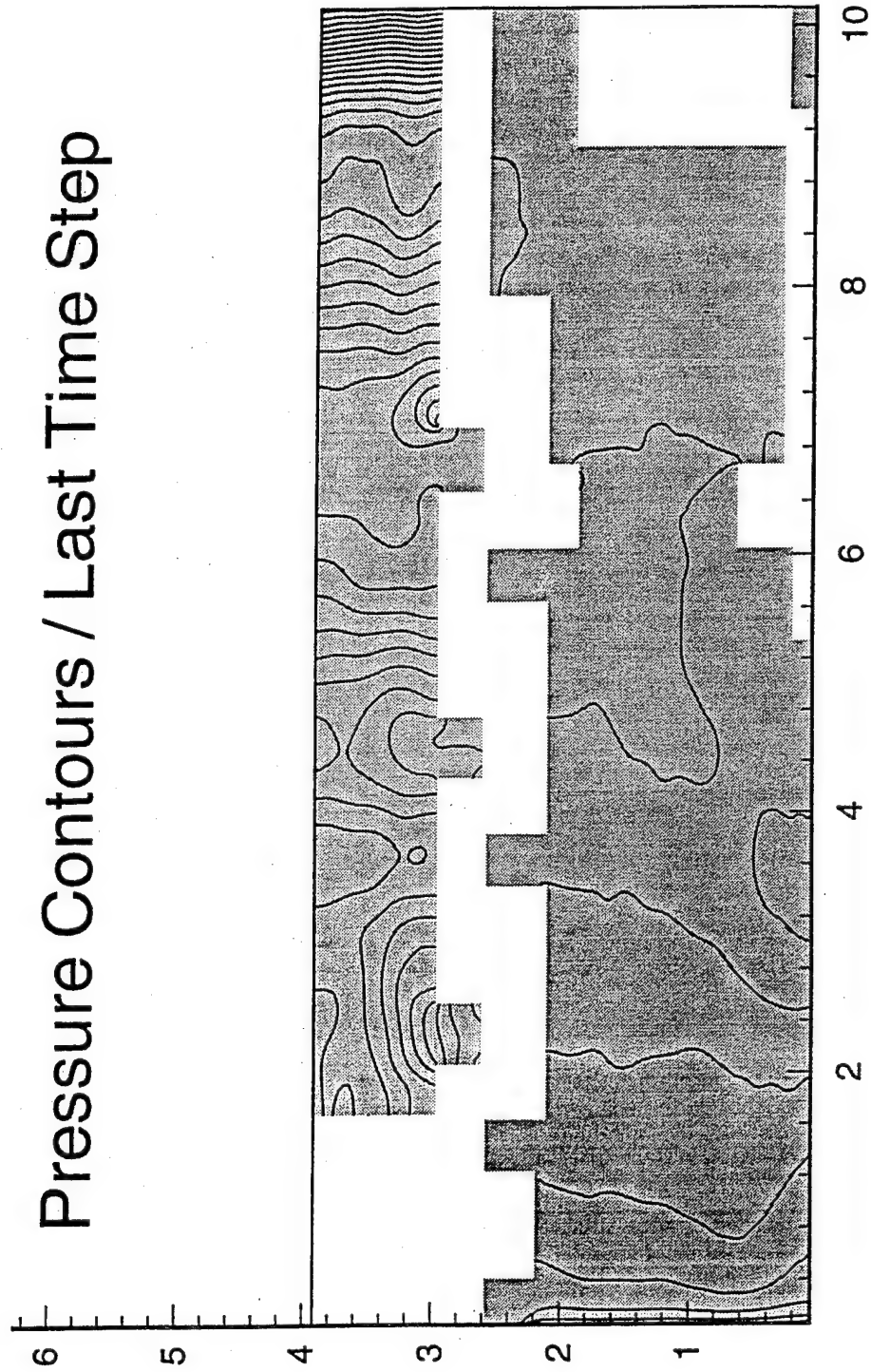
Figure E-3. Spatial pressure distribution at time = 0.042 sec. Isobars are at ~10-psi intervals.

16 % Viscous + 100 lbf Bellville Damping
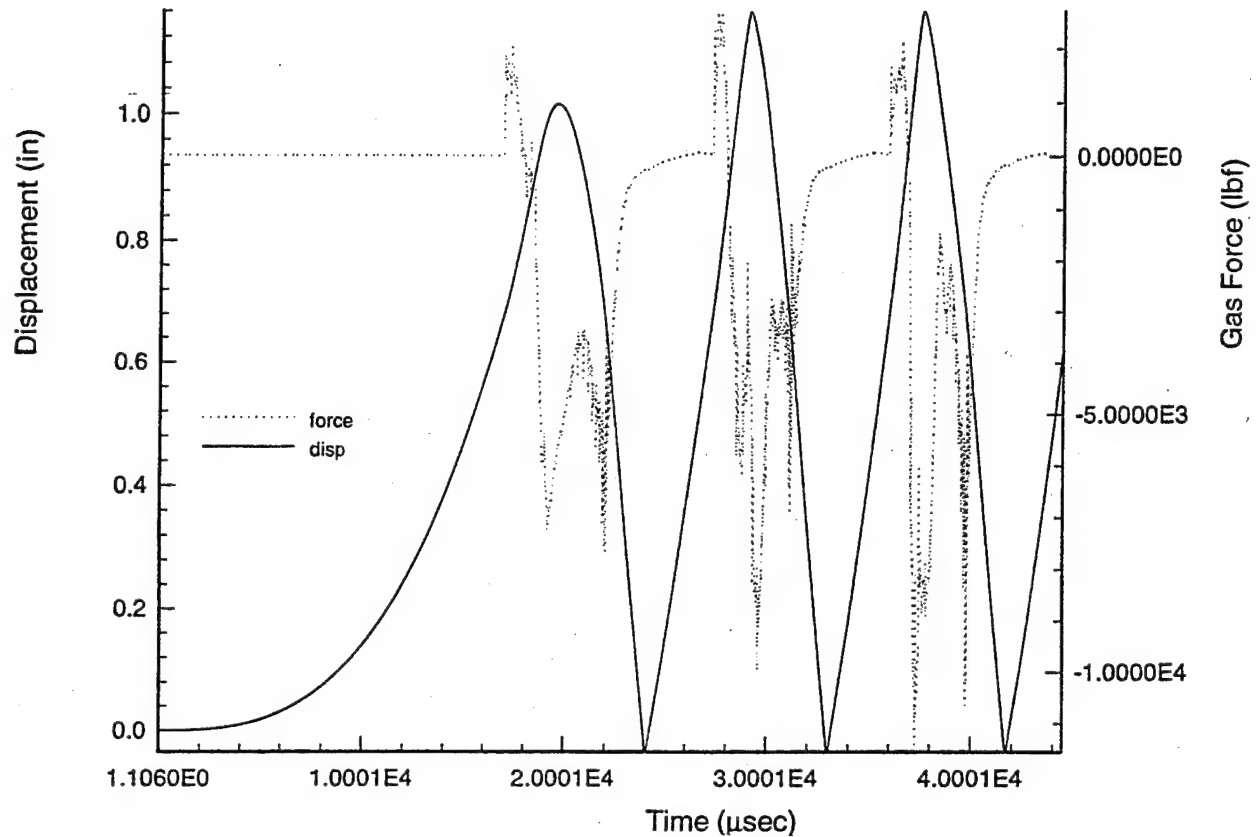
Figure E-4a. Histories of valve spool *displacement* and total gas dynamic force on valve spool. Damping forces are set at 16% viscous (on spool) plus 100lbf (on Belleville) Coulomb damping. The high-pressure boundary is 1400 psia; the low-pressure boundary is 14 psia.
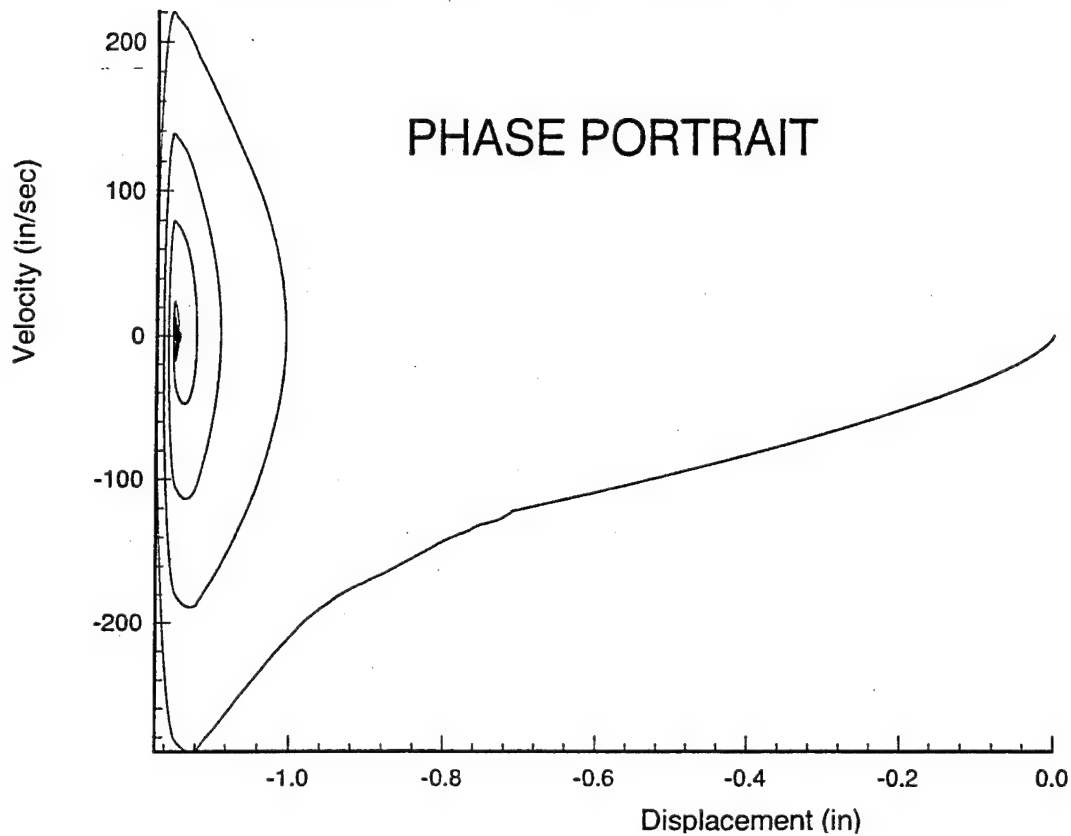
16 % Viscous + 100 lbf Bellville Damping
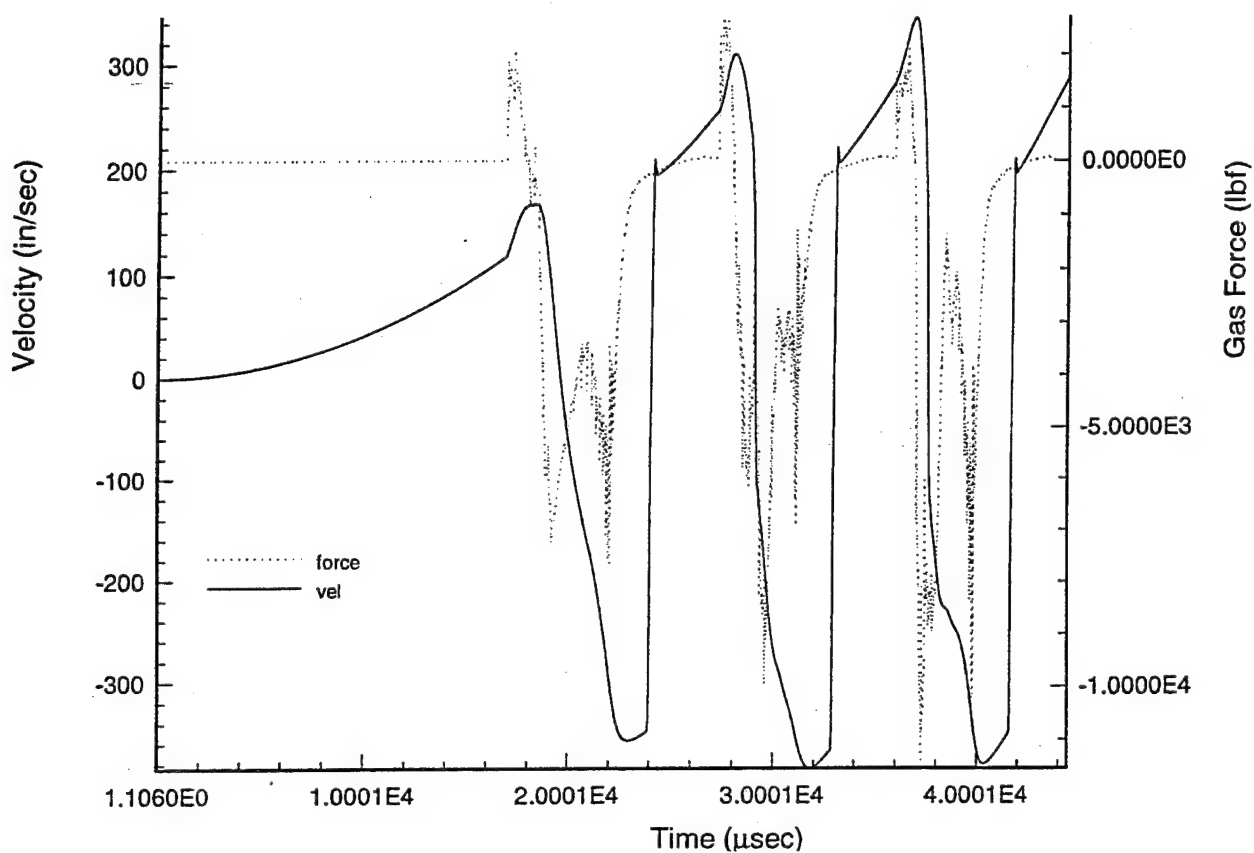
Figure E-4b. Histories of valve spool *velocity* and total gas dynamic force on valve spool. Damping forces are set at 16% viscous (on spool) plus 100lbf (on Belleville) Coulomb damping. The high-pressure boundary is 1400 psia; the low-pressure boundary is 14 psia.
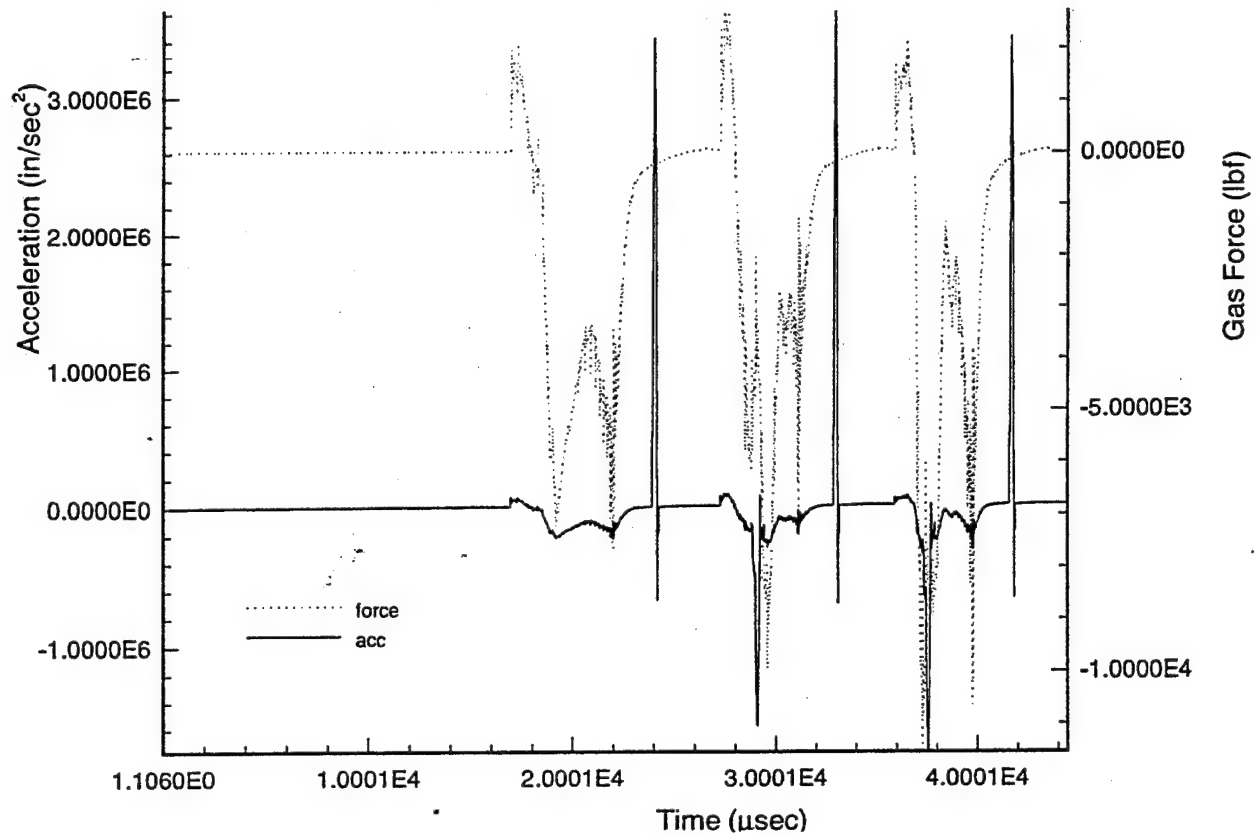
Figure E-4c. Histories of valve spool *acceleration* and total gas dynamic force on valve spool. Damping forces are set at 16% viscous (on spool) plus 100lbf (on Belleville) Coulomb damping. The high-pressure boundary is 1400 psia; the low-pressure boundary is 14 psia.
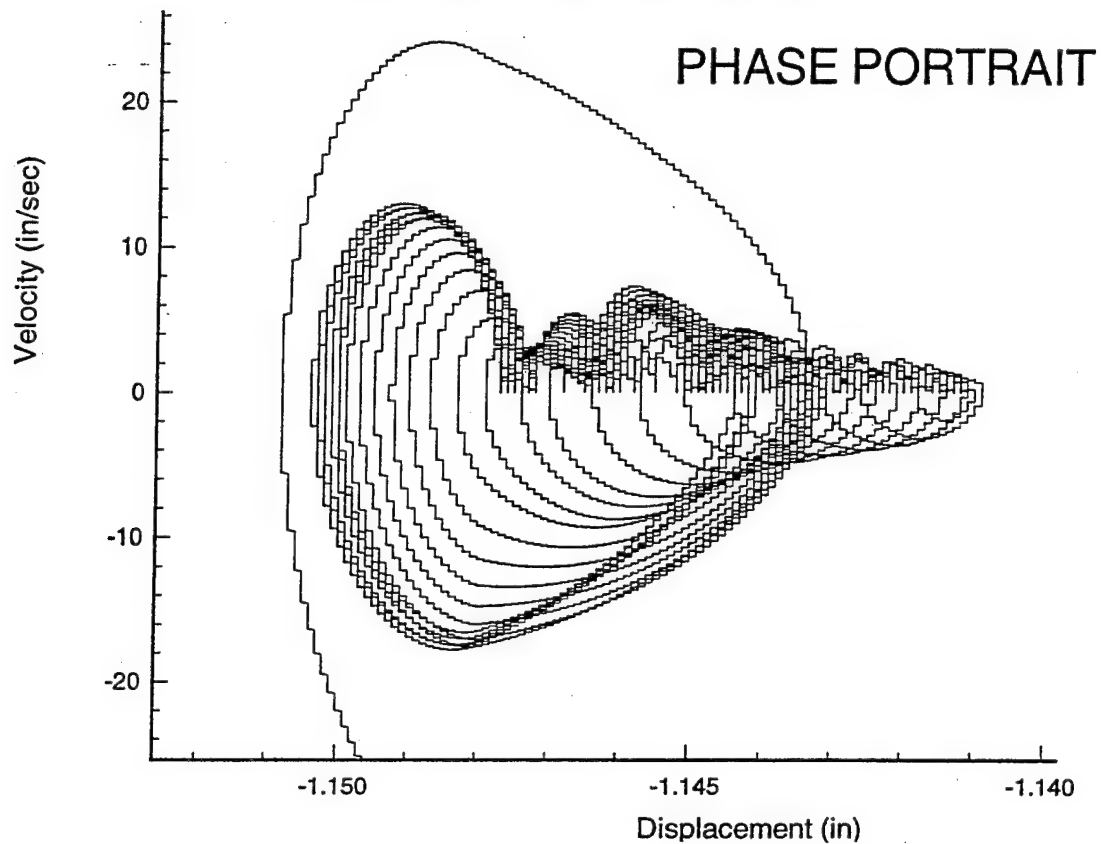
16 % Viscous + 100 lbf Bellville Damping

Figure E-4d. Histories of valve spool *acceleration (enlargement)* and total gas dynamic force on valve spool. Damping forces are set at 16% viscous (on spool) plus 100lbf (on Belleville) Coulomb damping. The high-pressure boundary is 1400 psia; the low-pressure boundary is 14 psia.

16 % Viscous + 100 lbf Bellville Damping

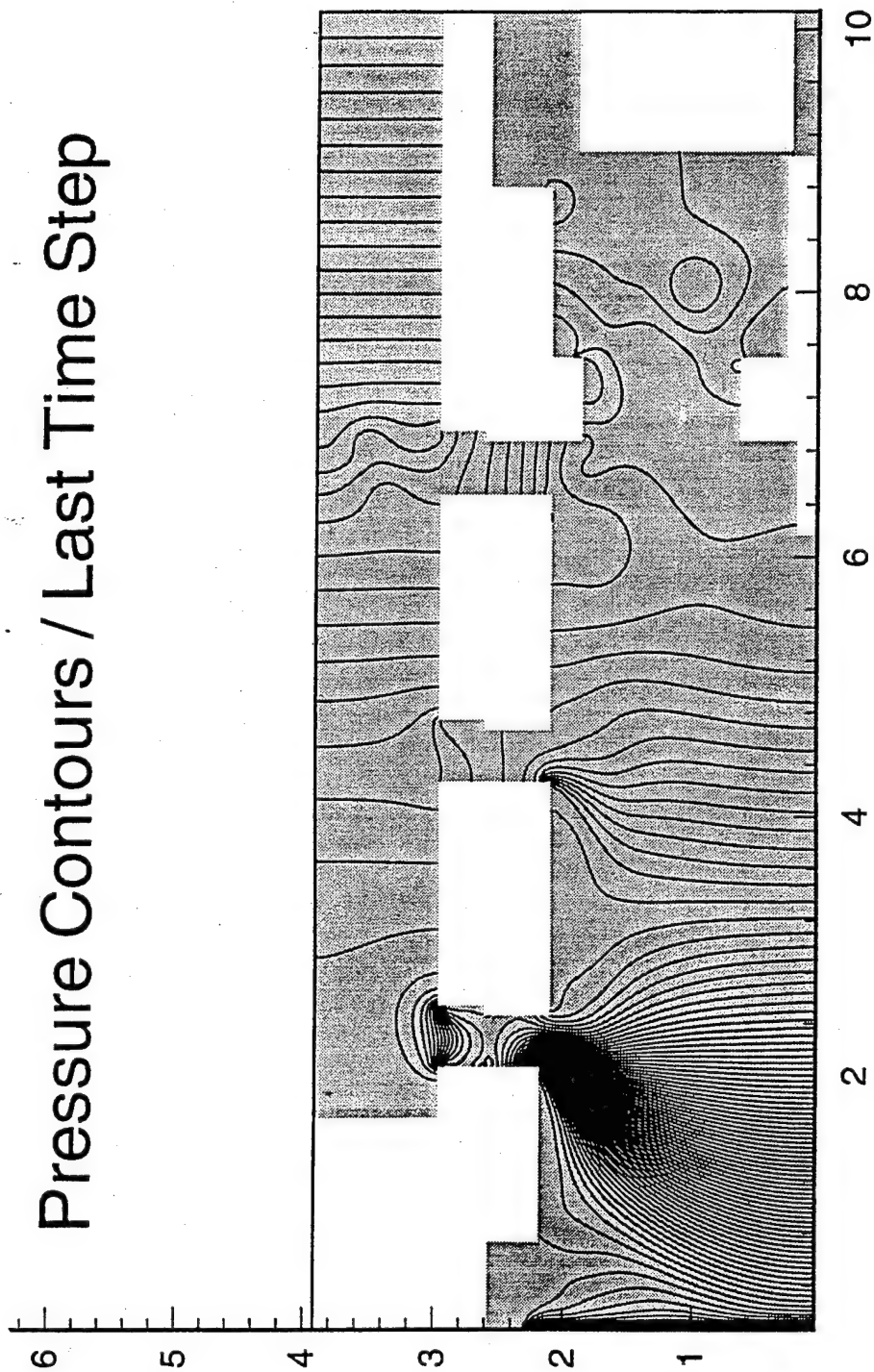**Figure E-4e.** Pressure history at the pressure history point and total gas dynamic force on valve spool. Damping forces are set at 16% viscous (on spool) plus 100lbf (on Belleville) Coulomb damping. The high-pressure boundary is 1400 psia; the low-pressure boundary is 14 psia.

Figure E-5. Spatial pressure distribution at time = 0.0443 sec. Isobars are at ~10-psi intervals.

Figure E-6. Proposed backward-opening ETVE gas dynamic simulation model. All dimensions are mm. (The schematic is not to scale.)

Figure E-7a. Histories of modified valve spool *displacement* and total gas dynamic force on modified valve spool. Damping forces are set at 8% viscous (on spool) plus 100 lbf (on Belleville) Coulomb Damping. The high-pressure boundary is 1400 psia; the low-pressure boundary is 14 psia.
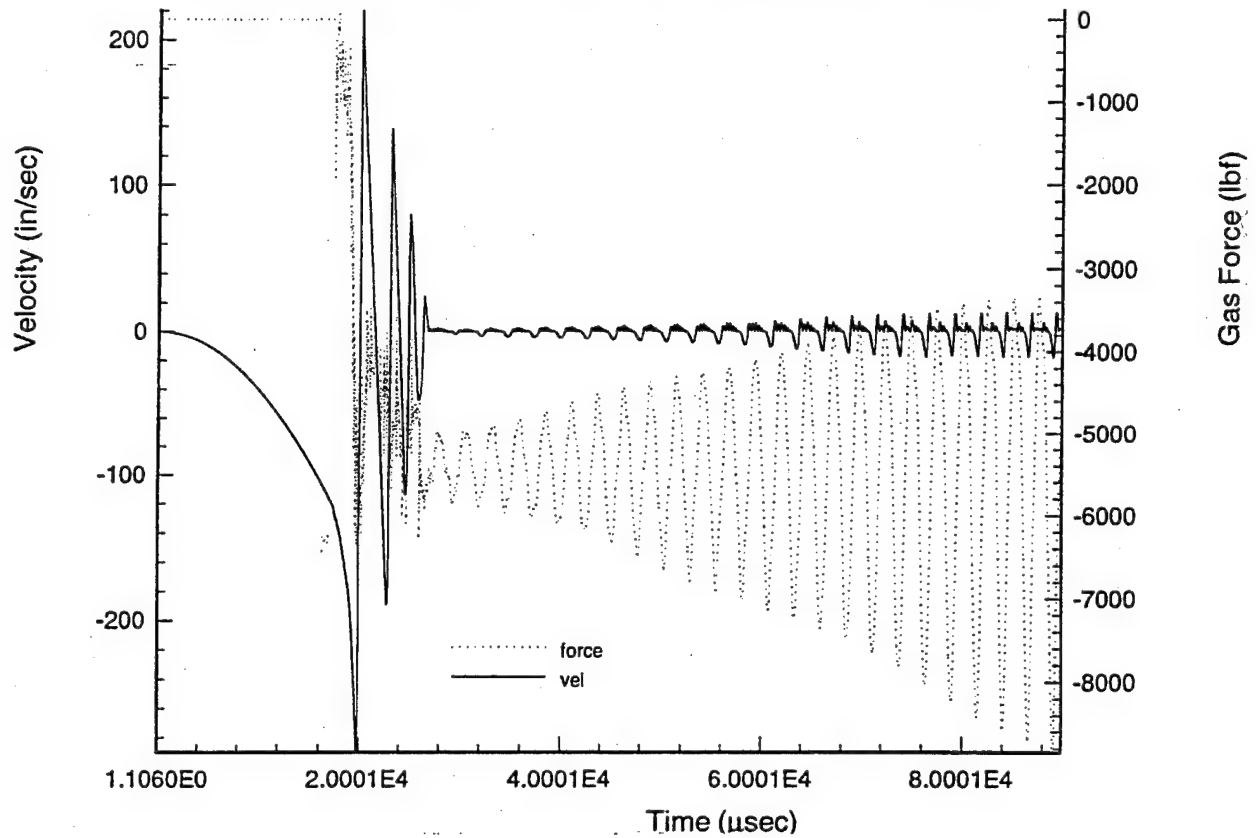
Figure 7-b. Histories of modified valve spool *velocity* and total gas dynamic force on modified valve spool. Damping forces are set at 8% viscous (on spool) plus 100 lbf (on Belleville) Coulomb Damping. The high-pressure boundary is 1400 psia; the low-pressure boundary is 14 psia.

Figure 7-c. Histories of modified valve spool *acceleration* and total gas dynamic force on modified valve spool. Damping forces are set at 8% viscous (on spool) plus 100 lbf (on Belleville) Coulomb Damping. The high-pressure boundary is 1400 psia; the low-pressure boundary is 14 psia.

E-28

8 % Viscous + 100 lbf Bellville Damping
Backward Opening / Lengthened Spool

Figure 7-d. Histories of modified valve spool *acceleration (enlarged)* and total gas dynamic force on modified valve spool. Damping forces are set at 8% viscous (on spool) plus 100 lbf (on Belleville) Coulomb Damping. The high-pressure boundary is 1400 psia; the low-pressure boundary is 14 psia.
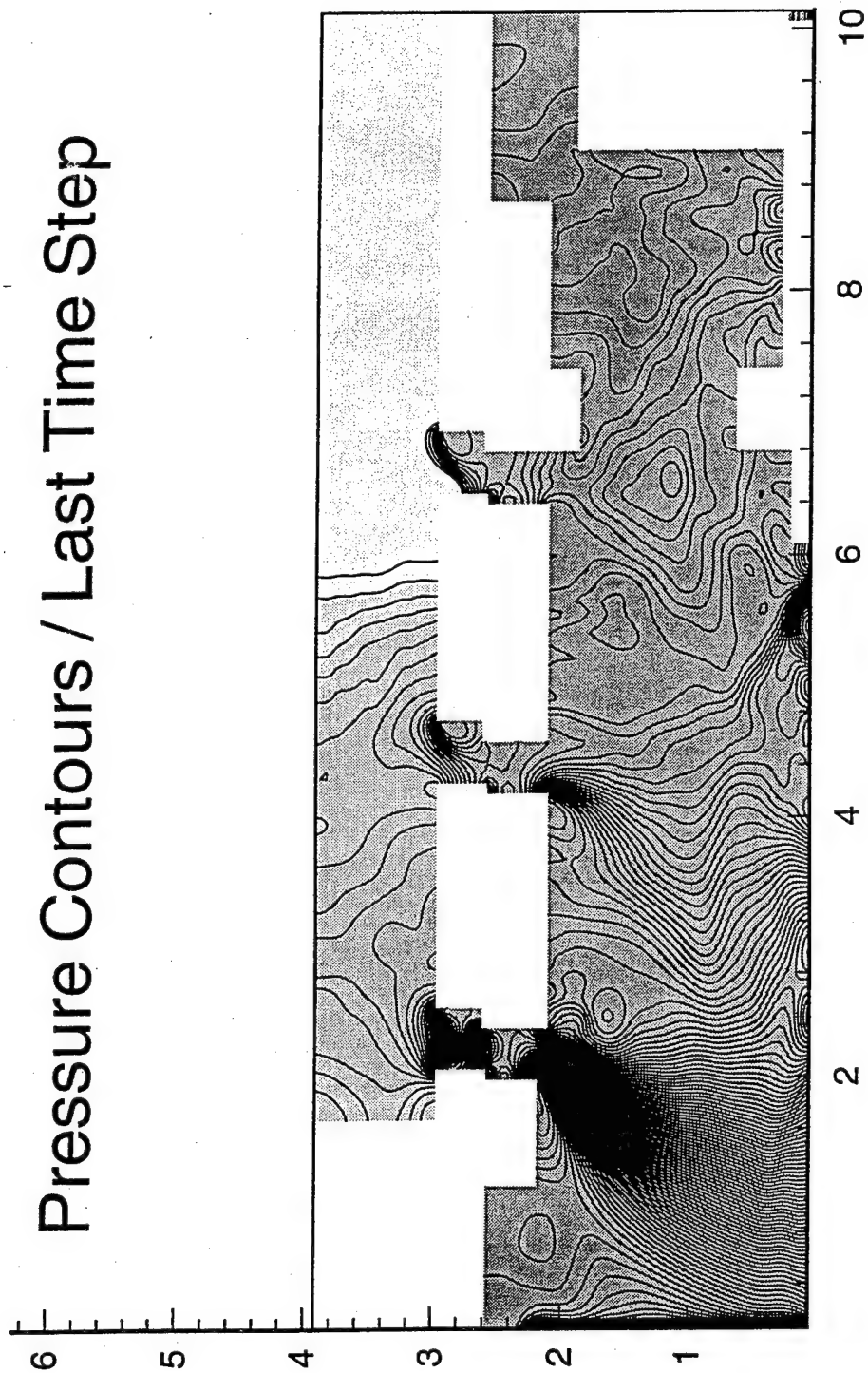
8 % Viscous + 100 lbf Bellville Damping
Backward Opening / Lengthened Spool

Figure 7-e. Pressure history at the pressure history point and total gas dynamic force on modified valve spool. Damping forces are set at 8% viscous (on spool) plus 100 lbf (on Belleville) Coulomb Damping. The high-pressure boundary is 1400 psia; the low-pressure boundary is 14 psia.

8 % Viscous + 100 lbf Bellville Damping
Backward Opening / Lengthened Spool

PHASE PORTRAIT

Velocity (in/sec) — *Displacement (in)*

Figure 8-a. Phase plane portrait for modified valve spool motion. Damping forces are set at 8% viscous (on spool) plus 100 lbf (on Belleville) Coulomb damping. The high-pressure boundary is 1400 psia; the low-pressure boundary is 14 psia.

Figure E-8b. Phase plane portrait enlargement of node region (Figure E-8a) around the valve open position.

Pressure Contours / Last Time Step

Figure E-9. Spatial pressure distribution about modified valve spool at time = 0.090 sec. Isobars are at ~10-psi intervals.
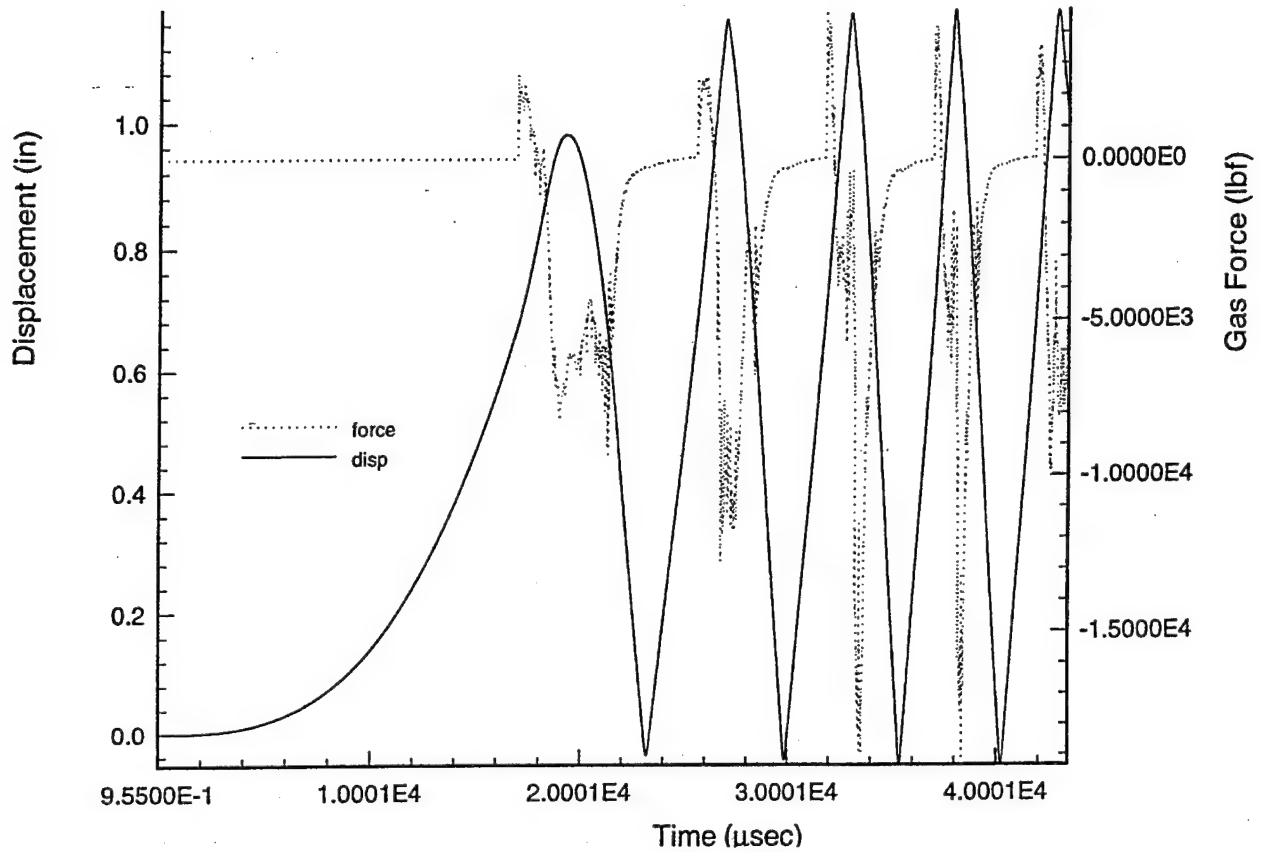
Figure E-10a. Histories of valve spool *displacement* and total gas dynamic force on valve spool. Damping forces are set at 8% viscous (on spool) plus 100lbf (on Belleville) Coulomb damping. The high-pressure boundary is 1800 psia; the low-pressure boundary is 12 psia.
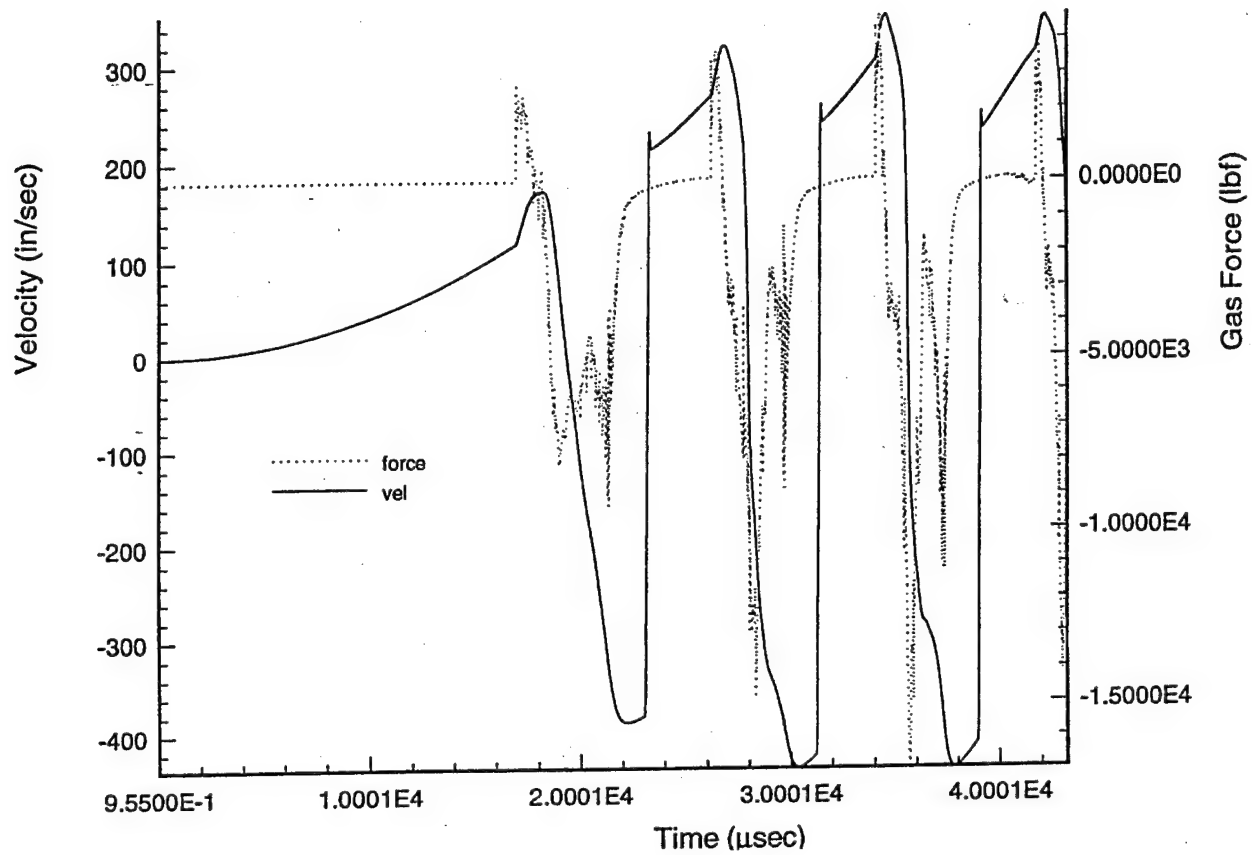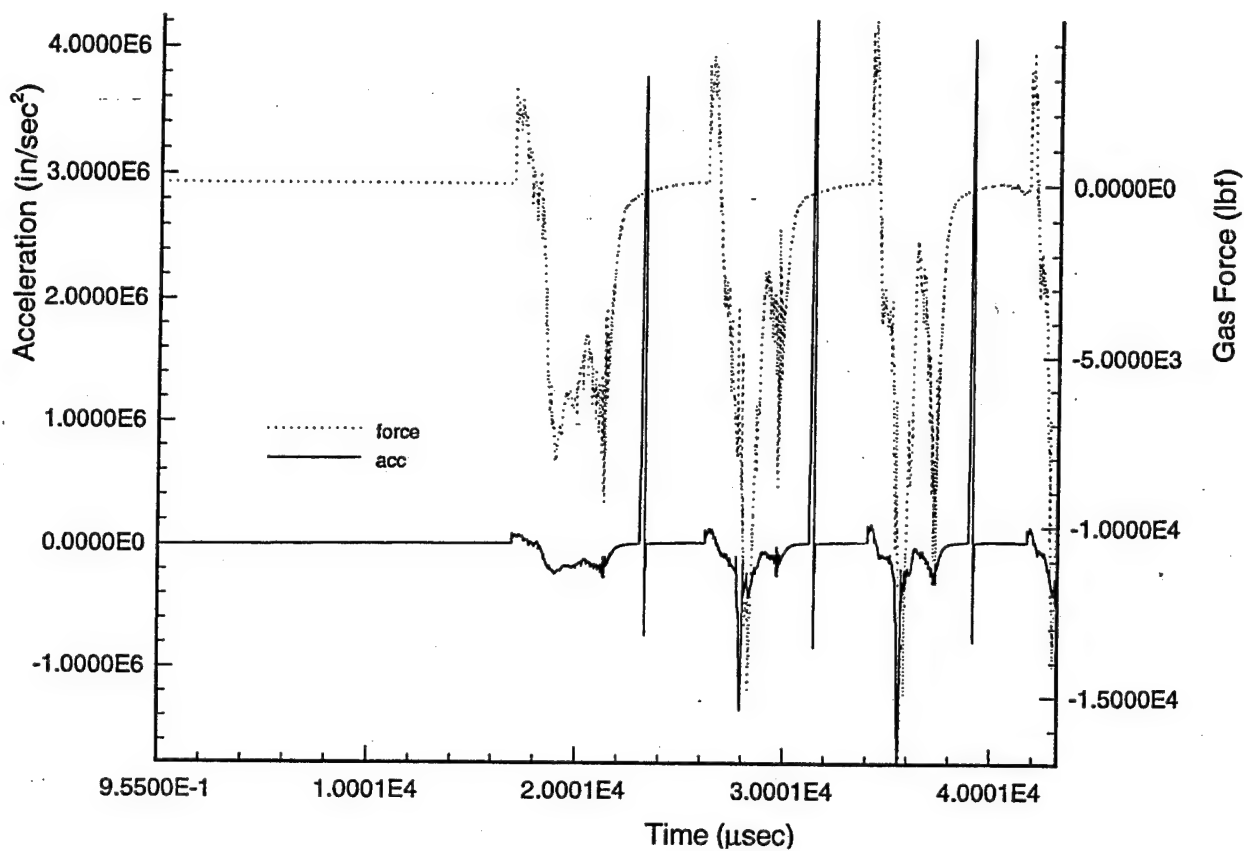
E-34

8% Viscous + 100 lbf Bellville Damping
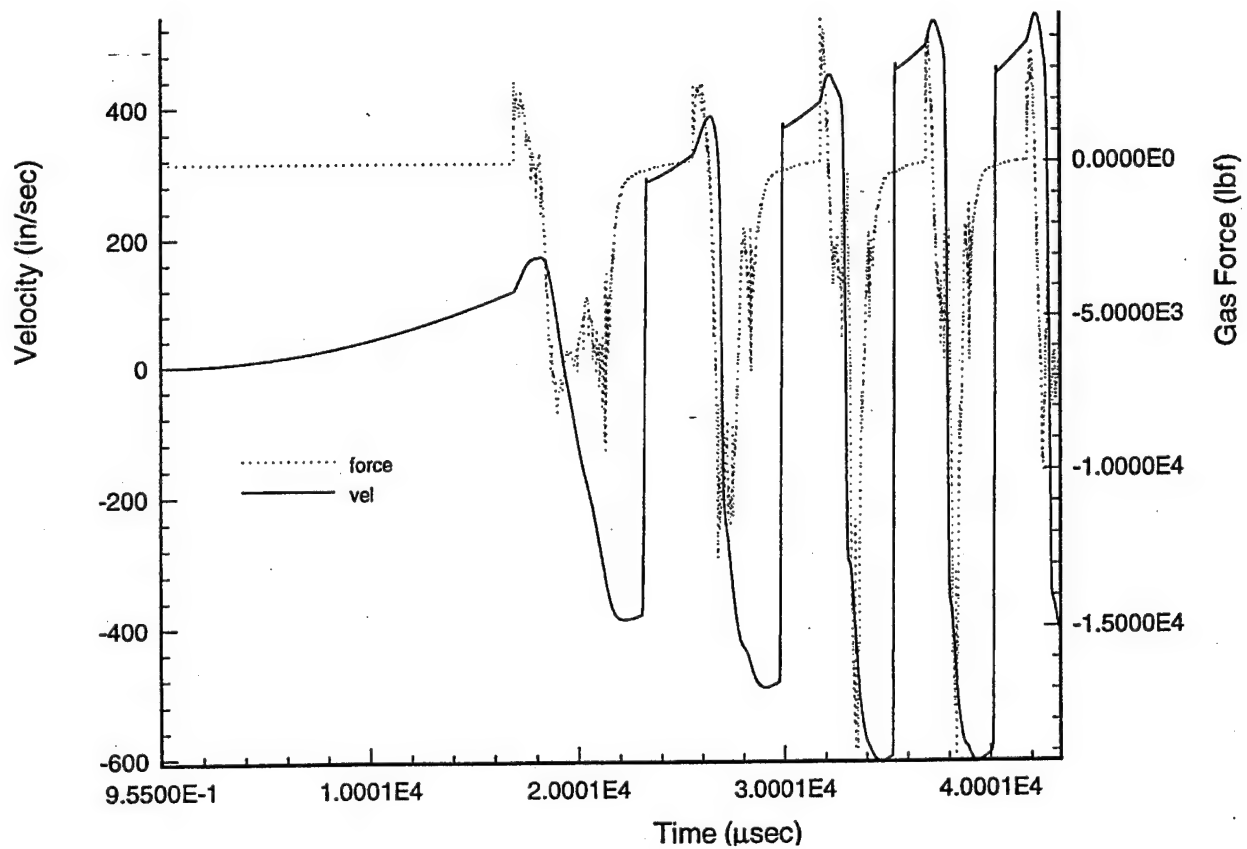
Figure E-10b. Histories of valve spool *velocity* and total gas dynamic force on valve spool. Damping forces are set at 8% viscous (on spool) plus 100lbf (on Belleville) Coulomb damping. The high-pressure boundary is 1800 psia; the low-pressure boundary is 12 psia.
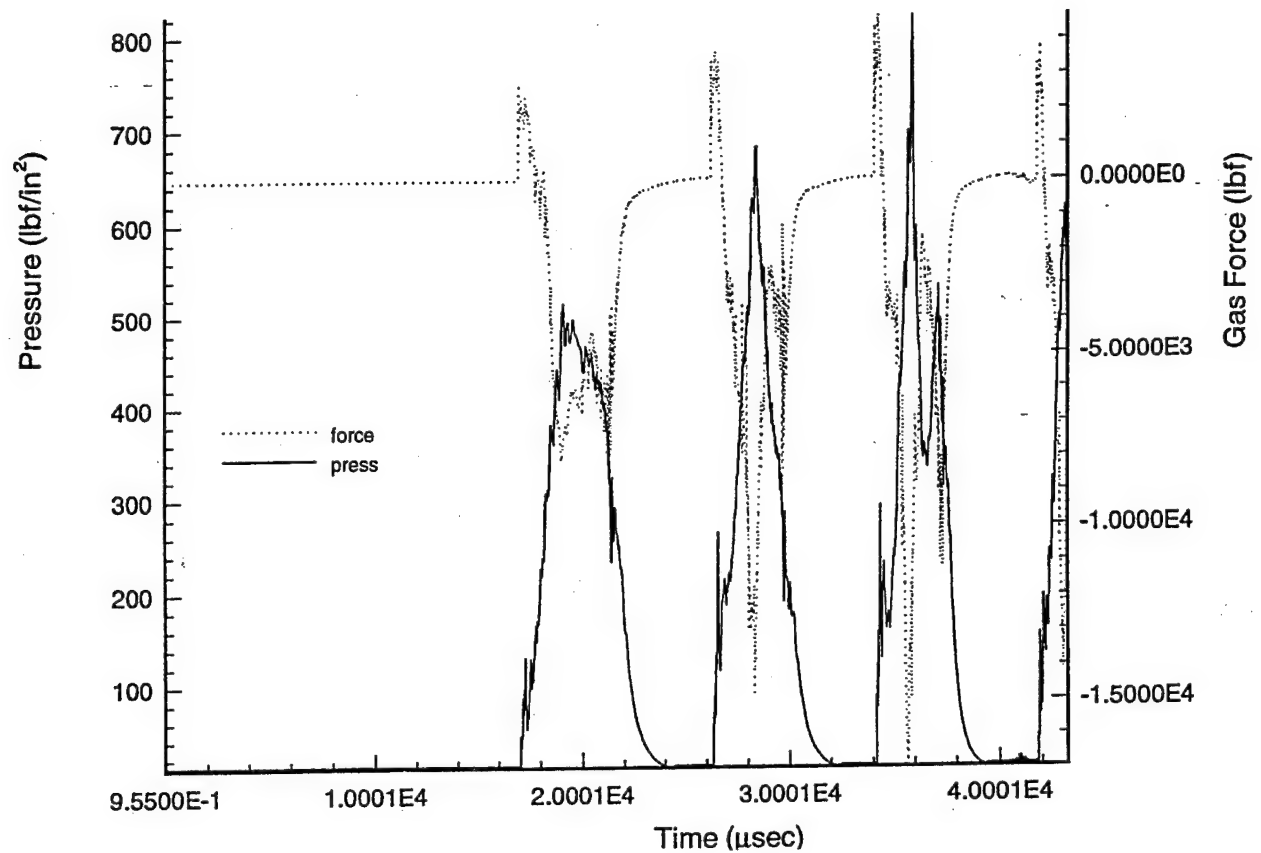
8% Viscous + 100 lbf Bellville Damping
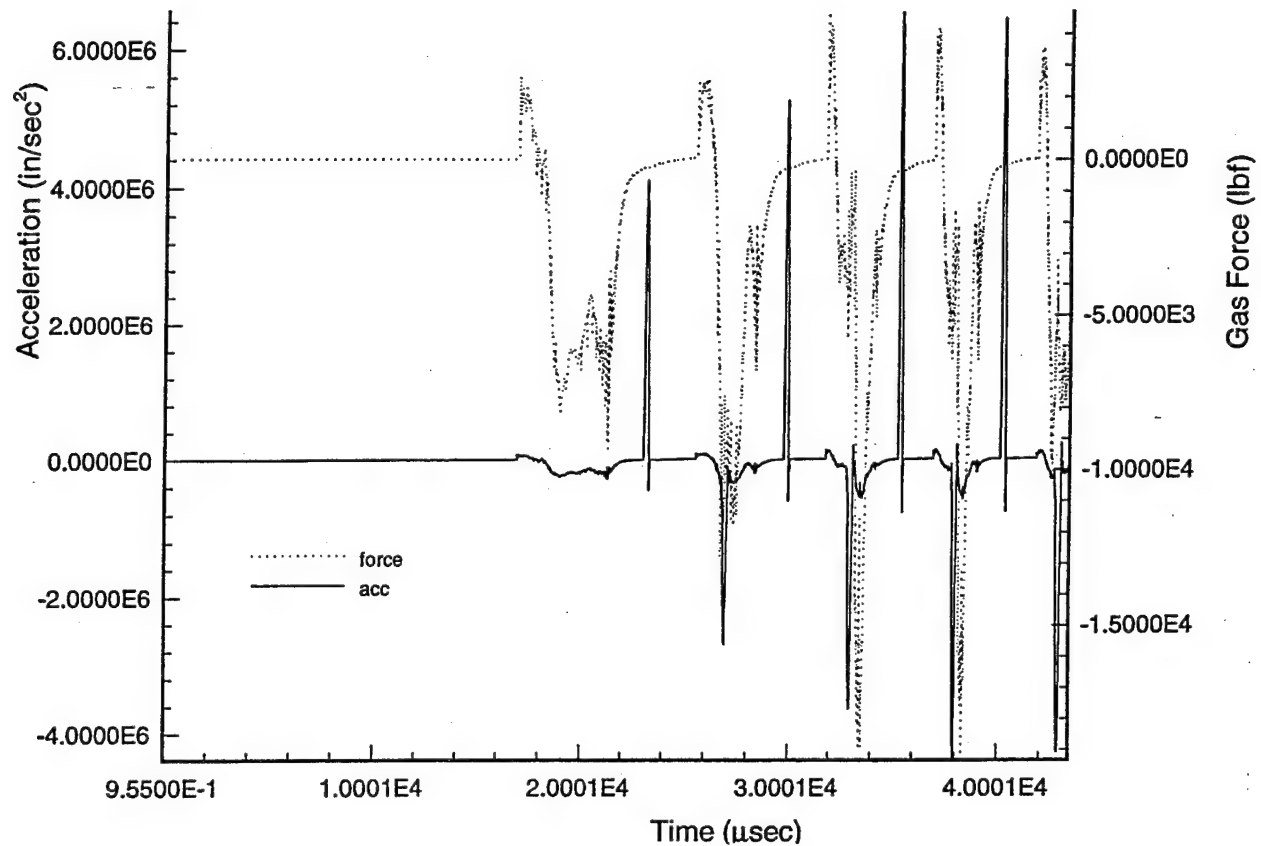
Figure E-10c. Histories of valve spool *acceleration* and total gas dynamic force on valve spool. Damping forces are set at 8% viscous (on spool) plus 100lbf (on Belleville) Coulomb damping. The high-pressure boundary is 1800 psia; the low-pressure boundary is 12 psia.
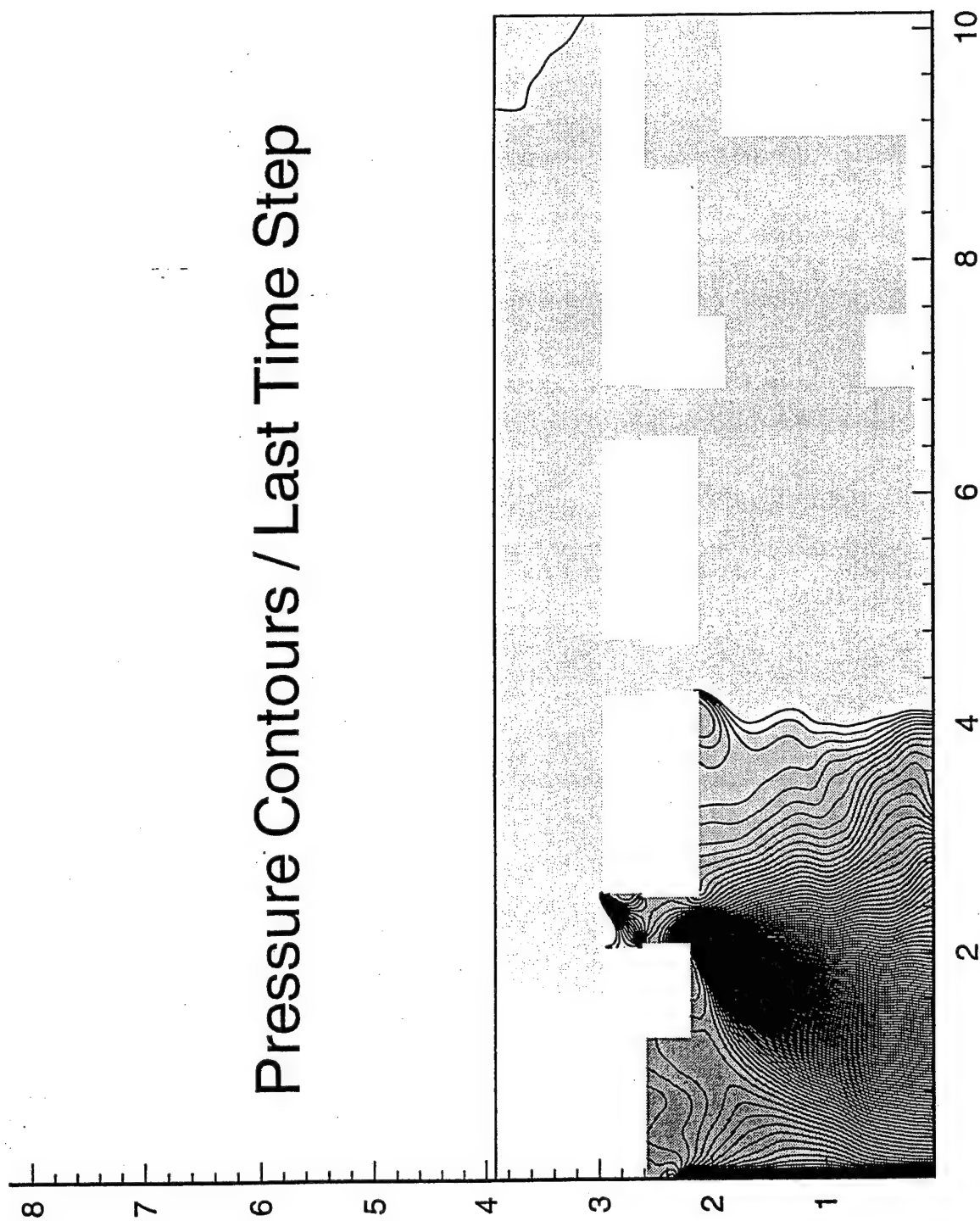
8% Viscous + 100 lbf Bellville Damping
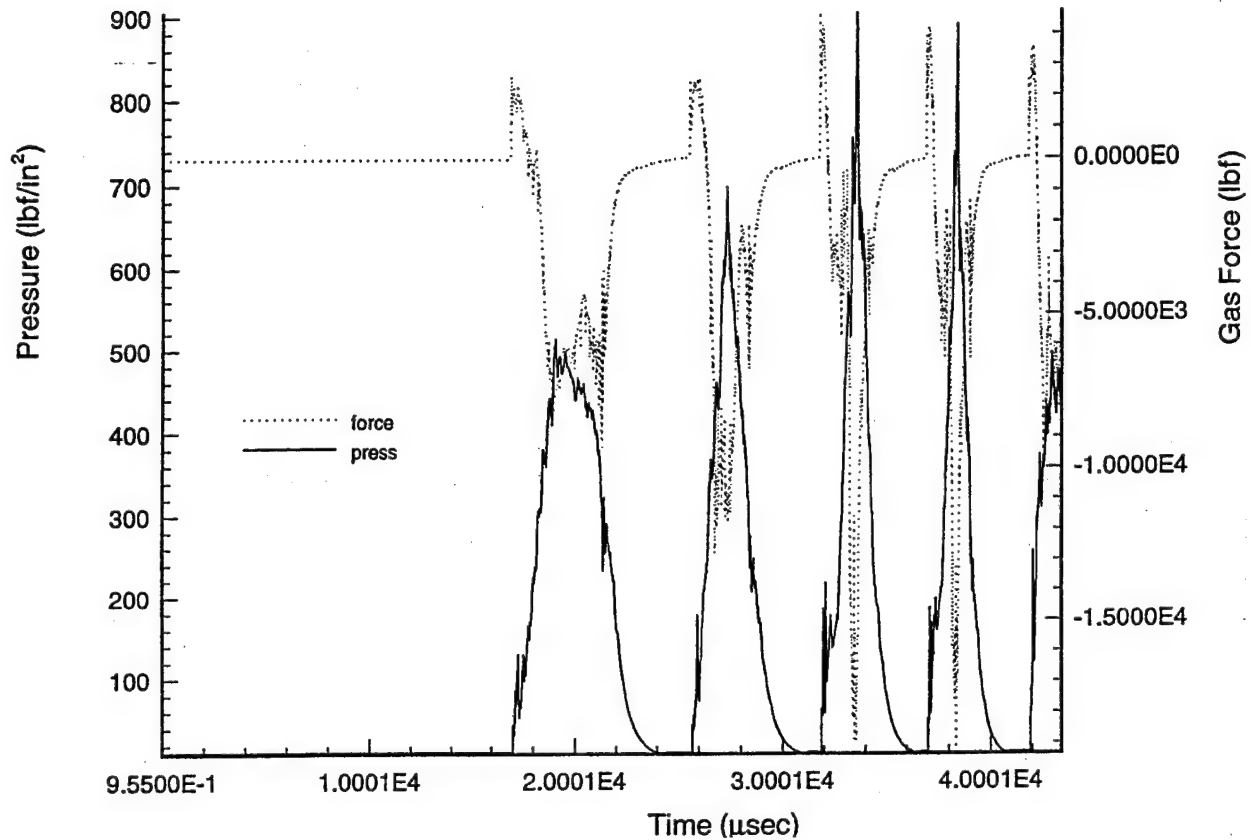
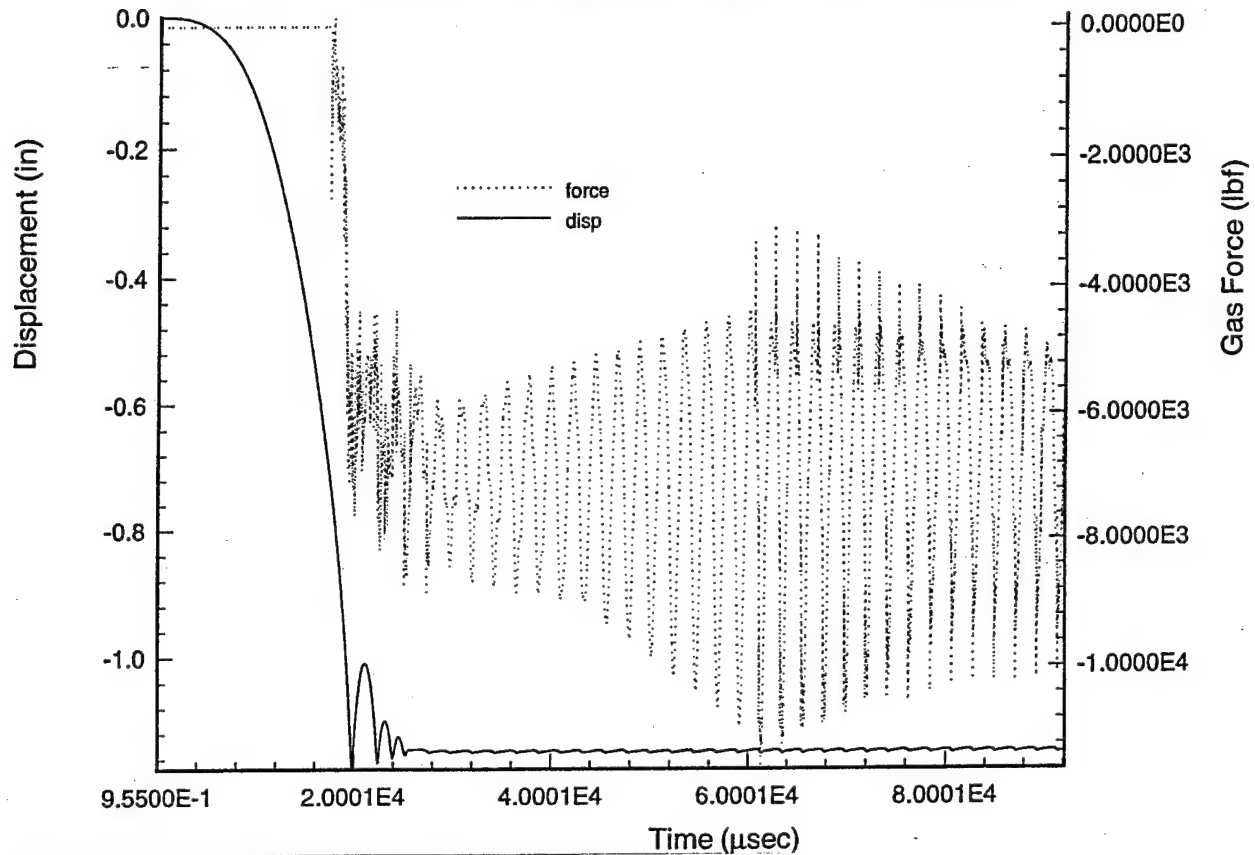**Figure E-10d.** Pressure history at the pressure history point and total gas dynamic force on valve spool. Damping forces are set at 8% viscous (on spool) plus 100lbf (on Belleville) Coulomb damping. The high-pressure boundary is 1800 psia; the low-pressure boundary is 12 psia.

Pressure Contours / Last Time Step

Figure E-11. Spatial pressure distribution at time = 0.0432 sec. Isobars are at 12-psi intervals.
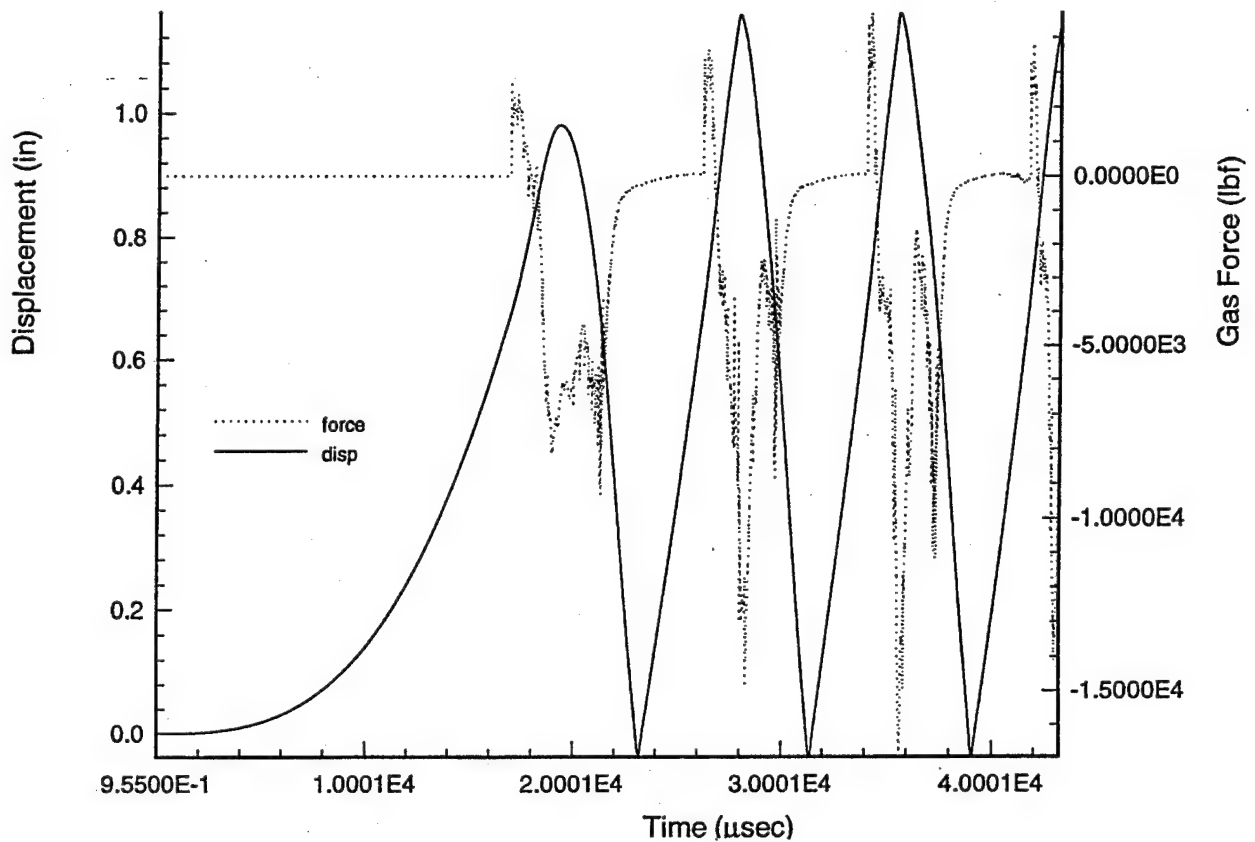
Figure E-12a. Histories of valve spool *displacement* and total gas dynamic force on valve spool. Damping forces are set at 16% viscous (on spool) plus 100lbf (on Belleville) Coulomb damping. The high-pressure boundary is 1800 psia; the low-pressure boundary is 12 psia.

Figure E-12b. Histories of valve spool *velocity* and total gas dynamic force on valve spool. Damping forces are set at 16% viscous (on spool) plus 100lbf (on Belleville) Coulomb damping. The high-pressure boundary is 1800 psia; the low-pressure boundary is 12 psia.
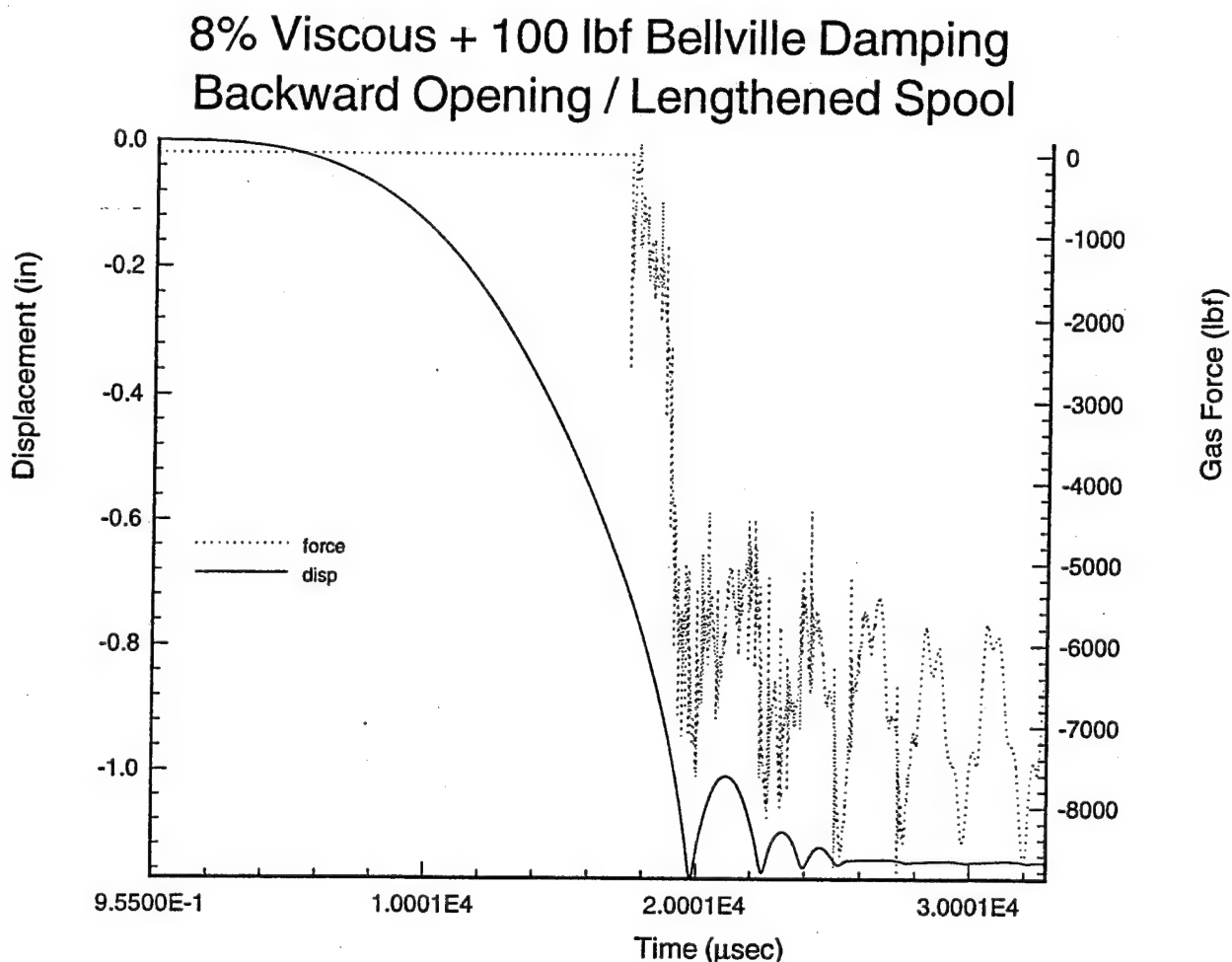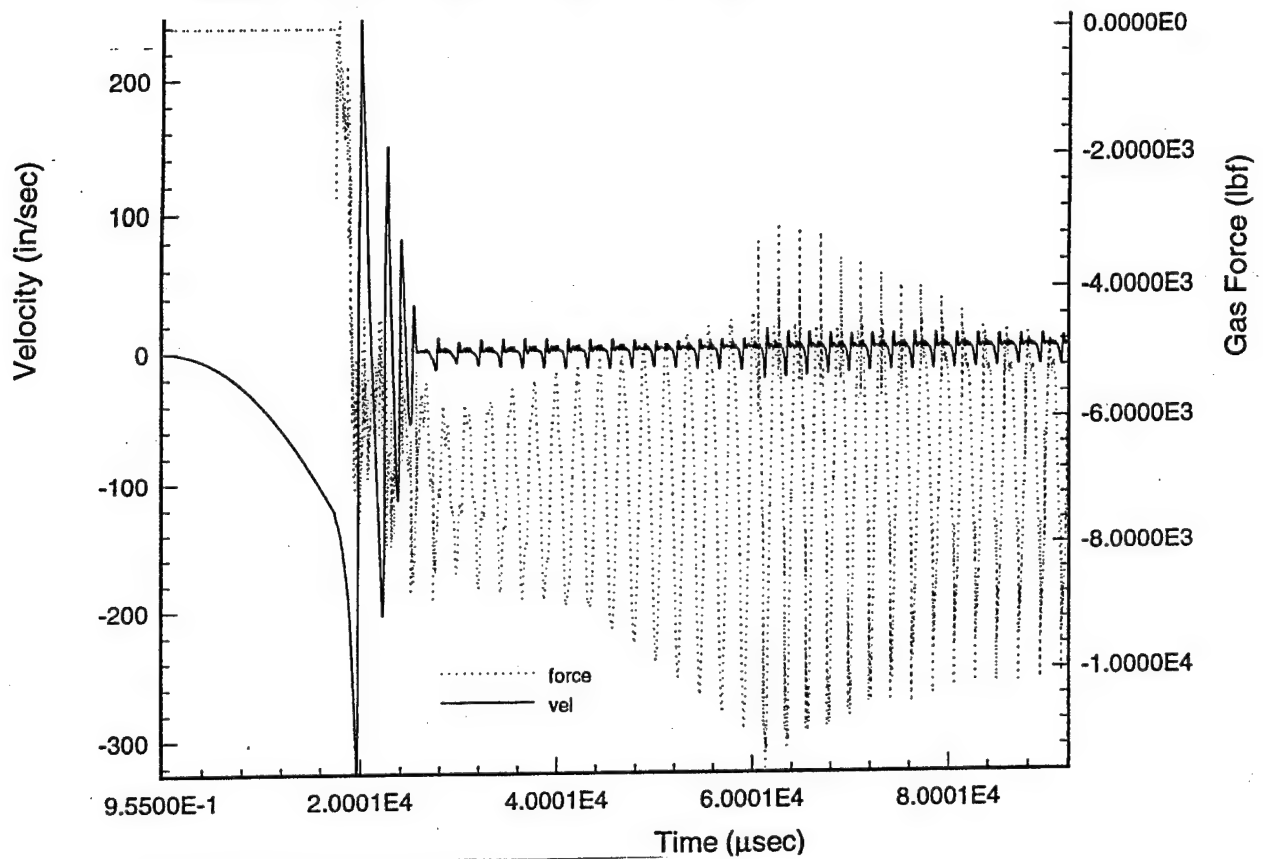
Figure E-12c. Histories of valve spool *acceleration* and total gas dynamic force on valve spool. Damping forces are set at 16% viscous (on spool) plus 100lbf (on Belleville) Coulomb damping. The high-pressure boundary is 1800 psia; the low-pressure boundary is 12 psia.

16% Viscous + 100 lbf Bellville Damping

Figure E-12d. Pressure history at the pressure history point and total gas dynamic force on valve spool. Damping forces are set at 16% viscous (on spool) plus 100lbf (on Belleville) Coulomb damping. The high-pressure boundary is 1800 psia; the low-pressure boundary is 12 psia.

Pressure Contours / Last Time Step

Figure E-13. Spatial pressure distribution at time = 0.0432 sec. Isobars are at 12-psi intervals.

Figure E-14a. Histories of modified valve spool *displacement* and total gas dynamic force on modified valve spool. Damping forces are set at 8% viscous (on spool) plus 100 lbf (on Belleville) Coulomb Damping. The high-pressure boundary is 1800 psia; the low-pressure boundary is 12 psia.
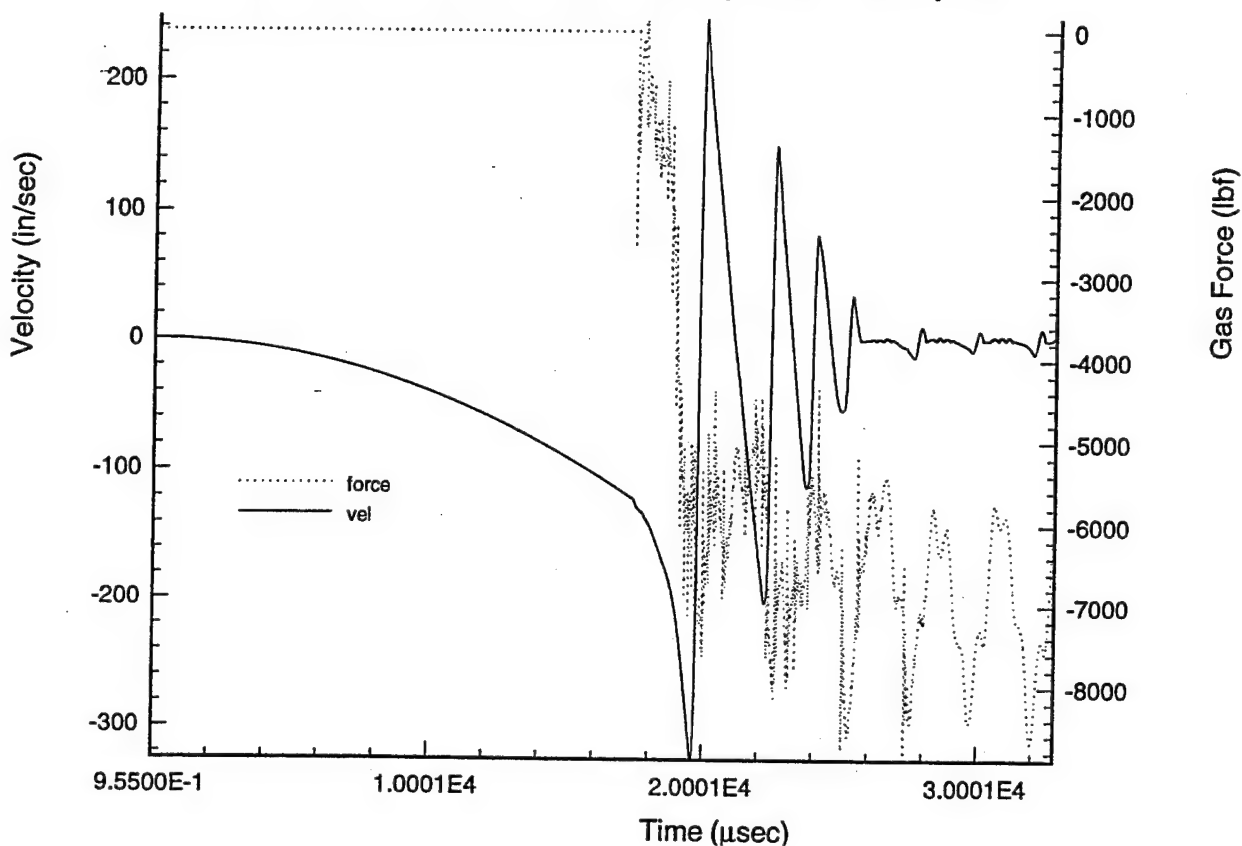
Figure E-14b. Histories of modified valve spool *displacement (enlargement)* and total gas dynamic force on modified valve spool. Damping forces are set at 8% viscous (on spool) plus 100 lbf (on Belleville) Coulomb Damping. The high-pressure boundary is 1800 psia; the low-pressure boundary is 12 psia.

Figure E-14c. Histories of modified valve spool *velocity* and total gas dynamic force on modified valve spool. Damping forces are set at 8% viscous (on spool) plus 100 lbf (on Belleville) Coulomb Damping. The high-pressure boundary is 1800 psia; the low-pressure boundary is 12 psia.
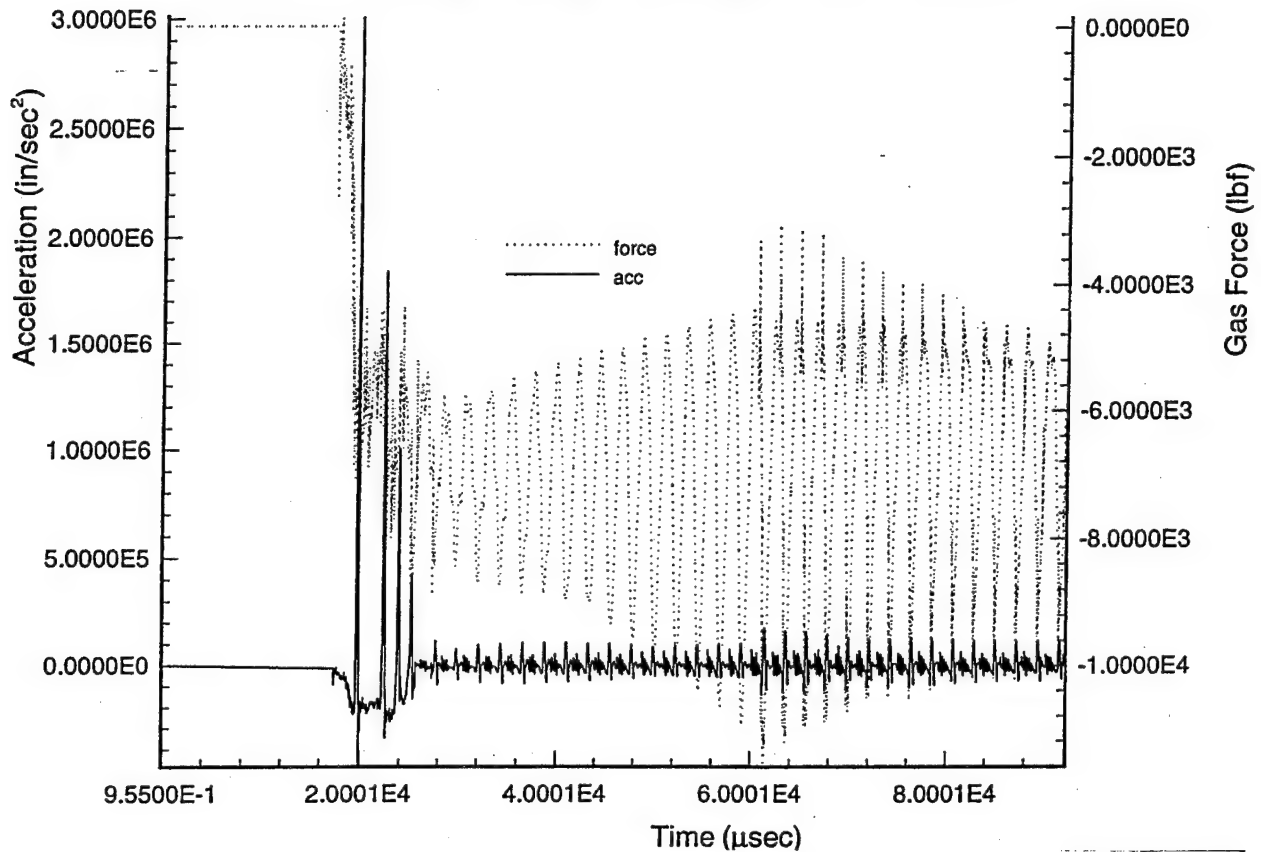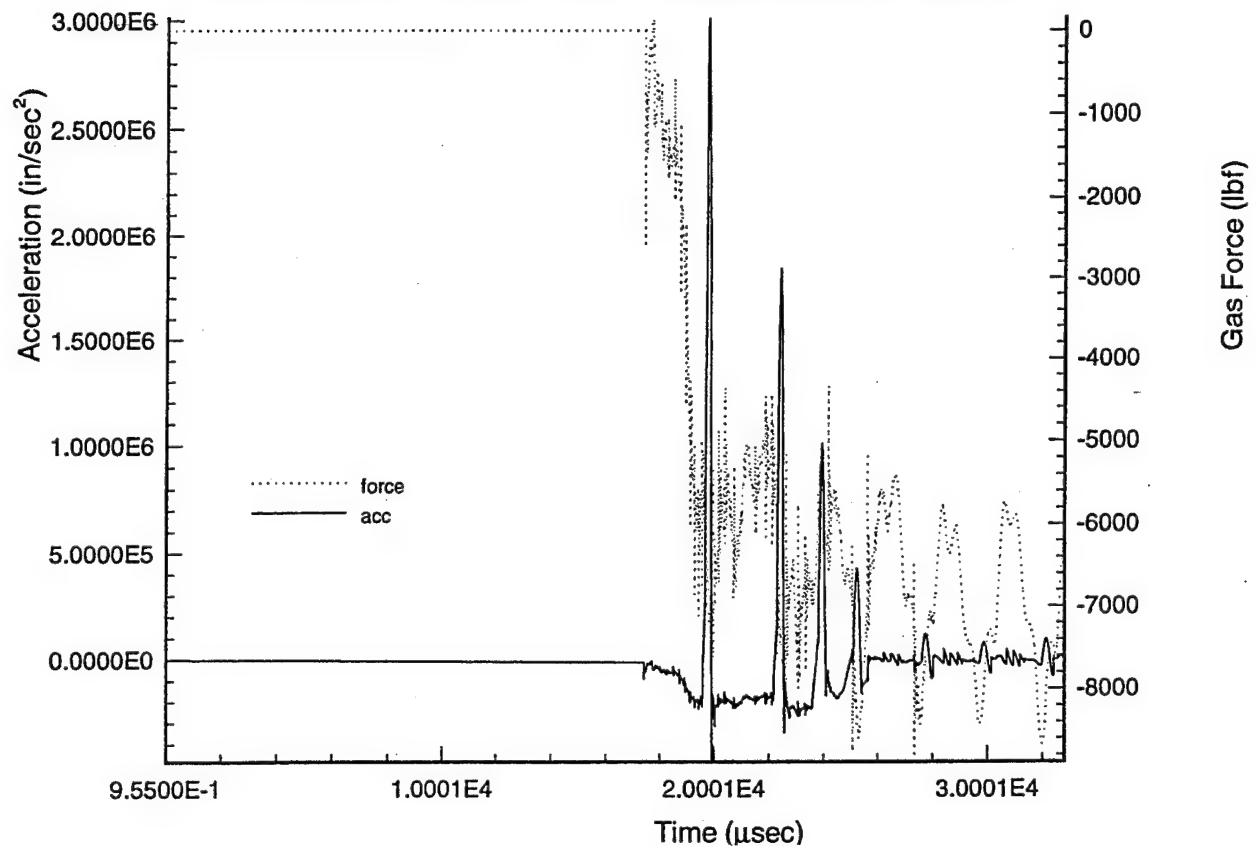
Figure E-14d. Histories of valve spool *velocity (enlargement)* and total gas dynamic force on modified valve spool. Damping forces are set at 8% viscous (on spool) plus 100 lbf (on Belleville) Coulomb Damping. The high-pressure boundary is 1800 psia; the low-pressure boundary is 12 psia.
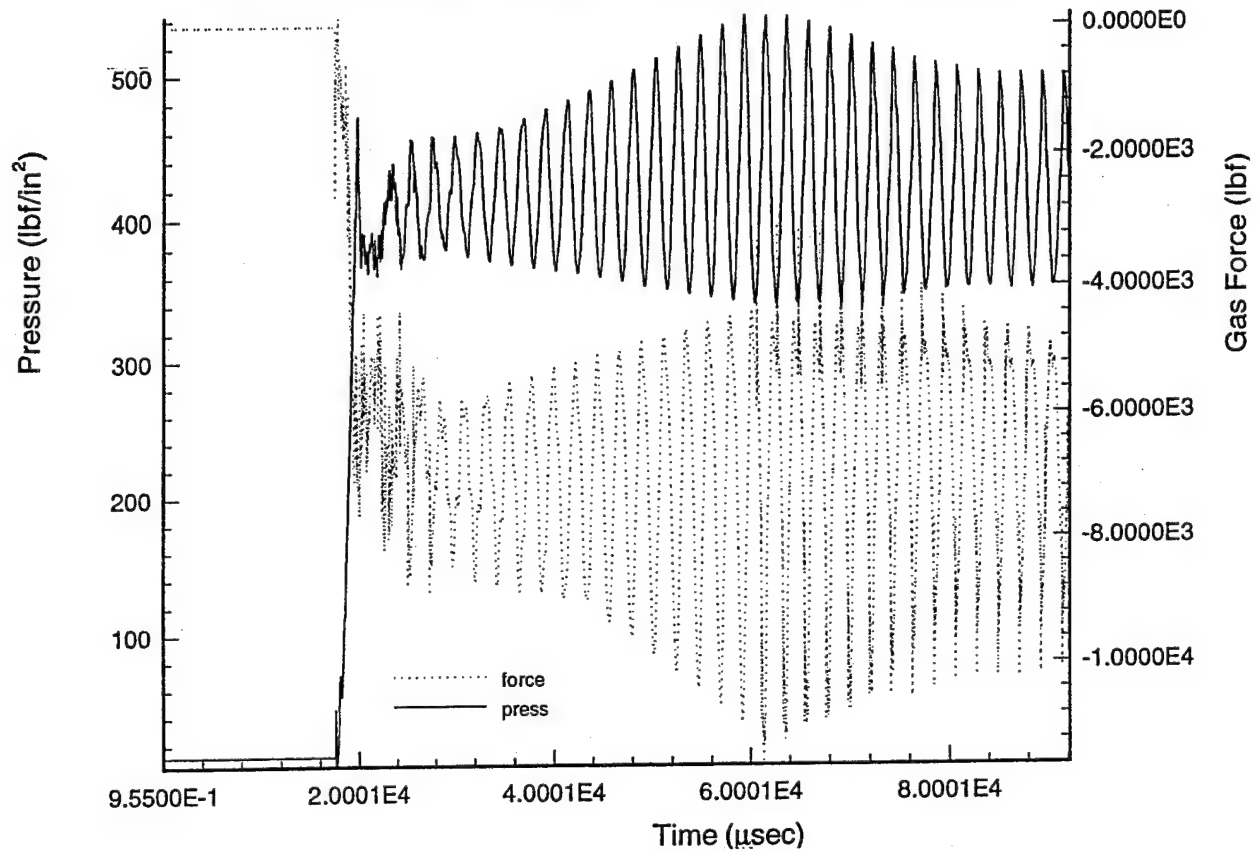
Figure E-14e. Histories of valve spool *acceleration* and total gas dynamic force on modified valve spool. Damping forces are set at 8% viscous (on spool) plus 100 lbf (on Belleville) Coulomb Damping. The high-pressure boundary is 1800 psia; the low-pressure boundary is 12 psia.
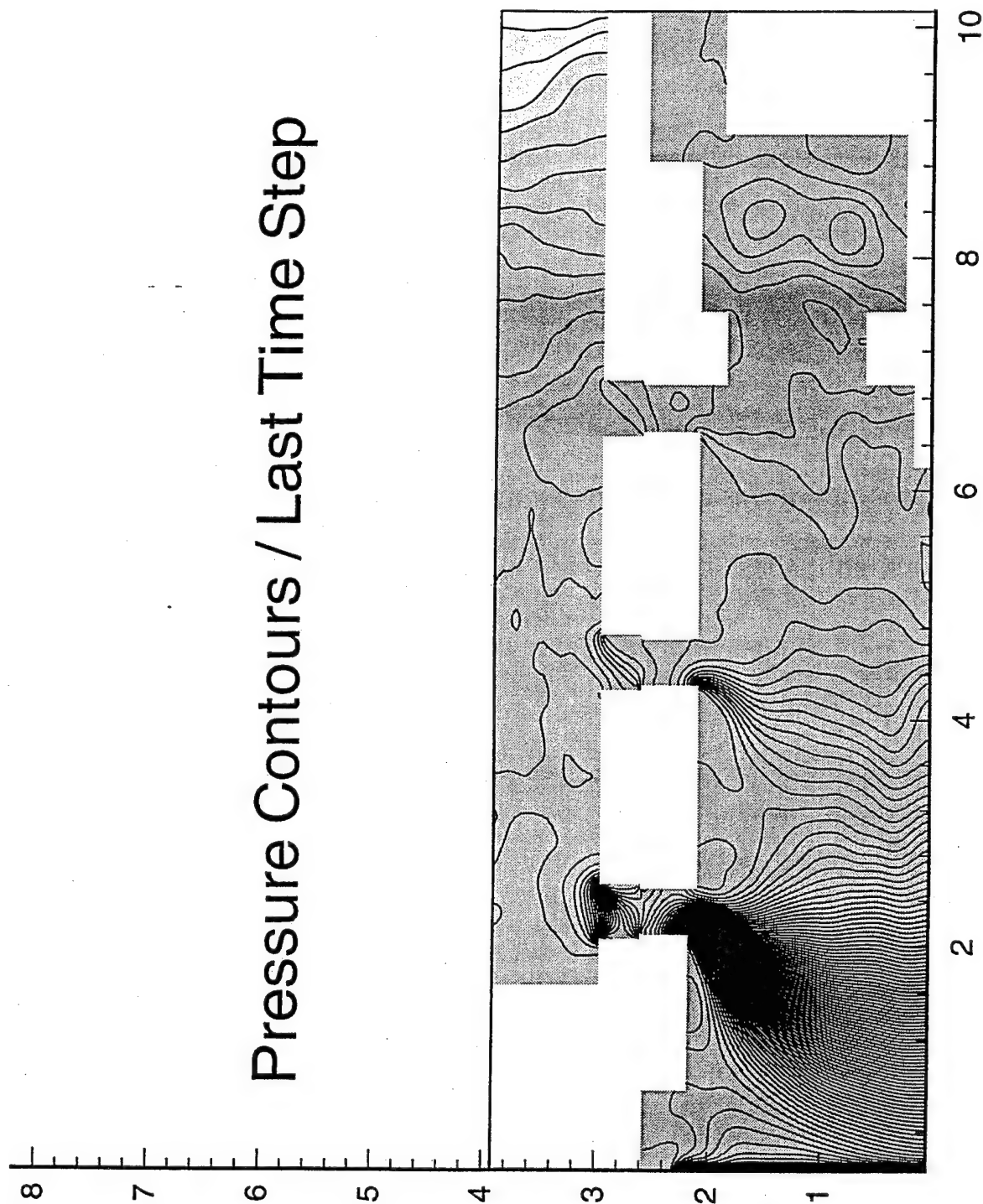
Figure E-14f. Histories of valve spool *Acceleration (enlargement)* and total gas dynamic force on modified valve spool. Damping forces are set at 8% viscous (on spool) plus 100 lbf (on Belleville) Coulomb Damping. The high-pressure boundary is 1800 psia; the low-pressure boundary is 12 psia.

8% Viscous + 100 lbf Bellville Damping Backward Opening / Lengthened Spool

Figure E-14g. Pressure history at the pressure history point and total gas dynamic force on modified valve spool. Damping forces are set at 8% viscous (on spool) plus 100 lbf (on Belleville) Coulomb Damping. The high-pressure boundary is 1800 psia; the low-pressure boundary is 12 psia.

Pressure Contours / Last Time Step

Figure E-15. Spatial pressure distribution about modified valve spool at time = 0.092 sec. Isobars are at 13-psi intervals.

Figure E-16a. Histories of modified valve spool displacement and total gas dynamic force on modified valve spool, with modified boundary condition. Damping forces are set at 8% viscous (on spool) plus 100 lbf (on Belleville) Coulomb Damping. The high-pressure boundary is 1800 psia; the low-pressure boundary is 12 psia.

Figure E-16b. Histories of modified valve spool *velocity* and total gas dynamic force on modified valve spool, with modified boundary condition. Damping forces are set at 8% viscous (on spool) plus 100 lbf (on Belleville) Coulomb Damping. The high-pressure boundary is 1800 psia; the low-pressure boundary is 12 psia.

8% Viscous + 100 lbf Bellville Damping
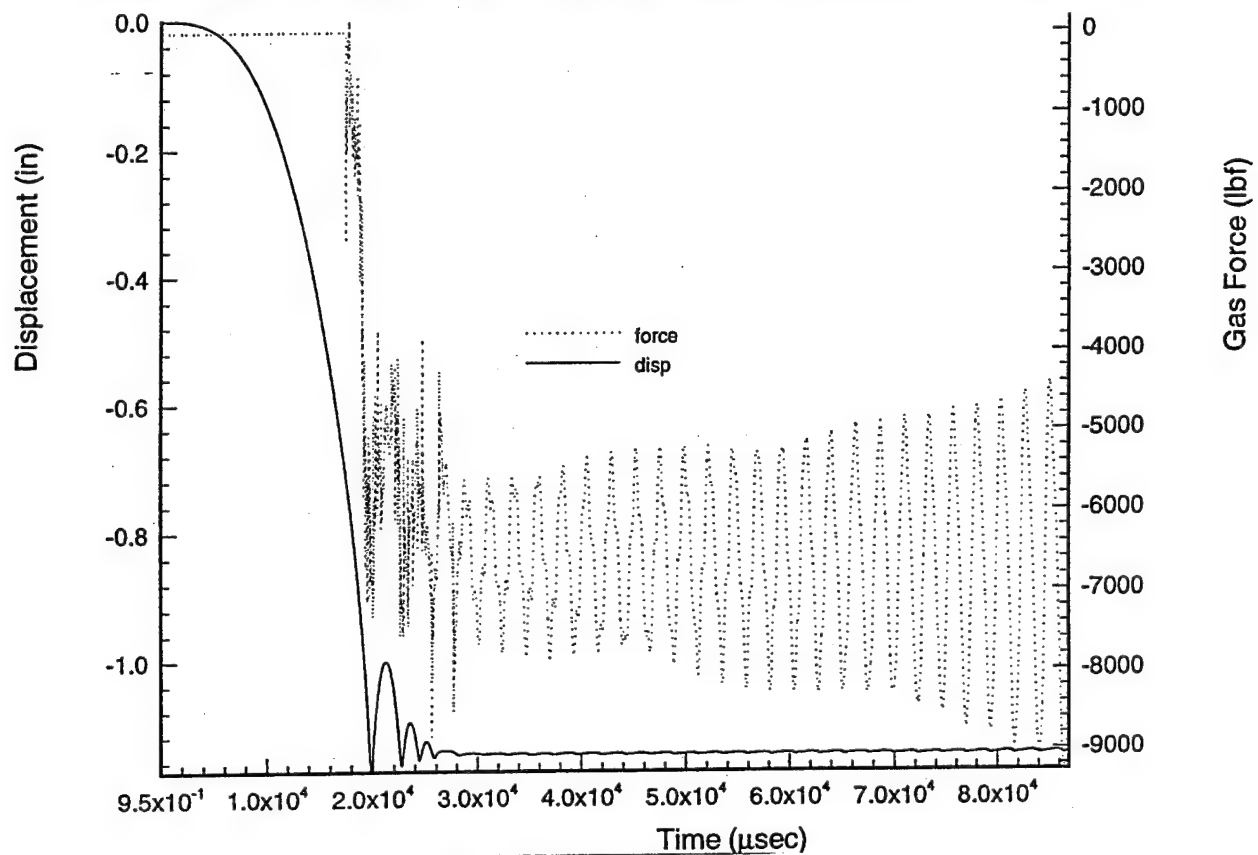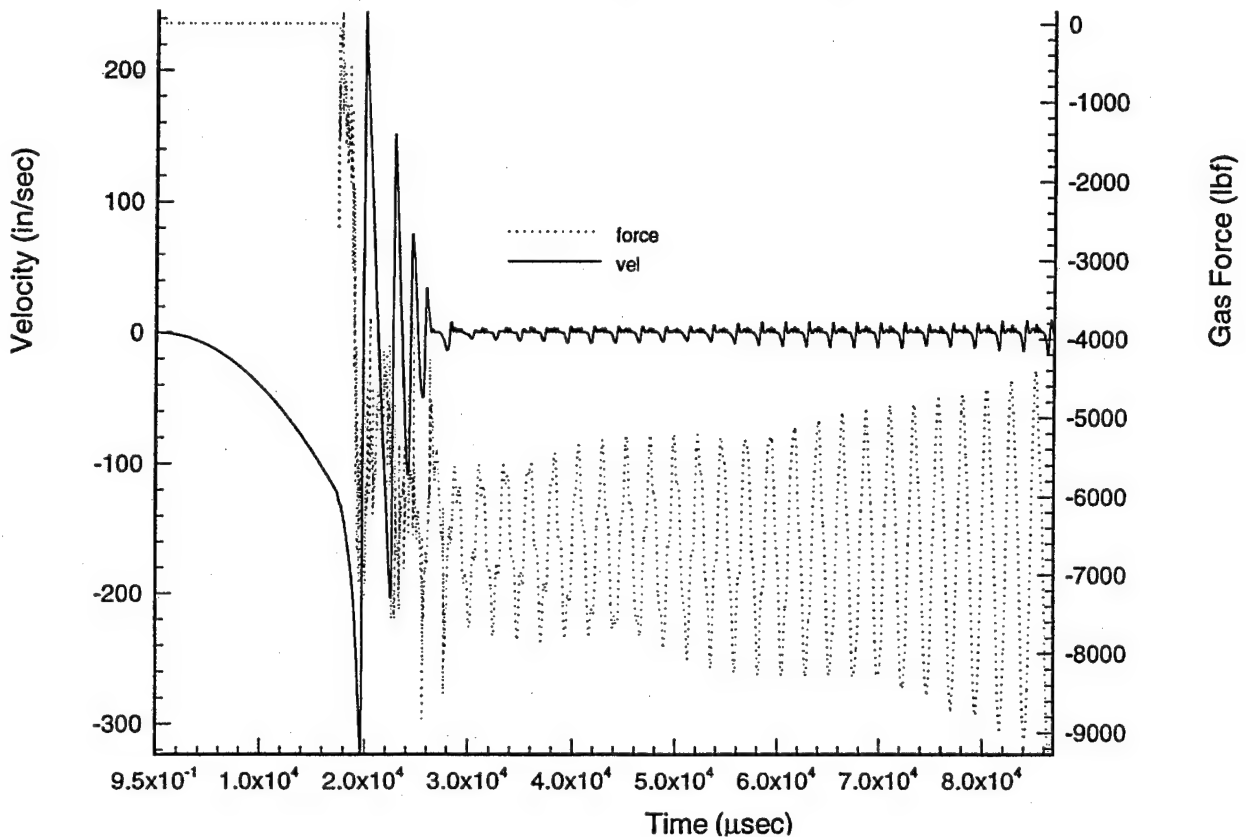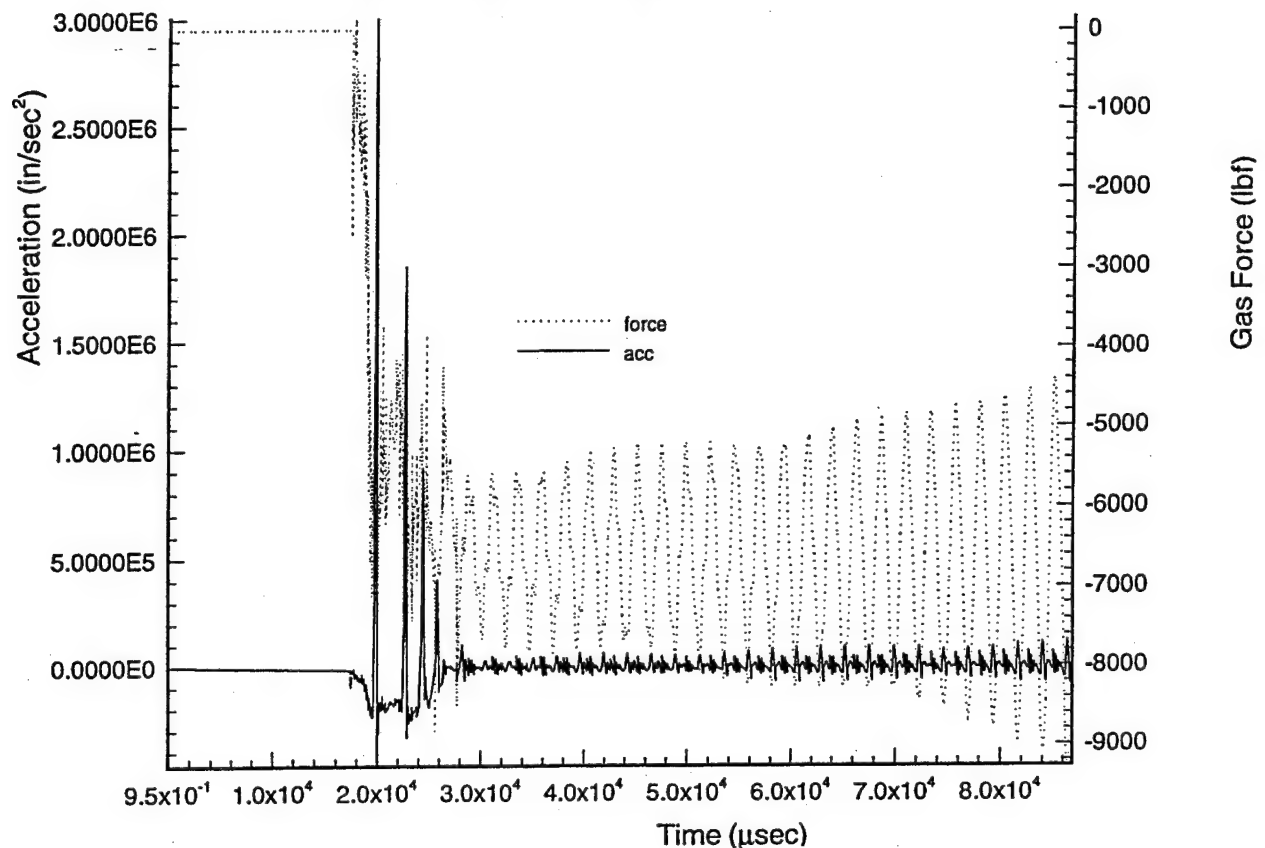**Backward Opening / Lengthened Spool / New B.C.**

Figure E-16c. Histories of valve spool *acceleration* and total gas dynamic force on modified valve spool, with modified boundary condition. Damping forces are set at 8% viscous (on spool) plus 100 lbf (on Belleville) Coulomb Damping. The high-pressure boundary is 1800 psia; the low-pressure boundary is 12 psia.
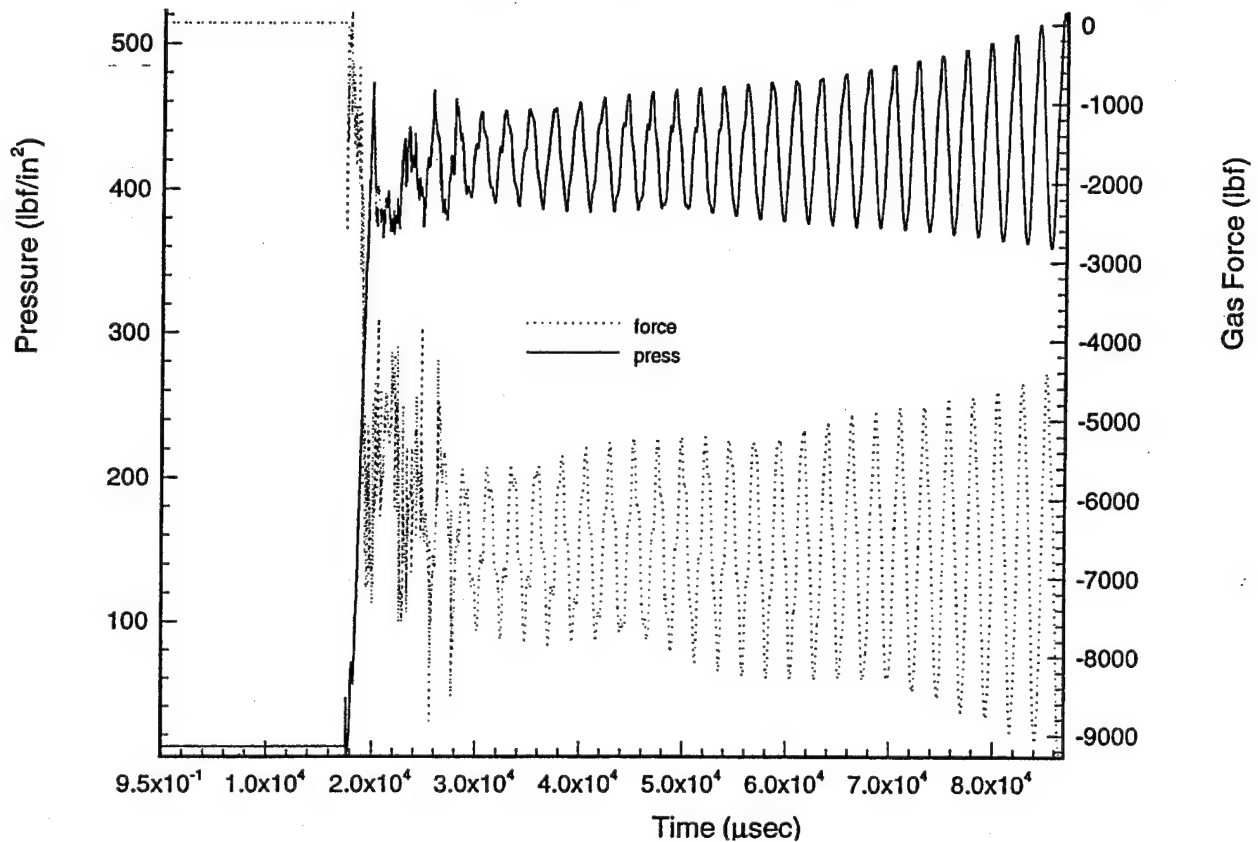
Figure E-16d. Pressure history at the pressure history point and total gas dynamic force on modified valve spool, with modified boundary condition. Damping forces are set at 8% viscous (on spool) plus 100 lbf (on Belleville) Coulomb Damping. The high-pressure boundary is 1800 psia; the low-pressure boundary is 12 psia.

Pressure Contours / Last Time Step
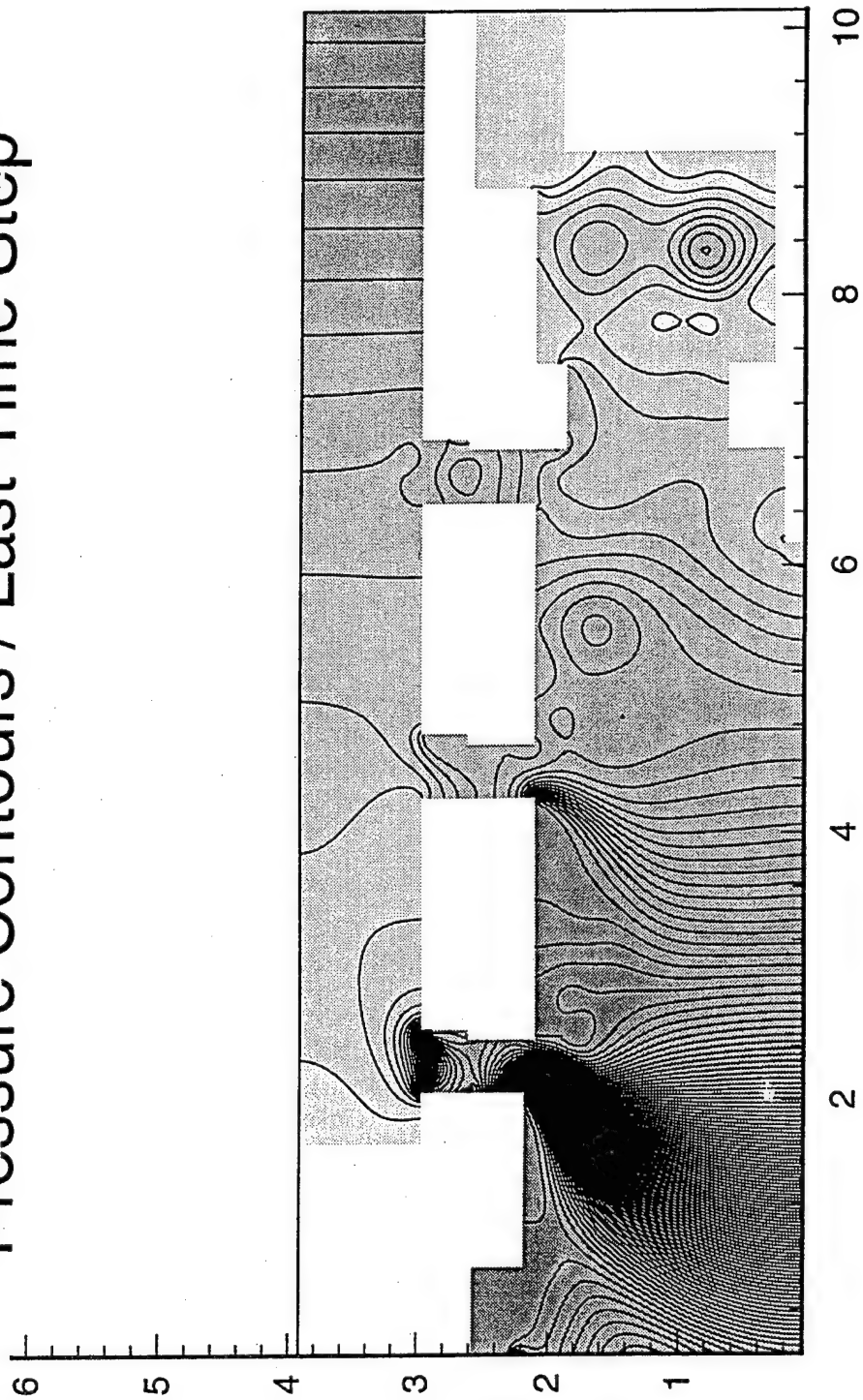
Figure E-17. Spatial pressure distribution about modified valve spool at time = 0.087 sec. Isobars are at 13-psi intervals.

APPENDIX F

ANALYSIS OF SELECTED EATON
THROAT-VALVE ELEMENT COMPONENTS

S. D. Snow

INTENTIONALLY LEFT BLANK.

CONTENTS

TABLES

FIGURES

2

1. SUMMARY OF RESULTS

Revision 1 to this report employed an updated acceleration history for the backward opening piston and sleeve. Section 7 contains that data.

Selected components of the Eaton Throat–Valve Element were evaluated with respect to the rules of the ASME Boiler and Pressure Vessel Code, Section VIII (Rules for Construction of Pressure Vessels). An exception was taken for the valve element because one of its materials (AMS 5643 in plate form) was not approved for use by the ASME Code Section VIII.

The body of the valve contained three rows of rectangular portholes sized 0.76" x 0.50" each. The analysis showed that the valve body could withstand the design conditions of 2,000 psi external pressure at 700 °F with its current porthole size and configuration. It also showed that the portholes could be enlarged to 0.76" x 0.76" square with 1/8" radius corners while under design conditions and remain stable, maintaining a factor of safety of 2 against buckling.

However, the dynamic forces associated with a backward opening piston and sleeve (used to "open" the portholes) caused excessive stresses throughout the valve. The location and magnitude of selected elastically calculated stresses were: (1) the valve body around the portholes (using the current porthole size) exceeded *58* ksi, (2) the piston stop plate exceeded *400* ksi, and (3) the stop plate attachment bolts reached *224.9* ksi. All above elastically calculated stresses exceeded the allowable stress level of 32.0 ksi defined by the ASME Boiler and Pressure Vessel Code, Section VIII (Rules for Construction of Pressure Vessels).

The large dynamic (impulse) forces created by the deceleration of the piston and sleeve were primarily due to the stiffness of the Belleville washer stack. The stack was clearly very "stiff", and had a short travel before bottoming out. The piston impulse forces would be greatly reduced if either of the following modifications were made:

(1) Arrange (or add to) the stack of Belleville washers so that the effective travel length (before bottoming out) is much longer. When the washers bottomed out their stiffness increased tremendously, thus increasing the piston/sleeve decelerations.

(2) Employ Belleville washers (or other springs) that have a lower stiffness value and a longer travel length. This will reduce the magnitude of the piston/sleeve decelerations.

2. INTRODUCTION

2.1. General: The Eaton Throat–Valve Element Prototype[1] is a quick–opening valve designed to vent gas at 2,000 psig. The valve element consisted of a cylindrical body with one end blocked and the other open. The body had three rows of slotted portholes around the circumference. An inner cylindrical sleeve also had three rows of portholes through which pressurized passed when the sleeve was positioned so that its portholes coincided with those of the body. The sleeve position was controlled by a piston, which was in turn located by a control system. Two components of the valve were evaluated in this analysis: (1) the valve body at the location of the portholes, and (2) the end plate that stops the travel of the piston when the sleeve is in the "open porthole" position.

2.2. Design Code: The design code followed was the ASME Boiler and Pressure Vessel Code Section VIII, Rules for Construction of Pressure Vessels[2] (ASME Code). Strict observance of the ASME Code requirements was not always kept – specific exceptions will be noted in this report as they were employed.

2.3. Design Conditions: The design conditions on the valve were: 2,000 psi external pressure, and 700 °F material temperature.

2.4. Materials: All components that were evaluated were constructed of the precipitation–hardened stainless steel AMS 5643 (SAE Standard)[3]. This material had an equivalent in the ASTM Standards[4], A–564 for bars, A–693 for plates, and A–705 for forgings. The ASME Code gave the properties for this material as listed in Table 1.

Table 1. Material Properties for ASTM A–564, A–693, & A–705

	Temperature °F							
Property	100	200	300	400	500	600	650	700
Yield Strength, ksi	115.0	106.3	101.9	98.3	95.2	92.8	91.5	*[90.0]
Modulus of Elasticity x 10^{-6}, psi	28.3	27.6	27.0	26.5	25.8	25.3	*[25.1]	24.8
ASME Code Allowable Stress, ksi	35.0	35.0	35.0	34.1	33.3	32.8	32.6	*[32.0]

*Properties not specified at this temperature. Number in brackets was either interpolated or extrapolated.

The minimum yield strength specified by the ASME Code (shown in Table 1) was somewhat lower than that specified by the AMS 5643 Standard. This appeared to be because the ASME Code applied a reduction factor (factor of safety) to the yield strength before it calculated allowable stress levels (from that yield strength). It was noted that the ASME Code only approved the bar material (A564) for Section VIII Code use. This design used the approved bar as well as unapproved plate material. An exception was taken from the ASME Code for the plate material.

3. VALVE BODY PORTHOLE EVALUATION

3.1. Purpose: The purpose of the valve body porthole evaluation was to determine if and (if so) how much the body portholes could be widened, given the design conditions. This was done by: (1) checking the body to determine the minimum required thickness at design conditions, (2) checking the portholes to determine the wall thickness around them required for reinforcement, and (3) determining the maximum allowable size of the portholes based on the actual valve body wall thickness. One additional condition that was evaluated on the portholes was due to the force produced by the piston, operating in a backward opening mode, on the stop plate. That force would be carried from the stop plate through its attachment bolts to the valve body.

3.2. Valve Body Minimum Thickness Under Design Conditions: The ASME Code developed charts to indicate the minimum required thickness for cylindrical components subject to external pressure. However, since the plate material that the valve body was made of was not approved by the Code, no external pressure chart was available. (The ASME Code did not set up a chart for the approved bar material because it was not expected to be used in vessel shell constructions). Therefore, the following process was followed to establish a minimum required thickness for the cylindrical wall of the valve body.

S. P. Timoshenko[5] developed a method for determining the thickness required for a cylindrical vessel subject to external radial and end pressure. It employed the modulus of elasticity and Poisson's Ratio of the material, the cylinder dimensions, and a variable buckling node term. The buckling node term accounted for the fact that the cylinder could collapse flat (2 nodes), collapse in a three corner shape (3 node), and so on. An initial assumption for his solution was that the cylinder edges were simply supported. Weingarten[6] further simplified Timoshenko's equation for cylinders that met the following additional requirement:

- $60 < (l/r)^2 * (r/t) < 2.5 * (r/t)^2$

The parameters for this cylinder were: l = unsupported length = 10.3", r = outside radius = 5.872 / 2 = 2.936", and t = thickness of wall (t nominal = 0.339"). This gave:

- $\mathbf{60} < (10.3/2.936)^2 * (2.936/0.339) = \mathbf{107} < 2.5 * (2.936/0.339)^2 = \mathbf{188}$

Therefore, the simplified equation was used, and was as follows:

- $q' = (0.92 * E) / (\{l/r\} * \{r/t\}^{2.5})$, where E = the modulus of Elasticity at 700 °F

The term q' was the critical buckling pressure for the cylinder. It is important to note that actual tests have shown that a cylinder may buckle at pressures that are 20% higher or lower that the calculated critical buckling pressure[7]. Table 2 shows the required valve body thickness for various factors of safety against the 2,000 psi external pressure.

Table 2. Minimum Valve Body Wall Thickness Required vs. Factors of Safety (External Pressure of 2,000 psi)

Factor of Safety Against Buckling	Thickness Required, in.
1.0	0.115
1.25	0.126
1.43	0.133
1.67	0.141
2.0	0.152
10.0	0.290

Since the actual valve body wall was 0.339" thick Table 2 shows that a factor of safety of 10 against buckling was maintained under a 2,000 psi external pressure load.

: Valve Body Thickness was Adequate!

3.3. Required Reinforcement for Portholes Under Design Conditions: The ASME Section VIII Code defined the required reinforcement for holes in the cylindrical shell of the valve body. Paragraph UG-37 (d) (1) stated that the required reinforcement around each porthole was 50% of that required by paragraph (c) which was:

- Reinforcement Area Required = $d * t_r * F$
  - where: d = cord length of porthole opening = 0.760"
    - t_r = required thickness of Table 2
    - F = correction factor = 1.0 for shells

The dimensioned portholes are shown in Figure 1 in solid lines. The valve body has three circumferential rows of 16 portholes, each circumferentially spaced as shown on the figure. The smaller circles indicate an equivalent hole with a diameter equal to the cord length of the portholes. The areas between the larger and smaller circles are those where reinforcement must be in order to qualify as material available to reinforce the portholes. Since the portholes were (area wise) smaller than the smaller circles, the calculations for reinforcement available will be somewhat conservative. However, the ASME Code does not define that magnitude of conservatism.

The areas required for reinforcement of the portholes overlap as shown on Figure 1 in the circumferential direction only (each row is longitudinally spaced, from center to center, at 2.214" apart, which equated to about 3 times the inner circle diameter). On the outside diameter of the valve body the areas do not cross into the portholes, but they do on the inside diameter. However, it was assumed that the material in the reinforcement areas lost to the portholes was made up by the extra material available in the longitudinal direction. The metal available for reinforcing the portholes was calculated using ASME Code Figure UG-37.1, as follows:

- Metal Available = $d * (E_1 * t - F * t_r) - 2 * t_n * (E_1 * t - F * t_r) * (1 - f_{r1})$
  - where: f_{r1} = 1.0 (no nozzle reduction)
    - E_1 = 1.0 (no welds at porthole)
    - F = 1.0 correction factor
  - which reduced Metal Available = $d * (t - t_r)$

6

Porthole Dimensions on Outside Diameter of Valve Body

Circumferential Direction

Porthole Dimensions on Inside Diameter of Valve Body
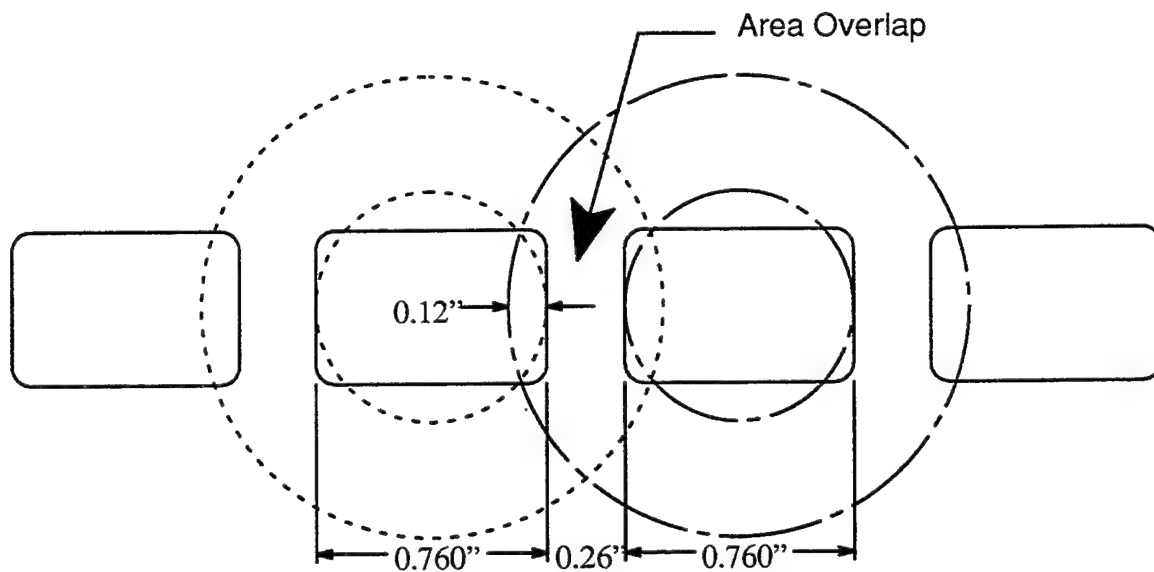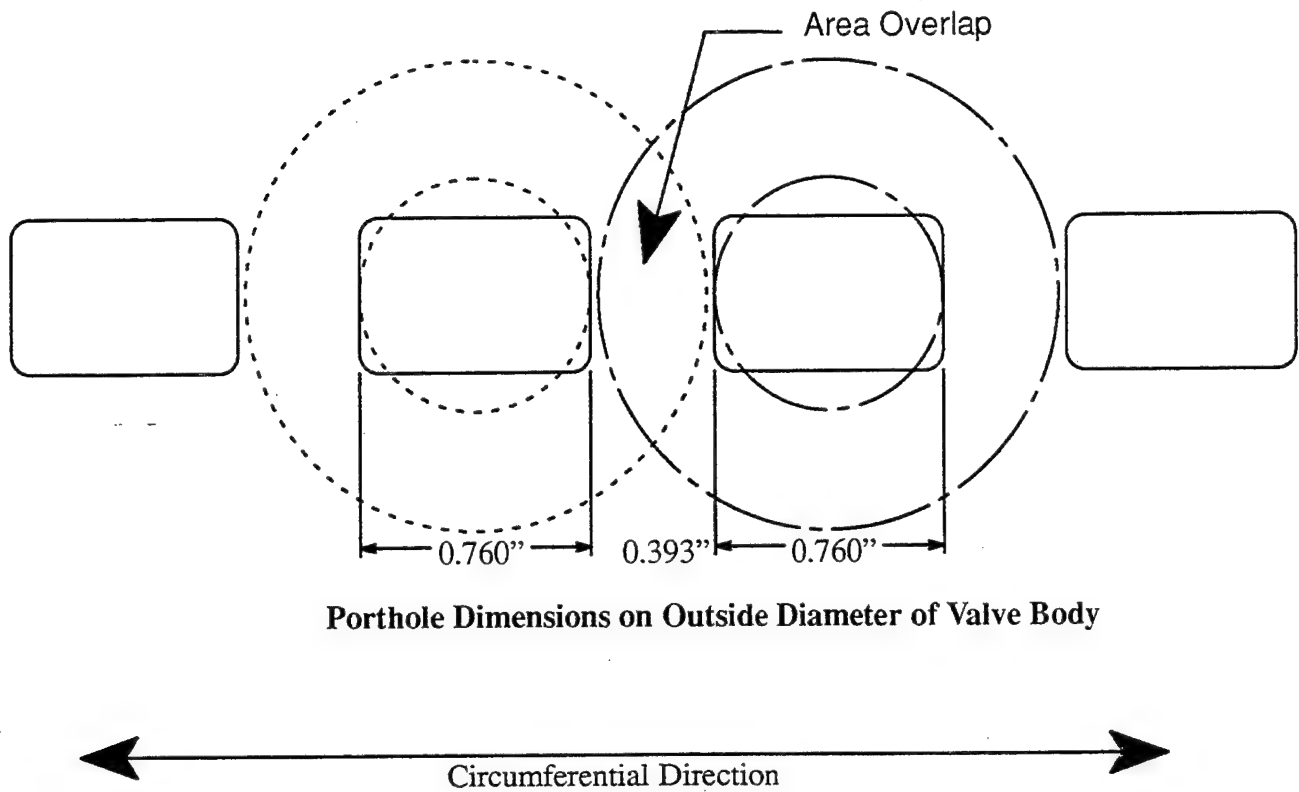
Figure 1. Porthole Dimensions on Valve Body Outside & Inside Diameters

7

Equating the required area (reduced by 50% as allowed) and the available area (dividing the available area of metal between two adjacent portholes equally) gave:

- $1/2 * d * t_r \leq d * 1/2 * (t - t_r)$

  —or—

  $2t_r \leq t$

The thickness of the valve body around the portholes had to be twice that required to maintain stability of the wall. Table 3 compares the required thickness for stability listed in Table 2, doubles it for that required for reinforcement, and lists the actual wall thickness.

Table 3. Valve Body Wall Thickness Required at Portholes (2,000 psi External Pressure)

Factor of Safety Against Buckling	Thickness Required for Stability, in.	Thickness Required for Reinforcement, in.	Actual Valve Body Wall Thickness, in.
1.0	0.115	0.230	0.339
1.25	0.126	0.252	0.339
1.43	0.133	0.266	0.339
1.67	0.141	0.282	0.339
2.0	0.152	0.304	0.339
10.0	0.290	0.580	0.339

: The reinforcement provided by the valve body wall at the portholes allowed a 2,000 psi external pressure with a factor of safety of 2 against buckling!

3.4. Maximum Allowable Porthole Size Under Design Conditions: The evaluation reported in the previous subsection used a "d" value equal to the cord length of the porthole opening. That "d" value would be the same if the hole were circular, with a diameter equal to "d". If the hole were square (with a corner radius) at the current dimension of 0.760" as shown on Figure 1, the cord length would still be that which was used above. A porthole with larger dimensions (than 0.760" square) would not maintain a factor of safety of 2 against the theoretical buckling pressure on the valve body.

: Maximum recommended porthole size was 0.760" square, with a corner radius value of 0.125"! This maintained a factor of safety of 2 against buckling under a 2,000 psi external pressure.

3.5. Valve Body Under Piston Loads: Section 4.4 calculates a maximum equivalent static force of *103,518* lbs that will be applied to the valve body via the stop plate. That force was produced by the dynamics of the sleeve being positioned by the piston operating in a backward opening mode. The force is compressive on the body of the valve, and will produce higher stresses on the row of "webs". Each web is that material between portholes in the circumferential direction. The total area of the webs, and the resulting stresses in them would be:

8

- **Web Area**   = 16 Webs * Area per Web ($\approx\{(0.26 + 0.0665) * 0.339\}$)
                 = 16 * 0.111
                 = **1.77 in.^{2}**

- **Compressive Stress in Webs** = Force / Area
                 = *103,518* lbs / 1.77 in.^{2}
                 = *58,485* **psi**

From Table 1 the allowable stress level of the material that the valve body was constructed of was 32.0 ksi. The actual compressive stress caused by the maximum force of the backward opening piston (*58,485* psi) exceeded the allowable stress level. It was also suspected that the valve body wall would be unstable under the above piston load. However, no further calculations were performed since the allowable compressive stress was unacceptable.

: Valve Body, in its Current Porthole Configuration Could Not Carry the Piston Impact Loading from Backward Opening!

9

4. PISTON STOP PLATE

4.1. General: The end plate that stops the travel of the sleeve-positioning piston was made of AMS 5643 steel. The stop plate consisted of a 3.75" diameter disc, 1.0" thick. A central hole allowed the piston guide rod to be attached to the valve sleeve. Two 180° opposed holes were provided for piston actuating pressure ports, along with six 0.33" holes for mounting the stop to the valve body with 5/16" bolts.

4.2. Load Conditions: The loading on the stop plate contained several components: (1) the actuation pressure on the piston, (2) the force caused by the nitrogen gas flowing through the portholes, and (3) the dynamics of the piston during its actuation.

4.3. Stop Plate Dynamics: A finite element model of the stop plate was developed in order to determine its fundamental frequency. This was needed to see how that frequency compared to the frequencies of the input forces. The stop plate was modeled and analyzed using the I-DEAS[8] software. Parabolic tetrahedron elements (1,355 total) simulated the stop itself and spring elements took the place of the attachment bolts. Two boundary conditions were considered possible for the stop plate: (1) the outside edge of the stop plate was simply supported (this assumed that the bolts always kept the stop plate in contact with the valve body), and (2) the stop plate was unrestrained except by the springs that took the place of the attachment bolts (this assumed that some small gap existed between the stop plate and the valve body). Figures 2 & 3 show the top and isometric views of the model (only half of the stop needed due to symmetrical geometry). Material properties from at 700 °F used were: Modulus of elasticity of 24.8×10^6 psi, Poisson's ratio of 0.29.

Figure 4 shows the fundamental frequency of the stop plate with simply supported edges. This mode shows the stop plate center flexing in and out at 12,367 Hz. The valve body will allow the outward movement but will restrain the inward movement of the stop plate. The second natural frequency, shown in Figure 5, shows the stop plate shifting from side-to-side. The geometry of the valve body should impede this mode.

Figures 6 & 7 show the first two natural frequencies of the stop plate that was restrained only by the attachment bolts (represented by nodal rigid restraints). Their frequencies were at 7,136 and 9,256 Hz. Much of their motion will also be restrained by the valve body.

One other possible motion of the stop plate not evaluated in the finite element model was that of the mass of the stop plate riding on six attachment bolts (i.e., rigid motion of the stop plate on springs). The spring constant of each bolt was:

- Spring Constant K = Modulus of Elasticity * Bolt Area / Spring Length of bolt
$$= (24.8 \times 10^6) * 0.077 \text{ in.}^2 / 1.0 \text{ in.}$$
$$= 1,909,600 \text{ lbs/in. per bolt}$$

- Total Spring Constant K_t = 6 bolts * K per bolt = **11,457,600 lbs/in.**

The weight of the stop plate was about 3 lbs. The fundamental frequency of this mass-spring system was

- $f_1 = (1 / 2\pi) * (K_t / \text{mass of stop plate})^{1/2}$
$$= (1 / 2\pi) * (11,457,600 / \{3 / 386.4\})^{1/2}$$
$$= \textbf{6,114 Hz}$$

10
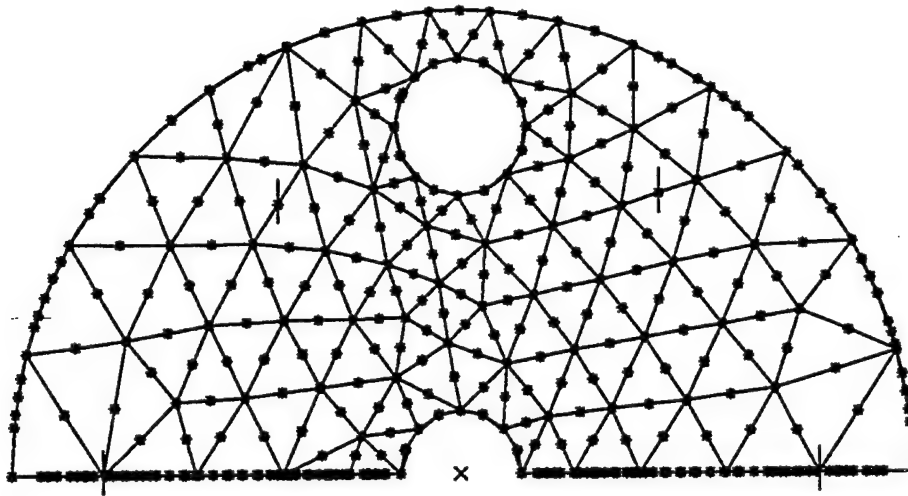
Figure 2. Model of Stop Plate (Top View)
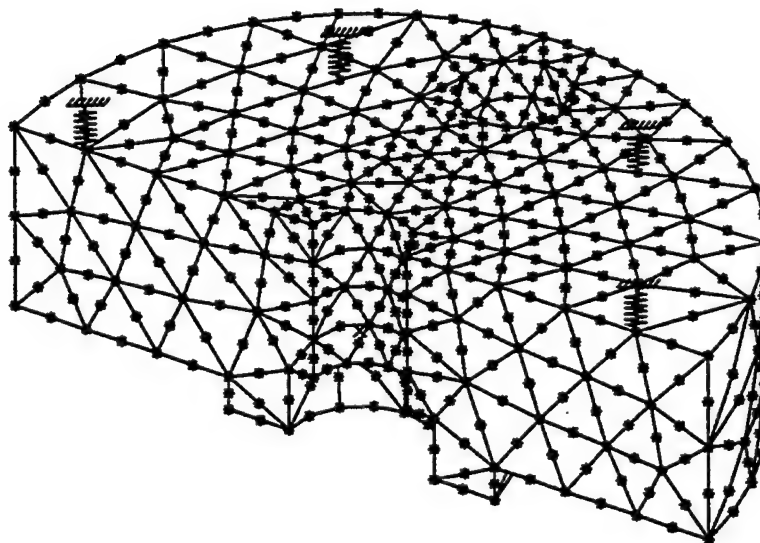
Figure 3. Model of Stop Plate (Isometric View)

11
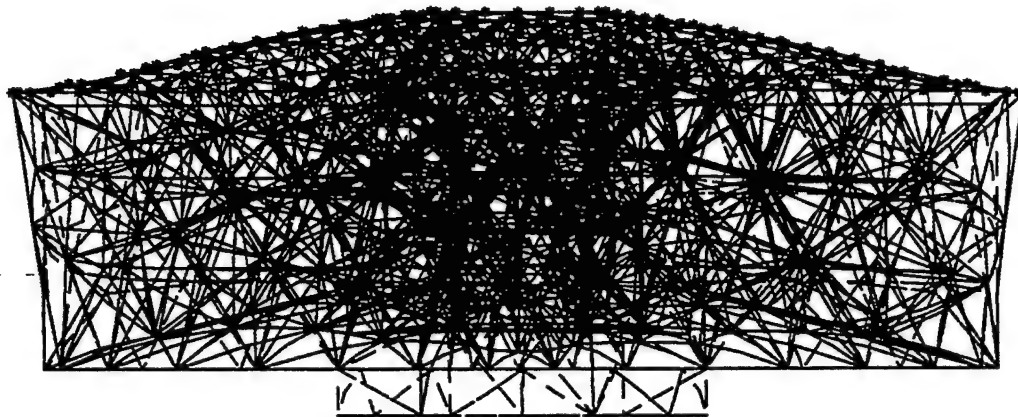
Figure 4. Mode Shape #1 for Simply Supported Edges at 12,367 Hz
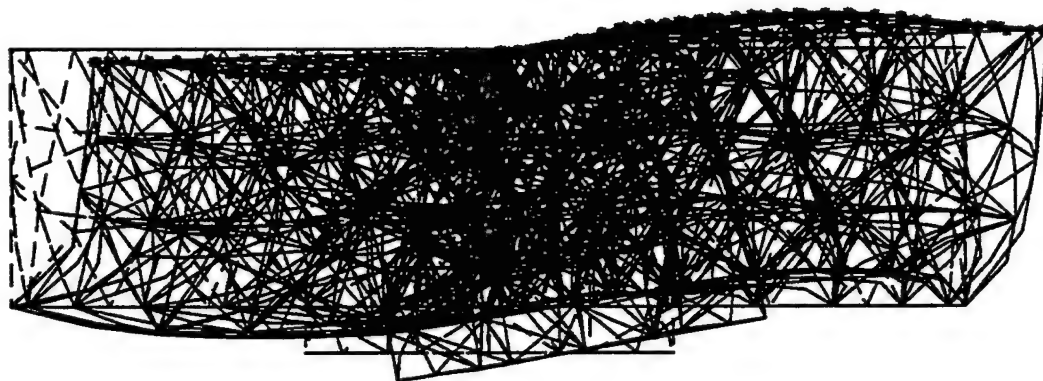
Figure 5. Mode Shape #2 for Simply Supported Edges at 12,895 Hz

12
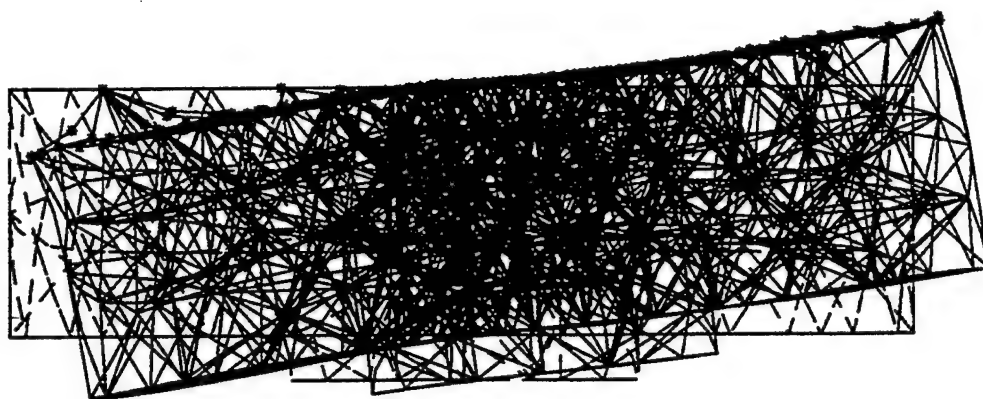
Figure 6. Mode Shape #1 for Stop Plate with Free Edges at 7,136 Hz
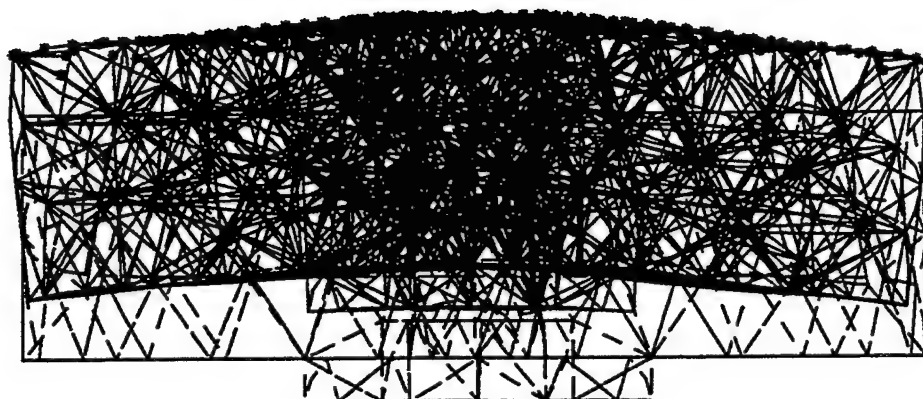
Figure 7. Mode Shape #2 for Stop Plate with Free Edges at 9,256 Hz

13

Therefore, of the three conditions on the stop plate the minimum calculated natural frequency was **6,114 Hz**.

4.4. Forces on Stop Plate: The actual forces applied to the stop plate were:

- **Piston Actuation Force:** The actuation force on the piston started at 0, linearly increased to 1,425 lbs at 0.05 seconds, continued to increase at a somewhat slower rate to 2,850 lbs at 0.5 seconds where it remained constant (See Reference 9).

- **Gas Forces on Sleeve:** The gas forces on the portholes in the sleeve began at zero at time 0 and remained there until the piston and sleeve slid just enough to allow flow through the portholes. At that time (roughly *0.017* seconds) the force fluctuated until the piston stopped moving (bouncing on the washers and the stop, at about 0.027 seconds). Then the gas force oscillated in a pattern that increased in magnitude with time (See Ref. 10).

- **Piston Impact Loads:** The piston actuation force and the gas force on the sleeve caused the motion of the piston. When the piston contacted the stop plate a spring–type washer stack (Belleville washers) compressed. The dynamics of the piston from the initial contact to when it came to rest on the stop plate were given in Reference 10. The force history associated with the piston impacting the stop was determined by multiplying the acceleration history of the piston by its mass (inc. the mass of the attached sleeve and etc.). Those forces were small until the piston moved the sleeve to "just begin to open" the portholes, at which time the force increased until the piston impacted the washers and the stop. Four piston impact loads occurred until the piston settled onto the stop, as follows:

Table 4. Piston Impulse Loads

| Piston Impulse or Impact	Max. Acceleration, in./sec^2	Associated Force, lbs	Frequency of Impulse, Hz	Freq. between this and next Impulse, Hz
First	3.0E6	97,200	1,515	382
Second	1.85E6	59,940	1,316	649
Third	1.0E6	32,400	1,000	794
Fourth	4.3E5	13,932	1,667	(last impulse)

Note that the piston impact frequencies were all less that the lowest natural frequency (6,114 Hz) of the stop plate. The magnitude of the piston impact force that was actually transmitted into the stop plate as an equivalent static force was dependent on the piston impact frequency and the natural frequency of the stop plate. The transmission ratio *for the first and most severe* impulse was calculated as follows:

Transmission Ratio[11] $= 1 / \{1 - (\text{Forcing Freq.}^2 / \text{Natural Freq.}^2)\}$
$$= 1 / \{1 - (1{,}515^2 / 6{,}114^2)\}$$
$$= \textbf{\textit{1.065}}$$

14

This meant that during the application of the first impulse load the equivalent static force applied to the stop plate was *97,200 lbs * 1.065 = **103,518 lbs**!* All other impulse loads were much smaller.

Note that if a triangular impulse approach[12] was taken to determine the "Dynamic Load Factor" (equivalent to transmission ratio) the results would give about the same value (1.06).

- **Total Load on Stop Plate:** The two cases of interest were:
  (1) Maximum equivalent static load on stop plate before the piston came to rest (from maximum piston impulse force) = **_103,518_ lbs**

  (2) Maximum load on stop plate after impulse loads ceased
     = actuation force + gas force
     = 2,850 lbs + Increasing Gas Forces
  Gas forces and their associated frequencies (< 1,000 Hz) did cause amplification in the stop plate response since the stop plate's lowest natural frequency was so much higher (6,114 Hz). This load could not be evaluated since it was not known if the gas forces continued to increase, or stabilized with time. However, it was not expected that the gas loads would approach those of the piston impulses.

Only the maximum equivalent piston impact static load of *103,518* lbs was used for calculating stresses.

4.5. Stresses in Stop Plate Bolts: The stresses in the stop plate bolts were tensile, due to the *103,518* lb maximum equivalent static load from the piston maximum impulse force. Six 5/16" attachment bolts were machined from the same material as the valve body and stop plate, AMS 5643. The elastically calculated stresses in the bolts were:

- Tensile Stress = Force / Area
     = *103,518* lbs / {6 * $(\pi/4)*(5/16/^2$}
     = ***224.9* ksi**

The elastically calculated stress in the bolts (*224.9* ksi) exceeded the tensile strength of the material(190 ksi per Ref. 3).

: Bolts Could Not Carry the Piston Impact Loading!

What bolt size and quantity would be needed to adequately carry the loads? Table 1 showed that the allowable tensile stress in the specified material was 32.0 ksi. The required area of the bolts to give a tensile stress at 32.0 ksi was:

- Bolt Area Required = Force / Allowable Stress
     = *103,519* lbs / 32,000 psi
     = ***3.23* in.**^{2}

Table 5 shows sizes and quantities of bolts required to limit the tensile stress to 32.0 ksi.

Subject: Analysis of Selected Eaton Throat—valve Element Components   Date: December 1998
Prepared by: S. D. Snow   Checked by G. K. Miller
Revision 1

Table 5. Bolts Required to Carry Maximum Piston Impulse Load

Bolt Size, in.	Tensile Area per Bolt, in.^{2}	Number of Bolts Required
1	0.606	6
7/8	0.462	7
3/4	0.334	10
5/8	0.226	15
9/16	0.182	18

4.6. Stresses in the Stop Plate: The finite element model of the stop plate was employed in a *linear* elastic analysis. The analysis used the equivalent static load of 92,728 lbs *(load used in the original release of this report)*. That force was converted into a pressure load on the face that contacts the piston. The piston (specifically the spring–type Belleville washers) did not contact the entire raised back face of the stop plate, shown cross–hatched in Figure 8 below, but that was assumed for a first approximation.

- **Pressure Load** = Force / Area of Application
  = 92,728 lbs / $\{(\pi/4)^* (1.426^2 - 0.780^2)\}$
  = **82,850 psi**

Revision 1 Note: Since a linear elastic analysis was used in the original analysis, those results were scaled to determine the results for the higher load of 103,518 lbs.
*Scale Factor = 103,518 / 92,728 = **1.116***

Back Raised Face of Stop Plate (d_o = 1.426", d_i = 0.780")
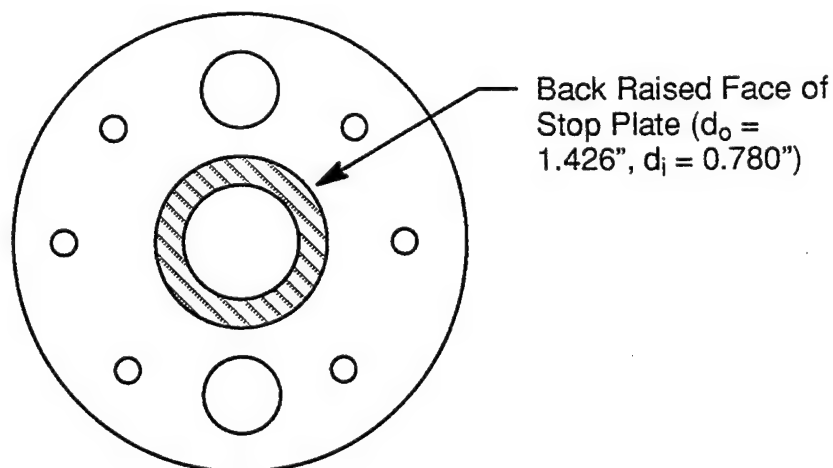
Figure 8. Assumed Piston Contact on Stop Plate

16

The above equivalent pressure load of (82,850 * 1.116 =) **92,461** psi was also the bearing stress at the face where the force was applied. That stress exceeded the level allowed by the ASME Code, listed in Table 1 of 32,000 psi. If the load was distributed over the somewhat smaller area that the piston washers actually contact that value of stress would be even greater.

The finite element model with restraints at the attachment bolts only was stressed as shown in Figure 9. The maximum elastically calculated von Mises stress level was located under the bolts in the stop plate at a magnitude of (362.0 * 1.116 =) **404.0** ksi.

: Stop Plate Could Not Carry the Maximum Piston Impact Force!

Eaton Throat-Valve Stop

LOAD SET: 1 - PISTON LOAD
FRAME OF REF: GLOBAL
STRESS - VON MISES MIN: 2199.83 MAX: 3.62E+05

Max. Stress of
362.0 ksi

Contour Level	Stress (psi)
1	3.11E5
2	2.59E5
3	2.08E5
4	1.56E5
5	1.05E5
6	53,608
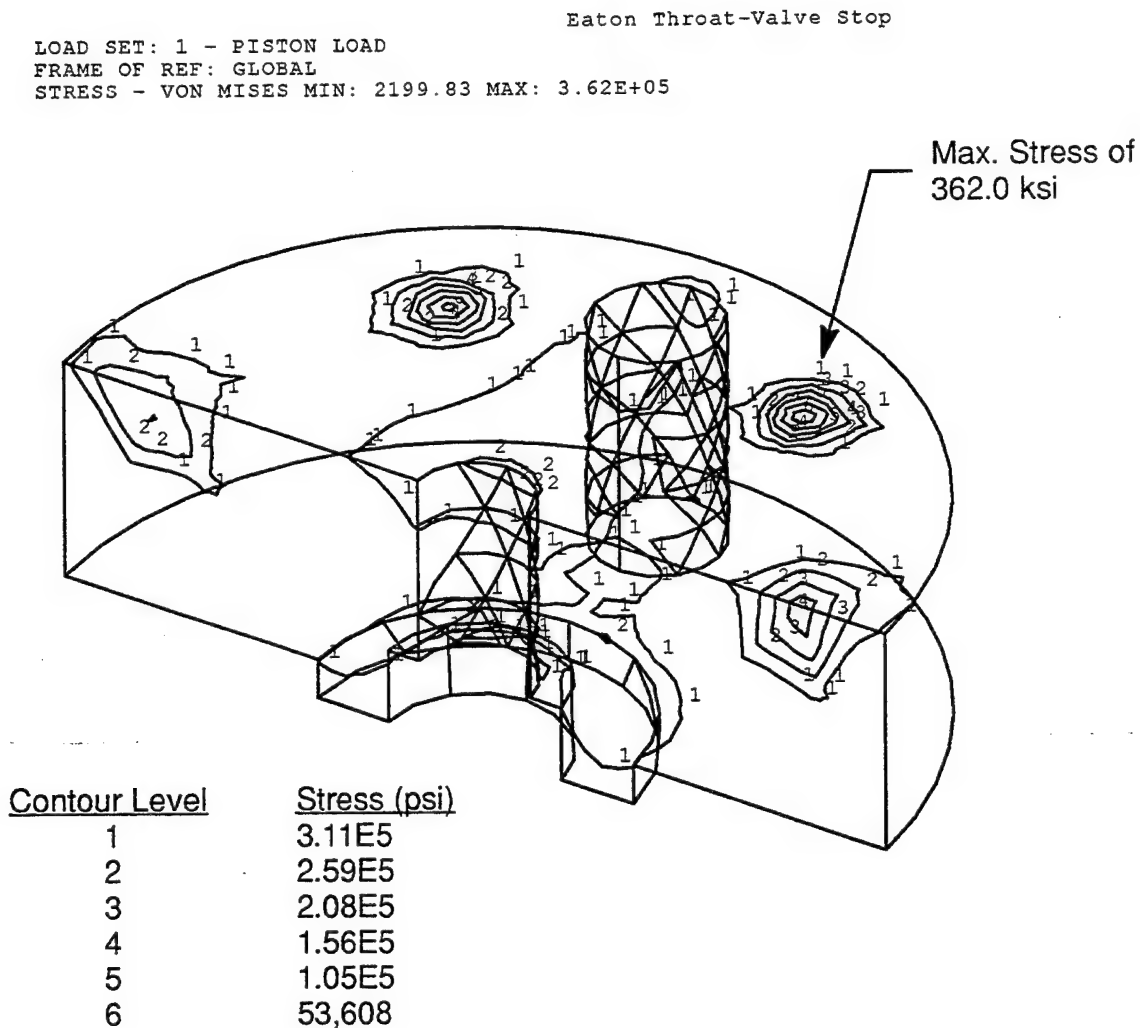
Figure 9. Stress Contour in Stop Plate Under 92,728 lbs Piston Load

17

5. COMPUTER PROGRAM CONFIGURATION DOCUMENTATION

The following documentation presents the traceability for computer programs used in the analysis reported here. This documentation should accompany any and all analysis reports transmitted by Applied Mechanics.

Task: Analysis of Selected Eaton Throat–Valve Element Components

Charge No. or Work Package: 820253914

Report Title: Same as task

Author: S. D. Snow   **Date:**   December 1993

Program Used: I–DEAS   **Version:** VI.i   **Module:** NA

Computer Used: WCUSV2   **Model:** DECstation 5000/200

Verification Manual/Test Problem Manual/Example Manual:
W. D. Richins letter to Applied Mechanics, "Verification of SDRC I–DEAS VI Software,"
WDR–28–91

Author: W. D. Richins   **Date:**   December 18, 1991

Comments: "SDRC I–DEAS V Verification Manual" is also available within the Applied
            Mechanics Unit.

18

6. FINITE ELEMENT MODEL INPUT & OUTPUT

(The finite element model input and output data from the original release of this report did not change in this revision. In the interest of conserving pater, that data was not included in this revision.)

19

7. ACCELERATION HISTORY FOR BACKWARD OPENING PISTON

8% Viscous + 100 lbf Bellville Damping
Backward Opening / Lengthened Spool

20.1

8% Viscous + 100 lbf Bellville Damping
Backward Opening / Lengthened Spool

8% Viscous + 100 lbf Bellville Damping
Backward Opening / Lengthened Spool

8% Viscous + 100 lbf Bellville Damping
Backward Opening / Lengthened Spool

20.4

8% Viscous + 100 lbf Bellville Damping
Backward Opening / Lengthened Spool

1

20.5

8% Viscous + 100 lbf Bellville Damping
Backward Opening / Lengthened Spool

2

20.6

8% Viscous + 100 lbf Bellville Damping
Backward Opening / Lengthened Spool

3

20.7

8% Viscous + 100 lbf Bellville Damping
Backward Opening / Lengthened Spool

4

20.8

8. REFERENCES

1. EG&G Idaho, Inc. Drawing 446082, LB/TS Eaton Throat–Valve Element Assembly Prototype As–Built, October 27, 1993.

2. American Society of Mechanical Engineers, "ASME Boiler and Pressure Vessel Code," Section VIII, Division 1, (Rules for Construction of Pressure Vessels), July 1, 1989 with addenda thru 1991.

3. AMS 5643J, Aerospace Material Specification for Steel Bars, Forgings, Tubing, and Rings, Corrosion Resistant, Society of Automotive Engineers, Inc., Warrendale, Pa., November 1, 1968.

4. ASTM, "1982 Annual Book of ASTM Standards", American Society for Testing and Materials, 1982.

5. S. P. Timoshenko and J. M. Gere, "Theory of Elastic Stability", Second Edition, McGraw–Hill Book Company, 1961.

6. Weingarten, V. I., et al, "Elastic Stability of Thin–Walled Cylindrical and Conical Shells under External Pressure and Axial Compression, AIAA J., vol 3, no. 5, May 1965.

7. W. C. Young, Roark's Formulas for Stress and Strain, 6th Edition, New York, NY: McGraw–Hill Book Company, 1989.

8. I–DEAS, Level VI.i, Milford, OH: Structural Dynamics Research Corporation, 1992.

9. Actuation Pressure History of ETVE Piston, personal communication by J. G. Arendts to S. D. Snow, EG&G Idaho,Inc., December 13, 1993.

10. *Force, Velocity, and Acceleration History of ETVE Piston, personal communication by R. A. Berry to M. R. Stacey, EG&G Idaho,Inc., December 23, 1993.*

11. R. F. Steidel, Jr, "An Introduction to Mechanical Vibrations", 2nd Edition, John Wiley & Sons, 1980.

12. J. M. Biggs, "Introduction to Structural Dynamics", McGraw–Hill Book Company,1964.

APPENDIX G

SEAL STUDY

J. P. Sekot

INTENTIONALLY LEFT BLANK.

SEAL STUDY

INTRODUCTION

A meeting was held with M.R.Stacy (Requester) on Dec 7, 1993 to develop scope of assignment, review problem, and identify design and operating conditions; and a follow up meeting was held with Jim Hall (Test Technician) to determine test scenario, test conditions and results.

o Scope of Assignment
   Review Valve operation and conduct scoping study to identify available seal materials and configurations capable of withstanding the conditions experienced by operation of the LB/TS Throat Valve Element. The study shall also identify Manufacturers, cost, and delivery. Schedule: Complete draft study by December 17, 1993
   Budget: 60 mhrs
   Charge No. 820253914

o Background
   EG&G was previously requested by the US Army to evaluate the performance of the LB/TS Throat Valve Element, which was supplied to them by Eaton Corporation. A series of tests were conducted. However, design conditions were never achieved because of seal failure and excessive leakage. The seals were completely destroyed during one of these tests. (see figure 1). Close examination of this photo, which was taken after the performance test, reveals that only three of the six seals were damaged. These are the three seals that cross the ports located on the valve body. Since the other three seals appear to be undamaged, it is reasonable to assume that damage was due to pinching rather than temperature, however, high temperature may be a significant contributor.

o Test Scenario, Test Conditions, and Results
   Three series of tests were conducted as follows:

First test using original seal design
Two different configurations of seals were used. The design of the seals crossing the cylinder ports was comprised of a teflon 15% graphite filled split overlapping joint ring (piston ring type) with a rectangular cross section, a radial metal spring (approx 0.010 thk x .25 wide), and a metal spacer (approx 0.010 thk x .25 wide) between the spring and the gland diameter. The design of the seals that were not required to cross the ports was comprised of a teflon 15% graphite filled guide ring with a lip on the leading edge. This guide ring was supported by a silicon o–ring with two segmented half washers 0.030 thk that backed up the o–ring. See figure 2. Experienced significant leakage. Unable to reach design temperatures or pressures. Leaked at approximately 400 psi and 350 degrees F. Installation of the teflon guide ring required use of an expanding mandrel type tool to expand the ring over the piston diameter and the use of a swaging type tool to then reduce the seal diameter after installation into the seal gland.

Second Test
The same seal design was used for all six seals. This design was of the same configuration used previously for those seals not crossing the ports (guide ring with o–ring energizer and segmented backup rings). The seals crossing the ports were destroyed. The lip of the teflon guide ring was sheared off during valve cycling. See figure 1. Unable to get any where near

design pressure or temperature.

Third series of tests

All six seals were of the same configuration. A thicker teflon 15% graphite filled guide ring with a rectangular cross section was backed up by a silicon o-ring energizer and the two segmented metal half rings. Tests were conducted at room temperature. Leakage was experienced at approximately 375 psi.

NOTE: *Many of the test details were recalled from memory and there was some difficulty in developing the actual test scenario. Hence, no real evidence of actual seal loading exists.*

o Valve Operating Conditions, Materials, Operation, and Configuration
The requester was consulted and drawings were reviewed to determine Valve operating conditions, materials, operation, and configuration as follows:

Valve Operating Conditions

inlet pressure : 2000 psig
outlet pressure : 0 psig
inlet temperature : 700 degree F
outlet temperature : 70 degree F (room)
flow media : nitrogen gas
ambient humidity : 10-100%
operating speed (close to open) : 45 ms
piston travel (close to open) : 1.12 inches
acceptable leakage (valve closed) : 87lbm/hr at 2000 psig and 59 degree F
seal design life : 150 cycles between replacements

Materials

Valve Body : CRES 17-4 PH Cond H925
Valve Sleeve : CRES 17-4 PH Cond H1025 (OD chrome plated by Electrolize process)
Seal : Teflon 15% graphite filled (drawing not available to EG&G) Seal configuration as described above.

Valve Operation

All components at room temperature, valve closed, exterior pressurized to 2000 psig with 700 degree F nitrogen gas and held for 15 minutes. Valve is then opened. Full rest to full open (1.12 inches) in 45 ms. Sleeve oscillates at open position until damped out.

Valve Configuration

Valve Body : Cylinder 5.197 dia. with 3 sets of 16 slots (ports) equally spaced around the circumference of the cylinder. Each port is 0.497 wide by 0.750 long. Each set of ports is spaced 2.20 inches apart.
Valve Sleeve : Cylinder 5.191 OD with 6 O-Ring glands and 3 set of slots (ports). Each set of ports consists of 8 slots 0.449 in wide equally spaced around the circumference of the cylinder and separated by 0.100 in wide webs. Each set of ports is spaced 2.20 inches apart.

ASSESSMENT OF PROBLEM

The O-Ring seal glands are located on the OD of the Valve sleeve, hence, a continuous ring seal must be stretched over the OD of the Sleeve for seal installation. During valve operation, the seals are moved at high speed across the cylinder ports. The present seal is

figure 1

SEAL CONFIGURATION for SEALS THAT CROSS PORTS

SPLIT-OVERLAPPING JOINT

— METAL SPRING
~ 0.010 THK × 0.25 WIDE

— SPLIT RING
Teflon 15% graphite filled

— SPLIT METAL RING
~ 0.010 THK × 0.25 WIDE

— GUIDE RING
Teflon 15% graphite filled

← Pressure

— SILICON O-RING

* SEAL CONFIGURATION for SEALS THAT DO NOT CROSS PORTS

2 HALF RING SEGMENTS
METAL ~ 0.030 THK
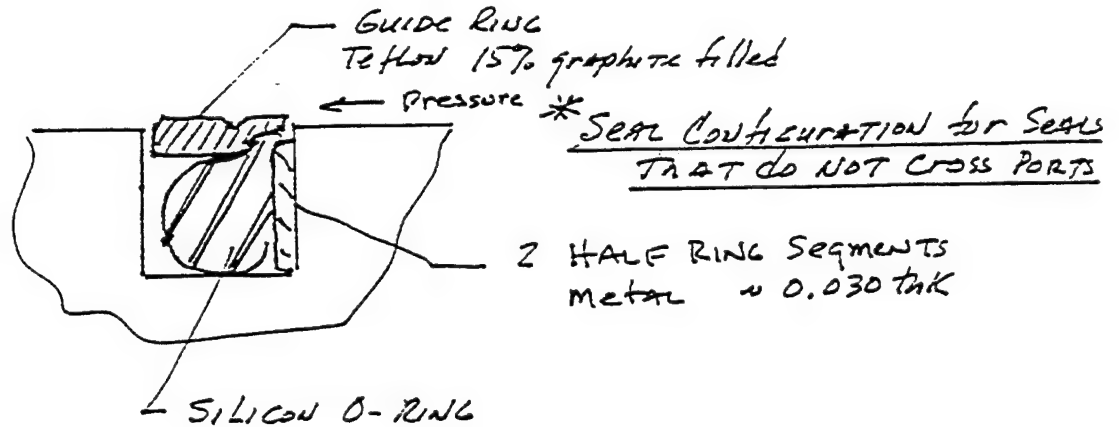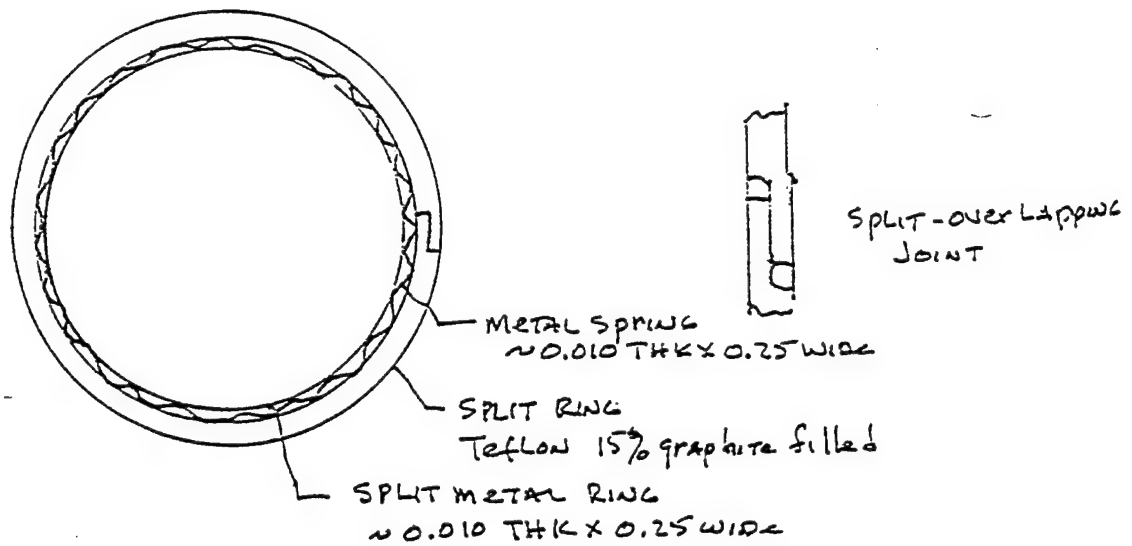
* This configuration was used for ALL SIX SEALS in the 2nd test.

— GUIDE RING
Teflon-15% graphite filled

3rd test

Pressure →

2 HALF RING SEGMENTS
METAL ~ 0.030 THK

— SILICON O-RING
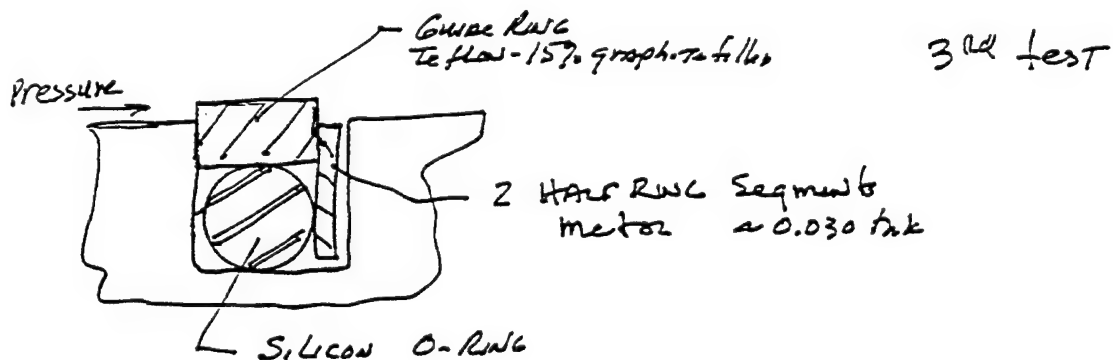
a fairly hard polymer (15% teflon graphite filled) at room temperature, however, teflon will cold flow and as the seal passes the cylinder port. it is left unsupported. The seal is then extruded into the port and pinched or stripped.

SURVEY OF MATERIALS
A literature search was conducted to identify candidate materials for this seal application. The most commonly used seal materials for piston/cylinder applications are the elastomers. However, silicon, which has the highest temperature limit for continued service is limited to 600 degree F. Table 1 provides temperature limits for these materials

Table 1 – Temperature for Continued Service (Elastomers)	
elastomer	Temp (F)
Nitrile rubber NBR	300
Natural Isoprene NR	250
Ethylene Propylene EPM,EPDM	350
Flurosilicon FVMQ	400
Flurocarbon, FPM	>550
Silicon VMQ	600
Ref: Materials Engineering, Material Selector–1987. p177–179	

Because of the low temperature limit, no manufacturers of elastomer seals other than silicons and flurocarbons were contacted.

Supplier literature from various Seal Manufactures was also reviewed to select candidate suppliers. These candidate suppliers were then contacted to determine their interest and capability. If they expressed interest, an information package consisting of drawings and fact sheet describing materials, operation, and operating conditions was sent to them by FAX. No manufacturers of silicon or flurocarbon seals have expressed interest in submitting a proposal for this application. See Appendix (Memos of conversation). They have expressed the following concerns:

      1 Temperature– Seals made of Teflon, a flurocarbon, are fabricated by the sintering (powder metallurgy) process at approximately 700 degree F. At approximately 720 degree F, teflon has the consistency of jelly. [Ref 2 and 3]

      2 Ports – Teflon will cold flow and with the high design pressure, the seals can be expected to expand into the ports and be pinched as they pass over the port. Teflon has a high temperature coefficient of expansion, hence, it can be expectected that under high temperature, it will expand to fill the gland space and when unsupported at the outer diameter, especially with high load , will expand into the port.

Information provided by the Flurocarbon Mechanical Seal Division indicates that temperature limits for their seal normally rated at 550 degree (F) is approximately 325 degree (F) at 2000 psi radial dynamic seal with reciprocating motion. See appendix (Data).

Manufacturers contacted include:
      Bal Seal Engineering Co. Inc.
      620 West Warner Ave
      Santa Ana, Ca 92707–3396
      Tel (714)–557–5192   Fax (714)–241–0185 Michael Binder

Hydra Pak Seal Div (Parker Hannafin)
Salt Lake City, Ut
Tel (801)−973−7325   Jeff Walker

FURON Mechanical Seal Div
(formerly FLUROCARBON)
PO box 520
4412 Corporate CenterDr
Los Alamitos, Ca 90720
Tel (714)−995−1818 Fax (714)−761−1270   Mark Maloney

Row, Inc
703−T Annoreno Dr
Addison,Il.60101
Tel (708)−628−9221 Fax (708)−628−9229 Ores Kozinczuk

Du Pont, manufacturers of VESPEL, a polyimide, claim that VESPEL will retain it's properties at temperatures from cryogenic to 500 degrees F, with excursions to 900 degrees F. Therefore, they were contacted to determine if VESPEL could be used as a piston/cylinder seal in our application and to determine if Du Pont would be interested in submitting a proposal. Mr. Ed Miller reaffirmed Du Pont's claim and expressed interest in submitting a proposal. An information package, including drawings and fact sheet were sent by Fax to Mr. Miller.

Du Pont Co.
Tel (302)−733−8120 Fax (302)−733−8362   Ed Miller

Temperature limitations for various metals and coatings are provided in tables 2 and 3. Piston rings fabricated from cast iron, commonly used in the hydraulic and automotive industries at temperatures of up to 850 degrees are not recommended for high pressure nitrogen service above 450 degree F. Severe leakage would be expected until the rings wear in.

Table 2 − Metal O−Ring Seals

matl	max temp (C)	max temp (F)
copper	400	752
mild steel	550	1022
cupra−nickel	600	1112
monel	600	1112
nickel	700	1292
stainless steel	800	1472
inconel	850	1562

Ref[1]

Table 3 — Plating materials for metal O—Ring seals		
matl	max temp (C)	max temp (F)
Indium	140	284
cadmium	200	392
silver	800	1472
gold	850	1562
PTFE	300	572

Various suppliers of metal piston/seal rings were contacted to determine their capabilities and interest. Information packages were sent via Fax to those expressing interest. These include:

Precision Ring Inc.
5611 Progress Road
PO box 418187
Indianapolis, In. 46241
Tel (317)—247—4786 Fax (317)—248—9781 Dave Dyer

C.Lee Cook/Dover Corp
PO box 1038
Louisville KY 40201—1038
Tel (5020—587—6783 Fax (502)587—6786 Paul Hanlon

Grover Piston Ring Co.
PO box 340080
Milwaukee, WI 53234—0080
Tel (414)—384—9472 Fax (414)—384—0201 Paul Cero Mike Knoebel

Superior Piston Ring Co.
6427 Epwort Blvd
Detroit, MI 48210
Tel 1—800—899—1827 Fax (313)—361—0530

A quotation has been received from C.Lee Cook/Dover. They quoted $115.02 each for quantiteis of 6—11 and $78.21 each for quanties of 12—49 with delivery of 10+ weeks. Their quotation did not include costs for any special quality control specifications. Any efforts required to meet these would be billed at cost.

SEAL CONFIGURATIONS
Seal rings are provided in various configuration, however, piston ring seals where the seal gland is machined on the piston require an expandable seal for installation over the piston diameter. Elastomer seals, which are expandable, are provided in a continous ring confiuration while metal seals must have a split joint for this type of application. Flurocarbons (Teflon) are expandable to a small extent and with tooling, thin teflon rings can be stretched over the piston and swaged back to original diameter after installed in the gland. However, thicker rings must be split for installation. Elastomeric seal can be provided with various cross sections including round, square, X, T, V, rectangular, and lip configurations. They are also sometimes used with back up face rings to prevent extrusion or blow out and with spring retainers or energizers. Flurocarbon seals can also be provided with a teflon outer layer and a silicon or viton core. Metal seals can also be provided with various cross sections including O,

X T, K, and C onfigurations, however, continuous metal rings are generally used as face seals or where they can be installed without expansion. They are are also sometimes used with back up rings and spring energizers or pressurized in some cases. However, a metal seal for this application would have to have a split joint. Joint configuration for Piston/Seal rings include 45 degree split joint, stepped, straight cut, stepped tongue, angled tongue, and stepped hook joint. They are also sometimes used in combination. See Appendix (Data— Design Update — Dover Corporation).

CONCLUSIONS
1 If Testing would have continued, there is fair probability that both the teflon guide ring and the silicon seal energizer ring would have failed since their operating temperature limit is 600 degree F.
2 Seal failure can be attributed to pinching of the seal while passing over the ports due to unsupported section of a material that will cold flow under high load conditions.

RECOMMENDATIONS
1 Consideration should be given to performance of a temperature test to determine behavior of teflon (15% graphite filled) at 700 degree F.
2 Conduct Seal Test Program to develop seals capable of meeting design conditions. Program should include testing of split metal piston ring type seals and VESPEL seals.
3 Continue efforts to obtain proposals from fabricators of split metal seals.
4 Continue to follow up DuPont on proposal of VESPEL seal.

REFERENCES
1 Seals that Survive Heat, G.J.Field, Machine Design reprint Designing with Seals and Gaskets
2 Memo of Conversation, Dec 12,1993, J.P.Sekot with O.Kozinczuk (Row,Inc.)
3 Machine Design, Plastics/Elastomers Referemce Issue 1973—1974, p 18

INTENTIONALLY LEFT BLANK.

APPENDIX H:
PROPOSED CONFIGURATION DRAWINGS

DRAWINGS

MEMOS OF CONVERSATION

MATERIAL DATA/SUPPLIER LITERATURE

CALCULATIONS

This appendix has been sent to R. J. Pearson file at the U.S. Army Research Laboratory, Aberdeen Proving Ground, Maryland.

INTENTIONALLY LEFT BLANK.

CONTENTS

- 2 Bernoulli disks containing data outputs from the model for the different runs:
  Disk 1 contains runs at 1400 psi driver gas pressure
  Disk 2 contains runs at 1800 psi driver gas pressure.

- 1 Bernoulli disk in the diskette mailer envelope, containing test data from the 1991 tests

- 2 floppy diskettes with ASCII files of the data obtained from testing the ETVE with the LVDT installed during 1993

- The LVDT and associated instrumentation

- Updated sheets for the camera-ready report

- Relevant information for future reference regarding ETVE hardware (seals, seals configurations used, Belleville washers, solenoid valves, etc.)

- ETVE as built drawings

- ETVE as built drawings with LVDT attached

- Final project status letter

INTENTIONALLY LEFT BLANK.

NO. OF
COPIES   ORGANIZATION

2   ADMINISTRATOR
         ATTN DTIC DDA
         DEFENSE TECHNICAL INFO CTR
         CAMERON STATION
         ALEXANDRIA VA 22304-6145

1   DIRECTOR
         ATTN AMSRL OP SD TA
         US ARMY RESEARCH LAB
         2800 POWDER MILL RD
         ADELPHI MD 20783-1145

3   DIRECTOR
         ATTN AMSRL OP SD TL
         US ARMY RESEARCH LAB
         2800 POWDER MILL RD
         ADELPHI MD 20783-1145

1   DIRECTOR
         ATTN AMSRL OP SD TP
         US ARMY RESEARCH LAB
         2800 POWDER MILL RD
         ADELPHI MD 20783-1145

         ABERDEEN PROVING GROUND

5   DIR USARL
         ATTN AMSRL OP AP L (305)

NO. OF COPIES	ORGANIZATION
2	HQDA ATTN SARD TR MS K KOMINOS DR R CHAIT PENTAGON WASHINGTON DC 20310-0103
2	HQDA ATTN SARD TT MS C NASH DR F MILTON PENTAGON WASHINGTON DC 20310-0103
1	DIR OF DEFNS RSRCH AND ENGRG ATTN DD TWP WASHINGTON DC 20301
1	ASST SECRETARY OF DEFNS ATTN DOCUMENT CONTROL ATOMIC ENERGY WASHINGTON DC 20301
1	CHAIRMAN ATTN J 5 R&D DIV JOINT CHIEFS OF STAFF WASHINGTON DC 20301
2	DA DCSOPS ATTN TECH LIB DIR OF CHEM & NUC OPS WASHINGTON DC 20310
1	EUROPEAN RSRCH OFC ATTN DR R REICHENBACH USARDSG UK PSC 802 BOX 15 FPO AE 09499-1500
1	DIR ATTN TECH LIB ADVNCD RSRCH PROJ AGCY 3701 N FAIRFAX DR ARLINGTON VA 22203-1714
2	CDR ATTN AMSEL RD AMSEL RO TPPO P US ARMY CECOM FT MONMOUTH NJ 07703-5301
1	MIT ATTN TECH LIB CAMBRIDGE MA 02139

NO. OF COPIES	ORGANIZATION
2	DIR ATTN PUBLIC RELATIONS OFC TECH LIB FED EMERG MGMT AGCY WASHINGTON DC 20472
1	CHAIRMAN DOD EXPLOSIVES SAFETY BOARD ROOM 856 C HOFFMAN BLDG 1 2461 EISENHOWER AVE ALEXANDRIA VA 22331-0600
1	DIR ATTN DT 2 WPNS & SYS DIV DEFNS INTLLGNC AGCY WASHINGTON DC 20301
8	DIR ATTN CSTI TECH LIB DDIR DFSP NANS OPNA SPSD SPTD DFTD DEFNS NUCLEAR AGENCY WASHINGTON DC 20305
3	CDR ATTN FCPR FCTMOF NMHE FIELD COMMAND DNA KIRTLAND ARB NM 87115
10	CIA ATTN GE 47 HQ DIR DB STANDARD WASHINGTON DC 20505
2	CDR ATTN AMSNA D DR D SIELING STRNC UE J CALLIGEROS US ARMY NRDEC NATICK MA 01762
1	CDR ATTN ASQNC ELC IS L R MYER CTR US ARMY CECOM R&D TECH LIB FT MONMOUTH NJ 07703-5000

NO. OF COPIES	ORGANIZATION
1	CDR ATTN SMCAR FSM W BARBER BLDG 94 US ARMY ARDEC PCTNY ARSNL NJ 07806-5000
1	DIR ATTN AIAMS YDL US ARMY MISSILE & SPACE INTLLGNC CTR REDSTONE ARSNL AL 35898-5500
1	DIR ATTN AMSMR ATL US ARMY RESEARCH LAB WATERTOWN MA 02172-0001
1	CDR ATTN HNDED FD US ARMY ENGINEER DIV PO BOX 1500 HUNTSVILLE AL 35807
1	CDR ATTN CESWF PM J US ARMY CORPS OF ENGRS FT WORTH DISTRICT PO BOX 17300 FT WORTH TX 76102-0300
1	CDR ATTN SLCRO D US ARMY RESEARCH OFFICE PO BOX 12211 RSCH TRI PK NC 27709-2211
1	DIR ATTN ATRC RPR RADDA HQ TRAC RPD FT MONROE VA 23651-5143
1	DIR ATTN ATRC WC KIRBY TRAC WSMR WSMR NM 88002-5502
1	CDR ATTN STEWS NED DR MEASON US ARMY WSMR WSMR NM 88002-5158

NO. OF COPIES	ORGANIZATION
2	CHIEF OF NAVAL OPERATIONS ATTN OP 03EG OP 985F DEPT OF THE NAVY WASHINGTON DC 20350
1	CDR ATTN RSRCH AND DATA BRANCH US ARMY NGIC 220 7TH STREET NE CHARLOTTESVILLE VA 22901-5396
1	DIR ATTN ATRC L MR CAMERON US ARMY TRAC FT LEE FORT LEE VA 23801-6140
2	CDR ATTN CSSD H MPL TECH LIB CSSD H XM DR DAVIES US ARMY STRATEGIC DEFENSE COMMAND PO BOX 1500 HUNTSVILLE AL 35807
3	CDR ATTN CEWES SS R J WATT CEWES SE R J INGRAM CEWES TL TECH LIBRARY US ARMY CORPS OF ENGINEERS WATERWAYS EXPERIMENT STATION PO BOX 631 VICKSBURG MS 39180-0631
3	CDR US ARMY NUCLEAR & CHEMICAL AGENCY 7150 HELLER LOOP, SUITE 101 SPRINGFIELD VA 22150-3198
1	DIR ATTN ATRC TRAC FLVN FORT LEAVENWORTH KS 66027-5200
1	CDR ATTN PME 117 21A NAVAL ELECTRONIC SYSTEMS COMMAND WASHINGTON DC 20360
2	OFFICE OF NAVAL RESEARCH ATTN DR A FAULSTICK CODE 23 800 N QUINCY STREET ARLINGTON VA 22217

NO. OF COPIES	ORGANIZATION
1	CDR ATTN CODE SEA 62R NAVAL SEA SYSTEMS COMMAND DEPARTMENT OF THE NAVY WASHINGTON DC 20362-5101
1	COMMANDING OFFICER CODE L51 ATTN J TANCRETO NAVAL CIVIL ENGINEERING LABORATORY PORT HUENEME CA 93043-5003
1	CIVIL ENGINEERING LABORATORY ATTN TECHNICAL LIBRARY CODE L31 NAVAL CONSTRUCTION BATTALION CTR PORT HUENEME CA 93041
1	CDR ATTN CODE E23 LIBRARY NAVAL SURFACE WARFARE CENTER DAHLGREN VA 22448-5000
1	WHITE OAK WARFARE CTR DETACHMENT ATTN CODE E232 TECHNICAL LIBRARY 10901 NEW HAMPSHIRE AVENUE SILVER SPRING MD 20903-5000
1	CDR ATTN DOCUMENT CONTROL NAVAL WEAPONS EVALUATION FAC KIRTLAND AFB NM 87117
1	AEDC ATTN R MCAMIS MAIL STOP 980 ARNOLD AFB TN 37389
1	OLAC PL TSTL ATTN D SHIPLETT EDWARDS AFB CA 93523-5000
2	AIR FORCE ARMAMENT LABORATORY ATTN AFATL DOIL AFATL DLYV EGLIN AFB FL 32541-5000
3	PHILLIPS LABORATORY (AFWL) ATTN NTE NTED NTES KIRTLAND AFB NM 87117-6008

NO. OF COPIES	ORGANIZATION
1	AFIT ATTN TECHNICAL LIBRARY BLDG 640 B WRIGHT PATTERSON AFB OH 45433
1	FTD NIIS WRIGHT PATTERSON AFB OH 45433
4	DIR ATTN R GUENZLER MS 3505 R HOLMAN MS-3510 R A BERRY W C REED IDAHO NATIONAL ENGINEERING LABORATORY EG&G IDAHO INC PO BOX 8757 BWI AIRPORT BALTIMORE MD 21240
3	KAMAN SCIENCES CORPORATION ATTN LIBRARY P A ELLIS F H SHELTON P O BOX 7463 COLORADO SPRINGS CO 80933-7463
2	DIR ATTN TH DOWLER MS F602 DOC CONTROL FOR REPORTS LIBRARY LOS ALAMOS NATIONAL LABORATORY PO BOX 1663 LOS ALAMOS NM 87545
1	DIR ATTN DOC CONTROL FOR TECH LIB SANDIA NATIONAL LABORATORIES LIVERMORE LABORATORY P O BOX 969 LIVERMORE CA 94550
1	DIR ATTN TECHNICAL LIBRARY NASA LANGLEY RESEARCH CENTER HAMPTON VA 23665
1	ADA TECHNOLOGIES INC ATTN JAMES R BUTZ HONEYWELL CENTER SUITE 110 304 INVERNESS WAY SOUTH ENGLEWOOD CO 80112

NO. OF COPIES	ORGANIZATION	NO. OF COPIES	ORGANIZATION
1	ALLIANT TECHSYSTEMS INC ATTN ROGER A RAUSCH MN48 3700 7225 NORTHLAND DRIVE BROOKLYN PARK MN 55428	1	DIRECTOR ATTN DR T HOLTZ MS 202-14 NASA-AMES RESEARCH CENTER APPLIED COMPUTATIONAL AERO BRANCH MOFFETT FIELD CA 94035
1	AEROSPACE CORPORATION ATTN TECH INFO SERVICES P O BOX 92957 LOS ANGELES CA 90009	2	APPLIED RESEARCH ASSOCIATES INC ATTN J KEEFER N H ETHRIDGE P O BOX 548 ABERDEEN MD 21001
1	THE BOEING COMPANY ATTN AEROSPACE LIBRARY P O BOX 3707 SEATTLE WA 98124	1	CARPENTER RESEARCH CORPORATION ATTN H JERRY CARPENTER 27520 HAWTHORNE BLVD SUITE 263 ROLLING HILLS ESTATES CA 90274
1	CALIFORNIA RES & TECH INC ATTN M ROSENBLATT 20943 DEVONSHIRE STREET CHATSWORTH CA 91311	1	GOODYEAR CORPORATION ATTN R M BROWN BLDG 1 SHELTER ENGINEERING LITCHFIELD PARK AZ 85340
1	DYNAMICS TECHNOLOGY INC ATTN D T HOVE G P MASON 21311 HAWTHORNE BLVD SUITE 300 TORRANCE CA 90503	2	FMC CORPORATION ATTN J DROTLEFF C KREBS MDP95 ADVANCED SYSTEMS CENTER BOX 58123 2890 DE LA CRUZ BLVD SANTA CLARA CA 95052
1	EATON CORPORATION ATTN J WADA DEFENSE VALVE & ACTUATOR DIV 2338 ALASKA AVE EL SEGUNDO CA 90245-4896	1	SVERDRUP TECHNOLOGY INC ATTN B D HEIKKINEN SVERDRUP CORPORATION AEDC MS 900 ARNOLD AFB TN 37389-9998
5	DIR ATTN DOC CONTROL 3141 C CAMERON DIV 6215 A CHABAI DIV 7112 D GARDNER DIV 1421 J MCGLAUN DIV 1541 SANDIA NATIONAL LABORATORIES P O BOX 5800 ALBUQUERQUE NM 87185-5800	1	KTECH CORPORATION ATTN DR E GAFFNEY 901 PENNSYLVANIA AVE NE ALBUQUERQUE NM 87111
1	BLACK & VEATCH ENGINEERS - ARCHITECTS ATTN H D LAVERENTZ 1500 MEADOW LAKE PARKWAY KANSAS CITY MO 64114	4	KAMAN AVIDYNE ATTN R RUETENIK (2 CYS) S CRISCIONE R MILLIGAN 83 SECOND AVENUE NORTHWEST INDUSTRIAL PARK BURLINGTON MA 01830

NO. OF COPIES	ORGANIZATION
2	KAMAN SCIENCES CORPORATION ATTN DASIAC (2 CYS) P O DRAWER 1479 816 STATE STREET SANTA BARBARA CA 93102-1479
1	LOCKHEED MISSILES & SPACE CO ATTN J J MURPHY DEPT 81 11 BLDG 154 P O BOX 504 SUNNYVALE CA 94086
1	ORLANDO TECHNOLOGY INC ATTN D MATUSKA 60 SECOND STREET BLDG 5 SHALIMAR FL 32579
2	THE RALPH M PARSONS COMPANY ATTN T M JACKSON LB TS PROJECT MANAGER 100 WEST WALNUT STREET PASADENA CA 91124
1	SAIC ATTN N SINHA 501 OFFICE CENTER DRIVE APT 420 FT WASHINGTON PA 19034 3211
1	SAIC ATTN J GUEST 2301 YALE BLVD SE SUITE E ALBUQUERQUE NM 87106
2	S CUBED A DIVISION OF MAXWELL LABS INC ATTN C E NEEDHAM L KENNEDY 2501 YALE BLVD SE ALBUQUERQUE NM 87106
1	TRW BALLISTIC MISSILE DIVISION ATTN H KORMAN MAIL STATION 526 614 P O BOX 1310 SAN BERNADINO CA 92402
1	THERMAL SCIENCE INC ATTN R FELDMAN 2200 CASSENS DR ST LOUIS MO 63026

NO. OF COPIES	ORGANIZATION
2	MCDONNELL DOUGLAS ASTRNTCS CORP ATTN ROBERT W HALPRIN K A HEINLY 5301 BOLSA AVENUE HUNTINGTON BEACH CA 92647
1	MDA ENGINEERING INC ATTN DR DALE ANDERSON 500 EAST BORDER STREET SUITE 401 ARLINGTON TX 07601
2	PHYSICS INTERNATIONAL CORPORATION P O BOX 5010 SAN LEANDRO CA 94577-0599
1	R&D ASSOCIATES ATTN G P GANONG P O BOX 9377 ALBUQUERQUE NM 87119
1	SCIENCE CENTER ROCKWELL INTERNATIONAL CORPORATION ATTN DR S CHAKRAVARTHY DR D OTA 1049 CAMINO DOS RIOS THOUSAND OAKS CA 91358
3	S CUBED A DIVISION OF MAXWELL LABS INC ATTN TECHNICAL LIBRARY R DUFF K PYATT P O BOX 1620 LA JOLLA CA 92037-1620
1	SUNBURST RECOVERY INC ATTN DR C YOUNG P O BOX 2129 STEAMBOAT SPRINGS CO 80477
1	SVERDRUP TECHNOLOGY INC ATTN R F STARR P O BOX 884 TULLAHOMA TN 37388
1	SRI INTERNATIONAL ATTN DR G R ABRAHAMSON DR J GRAN DR B HOLMES 333 RAVENWOOD AVENUE MENLO PARK CA 94025

NO. OF COPIES	ORGANIZATION
1	BATTELLE TWSTIAC 505 KING AVENUE COLUMBUS OH 43201-2693
2	THINKING MACHINES CORPORATION ATTN G SABOT R FERREL 245 FIRST STREET CAMBRIDGE MA 02142-1264
1	CALIFORNIA INSTITUTE OF TECHNOLOGY ATTN T J AHRENS 1201 E CALIFORNIA BLVD PASADENA CA 91109
1	UNIVERSITY OF MINNESOTA ARMY OF HIGH PERF COMP RES CTR ATTN DR TAYFUN E TEZDUYAR 1100 WASHINGTON AVE SOUTH MINNEAPOLIS MN 55415
2	CDR ATTN SSCNC YSD J ROACH SSCNC WST A MURPHY US ARMY NRDEC KANSAS STREET NATICK MA 10760-5018
3	SOUTHWEST RESEARCH INSTITUTE ATTN DR C ANDERSON S MULLIN A B WENZEL P O DRAWER 28255 SAN ANTONIO TX 78228-0255
1	STATE UNIVERSITY OF NEW YORK MECHANICAL & AEROSPACE ENGINEERING ATTN DR PEYMAN GIVI BUFFALO NY 14260
2	DENVER RESEARCH INSTITUTE ATTN J WISOTSKI TECHNICAL LIBRARY P O BOX 10758 DENVER CO 80210
2	UNIVERSITY OF MARYLAND INSTITUTE FOR ADV COMPUTER STUDIES ATTN L DAVIS G SOBIESKI COLLEGE PARK MD 20742

NO. OF COPIES	ORGANIZATION
1	NORTHROP UNIVERSITY ATTN DR F B SAFFORD 5800 W ARBOR VITAE STREET LOS ANGELES CA 90045
1	STANFORD UNIVERSITY ATTN DR D BERSHADER DURAND LABORATORY STANFORD CA 94305

ABERDEEN PROVING GROUND

1	CDR USATACOM ATTN AMSTE-TE-F (L TELETSKI)
1	CDR USATHAMA ATTN AMSTH-TE
1	CDR USACSTA ATTN STEC-LI
5	DIR USARL ATTN AMSRL-SL-CM (BLDG E3331) AMSRL-WT-NC (R LOTTERO)(2 CP) AMSRL-WT-NC (A. MIHALCIN)(2 CP)

INTENTIONALLY LEFT BLANK.

USER EVALUATION SHEET/CHANGE OF ADDRESS

This Laboratory undertakes a continuing effort to improve the quality of the reports it publishes. Your comments/answers to the items/questions below will aid us in our efforts.

1. ARL Report Number __ARL-CR-239_____ Date of Report __July 1995_____

2. Date Report Received _____

3. Does this report satisfy a need? (Comment on purpose, related project, or other area of interest for which the report will be used.) _____

_____

_____

4. Specifically, how is the report being used? (Information source, design data, procedure, source of ideas, etc.)

_____

_____

_____

5. Has the information in this report led to any quantitative savings as far as man-hours or dollars saved, operating costs avoided, or efficiencies achieved, etc? If so, please elaborate. _____

_____

_____

6. General Comments. What do you think should be changed to improve future reports? (Indicate changes to organization, technical content, format, etc.) _____

_____

_____

_____

CURRENT
ADDRESS

_____
Organization

_____
Name

_____
Street or P.O. Box No.

_____
City, State, Zip Code

7. If indicating a Change of Address or Address Correction, please provide the Current or Correct address above and the Old or Incorrect address below.

OLD
ADDRESS

_____
Organization

_____
Name

_____
Street or P.O. Box No.

_____
City, State, Zip Code

(Remove this sheet, fold as indicated, tape closed, and mail.)
(DO NOT STAPLE)

DEPARTMENT OF THE ARMY

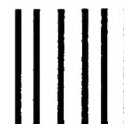OFFICIAL BUSINESS

BUSINESS REPLY MAIL
FIRST CLASS PERMIT NO 0001,APG,MD

POSTAGE WILL BE PAID BY ADDRESSEE

DIRECTOR
U.S. ARMY RESEARCH LABORATORY
ATTN: AMSRL-WT-NC
ABERDEEN PROVING GROUND, MD 21005-5066